Investigating the Mechanical Properties of Pharmaceutical Excipients in Granule and Tablet Production

by

Rachael Shinebaum

A thesis submitted to

The University of Birmingham

for the degree of

Engineering Doctorate

School of Chemical Engineering

University of Birmingham

June 2021

UNIVERSITY OF BIRMINGHAM

University of Birmingham Research Archive

e-theses repository

Abstract

Pharmaceutical tablets are commonly used as they are inexpensive to produce and have high acceptability amongst patients. Tablets are often made by direct compression of a powder formulation and when this is not achievable, a granular intermediate is produced before the compression process. Granulation is especially advantageous in the presence of powder handling difficulties such as poor flow or dusting. However, granulation can lead to a reduction in tablet tensile strength which is to be avoided to ensure a high-quality product. The current study investigates twin screw wet granulation and the result of changing process parameters on the tabletability of a range of materials. Granules were characterised by shape, internal structure and porosity while a compression simulator was used to find differences in tabletability based on the excipient used and process parameters.

To develop an understanding of the bonding mechanisms within tablets a comprehensive and thorough study of tablet properties surrounding the moisture content of materials was carried out. Pharmaceutical excipients were chosen based on their mechanical properties and hygroscopicity then directly compressed to identify the difference in tabletability due to the powder characteristics. A distinct difference in the tablet compaction process was identified between excipients which undergo brittle fracture and those which exhibit plastic deformation. The resultant tablet strength of hygroscopic powders is different depending on the moisture content gained by storage in changing relative humidity. This not only highlights the potential changes in material structure bought about by water, but also the importance of the control of storage conditions of hygroscopic materials for industrial purposes.

To further understand the role water plays in tabletability, magnesium stearate was used as a lubricant in microcrystalline cellulose (MCC) tablets. MCC is known to be highly lubricant sensitive, meaning that a reduction in tablet tensile strength is observed with increasing magnesium stearate concentration. However, a lubricant such as magnesium stearate is often required in the pharmaceutical tableting process. This study presents a hypothesis as to why magnesium stearate presents such problems during formulation work and how these problems are exacerbated by the presence of increasing moisture. To confirm the hypothesis, Raman spectroscopy was employed to visualise the areas of high magnesium stearate concentration within a tablet.

Alongside the powder characteristics identified as important in the prediction of tabletability presented within this study, surface energy presents an additional area of investigation for future study. Mannitol derivatives with different surface energies were successfully used in a tabletability feasibility study to assess the importance of surface energy in isolation to other differences in powder properties.

Acknowledgements

Contents

List of Figures

List of Tables

Nomenclature

Roman Symbols

Symbol	Definition	SI Units
a	Kawakita parameter	
A	Heckel parameter	
A'	Area	m^2
A_h	Area of the circumscribed convex hull	m^2
a_w	Water activity	
b	Kawakita parameter	
b'	Ryshkewitch empirical constant	
c	Cohesion	
C	Degree of volume reduction	
C'	Heat of sorption parameter	
C''	Powder deformability constant	
C_{BET}	BET constant	
CI	Carr's Index	
D	Relative density (solid fraction)	
d	Particle diameter	m
d_{10}	Diameter for which 10% of particles are smaller	m
d_{50}	Diameter for which 50% of particles are smaller	m
d_{90}	Diameter for which 90% of particles are smaller	m
D_t	Tablet diameter	m
F	Force	N
ffc	Flow function	
G_{21}	Mass of sample	g
G_{tot}	Total mass	g
H	Hausner Ratio	
k	Heckel parameter	
K'	Heat of sorption parameter	
l_{max}	Maximum Ferret length	m

Symbol	Definition	SI Units
l_{min}	Minimum Ferret length	m
m	Mass	kg
P	Compaction pressure	Pa
P_0	Saturation pressure	Pa
P_c	Perimeter of the equivalent circle	m
P_l	Total projection outline length	m
P_y	Yield pressure	Pa
S_A	Aspect ratio	
S_C	Convexity	
S_R	Roundness	
S_S	Sphericity	
T	Torque	Nm
t_h	Tablet height	m
V	Volume	m^3
V'	Specific tablet volume	$m^3\ kg^{-1}$
V'_{sp}	Specific volume at 1 MPa pressure	$m^3\ kg^{-1}$
V_0	Initial sample volume, bulk volume	m^3
V_{ej}	Tablet volume after ejection	
V_{ERS}	Tablet elastic recovery after storage	
V_f	Final tapped volume	m^3
V_m	Volume adsorbed in monolayer	m^3
W	Weight ratio of water to solid	
w_m	Water monolayer	
w'	Walker coefficient	
X_i	Mass fraction for specific particle size	

Greek Symbols

Symbol	Definition	SI Units
α	Coefficient of friction	
β	Deformation value	
∂	Angle of internal friction	
ε	Porosity	
ε_c	Critical porosity	
ε_n	Natural strain	
ρ_{bulk}	Bulk density	kg m^{-3}
ρ_{tablet}	Tablet density	kg m^{-3}
ρ_{tap}	Tapped density	kg m^{-3}
ρ_{true}	True density	kg m^{-3}
σ	Stress	Pa
σ_c	Unconfined yield stress	Pa
σ_{pre}	Pre-shear	Pa
σ_t	Tablet strength	Pa
σ_0	Maximum tablet tensile strength at zero tablet porosity	Pa
σ_1	Consolidation stress	Pa
τ	Shear failure stress	Pa
τ'	Second shear failure stress	Pa
τ_g	Granule strength	Pa
τ_0	Cohesive strength	Pa

1 Introduction

1.1 Introduction

This thesis will focus on the mechanical properties of pharmaceutical excipients in granulation and tableting. The work has been carried out as an Engineering Doctorate (EngD) in Formulation Engineering at the School of Chemical Engineering, University of Birmingham with AstraZeneca as the industrial sponsor. Pharmaceutical tablets are commonly made by either direct compression of a powder formulation or compression of a granular intermediate. Tablets require an adequate physical strength to ensure a high-quality product. Currently, trial and error lab scale experiments are carried out in order to optimise a formulation to produce the required tablet characteristics. This experimentation is costly and time consuming and could potentially result in a sub-optimal product. A greater understanding of the granulation and tableting procedures will lead to a reduction in pre-formulation experimentation and ease of scale-up. This may be done by optimizing granulation process parameters and applying knowledge of bond formation in tableting to better predict the compression process.

1.2 Direct compression or granulation

Direct compression of powders is preferable due to the reduction in manufacturing costs and the low risk of an active pharmaceutical ingredient (API) undergoing a physical or chemical change with the addition of solvents or extra manufacturing steps (Thoorens, et al., 2014). However, an intermediate granulation step is often required in order to improve flowability, reduce dustiness or ensure formulation uniformity (Thompson, 2015). Flowability can be defined as the propensity of powders to flow under given circumstances (Conceição, et al.,

2014) and dustiness is the tendency of a powder to produce an aerosol after an energy input (Boundy, et al., 2006). Granulation is a size enlargement process which can be carried out whether wet or dry. The characteristics of both API and excipients need to be considered when choosing a granulation process due to the chemical and physical changes that may take place as a result of interactions with heat, water, physical stress, or a combination of all three (Thompson, 2015).

Within this thesis the focus is upon wet granulation, and more specifically twin screw granulation (TSG). TSG has gained popularity over recent years due to the ability to incorporate it into a continuous process. Unlike batch granulation techniques, such as high shear granulation, continuous processes reduce manufacturing costs, allow for in-line quality measurements and reduce operator process interaction time. Previous literature has reported a reduction in tabletability after both wet and dry granulation (Nguyen, et al., 2013; Sun & Kleinebudde, 2016). However, there has been little work surrounding the change in tabletability after the TSG process. There is a need for links to be made between TSG process parameters, granule attributes and tablet compaction properties in order to improve understanding and reduce time consuming experimental work in the future.

As a result of findings within the TSG study and ongoing collaboration with AstraZeneca leading to prioritized research areas, this thesis also studies the effect of moisture on tablet properties from directly compressed material. The effect of moisture on tablet strength has been investigated previously (Sun, 2008; Thapa, et al., 2017). However, there has been little work carried out towards understanding the mechanical properties of materials that lead to a difference in tablet tensile strength in the presence of varying quantities of moisture.

1.3 Aims and objectives

This research aims to understand the effect of material mechanical properties on tablet tensile strength and whether they can be used to predict the tabletability of powders or granules. The first objective is to investigate how the TSG process modifies pharmaceutical excipients and how process parameters can be changed to gain the required granule quality attributes. The second objective of this work is to improve the understanding of tabletability and knowledge surrounding bonding mechanisms. This will lead to additional information that can later be used in material tabletability prediction based on their mechanical properties.

1.4 Thesis overview

Chapter 2 – Literature Review: In this chapter the available literature surrounding granulation and, more specifically, the TSG process will be reviewed. This chapter also explains the main mechanisms of tablet formation and current understanding of bonding mechanisms.

Chapter 3 – Experimental materials and methods: The materials and methods used within the study are discussed along with justification of the experimental procedures used.

Chapter 4 – Investigating twin screw granulation: This chapter focuses on TSG as a granulation process, using a selection of pharmaceutical excipients to investigate the impact of varying process parameters on final granule quality attributes and tabletability.

Chapter 5 – Investigating the role of moisture in tablet compaction and tensile strength: The role moisture plays on tabletability of pharmaceutical excipients with varying material characteristics is investigated.

Chapter 6 – Investigating microcrystalline cellulose tabletability and storage: Based on the wide variation in tabletability with varying amounts of moisture within microcrystalline cellulose (MCC), this chapter investigates the tablet bonding mechanisms within the material further.

Chapter 7 – The role of magnesium stearate in the reduction of tablet tensile strength: This chapter investigates the role magnesium stearate plays in tabletability and provides an explanation for the reduction in tablet tensile strength with increasing lubricant concentration.

Chapter 8 – Functionalized mannitol case study and an introduction to future work: Functionalized mannitol was provided for a tabletability study. The four mannitol grades were modified to change surface energy but keep other mechanical properties the same. Tablet attributes were assessed for each material in order to provide greater understanding for the potential to manipulate certain required characteristics within manufacture. The potential for future work around tabletability prediction is also discussed within this chapter.

Chapter 9 – Conclusions: A conclusion of the main findings for each study are presented.

1.5   Publications arising from this work

Poster R. Shinebaum, H. K. Batchelor, I. Gabbott, G. K. Reynolds, A. Ingram, Twin Screw Granulation and resultant granule characteristics. Formulation Forum Launch Event, January 2018, SCI, London, UK.

Oral presentation R. Shinebaum, H. K. Batchelor, I. Gabbott, G. K. Reynolds, A. Ingram, Granule characteristics after twin screw granulation, World Congress on Particle Technology, April 2018, Orlando, USA.

Poster R. Shinebaum, H. K. Batchelor, E. Stone, I. Gabbott, G. K. Reynolds, A. Ingram, Compaction simulation of granules produced via twin screw granulation, Compaction Simulation Forum, June 2018, San Francisco, USA (presented by E. Stone).

Poster R. Shinebaum, H. K. Batchelor, I. Gabbott, G. K. Reynolds, A. Ingram, Twin screw granulation: Can continuous manufacture result in superior granules? IFPRI 40th Annual General Meeting, June 2018, Edinburgh, UK.

Poster R. Shinebaum, H. K. Batchelor, I. Gabbott, G. K. Reynolds, A. Ingram, Granule attributes and resulting compaction behavior after twin screw granulation, PARTEC, April 2019, Nuremburg, Germany. Poster competition 3rd prize winner.

Conference paper and oral presentation R. Shinebaum, H. K. Batchelor, I. Gabbott, G. K. Reynolds, A. Ingram, Granule characteristics after twin screw granulation, **Poster** Linking moisture induced variations in pharmaceutical primary powders to their tableting performance, 9th International Granulation Conference, June 2019, Lausanne, Switzerland.

Oral presentation R. Shinebaum, H. K. Batchelor, I. Gabbott, G. K. Reynolds, A. Ingram, Linking moisture induced variations in pharmaceutical primary powders to their tableting performance, AIChE Annual General Meeting, November 2019, Orlando, USA.

2 Literature Review

2.1 Introduction

Tablets are the most commonly used oral dosage form, this is mainly due to their ease of production and administration in comparison to other medication administration routes . Tablets require adequate physical strength to ensure a high quality product that can withstand the maufacturing process, packaging and transportation (Pitt & Sinka, 2001). They may be produced by directly compressing a powder formulation, but this does not always result in an adequate compact. If direct compression is to be undertaken, the powder must have good flowability, minimal dusting, suitable mechanical properties and a low tendency towards segregation (Thompson, 2015;Rosato & Windows-Yule, 2020). If a powder does not meet these requirements, the process of granulation prior to tablet production may produce a suitably compactible formulation. Granulation can be either a wet or dry process (Thompson, 2015).

This literature review provides an introduction to twin screw wet granulation and the effect of process parameters on the granules that are produced. The properties of the primary powders before granulation are also discussed and how these impact granules and the final tablet form. The review also covers previous work that has taken place to study the mechanisms involved in tablet formation and how these may be modified.

2.2 Twin screw wet granulation

The use of a twin-screw granulator (TSG) has gained considerable interest in recent years as a continuous wet granulation method in the pharmaceutical industry. This is mainly due to the

advent of Process Analytical Technology (PAT) and Quality by Design (QbD), as a continuous process such as TSG lends itself well to the application of both. It has been noted that the granulation process has an influence on the final tablet strength (Dhenge, et al., 2012(a); Seem, et al., 2015; Vercruysse, et al., 2015). Therefore, it is important to gain an understanding of TSG process parameters and the resultant effect on material behaviour during tableting.

The TSG is a modified extruder consisting of a pair of screws that rotate in the same direction (co-rotating), housed inside a temperature-controlled barrel (Figure 2-1). The length of the barrel is measured in terms of its length to diameter ratio (L/D). Industrially, screw lengths are 12-20 L/D for powder formulations and 30-50 L/D in the food and plastics industries (Thompson, 2015). At the start of the barrel is a powder feeder which may be a screw, gravity or vibratory feeder and must provide a consistent feed of material. The liquid feed is introduced early along the barrel length through liquid feed ports, located centrally above the screws within the barrel. The screw composition can be adapted with the use of modular elements which directly impact granule attributes (Table 2-1). There are three main screw element types in use, these being conveying, kneading and comb-mixing elements (Thompson, 2015). Kneading blocks are composed of kneading elements placed in a group and aligned at either 30°, 60° or 90° angles. The use of kneading elements causes a rise in product temperature due to friction between the material and barrel through the increase in shear stress (Seem, et al., 2015). This has led to the use of a temperature-controlled jacket around the barrel to ensure there is no unfavourable effect of temperature on the material.
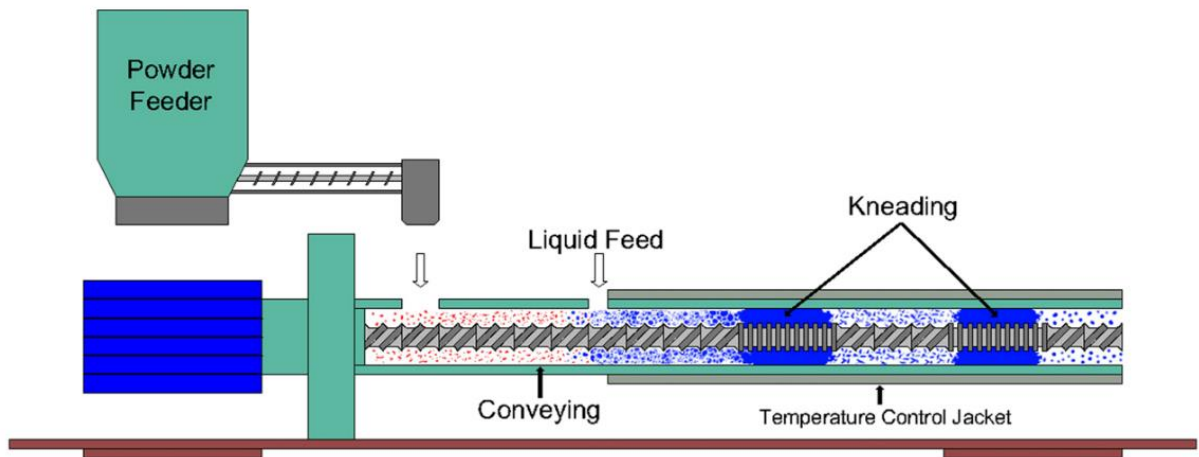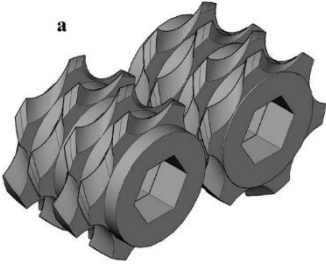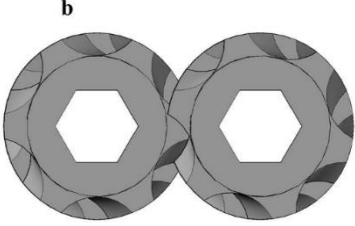
Figure 2-1 The components of a typical TSG (Seem, et al., 2015).

Table 2-1 The modular elements used to make up screw lengths within the TSG (adapted from Seem, et al., 2015).
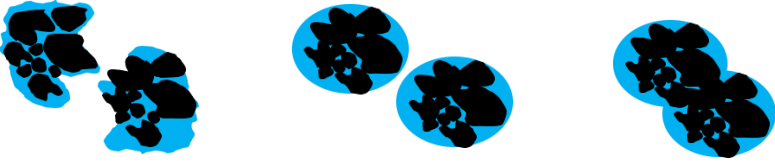
Element	Isometric view	End view
Intermeshed conveying elements		
60° forwarding kneading block		

Element	Isometric view	End view
Comb mixer elements	a	b

2.3 The mechanism of wet granulation

Wet granulation is a process that produces free-flowing granules by the addition of a liquid to a powder. Wet granulation is a complex process which sees a number of phenomena occur to control the granule size distribution, density and morphology (Lister, 2016). Although there are varying types of wet granulating equipment, the fundamental mechanisms in which granules are formed remain the same. The three main stages of wet granulation are wetting and nucleation, consolidation and growth and breakage and attrition. These are shown in Table 2-2.

Table 2-2 The wet granulation rate processes (Litster, 2016).

I.   Wetting and nucleation: Liquid is added to the powder and 'nuclei' granules are formed.
II.   Consolidation and growth: Granules collide with other granules and densify.
III.   Breakage and attrition: Granules break to form small granules as a result of high shear in the powder bed.

2.3.1   Wetting and nucleation

The first stage in wet granulation is wetting and nucleation (Table 2-2). In this stage the liquid binder is distributed through the feed powder. Two situations may be considered:

I.   If the liquid binder drop size is larger than the powder particle size then seed granules or nuclei will be formed, also known as immersion.

II. If the liquid binder drop size is smaller than the powder particle size, the liquid will coat the particles and if the particle is porous then liquid will enter these pores via capillary action.

These initial stages have an impact on the later stages of granule growth: poor nucleation and binder distribution almost always leads to difficulty in the control of granule properties. This may be in the form of broad granule size distribution or clump formation (Litster & Ennis, 2004).

The initial wetting of a powder was studied further by Emady, et al. (2011). A single drop of binder solution was dropped onto a powder bed from two controlled drop heights. Granules were excavated and further investigated. Granule nuclei formation was recorded using a high speed camera resulting in the observation of three different granule formation mechanisms (Figure 2-2):

I. *Tunnelling* where powder particles are sucked into the liquid binder drop which then tunnels into the powder bed. This was seen for fine, cohesive powders;

II. *Spreading* in which the liquid binder droplet spreads to equilibrium before penetrating the powder bed via capillary suction. This mechanism was reported for coarser powders; and

III. *Crater formation* where the momentum of the liquid binder droplet on impact forms a crater in the powder bed, forming a layer of powder on the droplet surface. This mechanism was observed for cohesive powders that formed a denser powder bed than those in the tunnelling mechanism.

28
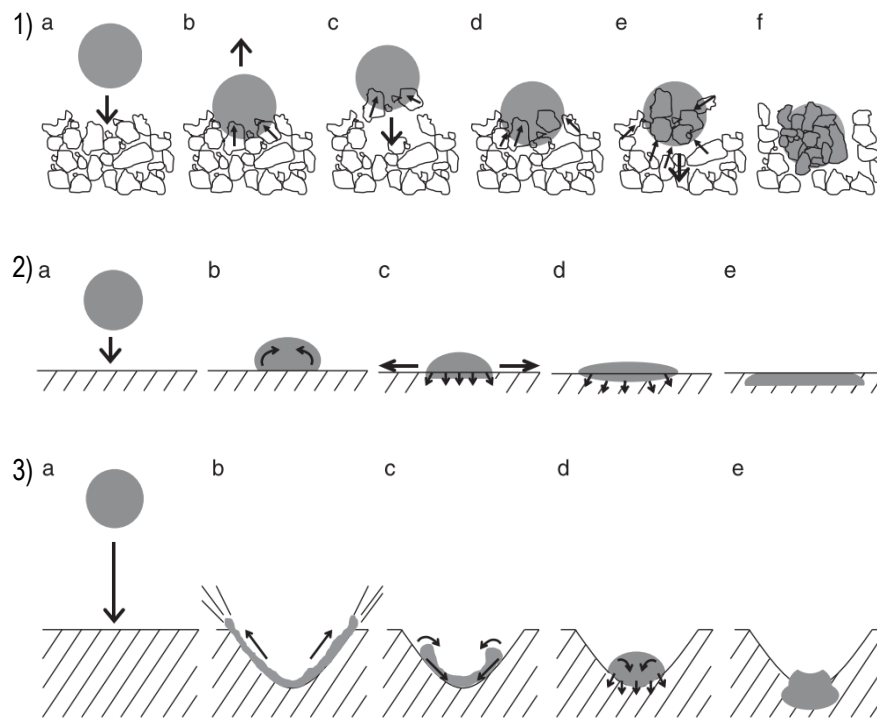
Figure 2-2 (1) The tunnelling mechanism, (2) The spreading mechanism and (3) The crater formation mechanism (Emady, et al., 2011).

These mechanisms are dependent on the powder properties and the structure of the powder bed, thereby showing that an understanding of both the feed powder and the process are required in order to optimise wetting and nucleation.

Surface energy describes the excess energy that a surface has compared to the bulk of a material. At an air-solid interface, molecules have similar molecules neighbouring them on the sides and below. There is little interaction with molecules in air which causes excess energy at the solid interface (Aliofkhazraei, 2015). Wetting may be improved by maximising the surface energy, or by minimising the surface tension, of the liquid binder or decreasing the binder viscosity. The powder may also be modified in order to maximise wetting by increasing the pore size to increase the rate of fluid penetration (Litster & Ennis, 2004).

2.3.2 Coalescence and consolidation

Once wetting and nucleation has taken place, granules may increase in size and density and the extent of this growth and consolidation plays a role in determining final granule properties (Litster & Ennis, 2004).

The stages of wet granulation along the length of a TSG barrel have previously been studied. Dhenge, et al. (2012) divided the barrel into five compartments showing the series of granulation steps along the length in order to track the progression of granulationion along the lengths of the screws (Figure 2-3). For compartment C1 where only conveying elements were present it was reported that nucleation occurred. Compartment C2 which consisted of eight kneading blocks provided an area of high shear resulting in consolidation and breakage of the granules. Within the longer area of conveying elements, C3, coalescence and breakage took place, even with a lesser extent of shearing than C2. The coalescence that occurs in C3 is dependent on the surface wetting of granules in C2. If coalescence is the dominating factor, granules will grow. However, if breakage is the dominating factor, granules will reduce in size. Granule, even with a lesser extent of shearing than C2. The coalescence that occurs in C3 is dependent on the surface wetting of granules in C2. If coalescence is the dominating factor, granules will grow, however if breakage is the dominating factor, granules will reduce in size. Granule size increased in the second kneading section, C4, due to growth being the dominating factor, due to growth being the dominating factor. And finally, granule size reduction took place in compartment C5 before tablet ejection from the barrell (Dhenge, et al., 2012(a)). The authors noted that the granule growth that occurred in the conveying areas

took place via layering of the material, whereas in an area with kneading elements, granule growth was due to continuous breakage and coalescence.
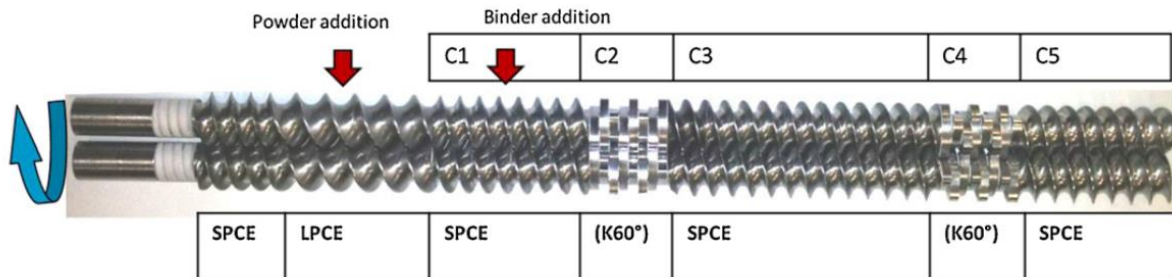
Figure 2-3 The different compartments (C1 to C5) along the TSG barrel (where SPCE is short pitch conveying element, LPCE is long pitch conveying element and K60° is a forward-facing kneading block) (Dhenge, et al., 2012(a)).

Seem, et al. (2016) further understood the movement of material along the barell length by carrying out Positron Emission Particle Technology (PEPT). In this technique, a single radioactively labelled tracer particle is put into the system and its location can be determined accurately and frequently as it moves, in this case along the length of the TSG barrrel (Figure 2-4). The authors found that the distribution of material within conveying zones is highly asymmetric, where one screw carries the bulk of the material. The extent to which the system was asymmetric was dependent on the fill level of the barell. The lower the fill level, the more asymmetric the loading of the screws. It was also shown that there is a much longer residence time in the kneading zones of the screw.
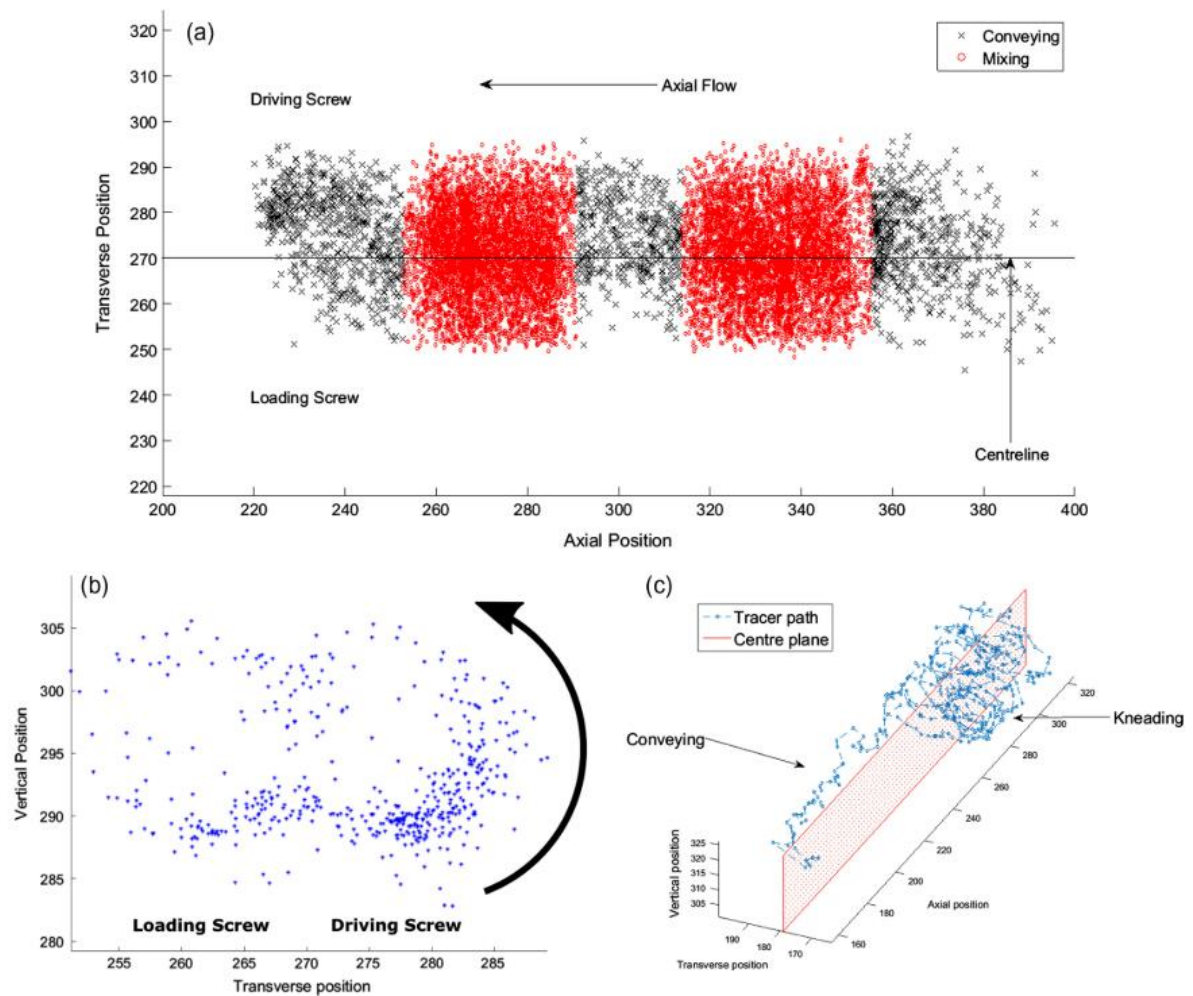
Figure 2-4 (a) The overhead view of the TSG barrel showing each detection of the PEPT tracer in 100 passes through the TSG, the red areas show kneading blocks along the screw. (b) End view of the screws showing asymmetry with a larger material loading on the driving screw. (c) A single pass of a tracer through the TSG showing a longer residence time in the kneading zone (Seem, et al. 2016).

2.3.3 Breakage and attrition

When considering the final stage of the granulation process it is suitable to separate it into two potential phenomena. Firstly, the breakage of wet granules within the granulator and secondly, the attrition or fracture of dried granules. The second phenomena may occur within

the granulator itself, in the drier or upon handling (Litster & Ennis, 2004). Vonk, et al. (1997) proposed a destructive nucleation-growth mechanism during high-shear wet granulation. It was suggested that after initial nucleation, small secondary nuclei are formed from the break-up of primary nuclei. Firstly, weak nuclei break by nuclei-nuclei and nuclei-wall collisions (attrition) and secondly, they can break into fragments from the action of the impeller and chopper (fragmentation). The small, secondary nuclei that are formed can then subsequently grow upon sufficient wetting and consolidation. The secondary nuclei are stronger and can withstand further impacts (Vonk, et al., 1997). Primary nuclei consist of loose agglomerates and resultant granules are produced by layering. However secondary nuclei produce granules by densification which are less porous and therefore stronger than those produced by a layering of material (Vonk, et al., 1997).

If wet granulation breakage can be controlled, by growing granules up to a breakage limit, then a possibility for a narrow granule size distribution can occur (Litster & Ennis, 2004). However, granulators that have an uncontrolled turnover of granules through the high impact region are unlikely to have a granule size distribution that is easy to control. Owing to its modular nature, the twin screw granulator may provide an appropriate level of control to allow the turnover of material in regions of high shear regions of high shear to be adequate to produce a narrow granule size distribution.

Any drying processes that take place after granulation pose a threat by being a source of undesirable attrition or fracture of granules. An understanding of the drying process is required in order to minimise unwanted results, alongside an understanding of the fracture of dry granules (Litster & Ennis, 2004).

2.4 Regime maps for twin screw granulation

There has been previous work to develop a regime map for the twin screw granulation process (Dhenge, et al. (2012(b)). Dhenge, et al. (2012(b) used a range in concentraion of binder (hydroxypropylcellulose, HPC) at different liquid to solid ratios (L/S) and found that torque increased with increasing HPC concentration or L/S. An increase in binder quantity decreased the fraction of fines and very small granules, therefore producing a mono-modal size distribution and improved flow due to increased granule sphericity. At low L/S with no binder, the granule size distribution was bimodal. The developed regime map was based on those previously produced for high shear (HSG) and fluid bed (FBG) granulation by Iveson and Lister (1998) where the map is classified into granulation behaviours such as, under-wetted (dry), nucleation (crumb), growth and over-wetting (paste). HSG and FBG are both batch processes, therefore some of the granulation behaviours occur simulataneously. Within the continuous TSG process there is no re-circulation of material so granulation behaviours are separated from one another. As demonstrated in previous work (Dhenge, et al., 2012(a)), granulation behaviours occur one after the other along the length of the TSG screws, therefore all powder particles that are fed into the system are subjected to similar processes within the barrel. TSG, unlike HSG and FBG, has a high volume of materials within the barrel and little free volume at various points along the system at various points along the system. This results in higher stresses acting on the material and higher torque output. The torque (T) changes with barrel fill level, or volume of material in the barrel (V). Together torque and volume represent the stresses acting on the material (σ) (Equation 2-1) (Dhenge, et al., 2012(b)).

$$\sigma \approx \frac{T}{V} \qquad\qquad\qquad \textit{Equation 2-1}$$

Dhenge, et al. (2012(b)) found that kneading elements increase the holdup time of the material due to their low conveying capability, thereby increasing fill level and stresses. Conversely, low stresses are observed with conveying elements because material is transported quickly with shorter hold up time and lower volume of material in the barrel. The deformation value, β, can be used as an indication of deformability in a TSG system and forms the basis of a regime map produced by Dhenge, et al. (2012(b)). The deformation value can be found using Equation 2-2.

$$\beta = \frac{\sigma}{\tau_g} \qquad\qquad\qquad \textit{Equation 2-2}$$

where σ is the stress acting on the powder from Equation 2-1 and τ_g is granule strength. A smaller value for β indicates a stronger granulation system and a larger value, a weaker system. A later regime map (Dhenge, et al., 2013) shows that not only L/S and binder viscosity have an effect on the deformation value, but also the powder feed rate and therefore barrel fill level (Figure 2-5). The boundaries within the regime map are highly dependent on the system and will move due to changes in parameters, for example screw configuration, primary material properties and operating conditions.
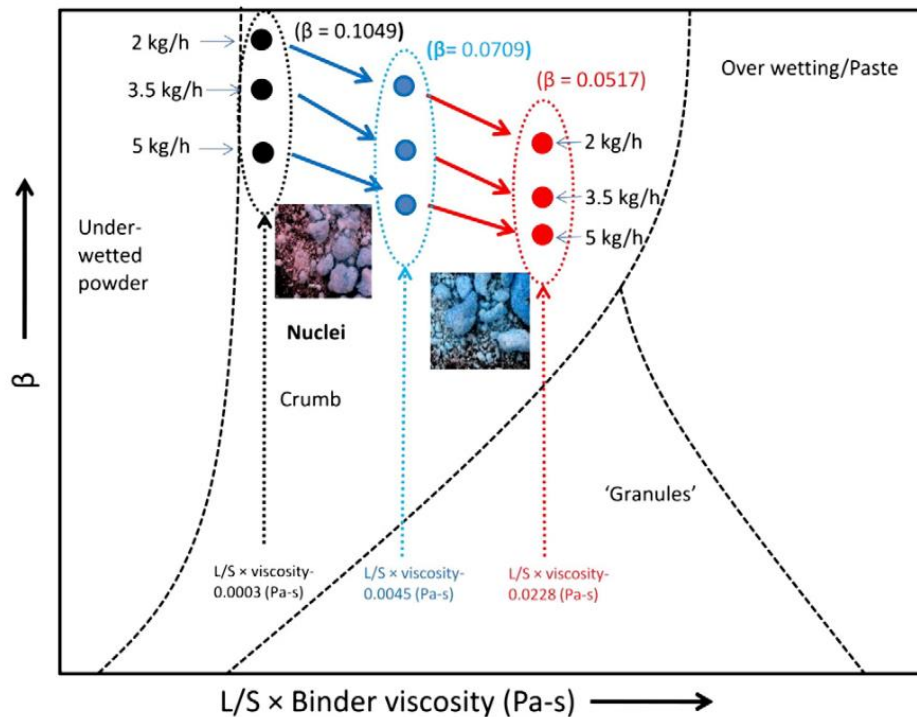
Figure 2-5 A granule regime map for TSG using conveying screws (Dhenge, et al., 2013).

Kumar, et al. (2016) undertook further work on the development of a regime map by presenting a range of process maps. It was recognised that there is difficulty in producing a scaleable regime map for the TSG process due to the highly adaptable nature of the process. There are not only a large number of potential process parameters but also many different combinations of screw length adaptations making it difficult to incorporate into a regime map. The study showed that an increase in L/S ratio results in an increase in granule size. However most of the additional liquid contributes to the production of oversized granules. The authors conclude that the L/S ratio should be kept in a lower range and the energy input to the system should be the main source of producing an increase in granule size (Kumar, et al., 2016).

Regime maps can provide a step towards reducing development time by providing a basis upon which to set up the TSG process in order to obtain granules of the required size and

shape. These and other granule attributes such as porosity and strength have an effect on final tablet properties such as compactibility and dissolution rate. Therefore, it is important to further investigate the prediction of granule characteristics based on TSG process parameters to further the use of this continuous process in the furture of pharmaceuticals manufacture.

2.5   Process parameters and their effect on granule attributes

The effects of the process on granule attributes can be split into two groups (Thompson, 2015):

I.   Operational parameters, such as powder feed rate and screw speed, and

II.   Formulation parameters, such as L/S ratio and powder properties.

2.5.1   Operational parameters

Powder feed

Gravimetric feeders or loss-in-weight feeders are the most commonly used powder feeders for the TSG process. These may be a single screw auger, twin screw auger, vibrating pan or a conveying belt and each will vary in dosing accuracy and available feed rates (Thompson, 2015). Meier, et al. (2016) identified that powder feeders present problems due to pharmaceutical powders often being cohesive and poorly flowing, resulting in poor feeder performance. The authors showed the importance of accurate powder feeding throughout the process and stressed that any short term fluctuations due to process disturbances during batch production would be compensated by the overall size of the whole batch. Conversely, during a continuous process such as TSG, running in steady-state can lead to inaccuracies

leading to lower than required quality of products. Feeder deviation times were used to produce 'good' and 'poor' settings by changing the display filter values. For example, if a display filter time of 1 s is observed, there are a lot of deviations from the set value. However, at a display filter time of 30 s there is very little deviation from the set value. By using these settings to investigate the influence of the feeding system on granule size distributions it was found that just a small shift in feed settings produced a distinct difference in granule quality. Figure 2-6 shows the particle size distribution for ungranulated and granulated material using 'good' and 'poor' feeder settings. It can be seen that when 'good' settings are used there is a successful particle size increase and a monomodal distribution. However, when 'poor' settings are used there is particle size enlargement but it is shown as a bimodal distribution and a large fraction of oversized granules (Meier, et al., 2016). The result of the 'poor' feed settings are granules which may not compress as successfully and could be likely to segregate due to the presence of more fines.
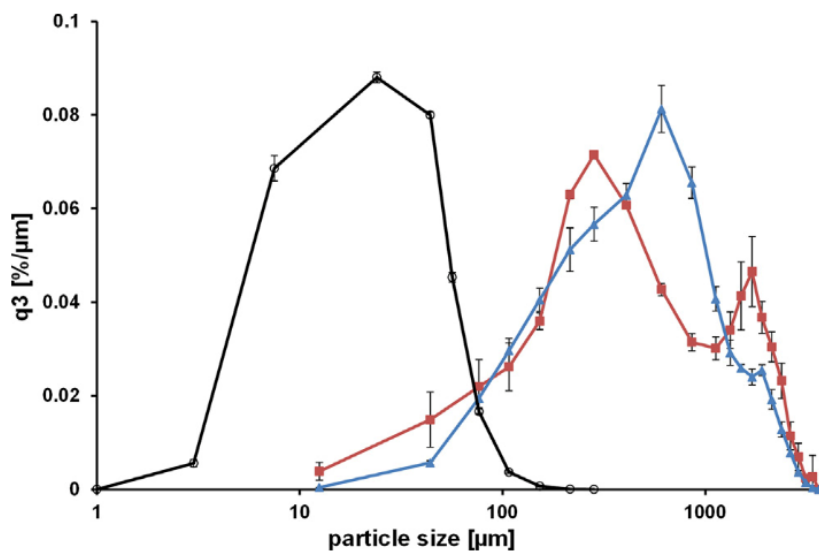
Figure 2-6 Granule size distributions of ibuprofen/croscarmellose sodium granules produced with conveying screws only. Black circles represent raw powder formulation, blue triangles are granules produced with 'good' feeder settings, and red squares are granules produced with 'poor' feeder settings (Meier, et al., 2016).

A study by Dhenge, et al. (2011) showed that granule size decreased with higher powder feed rate. The powder feed rate had a direct impact on residence time distribution, barrel filling and torque. As a consequence there were changes in granule size, shape, structure, porosity, strength and dissolution. There was an effect on granule surface structure, where a lower feed rate (2 kg/h) produced rough and loosely packed granules, whereas a higher feed rate (6.5 kg/h) produced smooth and closely packed granules. Granule porosity was reduced with an increase in powder feed rate. This was attributed to changes in barrel filling and torque. At higher feed rates there is a higher barrel fill and an increased torque, therefore increased compaction amongst the material resulting in lower porosity, higher granule strength and increased dissolution time (Dhenge, et al., 2011).

During powder feeding, contact and separation of particles can give rise to electrostatic charges, also termed tribo-charging (Beretta, et al., 2020). Tribo-charging can represent a safety hazard, as well as cause manufacturing issues such as particle agglomeration, reduced powder flow, adhesion to the surface of equipment and segregation (Beretta, et al., 2020).

Screw speed

Screw speeds between 200 and 400 rpm are regularly used for the TSG process and have been found to have little effect on granule properties (Thompson, 2015). However, under some circumstances, lower screw speeds can generate higher torque values as a result of increased screw filling and higher screw speeds at the same throughput can reduce torque because of an increased conveying capacity (Thompson & Sun, 2010). In my own opinion, a difference in granule properties would be expected due to changing screw speed and its effect on barrel fill and shear rate within the kneading zone. With a higher screw speed, and therefore lower barrel fill, there would be less consolidation of granules taking place and a potential reduction in granule size. The opposite being true for slower screw speeds.

Liu, et al. (2017) confirmed that differences in L/S ratio has a greater effect on granule attributes than changes in screw speed. The authors found that increasing L/S ratio reduced fines and increased the oversized fraction. By decreasing barrel fill level, by reducing throughput or increasing screw speed, an improved flowability of granules was found. However this improvement was greater when the L/S ratio was increased. An increase in tablet tensile strength was observed when screw speed and L/S ratio were increased (Liu, et al., 2017).

Keleb, et al. (2002) found that screw speed had an effect on granule friability when polyvinylpyrrolidone (PVP) was used as a binder with lactose as the bulk material. When screw speed was increased from 200 to 450 rpm, granule friability significantly increased for granules produced with PVP. No significant difference in friability with increasing screw speed was observed for granules produced from lactose and water only. This is further supported by Vanhoorne, et al. (2016) where it is noted that screw speed has an influence on torque and this is potentially formulation dependent. If material throughput is kept constant, increasing the screw speed results in a lower barrel filling, which in turn yields lower torque values.

Screw configuration

Conveying elements are available as either single- or double-flighted modules, and differ in the axial distance between two adjacent flights along the axis of the screw. A double-flighted conveying element has the largest available space for material to fill in comparison to a kneading element. Thompson (2015) concludes that the type of conveying element used is not important. However, there is a suggestion that double-flighted conveying elements should be placed before and after a kneading block to minimise large clumps from exiting the process.

A kneading block is effective in the compaction of wetted powders and ensures the densely packed material produces strong granules. Within the kneading block there is a higher fill volume of the material (shown in Figure 2-7), therefore a pressure rise that conveys material along the barrel, differing to the drag flow seen in a conveying zone. Djuric, et al. (2009) demonstrated that kneading elements produce larger, denser and stronger granules, however these resulted in weaker tablets due to the lack of ability for the granules to deform under

41

pressure and therefore increase contact area for more widespread bonding. Thompson and

Sun (2010) took the unusual step of pre-wetting lactose with an aqueous PVP binder before

using different screw designs to granulate the material. The authors showed that kneading

blocks were effective for generating coarser particles. The authors acknowledge that the

difference in aqueous binder system would increase the liquid bridging forces present and

therefore change the size distribution dependending upon the strength of liquid bridges

present and how well they withstand the compressive and shear forces from each different

type of screw element. However, despite the differences in aqueous binder system, granule

characteristics showed similar trends to previous work (Thompson & Sun, 2010).
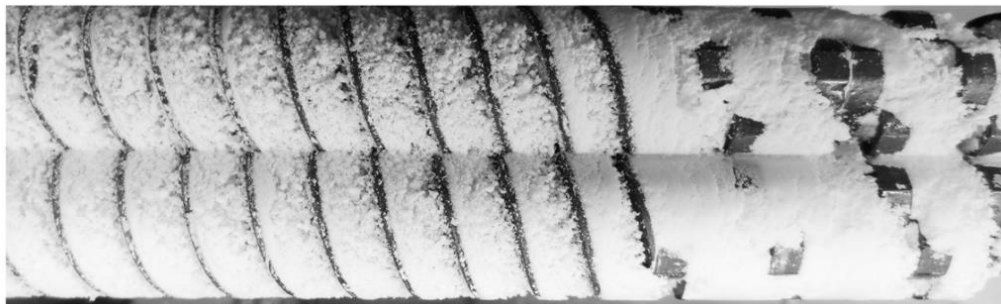
Figure 2-7 Screws pulled out from a TSG process after reaching steady state showing the kneading block at the far right of the image. The material flows from left to right (Thompson, 2015).

Kneading elements can be staggered at different angles (30°, 45°, 60° or 90°) and this can

have an effect on conveyance, residence time, torque, barrel fill and granule properties within

the TSG process (Lee, et al., 2012). It was shown that a kneading block with a 90° staggered

angle increased residence time and torque in comparisson to the 30° and 60° blocks. This led

to the production of denser granules. However, it has been noted that there is a limit to how

many of these kneading elements can be placed in the system before there is excess barrel fill

leading to failure of the machinery due to screws jamming.

Barrel temperature

There are few studies that have focused on barrel temperature and how it affects the TSG

process. Fonteyne et al. (2013) found that barrel temperature significantly increases granule

size; increasing the barrel temperature leads to large and oversized granules. It was concluded

that this was due to an increase in solubility with increased temperature of the materials used

in the formulation, and therefore more bridge formation between particles (Fonteyne, et al.,

2013).

Table 2-3 A summary of key parameter settings and their effect on TSG.

Parameter	Key findings	References
Powder feed	- Problematic area if powder is cohesive and poorly flowing. - Inconsistency of feed is reflected in granule PSD e.g. 'poor' setting produce a bimodal distribution and large fraction of oversized granules. - Granule size decreases with higher powder feed rate.	Meier et al. (2016) Dhenge et al. (2011)
Screw speed	- Speeds between 200 and 400 rpm regularly used. - Screw speed shown to have little effect on granule properties. - Increase in tablet tensile strength found when screw speed and L/S increased. - Friability of granules is likely to be formulation dependent, however there is	Thompson (2015) Thompson & Sun (2010) Liu et al. (2017) Keleb et al. (2002) Vanhoorne et al. (2016)

Parameter	Key findings	References
	literature to suggest that increased screw speed increases granule friability.	
L/S ratio	• Reduced fines and increased oversized fraction with increasing L/S.	Liu et al. (2017)
Screw configuration	• Type of conveying element used (single or double flighted) not important. • Can be staggered at different angles which has an effect on conveyance, residence time, torque and barrel fill. • Kneading elements produce larger, denser and stronger granules. • 90° staggered angle increases residence time and torque in comparisson to the 30° and 60° blocks, producing denser granules.	Thompson (2015) Djuric et al. (2009) Thompson & Sun (2010) Lee et al. (2012)
Barrel temperature	• Barrel temperature slightly increases granule size but this may be due to an increase in solubility of materials at higher temperature.	Fonteyne et al. (2013)

2.5.2   Material and formulation parameters

The influence of L/S ratio

The L/S ratio is the ratio of liquid and powder feed rates (kg/h) within the TSG and has been widely studied in previous literature. As previously discussed, the addition of kneading blocks and a reduction in screw speed reduce residence time; an increase in L/S ratio also increases residence time due to change in mass and consistency of the material (Dhenge, et al., 2010). It was found that a L/S ratio of 0.4 gave monomodal size distribution for a formulation containing lactose, microcrystalline cellulose, croscarmellose sodium and hydroxypropyl

cellulose with water as a granulation liquid. Below a L/S ratio of 0.4 there is bimodal distribution suggesting that there is not enough binder present to form sufficient granules. The higher L/S ratio also produced the smallest d_{50}. However, the data is distorted due to the granules formed at lower L/S ratios having an elongated shape and a rougher surface. The authors conclude that granules produced at lower liquid fractions contained less liquid and therefore formed fewer liquid bridges. The more spherical shape of granules produced at higher L/S ratio is due to the availability of more liquid bridges being formed. Previous studies have consistently found that increasing L/S ratio results in an increase in granule size (Keleb, et al., 2002; Djuric, et al., 2009; Dhenge, et al., 2010; Lee, et al., 2012).

The influence of binder choice

As discussed in Section 2.3 the initial stage of granulation, nucleation, involves wetting of the powder bed and has a large influence on the final properties of granules. During the addition of liquid to the powder bed, liquid bridges are formed giving a mechanical strength to the granules within the TSG barrel. A binder powder can be dissolved in a liquid to produce a viscous granulation liquid which can produce stronger granules than those produced with water alone. Dhenge, et al. (2012(a)) found that adding varying amounts of hydroxypropyl cellulose (HPC) in water to lactose within the TSG process produced granules with different properties. As HPC concentration was increased, torque, residence time, granule size and granule strength increased. These results were in agreement with those found by Keleb, et al. (2002), where increasing the concentration of PVP in the liquid addition had the same effects on granule properties.

The influence of powder properties

Due to the wide range of powder properties within formulations that are used within TSG there are few studies that have investigated the effects of changing this input alone. Each material will require different L/S ratios to provide granules with the required properties. As a result, previous literature focuses on process influences rather than differences caused directly by the materials used and the role they play in final granule attributes. Previous studies have used common pharmaceutical excipients such as α-lactose monohydrate (Keleb, et al., 2002; Djuric, et al., 2009; Thompson & Sun, 2010; Kumar, et al., 2016), microcrystalline

cellulose (Tu, et al., 2013) or a mixture of both (Dhenge, et al., 2012(b); Dhenge, et al., 2013; Lee, et al., 2012).

An investigation into improved tabletability after the moisture-induced polymorphic transition of δ-mannitol to β-mannitol during the TSG process was carried out by Vanhoorne, et al. (2016). The authors succesfully carried out the transition and showed an increase in tabletability in comparison to those produced from β-mannitol as a starting material. It is important to note the possibility of materials undergoing structural changes as a result of the process enviroment. Although in this circumstance the changes resulted in a positive response, it may be possible for any changes to have a negative effect on the final tablet.

El Hagrasy, et al. (2013) used a formulation composed of lactose, MCC, HPC and croscarmellose sodium and varied the feed particle size using three grades of lactose. The authors noted that the TSG process was robust, showing that all three grades displayed similar growth behaviour. The granule d_{50} remained similar for all three grades at low L/S ratios but above a L/S ratio of 0.35 the formulation containing the largest particle size demostrated rapid growth and a larger granule d_{50}. An increase in granule d_{50} with increasing particle size was also noted by Fonteyne, et al. (2013), where differing particle sizes of theophylline were studied.

2.6   Powder and granule characterisation

It is essential to characterise the mechanical properties of materials as they play an important role in powder flow and compaction and the true areas of contact between particles. In this section the properties of powders and granules that can contribute to the TSG and tableting

processes are discussed, including shape, size, internal structure, density, flowability, compactibility and compressibility.

2.6.1 Shape

The shape of powders and granules is an important property that influences processing techniques and final tableting. Wong and Pilpel (1990) found that for materials that consolidate by plastic deformation, there is a large increase in compressibility when going from regular to irregular particle shapes. This may be due to more effective packing of regular shaped particles, therefore achieving a lower initial voidage and appearing less compressible. Flowability was improved with spherical paracetamol particles when compared to those that were needle-shaped (Kaerger, et al., 2004). Powders are produced in a wide range of ways and these manufacturing processes will result in different particle shapes, much like various granulation techniques will result in a range of granule shapes. For example, Garekani, et al., (2001) observed that ibuprofen crystallised from different solvents showed different size and shape. Particles that were produced from methanol and ethanol were plate-shaped resulting in better flow properties than those produced from hexane that were needle-shaped. Although particle shape can be assessed using 3D methods such as x-ray computer tomography, it can be difficult to ensure that the data obtained is reliable and representative of the sample (Seville & Wu, 2015). Therefore, 2D shape analysis has been used in this thesis. 2D shape analysis requires a projected image of a particle in a 2D plane, which is then measured in pixels (Seville & Wu, 2015). Feret dimensions are used in shape analysis as length measurements and can be defined as the distance between two tangents to the contour of

the particle in a specified direction. The most commonly used Feret lengths are maximum Feret length, l_{max} and minimum Feret length, l_{min} (Figure 2-8). From these measurements, a number of shape factors can be defined (Table 2-4).
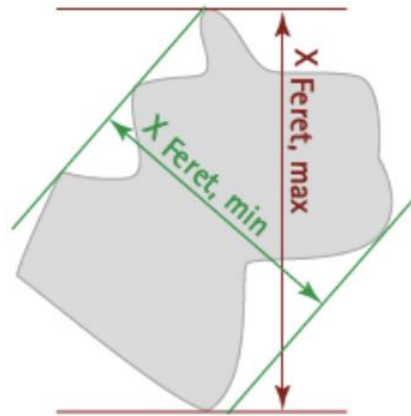
Figure 2-8 Commonly used Feret lengths demonstrated on a single particle (Sympatec, 2021).

Table 2-4 Details of shape factors (Litster, 2016)

Shape factor	Formula	Description
Aspect ratio, S_A	$$S_A = \frac{l_{min}}{l_{max}}$$	Indicates the degree of elongation. The lower the value, the more elongated the particle.
Roundness, S_R	$$S_R = \frac{4\pi A'}{P_l{}^2}$$	where P_l is the total length of the outline surrounding the projection of the particle determined in pixels and A is the total number of pixels in a particle image. For a perfect sphere S_R is equal to 1.
Sphericity, S_S	$$S_S = \frac{P_c}{P_l} = \frac{2\sqrt{\pi A'}}{P_l} = \sqrt{S_R}$$	The ratio of the perimeter of the equivalent circle, P_c, to the perimeter of the projection of the particle. For a spherical particle $S_S=1$.

Shape factor	Formula	Description
Convexity, S_C	$$S_C = \frac{A'}{A_h}$$	where A_h is the area of the circumscribed convex hull. If there are no concave features S_C is equal to 1.

Image analysis with a high level of manual operation for sample preparation, measurement and data analysis is time consuming and the number of particles analysed is relatively small (Yu & Hancock, 2008). With the advent of high-speed digital cameras there has been the ability to develop automated image analysis to capture 2D images of samples via either stationary image analysis (SIA) or dynamic image analysis (DIA) . For SIA, the sample is present as a thin layer on a glass slide and images of particles are captured using a microscope. The main disadvantage of this method is that the number of particles being assessed is limited to the number that fit to the size of the slide. However, DIA allows the capture of images of particles that are in motion, allowing for a much higher number of particles to be assessed. According to ISO standard 14488 (2007), to ensure the accuracy and reliability of measured data, the number of calculated particles should be above 2,000,000 and an optical concentration of 0.5-1% per measurement. The QicPic dynamic image analysis system (Sympatec Inc, Germany) uses a fast-moving airstream to disperse particles and move them down a tube past a high-speed digital camera with synchronized light source to obtain images.

2.6.2 Size

Particle size distribution (PSD) plays an important role on the compaction process and final tablet properties (Roberts & Rowe, 1986). The sieving technique is a simple way of determining the PSD of a material. The method is based on the size of a particle that can pass through a mesh with openings of a known size. This technique is most commonly performed on dry material. However, a wet sieving method can also be used. The system is composed of a stack of sieves with mesh sizes getting progressively smaller from top to bottom. The stack is placed on a vibrating plate which allows the particles to distribute throughout the stack depending on their size. Each sieve is weighed, post-vibration, to determine the mass of particles as a proportion of the total that are present in each size portion (Retsch, 2015). Excessive vibration can cause the breakage of fragile particles, leading to an error in results. However, if care is taken, the technique can be non-destructive allowing for further use of the tested material (Seem, 2015).

Light scattering techniques use a small sample size which is illuminated by a laser or other light source and the scattered light is collected and converted to a voltage pulse. These pulses are analysed using different amplitudes of peaks to find the number of particles present in a measurement range to obtain a particle size distribution (Malvern Panalytical, 2022). Microscopy is an example of a static method where the particles are stationary. Laser diffraction measures particle size distributions of a sample that is dispersed in a liquid or gas. The angular variation in intensity of light scattered from a laser beam passing through the sample is measured. Small particles scatter light at large angles relative to the laser beam and

the opposite is true for large particles (Schiano, 2017). Laser diffraction is a technique that is simple to use and has better resolution than traditional sieve analysis techniques.

2.6.3   Density

Density is described as the ratio between mass and volume and three definitions are used when characterising powders:

I.   True density,

II.   Bulk density, and

III.   Tapped density.

True density, or absolute density, is an intrinsic property of a material which is independent of material packing and can be defined as the mass of the particle divided by its volume, excluding pores. Gas pycnometry is the most commonly used technique due to its ease of use and ability to be fully automated. Helium is the gas of choice for the method because it can penetrate into very small pores. Hygroscopic materials have shown a difference in true density values across previous research due to changes in moisture during the course of the measurement (Sun, 2004). Sun (2004) recognised this discrepancy and proposed a method using the modified Heckel equation proposed by Kuentz and Leuenberger (1999) (Equation 2-3).

$$P = \frac{1}{C''}\left[(1 - \varepsilon_c) - \frac{\rho_{tablet}}{\rho_{true}} - \varepsilon_c ln\left[\frac{1 - \left(\frac{\rho_{tablet}}{\rho_{true}}\right)}{\varepsilon_c}\right]\right] \qquad\qquad \textit{Equation 2-3}$$

where P is the compaction pressure, C'' is a constant indicating the deformability of the powder, ε_c is the material critical porosity which indicates a critical state where the powder mass starts to gain some rigidity or strength, ρ_{tablet} is tablet density and ρ_{true} is the true density of the powder. The authors found higher values for true density in water-containing powders when measured by helium pycnometry in comparison to the calculated values. However, the samples used were vacuumed to remove surface moisture before testing, vastly changing the moisture and expected true density. The helium pycnometer performs the test in a closed chamber, therefore if the test is run within a minimal amount of time between taking the powder from its controlled storage conditions and placing in the sealed chamber, minimal changes should be observed. This was also confirmed by an investigation into the accuracy of a helium pycnometer by Viana, et al. (2002).

The *bulk density* of a powder is the ratio of the mass of an untapped powder sample to its volume, therefore taking the interparticulate void volume into account (EDQM, Council of Europe, 2014). The measurement is often difficult to reproduce due to even a slight disturbance in the powder bed resulting in a change in packing. The most common method of measurement is measuring the volume of a known powder mass according to the European Pharmacopoeia (EDQM, Council of Europe, 2014).

The *tapped density* is measured by increasing the bulk density of the powder by mechanically tapping the sample and is changed by the total number and amplitude of the taps during the experiment. As with the measurements for bulk density there is a standard procedure from the European Pharmacopoeia to minimise variation when testing across a range of materials (EDQM, Council of Europe, 2014). Bulk and tapped density values can be used to estimate

flowability of particulate materials. The Carr's Index (or Compressibility Index) (Equation 2-4) and Hausner Ratio (Equation 2-5) are used to predict the flow properties of particulate products based on the bulk and tapped density values (Table 2-5) (Seville & Wu, 2015).

$$CI = \frac{(\rho_{tap} - \rho_{bulk})}{\rho_{tap}} x100 \qquad \textit{Equation 2-4}$$

$$H = \frac{\rho_{tap}}{\rho_{bulk}} \qquad \textit{Equation 2-5}$$

where ρ_b and ρ_{tap} are the bulk and tapped densities respectively. In a free-flowing powder, interparticulate interactions are less significant and therefore the bulk and tapped densities will be closer in value. For poorly flowing materials, there are greater interparticulate interactions and a larger difference between bulk and tapped densities.

Table 2-5 Flowability predictions based on Carr's Index and Hausner Ratio (Seville & Wu, 2015).

Flowability prediction	Carr's Index (%)	Hausner Ratio
Excellent	10	1.00-1.11
Good	11-15	1.12-1.18
Fair	16-20	1.19-1.25
Passable	21-25	1.26-1.34
Poor	26-31	1.35-1.45
Very poor	32-37	1.46-1.59
Very, very poor	>38	>1.6

Sørensen, et al. (2005) identified that bulk and tapped density measurements carried out in accordance with the European Pharmacopoiea are very material consuming; minimum samples of 100 g are required. This presents a problem if expensive pharmaceuticals are being tested, where only a few grams may be available. Volume determinations are also made visually which presents a major source of error within the procedure.

2.6.4 Flowability

Flowability can be defined as the propensity of powders to flow under given circumstances and can be used to predict the compression ability of a powder (Conceição, et al., 2014). It is important when considering applications such as hopper design and die filling to ensure uniform flow properties of the powder to reduce segregation and blockages (Pitt & Sinka, 2001). There are a number of methods that can be used to characterise flowability, one of the most common being the uniaxial compression test and Jenike method (Jenike, 1964). Figure 2-9 shows a bulk solid being consolidated under a stress (σ_1) where there is a rearrangement of particles and collapsing of the voids within the bulk solid. After consolidation, the bulk solid is relieved of consolidation stress and the hollow cylinder is removed. Upon vertical compressive stress of the bulk solid, the specimen will fail at a certain stress, the unconfined yield stress (σ_c) (Schulze, 2010).
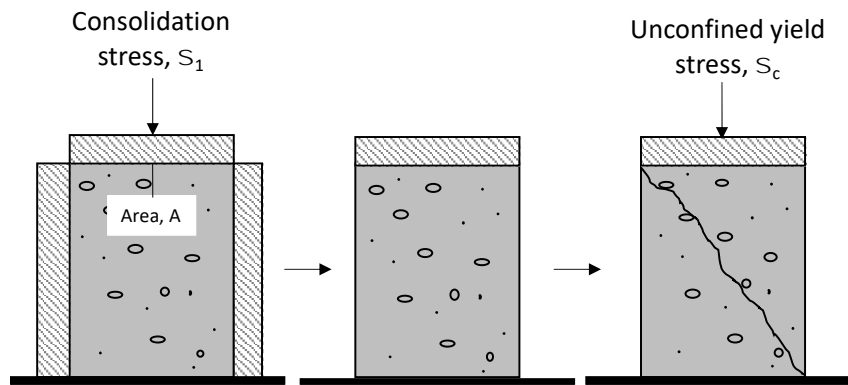
Figure 2-9 A uniaxial compression test showing unconfined yield stress (σ_c). Adapted from Schulze (2010).

A shear test procedure using a Schulze ring shear tester directly measures the yield limit of a consolidated bulk solid or yield locus. Firstly, a bulk solid is loaded vertically by a normal stress or pre-shear, σ_{pre}, then an increasing horizontal shear stress, τ, is applied until it reaches a maximum constant value (τ_{pre}) and steady state flow is achieved. Following this, the shear stress, τ, is reduced to zero and then a normal stress is applied ($\sigma' < \sigma_{pre}$), shear stress is then gradually increased until to a second failure value, τ'. By repeating these steps (including the pre-shear), a plot of failure shear stress, τ', versus normal stress, σ', can be plotted and used to calculate flow function, *ffc*, according to Equation 2-6.

Equation 2-6

$$ff_c = \frac{\sigma_1}{\sigma_c}$$

where σ_1 is the major principal compressive stress and σ_c is the unconfined yield strength. The larger the value of *ffc*, the more freely the bulk solid flows as shown in Figure 2-10 (Schulze, 2010). Figure 2-11 illustrates the values of σ_c, σ_1, effective angle of internal friction (δ_e) and flow function coefficient (ffc) (Schulze, 2010). These values are determined through the

application of two Mohr stress circles that are drawn tangent to the derived yield locus. The first circle passes through the origin and gives σ_c, the unconfined yield stress, while the second passes through the pre-shear point and gives the major principal stress corresponding to that shear state.
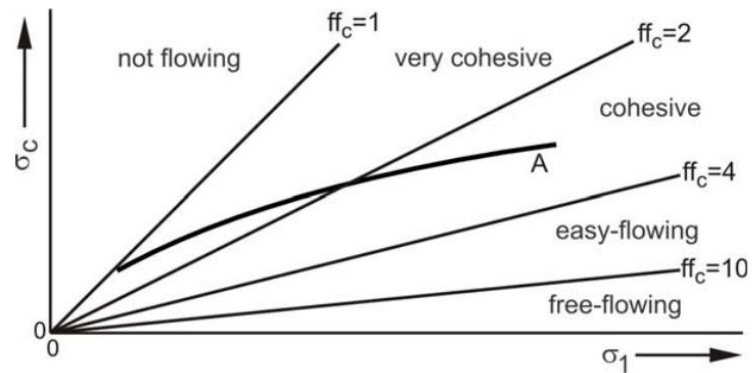
Figure 2-10 Flow function and lines of constant flowability (Schulze, 2010).
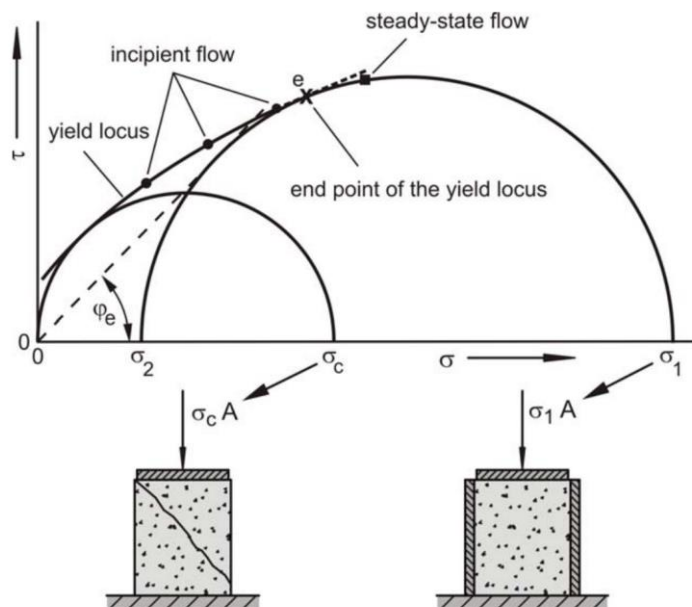
Figure 2-11 An example of a yield locus test and powder flow properties obtained (Schulze, 2010).

Flowability can be influenced by particle shape. Garekani, et al. (2001) crystallized ibuprofen in various solvents to produce differing particle shapes. Crystallization from methanol and ethanol provided lath/plate-shaped particles with improved flow properties over needle-shaped particles produced from hexane. Previous studies have found that flowability is also affected by particle size distribution. For powders with a narrow size distribution, the flowability increases with increasing particle size (Liu, et al., 2008). This was explained by a reduction in surface area for larger particles, reducing the area available for cohesive forces between particles. Liu, et al. (2008) found that adding magnesium stearate to ibuprofen increased the powder flow function and reduced the internal friction angle.

There are other experimental methods that can be used to measure flowability, however they focus on differing properties to that of the Schulze shear cell. For example, the powder rheometer which measures a powders resistance to flow by moving a rotating blade downwards through the powder bed to establish a flow pattern. The resistance experienced by the blade represents the difficulty of the relative particle movement, or bulk flow properties (Freeman Technology, Undated). A rotating drum can also be used to analyse granular flow (Granutools, Undated). A transparent cylinder is half-filled with a sample of powder and rotates around its axis. A camera takes multiple snapshots during the rotation and they can analysed to give measurements for the cohesive index and flowing angle per speed (Granutools, Undated). This method uses the characteristics of a powder as it cascades upon istself upon rotation to quantify its flowability and cohesion. Although both the powder rhemometry and rotating drum methods appear to be interesting and would warrant future exploration, it was decided that the Schulze shear cell would be used for the current study

because it has been used in simialr studies (Pitt & Sinka, 2001; Liu, et al., 2008; Conceição, et al., 2014; Schiano 2017), allowing for comparison against previous results.

2.7 Tableting characteristics

Compaction properties of pharmaceutical materials are assessed based on tabletability, compressibility and compactibility. This section explores the methods used to investigate these characteristics and the underlying material properties that change compaction properties in terms of powder plasticity and bonding strength.

2.7.1 Tablet compression

During the tableting process, the volume of the powder or granule bed is decreased with applied compression pressure. As the particles are forced into close proximity, inter-particle bonds are formed, thus producing a compact. The stages involved in compression are as follows:

    I.   Particle rearrangement

   II.   Deformation of the material at contact points

  III.   Elastic deformation (reversible)

  IV.   Irreversible deformation which may be via plastic deformation or brittle fracture

   V.   Formation of interparticulate bonds

Particle rearrangement occurs under low compression pressures and the powder bed is rearranged to a closely packed structure. Once there is no further possibility of rearrangement deformation of the material occurs. The deformation of the material is dependent on the

consolidation mechanism and the dynamics of the consolidation process (Amidon, et al., 2017). For example, brittle materials consolidate predominately via fragmentation under compression, whereas plastic materials deform via plastic flow. MCC and starch are examples of plastically deforming materials, whereas lactose and calcium phosphate are examples of materials that undergo brittle fracture. During elastic deformation, any change in shape caused by an applied stress is reversible, therefore the particle will return to its original shape on removal of the applied stress. The elastic properties of a material can be understood by the attractive and repulsive forces between atoms and molecules as elastic strain results from a change in intermolecular spacing (Amidon, et al., 2017). Plastic deformation results in a permanent structural change in the material due to the applied stress. The large areas of contact can remain on decompression, therefore forming strong compacts. Brittle or ductile fracture occurs when there is separation of a body into two or more parts. Brittle fracture is when there is rapid propagation of a crack throughout a specimen. Ductile fracture is described as extensive plastic deformation followed by fracture though is not commonly observed in pharmaceutical materials (Amidon, et al., 2017). Viscoelasticity is a time-dependent property of the stress-strain relationship. Amidon, et al. (2017) states that higher compaction forces are required to produce a tablet with a given strength in the case of rapid compaction speed. It is important to keep in mind that all materials demostrate a degree of elastic, plastic, brittle and viscoelastic behaviour.

2.7.2   Tabletability

Joiris, et al. (1998) define tabletability as the capacity of a powdered material to be transformed into a tablet of specified strength under the effect of compression pressure. A diametrical compression test is regularly used to test the strength of tablets. However, the breaking force needs to be converted to take into consideration the shape and dimension of the tablet.

A tabletability profile is presented as a plot of tensile strength versus compaction pressure (Figure 2-12). The tabletability profile shows the tablet in three different stages. Firstly, at low compaction pressures, the tablet does not form a coherent dosage form. Previous literature states that generally, a tensile strength greater than 1.7 MPa will be acceptable to ensure a tablet that is strong enough to withstand processing and distribution. However, tensile strengths above 2 MPa should be targeted (Pitt, et al., 2015) and this is indicated within Figure 2-12. The tabletability profile presented in Figure 2-12 is an example only, this does not represent a curve produced by any specific material, it is for visualisation purposes only. During the second stage, there is an increase in tablet tensile strength with increasing compaction pressure until the third stage is reached where no additional tablet strength can be achieved even with additional compaction pressure. An upper limit of tablet tensile strength should also be considered, 'the stronger, the better' should not be assumed. Biopharmaceutical aspects of tablet design should be taken into account when designing a tablet, where a tablet with a higher tensile strength will potentially provide slower dissolution (Odeku & Itiola, 2003).
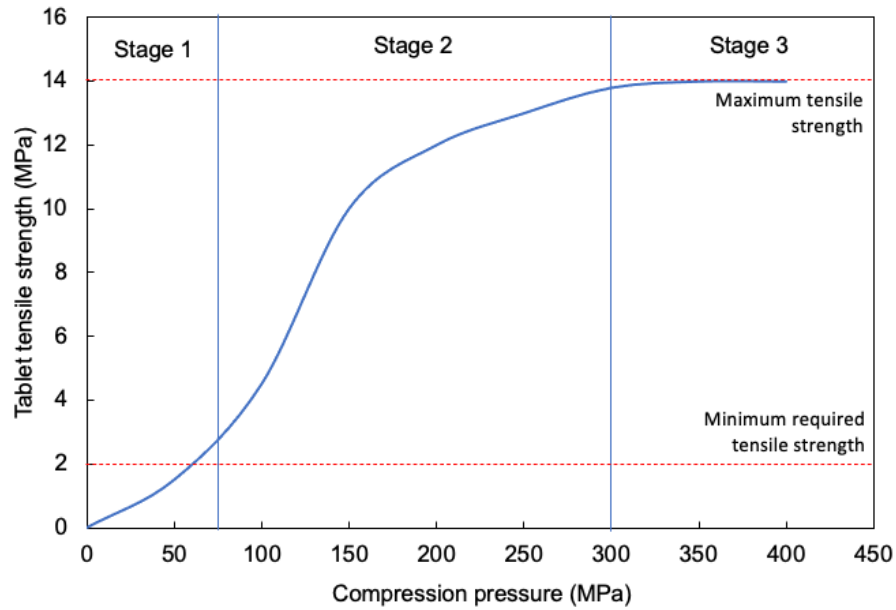
Figure 2-12 An example tabletability profile showing the three stages of compaction with minimum required and maximum tablet tensile strength.

2.7.3 Compressibility

As the pressure acting on a powder bed increases, the density of the powder also increases resulting in a decrease in porosity (Sun, 2008). The change in porosity of the powder bed under pressure is described as the compressibility. Rather than one process, the compression of a powder bed is described as a sequence of stages as shown in Figure 2-13.
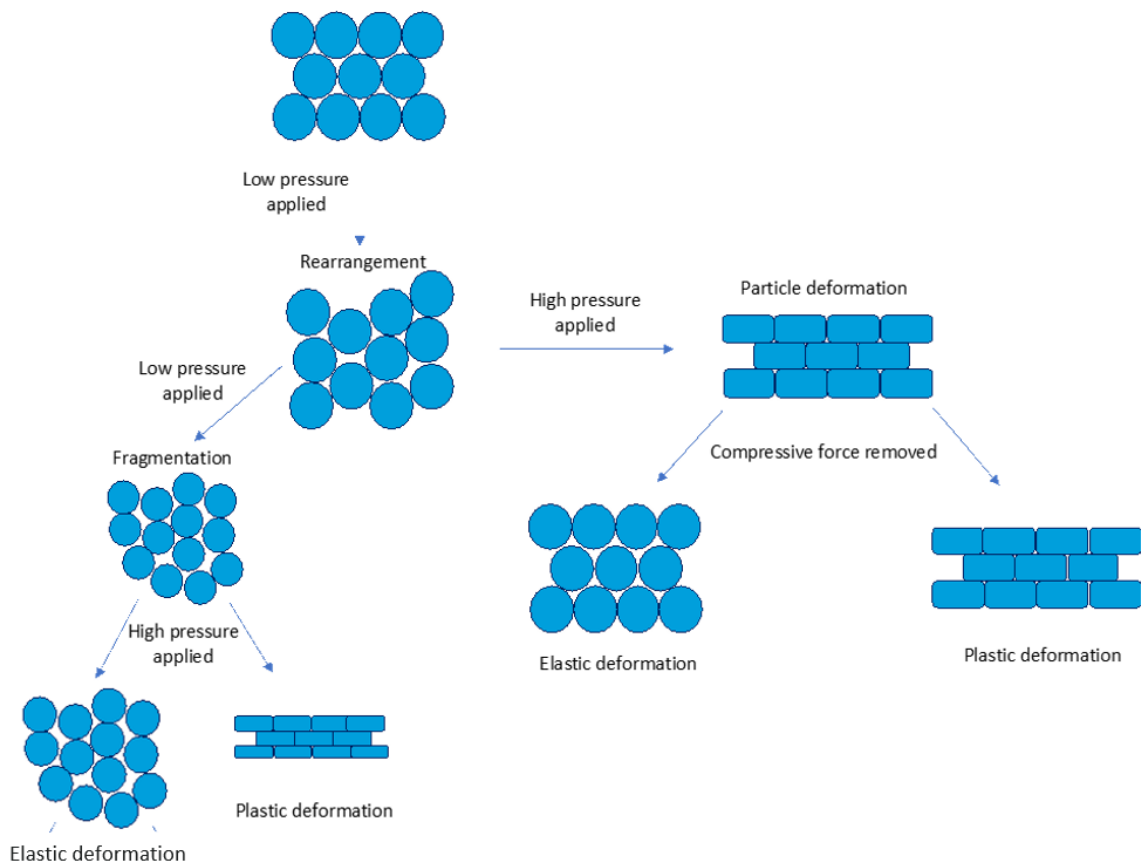
Figure 2-13 The stages of compression of a powder bed, adapted from Aulton & Taylor (2013).

Particles change shape temporarily by elastic deformation and permanently by plastic deformation. Alternatively, they may firstly undergo fragmentation to smaller particles which fill voids in the powder bed and further increase its density before undergoing deformation with further applied pressure. Fragmentation results in an increase in particle surface area, therefore producing a greater contact area for bonds to be formed. The same increase in surface area is seen for plastic deformation where the contact area between particles is increased where they were previously separated. A number of methods have been adopted

in previous literature to investigate powder behaviour under compression such as Heckel (1961), Kawakita (1970) and Adams, et al. (1994).

The Heckel equation was derived assuming that particles will undergo plastic deformation with the application of pressure. The volume reduction of a powder bed obeys first-order kinetics where the "reactants" are the pores, as shown in Equation 2-7 (Heckel, 1961). Equation 2-7 can be integrated with ε equal to zero (ε_0) at zero pressure to give Equation 2-9. It can then be defined that D is equal to *(1-ε)* and A is equal to $ln\frac{1}{\varepsilon_0}$ to make it possible for Equation 2-8 to be rearranged to give Equation 2-9.

$$\frac{d\varepsilon}{dP} = -k\varepsilon \qquad\qquad \textit{Equation 2-7}$$

$$\ln\left(\frac{1}{\varepsilon}\right) = \ln\frac{1}{\varepsilon_0} + kP \qquad\qquad \textit{Equation 2-8}$$

$$\ln\left(\frac{1}{1-D}\right) = kP + A \qquad\qquad \textit{Equation 2-9}$$

where ε is porosity, P is pressure, D is equal to the solid fraction and the constant, k, describes the influence of pressure in increasing the density of the tablet and is known as the Heckel parameter (Sun & Grant, 2001). The reciprocal of k represents yield pressure, P_y (Hersey & Rees, 1971). The dimensionless constant, A, is related to the bulk density of the powder upon initial filling and particle rearrangement and fracture upon increasing pressure. When P=0 and ε=ε_0, *A will be equal to* $-\ln(\varepsilon_0)$, however, the Heckel model is not obeyed uniformly over the

whole curve so this extrapolation is not valid. Therefore, the equation does not refer to the actual initial porosity, but the porosity after some initial rearrangement before particles start to deform or undergo fracture.

The Heckel plot is divided into three regions describing the different stages of compaction (Figure 2-14). Region I is an area of low compaction pressure and therefore the main mechanism of volume reduction is particle rearrangement. Region II is dominated by plastic deformation of the powder bed and is often a linear region. The constant, k, is equal to the slope of this region. Region III shows an elastic region, deformation that recovers after the compaction pressure has been removed from the powder bed (Sun & Grant, 2001).
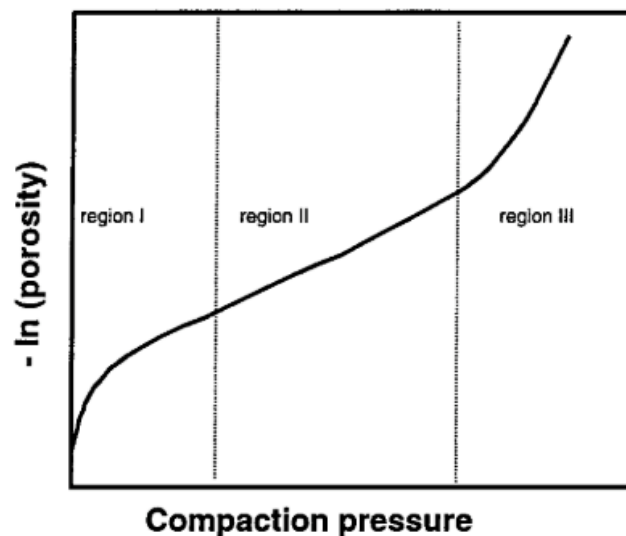
Figure 2-14 A Heckel plot with three regions of compaction, these are discussed in the text (Sun & Grant, 2001).

Data can be collected from the 'in-die', or the 'out-of-die' method. A reliable value for yield pressure should come from 'out-of-die' measurements because elastic deformation contributes to the densification of powder under pressure, therefore affecting tablet porosity

65

for the 'in-die' method (Sun & Grant, 2001). The methodology used for data collection when comparing Heckel analyses should be considered. Several parameters and their effect on mean yield pressure during Heckel modelling have been shown to influence results (Tarlier, et al., 2018). Die size, die filling mode, compaction speed, particle size distribution, dwell time and sensibility of true density have previously been shown to influence the determination of Heckel modelling (Tarlier, et al., 2018).

The use of a modified Walker equation is considered more reproducible. The Heckel model has received criticism regarding accuracy and robustness (Ilić, et al., 2013). The Walker model (Walker, 1923) is an empirically based model which relies on the change in tablet relative volume with changing compression pressure. Sonnergard (1999) modified the equation to replace relative volume with specific volume and is represented by Equation 2-10.

$$V' = -w' \times logP + V'_{sp}$$
<div align="right">*Equation 2-10*</div>

where V' is the specific volume of the tablet, w' is the Walker coefficient represented by the slope of a plot of *logP* against specific volume. The Walker coefficient expresses the volume reduction corresponding to one-decade change in pressure *P*. V'_{sp} is the specific volume at 1 MPa of pressure (Sonnergard, 1999).

An in-die or out-die approach can be used for both Heckel and Walker models. The in-die compressibility profile is attained by compressing one tablet only and data are obtained under load during compression. At this point the tablet has not returned the elastic energy it has stored within. Therefore, in-die coefficients include both the plasticity and elasticity of the

powder. For out-die methods, several tablets are required to be produced, therefore more material is required. Unlike in-die methods, the out-die approach describes only the plastic deformation of the material (Egart, et al., 2014). Ilić, et al. (2013) confirmed that the modified Walker model was found to be more robust and smaller differences between in-die and out-die methods were observed.

Kawakita and Ludde (1970) similarly investigated the relationship between applied pressure and volume reduction using Equation 2-11.

$$C = \frac{V_0 - V}{V_0} = \frac{abP}{1 + bP}$$

Equation 2-11

where *C* is the degree of volume reduction, V_0 is the initial volume of the sample, *V* is the volume of the sample at pressure *P*, *P* is the applied compaction pressure, *a* is a constant related to the initial powder porosity and b^{-1} is constant related to the yield stress of the particles. Equation 2-12 can be obtained by linearizing Equation 2-11.

$$\frac{P}{C} = \frac{P}{a} + \frac{1}{ab}$$

Equation 2-12

The slope from the linear portion of a plot of *P/C* as a function of *P* will give the reciprocal of *a* and the intercept on the x axis will give a value for *1/ab*. Conversely to the Heckel plot, the Kawakita plot takes the initial packing of the powder bed into account (V_0) and determining this value is a sensitive process. For example, the process of filling the compaction die may

lead to a degree of compaction by particle rearrangement, therefore lowering the value for the constant, b^{-1}, that is recorded.

The Adams model (Adams, et al., 1994) provides a further alternative to the Heckel and Kawakita models where the powder within the compression die is considered a collection of parallel columns that fail during upon the application of compaction pressure. Here, the relationship between pressure and volume during compression is described using Equation 2-13.

$$lnP = ln\frac{\tau_0}{\alpha} + \alpha\varepsilon_n + ln(1 - e^{-\alpha\varepsilon_n})$$
Equation 2-13

where P is compaction pressure, τ_0 is cohesive strength, α is the dimensionless coefficient of friction and ε_n is the natural strain defined as $ln(V_0/V)$. At high values of ε_n, the final term in Equation 2-13 approaches zero. Therefore, a plot of lnP versus ε_n can be used to find values for τ_0 and α from the gradient and intercept of the linear section of the equation. Adams, et al. (1994) identified a strong correlation between the Adams τ_0 and Kawakita b^{-1} parameters using experimental methods and concluded that both parameters give a reasonable indication of single particle yield stress (Figure 2-15).
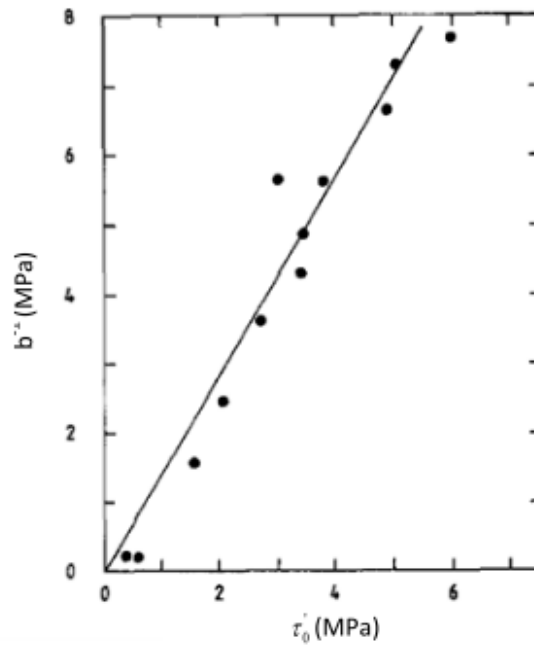
Figure 2-15 Comparing the Kawakita parameter b^{-1} with Adams parameter, τ_0 for quartz sand and polyvinylpyrrolidone binder agglomerates (Adams, et al., 1994).

Yap, et al. (2008) determined that the Kawakita model achieved a good fit to experimental data for all investigated powders. The values for the Adams parameter, τ_0, were of a similar magnitude to b^{-1}. The Heckel parameter, k, provided the worst correlation and were significantly greater in magnitude than both b^{-1} and τ_0.

2.7.4 Compactibility

Compactibility is the relationship between tablet tensile strength and porosity. In most circumstances, tensile strength decreases exponentially with increasing porosity (Sun, 2008). The Ryshkewitch equation (Equation 2-14) is commonly used to analyse this relationship (Ryshkewitch, 1953).

$$\sigma_t = \sigma_0 e^{-b'\varepsilon}$$

<div align="right">*Equation 2-14*</div>

where σ_t is the tablet tensile strength, σ_0 is the maximum tensile strength at zero tablet porosity and *b'* is an empirical constant.

Sun (2008) used a common batch of MCC to ensure that particle size distribution and particle morphology were constant whilst changing the moisture content of the powder by storing at a range of relative humidity. The author expected the bonding pattern of tablets of identical porosity to be similar for MCC containing different amounts of moisture. Therefore, tablet tensile strength at a common porosity was used to evaluate the effects of moisture on bonding strength per unit bonding area. Figure 2-16 shows that tablet tensile strength at a given porosity remains constant up to ~3.3% moisture (corresponding to monolayer coverage) but decreases linearly with increasing moisture. Sun concluded that any moisture present past the monolayer coverage reduces bonding strength and any water content below this does not significantly reduce the integrity of the hydrogen-bonding between MCC particles. Sun also shows that the constant, *b'* from Equation 2-14, relating to pore distribution changes with different moisture content. Therefore, *b* is affected by factors other than pore distribution.
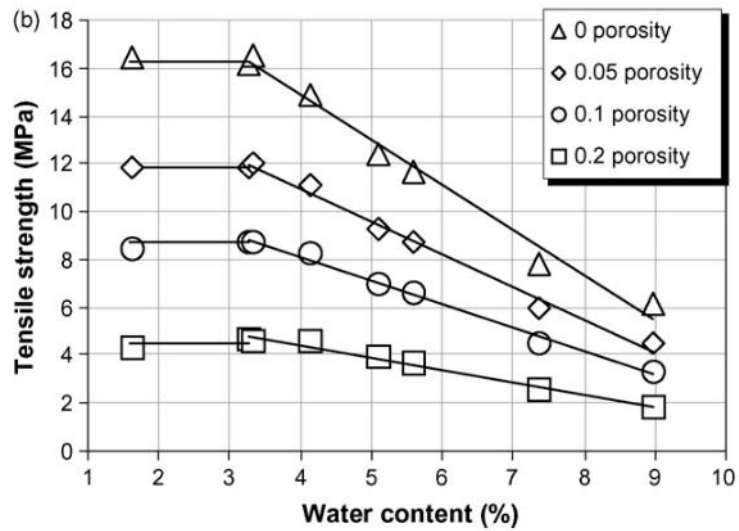
Figure 2-16 Tablet tensile strength at varying porosity as a function of water content (Sun, 2008).

Particle size was first found to be an important factor in final tablet tensile strength by Shotton and Ganderton (1961) who correlated tablet tensile strength and particle size in tablets produced with sodium chloride and hexamine. They observed three volume reduction mechanisms:

I.   Particle rearrangement,

II.   Deformation, and

III. Fragmentation.

For materials undergoing fragmentation, the particle size had a greater effect on tablet tensile strength than it did for those undergoing permanent deformation.

2.8 Tablet bonding mechanisms

2.8.1 Types of bonding mechanism

Particulate materials may be bonded via two main types of bonds. Firstly, primary bonds include ionic, covalent and metallic bonding. Secondly, weaker long-range attractive forces or intermolecular bonds can form. Tablets are most commonly held together by secondary bonds and the maximum achievable bonding force will depend on how many bonding mechanisms are present.

2.8.1.1 Primary bonds

The well-known C—C and C—H bond are examples of covalent bonds where atoms fill their outer shell by sharing pairs of outer electrons between both atomic nuclei. Metallic bonds occur when all atoms share all outer electrons and the resultant free electrons lead to electrical conductivity in metals (Houwink & De Decker, 1971).

2.8.1.2 Secondary bonds

Secondary bonds are responsible for weaker structures that easily undergo rupture, such as tablets. Van der Waals bonds are the result of interactions between various types of forces which occur due to the displacement of charge within electrically neutral atoms or groups of atoms in the following ways (Houwink & De Decker, 1971):

Permanent dipoles occur when a permanent magnet is formed. For this to happen the centres of gravity of the positive and negative charges cannot coincide. An example of a special dipole

is the hydrogen bond which is responsible for the association of molecules in water, alcohols and carboxylic acids. Hydrogen bonds are the strongest of the secondary bonds and form due to the interaction of OH groups (Houwink & De Decker, 1971).

Induced dipoles are generated in neutral molecules by permanent dipoles and may be permanent or alternating, depending on the inducing source.

Dispersion forces. As electrons move around positive nuclei, continuously changing dipoles are formed and, in turn, these have an inducing effect on neighbouring atoms which results in mutual attraction. Dispersion forces are the weakest of the van der Waals interactions, but often considered the most important because they are always present between materials and do not decrease with temperature (Mate, 2007).

2.8.2 Liquid and the bonding of solids

Van der Waals forces between solid surfaces are typically reduced in the presence of liquid. They may still be present, but more importance is placed on capillary or meniscus forces (Houwink & De Decker, 1971). The extent to which the van der Waals forces are reduced is dependent upon the layers of liquid molecules present between the separating distance of the two solids (Mate, 2007). For a hygroscopic material, such as MCC, the addition of water will involve liquid-solid interactions and therefore the effects of this water addition on the properties of the material may influence the process and final outcome of a dosage form. Sahputra, et al. (2019) investigated the influence of absorbed water on the physical properties of MCC using a molecular mechanics (MM) – molecular dynamics (MD) simulation method. It was demonstrated that the specific volume of MCC increases with moisture content and

simulations are in close agreement with experimental values. Figure 2-17 shows that energies of MCC decrease with increasing moisture due to the availability of more water molecules to change the material structure which is confirmed by the increase in specific volume. Sahputra, et al. (2019) state that the decreasing value for hydrogen bonding energy as moisture content increases is related to the breaking of some hydrogen bonds due to the additional space occupied by water molecules. With the addition of water, there is expansion of the MCC structure because polymer chains are less restricted leading to a reduction in hydrogen bonds. Torsional energy changes as a result in conformational variations in the MCC chains. The torsional energy reduces as the increase in water molecules present increase internal pressure and repel adjoining MCC chains, resulting in an overall increase in the volume of the material. The authors quote that the changes in hydrogen bonding and resultant changes in torsional energy as a function of moisture content are critical factors in the plasticisation of MCC by water.
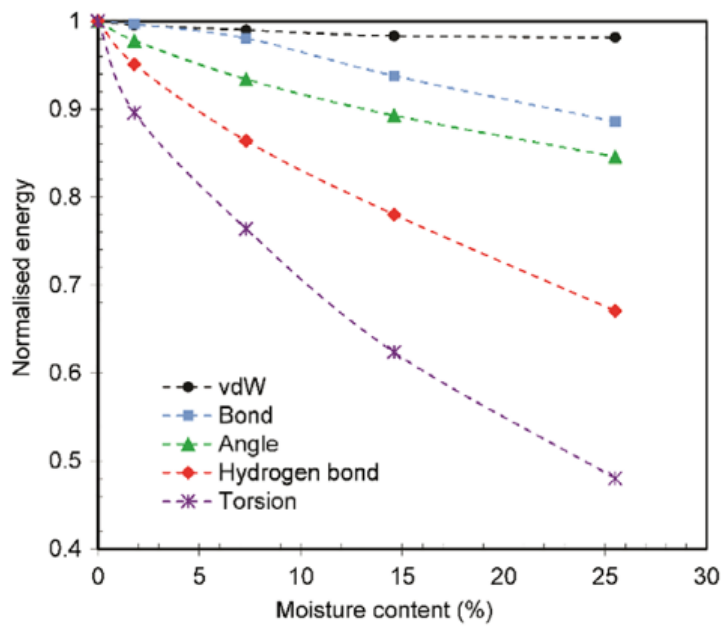
Figure 2-17 Normalized energy of MCC as a function of moisture content (Sahputra, et al., 2019).

In addition to the possibility of water creating an expansion of the material and therefore reduction in hydrogen bonding as discussed for MCC, it is also important to consider water that may become trapped in the spaces between particles. Water could be adsorbed onto the surface of a particle or absorbed within materials, having to find somewhere to move as a result of compression or get pulled into the material as a result of capillary condensation. The capillary pressure is the pressure associated with a curved surface of a liquid and can be positive or negative. If a liquid is present between two surfaces that have favourable surface energy, the liquid will have a negative capillary pressure and the surfaces of the particles will be pulled closer together (Figure 2-18) (Bocquet, et al., 1998). In the opposite situation, where liquid is present between two surfaces of unfavourable surface energy (e.g., two hydrophobic surfaces), a positive capillary pressure will force the two surfaces away from each other. This phenomenon is also reliant upon the quantity of water present. For example, if too little water

75

is present, there will be less changes of capillary bonding, however, too much water may flood

the spaces between particles and lead to particle-particle lubrication (You & Pun Wan, 2013).
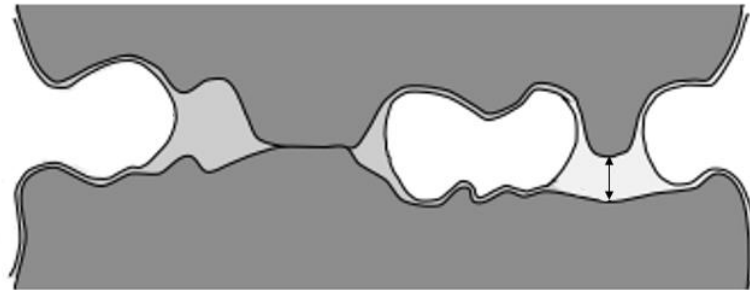
Figure 2-18 Demonstrating a negative capillary pressure between two surfaces of favourable surface energy. Adapted from (Bocquet, et al., 1998).

2.8.3   Surface area and bonding

The surface area over which bonding can take place is an important factor in determining a

final tablet strength. For a predominantly plastically deforming material, such as MCC, the

surface area will decrease as a function of compaction pressure as a result of deformation.

However, a brittle material, such as lactose, will undergo brittle fracture during compaction,

resulting in an increase in available surface area over which bonding can occur. The method

by which surface area is measured is discussed later in Section 3.4.7.

2.9   Summary

In order to improve the performance of tablets produced using pharmaceutical materials, it is

vital to gain an understanding of the physical properties of each material and the process by

which the tablet is manufactured. As described in previous sections, particle characteristics

such as shape, density, flowability and size can influence the resultant tablet product. This

thesis focuses on the study of compaction behaviour of pharmaceutical excipients as a result

of different processing steps and storage conditions with an aim to improve the potential to

predict tablet tensile strength and reduce future pre-formulation studies.

3 Experimental materials and method

3.1 Introduction

In this chapter the materials and the experimental methods used in the production of this thesis are discussed. Each technique that has been chosen is discussed and justified to ensure an understanding of each method.

3.2 Materials

For the purpose of this study, pharmaceutical excipient powders are considered. Excipients such as lactose and microcrystalline cellulose have been chosen due to their high use and relevance within pharmaceutical formulation (Keleb, et al., 2002; Djuric, et al., 2009; Thompson & Sun, 2010; Tu, et al., 2013; Kumar, et al., 2016). The chosen excipients were selected to give a range in mechanical properties and solubility in water. The study includes both plastically deforming and brittle materials along with both water soluble and insoluble materials to present a wide range of material characteristics.

3.2.1 Pharmaceutical excipient powders

Dicalcium Phosphate in the dihydrous form (DCPD) has excellent flow properties and low hygroscopicity, therefore, it is an excipient widely used for direct compression (Doldán, et al., 1995). However, due to variation in temperature and humidity it can lose its hydration water. It is a white, free-flowing, crystalline powder which is practically insoluble in water and alcohol (Eyjolfsson, 2015). DCPD used within this study is Di-Tab, unmilled (Innophos, UK).

Lactose is a white, odourless powder that is soluble in water. It is non-hygroscopic, crystalline and has high chemical stability. Lactose is commonly used as a diluent and filler in tablets and capsules. Lactose is available in a wide range of particle sizes and grades such as spray-dried, beta-anhydrous and alpha-anhydrous to allow it to be targeted for purpose. For example, a fine grade may be used for inhalation formulations and a larger particle size may be used within the food industry (DFE Pharma, Undated). Two types of lactose were used, firstly a spray-dried lactose monohydrate, Fast flo 316 (Foremost Farms, Clayton, USA) and secondly, a crystalline, milled lactose monohydrate, Pharmatose 200M (DFE Pharma, Goch, Germany). For the purpose of this study Pharmatose 200M and Fast flo 316 will often be referred to as P200M and FF316 respectively.

Mannitol is a polyol isomer of sorbitol and commonly used within the pharmaceutical and food industries (Hiremath, et al., 2019). It has a sweet taste; therefore, it can be used within formulations designed to dissolve in the mouth to give a pleasant taste and cooling sensation to the consumer. It is partially insoluble in water and non-hygroscopic, however, can be used to enhance the dissolution of tablets, especially chewable tablet formulations. Mannitol is a white, odourless, crystalline powder. It is present in different polymorphic forms which have varying compression characteristics. A crystalline grade is generally used for wet granulation and a spray-dried form can be used for direct compression (Hiremath, et al., 2019). The mannitol grade used in this study is Pearlitol 160C and is a standard, crystalline grade (Roquette, UK).

Microcrystalline cellulose (MCC) is a white, free-flowing, hygroscopic, tasteless and odourless powder. It is produced by acid hydrolysis of cellulose and the degree of polymerization is

defined by size of crystalline domains known as microfibrils (Figure 3-1) (Sun, 2008). Previous studies have suggested that the crystallinity of commercially available MCC was 60-80% (Rowe, et al., 1994). Spray drying of MCC can be controlled in order to change the particle size distribution and moisture content. The primary use of MCC within pharmaceutical formulation is as a binder or diluent. Owing to its free-flowing nature, it can also be used as a lubricant in tableting and can be processed via wet granulation or direct compression. In this study, MCC Avicel PH101 (FMC, Biopolymer, USA) was used.
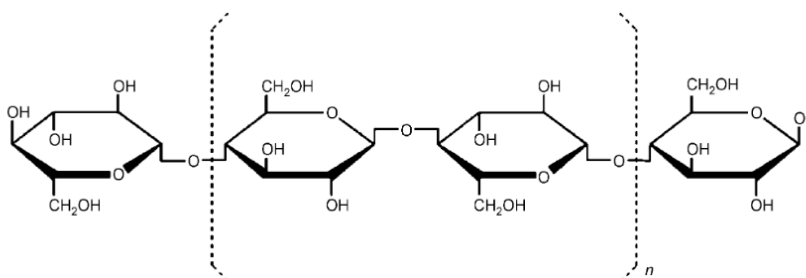
Figure 3-1 The chemical structure of MCC (Sun, 2008).

Starch is a white, free-flowing, fine granular powder which swells in cold water due to its hygroscopic nature (Eyjolfsson, 2015). Within this study, Starch 1500 (Colorcon Inc., Harleysville, USA) is used. It is a starch that has been previously gelatinized and dried to powder form. More specifically, Starch 1500 is a partially pregelatinized starch which has a mixture of properties of both native and fully gelatinized starches. Due to these properties, it can be used as both a binder and disintegrant within formulations that are wet granulated (Colorcon Inc., 2016).

Magnesium stearate is a commonly used lubricant (Hiremath, et al., 2019). It is relatively inexpensive, chemically stable and has a high melting point making it suitable for use in most

processes. Concentrations between 0.25% and 5% w/w in formulations have been used in previous studies (Paul & Sun, 2017; Koskela, et al., 2018). It has a capacity to form a hydrophobic layer around particles which leads to decreased tablet strength and dissolution rate (Hiremath, et al., 2019). Magnesium stearate used within this study was Ligamed MF-2-V (Peter Greven, Germany).

Table 3-1 Details of material properties used within the current study

Material	Brand name	Supplier	D50 (μm)	Bulk density (g/cm³)	References
Dicalcium phosphate dihydrous	Di-Tab	Innophos	180	0.87	Charoo (2020)
Lactose	Fast flo 316	Foremost Farms	150	0.50	Charoo (2020)
Lactose	Pharmatose 200M	DFE Pharma	35	0.59	Charoo (2020), DFE Pharma (2022)
Mannitol	Pearlitol 160C	Roquette	160	0.64	Charoo (2020), Roquette (2022)
Microcrystalline cellulose	Avicel PH101	FMC Biopolymer	50	0.26-0.31	Charoo (2020)
Starch	Starch 1500	Colorcon	65	0.61	Charoo (2020)
Magnesium stearate	Ligamed MF-2-V	Peter Greven	7-11	Not given	Charoo (2020), Peter Greven (2018)

3.3   Granule production by Twin Screw Granulation

Wet granulation was performed using a lab scale co-rotating twin screw extruder (Haake, Thermo Scientific, Germany) with screw diameter (D) of 16 mm and length to diameter ratio of 25:1. Powder was fed into the barrel at the base of the screws via a volumetric twin screw feeder (T20, K-Tron, Soder) at a speed of 2 kg/h. Granulation fluid (distilled water) was added through a single injection port positioned approximately 9 diameters length from the base of the screws via an 8-roller peristaltic pump (REGLO Digital, Ismatec, Switzerland). The output of the pump was regularly calibrated in order to ensure the flow rate was accurate according to the required liquid to solid ratio (L/S). There are four inlet points along the top of the barrel, the first being the powder inlet from the volumetric feeder and the next three being available for optional addition ports. The decision was made to use the second port (or 9 diameters length from the base) to allow for wetting near the start of the barrel length rather than water being added a short distance before the granule outlet. Changing water addition points were previously studied by Dhenghe et al. (2012(b)).

The temperature of the barrel was maintained at 21°C by circulating silicone oil via a refrigerated circulator through a jacket around the barrel of the TSE. Temperature has previously been shown to affect final granule characteristics due to increased solubility rate of the powder (Vercruysse, et al., 2012), therefore, to dismiss it as a variable from this study it was important to maintain it as a constant. A temperature of 21°C was chosen as it would be sustainable given the limitations of the equipment being used and it is below the melting point of any of the materials being used.

Mannitol and lactose (both Pharmatose and Fast flo 316 lactose) were granulated using a powder feed rate of 2 kg/h and screw speed of 400 rpm based on previous work carried out by Seem et al (2016). Preliminary tests were done to find the maximum L/S possible. At an L/S of 0.28, all materials were over-wetted and produced a paste which was unsuitable for characterisation for all the powders. Therefore, in the following experiments ratios of 0.11, 0.18 and 0.25 were used.

Twin screw elements can be configured in varying ways and based on previous studies by Seem (2017) that used the same lab-scale extruder. The configurations used consisted of either conveying only elements (C) or kneading elements (K), making up 1 or 2 kneading zones and are described in terms of ratio of length to diameter. Previous studies by Seem (2017) used one kneading zone after 18 conveying elements, however the current study also investigates the addition of a second kneading zone after 7 conveying elements. An example TSG set-up is shown in Figure 3-2. Each kneading zone consisted of four 60° forward kneading blocks. For the purpose of this study, when 2 kneading zones are referred to it is important to clarify that this is made up of 1 kneading zone immediately before the liquid injection port (pre-kneading section) and 1 kneading zone later along the barrel. A pre-kneading zone was inserted to investigate the extent of the effect of a kneading zone without the presence of binder.

Once the instrument was started, the equipment software (Polylab, Haake, Thermo Scientific, Germany) provided a live torque reading. This was used to ensure steady state had been reached after a few minutes before granules for further processing were collected from the outlet. After granules were collected they were transferred to large trays in to provide a

83

shallow granule bed (no deeper than 1.5 cm) for drying at room temperature for a minimum of 72 hours.

Figure 3-2 The screw configurations used within the study: conveying elements only (C), 1 kneading zone (1K) and 2 kneading zones (2K). The picture to the right shows a single 60° kneading zone.

3.4   Powder and granule characterisation

3.4.1   Powder conditioning

By storing materials at a range of relative humidity (RH) it is possible to investigate if there is any uptake of water by the material and if so, to what extent. Any differences in moisture content can then be used to find the variation in material characteristics due to this change. In experiments where materials were required to be conditioned before testing, they were placed in desiccator cabinets after being placed into petri dishes (Figure 3-3). Powders were left for 28 days at the required RH using a saturated salt solution as desiccant (Table 3-2) and mass was taken at 7-day intervals until no change in mass was observed to ensure equilibrium had been reached. Moisture content was assessed using a halogen moisture balance immediately before further experimentation (HC103, Mettler Toledo, Leicester, UK). The balance heated $2\,g \pm 0.5\,g$ of powder to $120\,°C$ for 20 minutes to ensure all moisture had been removed from the sample. Higher temperatures were not used to ensure the heating temperature was not above the melting point for any of the powders.
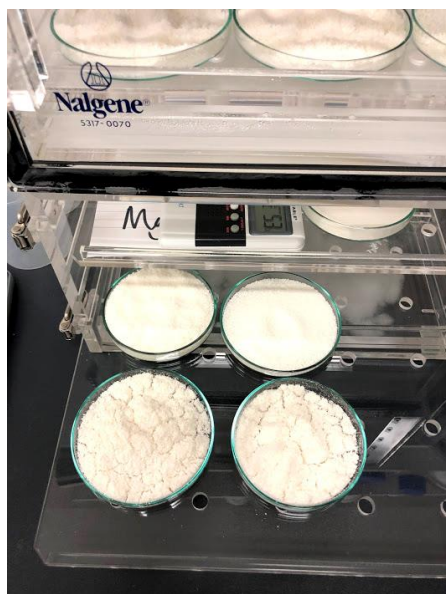
Figure 3-3 Material storage set-up for conditioning at various RH.

Table 3-2 Target relative humidity (RH) and corresponding desiccant material (Greenspan, 1976).

Desiccant	Target RH (%)
Caesium fluoride	3
Lithium chloride	11
Potassium acetate	22
Magnesium chloride	34
Potassium carbonate	43
Magnesium nitrate	60
Sodium chloride	79

The measured moisture content of each powder was validated by investigating their moisture sorption characteristics using DVS. Approximately 10 mg of powder was placed on an atmosphere-controlled microbalance (DVS Advantage, Surface Measurement Systems, Middlesex, UK). Each sample was dried on the balance using a stream of nitrogen gas to purge

until a stable weight was achieved. Samples were then subjected to a series of RH from 0% to 90% with a 10% increment. It was assumed that equilibrium was achieved when there was <0.5 µg weight increase in ten minutes at a given RH.

3.4.2 *Particle size distribution*

The particle size distribution of a material can have an impact on many aspects of the processing of a formulation. For example, content uniformity, flow properties, bulk density and compaction properties. Therefore, it is important to investigate the particle size distribution of each material and potentially relate this to some of the observed characteristics.

Particle size analysis was carried out for raw powders and granules using either vibratory sieving analysis (Fritsch Analysette 3 Pro, Idar-Oberstein, Germany), dynamic imaging (QicPic, Sympatec Inc., Germany) or laser diffraction (Malvern Mastersizer 2000, Malvern Instruments, UK). Nathier-Dufour, et al. (1993) assessed the differences between traditional sieving and laser diffraction and found that any discrepancies between the methods were attributable to shape factors which were dependent on the size fractions examined. Laser diffraction presented suitable accuracy when applied to products with a small range of particle size. However, sieve analysis can provide mass distributions over a wide range of size, which in the case of TSG where it would be expected to have a large span of particle size, sieving may be a more appropriate choice. Dynamic imaging and laser diffraction are rapid techniques and can be reported as a 'volume' distribution which is most appropriate for bulk material characterisation (Malvern Panalytical, 2022).

For sieving analysis, powders and granules were separated using a sieve series of 90, 180, 355, 710, 1400 and 2800 μm (ISO standard, every second number of fourth root of two series) at an amplitude of 5 mm for 10 minutes on a sieve shaker (Retsch VE 1000, Haan, Germany), to obtain size distribution data. This method was based on the USP-NF standard testing procedure (The United States Pharmacopeial Convention, 2012). The fraction of powder or granules retained on each sieve were weighed. The mass fraction X_i for a specific size range d_2 – d_1, is calculated as:

$$X_i = \frac{G_{21}}{G_{tot}}$$
Equation 3-1

where G_{21} is the mass of sample (g) in the size range $d_2 \sim d_1$ and G_{tot} is the total mass (g) used for each experiment. Granules less than 180 μm, 180-1400 μm and more than 1400 μm were defined as fines, usable and oversized granules respectively based on sizes most commonly used in industrial tableting. Although the sieve shaker method is well practiced and commonly used, it does not give such detailed results as other methods such as dynamic imaging and laser diffraction. Granules that are produced using only water as a binder may be easily broken up as a result of the sieve shaking process, even at low amplitudes and produce a higher quantity of fines than those found prior to sieving. Therefore, it may be appropriate to carry out another or additional method of particle sizing to ensure reliable results.

For QicPic dynamic imaging, approximately 3 g of material is fed into a funnel held 4 mm above a vibrating feeder (Vibri/L, Sympatec Inc., Germany) (Figure 3-4). This quantity is based on granulated material and the mass added before measurement is based on number of particles

that enter the system. By introducing 3 g of material and allowing a long dispersion time (3 minutes) it ensures a high number of particles are imaged. At least 1000 representative objects (i.e. particles in focus) were collected per measurement (Cardona, et al., 2018). The material is fed into the Gradis/L (Sympatec Inc., Germany) attachment at a constant rate for dynamic imaging. The experiment was run for 3 minutes at a constant pressure of 0.2 bar and data was collected and analysed by the computer software (Windox 5.0 software, Sympatec Inc., Germany). A dispersion pressure of 0.2 bar was chosen to ensure minimal attrition and granule breakage as a result of the experimental conditions. The diameter for which 10% of the particles are smaller, the median particle size and the diameter for which 90% of the particles are smaller are known as d_{10}, d_{50} and d_{90} respectively. The span, or breadth of distribution is calculated according to Equation 3-2.

$$Span = \frac{d_{90} - d_{10}}{d_{50}}$$

Equation 3-2

Figure 3-4 The QicPic system including Vibri/L and Gradis/L attachments (Sympatec GmbH, 2017).

Dynamic imaging offers the advantage of providing binary images of the particles assessed through the process. These images are used to calculate particle shape factors. However, they also provide a qualitative view of individual granules if required. This method has the disadvantage of not being able to distinguish between particles or granules that may have overlap in the chute when being imaged. A powder or granule should have suitable flowability to ensure minimal risk for overlap of particles upon imaging.

Laser diffraction (Malvern Mastersizer 2000, Malvern Instruments, UK) was used for particle size analysis of powders that were not suitably free flowing to ensure accurate results from dynamic image analysis. More details on the principle of laser diffraction are given in Section 2.6.2. The method was selected based on application notes from the manufacturer of the equipment (Malvern Instruments Worldwide, 2013). The wet dispersion method was selected with sunflower oil as the dispersant as some materials being investigated are water-soluble and sunflower oil is a non-polar carrier. Approximately 1 g of material was dispersed in 150 ml dispersant until there was between 10% and 20% obscuration. From the measurement of the particle size distribution, d10, d50 and d90 values were computed.

3.4.3   Particle shape

In addition to particle size distribution, particle shape can influence the physical properties of a material. Therefore, it is important to consider when characterising each material. By using QicPic dynamic imaging it is possible to gain particle shape factors at the same time as particle size analysis, therefore offering an advantage over laser diffraction.

Dynamic imaging and scanning electron microscopy (SEM) were used to perform shape characterisation of powders and granules. Image analysis using an SEM microscope (TM-1000, Hitachi, Japan) was carried out for each excipient powder at magnifications of x100, x400, x800, x1000 and x2500. Samples were sputter-coated with a thin layer (2 nm) of gold using a pumped coater (Quorum, Q150T, UK).

Shape analysis using QicPic (Sympatec Inc., Germany) is carried out by software (Windox 5.0, Sympatec Inc., Germany) during particle size distribution analysis. Shape factors sphericity (S_S), aspect ratio (S_A) and convexity (S_C) were also collected. A binary image of each frame analysed during a run through dynamic imaging can be viewed, giving a qualitative view of the particle size and shape distribution. An example of the binary images that can be viewed using the software is given in Figure 3-5.
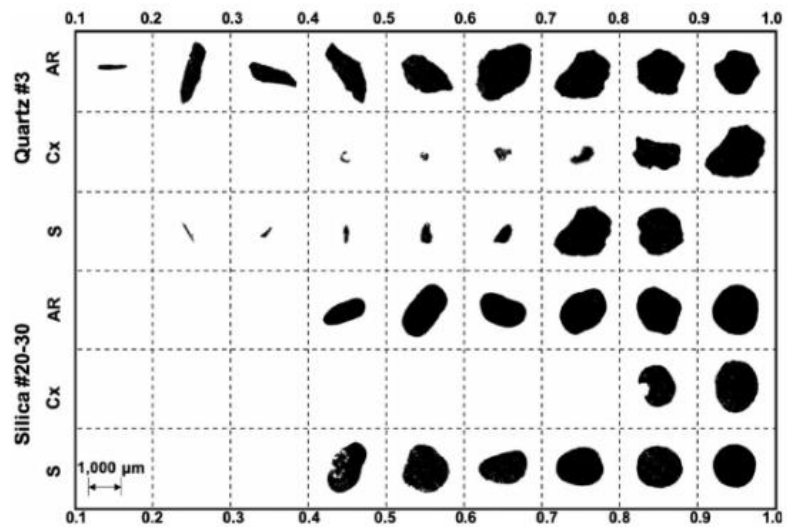
Figure 3-5 An example of particle shape detail that is given by the QicPic software. In this example silica and quartz samples were measured by Li & Iskander (2019).

91

3.4.4 Visualisation of granule internal structure

Micro X-ray computer tomography (uXRCT) (SkyScan 1172, Bruker, Belgium) was utilised to provide information on the internal structure of granules within the size range 180-1400 µm for each granulation set-up. A voltage of 34 kV and current of 37 mA without a sample filter was used. Each granule was scanned at a total rotation of 180° with a pixel resolution of 4000 x 2664 and 0.2° rotation between frames. All images were reconstructed using a filtered back-projection algorithm. The slice thickness selected was 35 µm. The voxel size is directly linked to the field of view and reconstructed with an isotropic voxel size of 10 µm. The scans were reconstructed into 3D images using NRecon software (SkyScan, Bruker, Belgium) and the centre horizontal 2D image was selected for each granule to produce a binary image. The binary image was then analysed using CTAn software (SkyScan, Bruker, Belgium) to calculate the total, open and closed pore volume. The total porosity is taken as the fraction of all void space in the total volume. The method used was based on that previously used by Lute et al. (2018) and developed according to the current software and instrumentation during method development.

XRCT is able to see internal structures at high resolution and has the added benefit of being non-destructive. An example of an application of XRCT is given in Figure 3-6, where the internal structure of dental resin can be viewed.
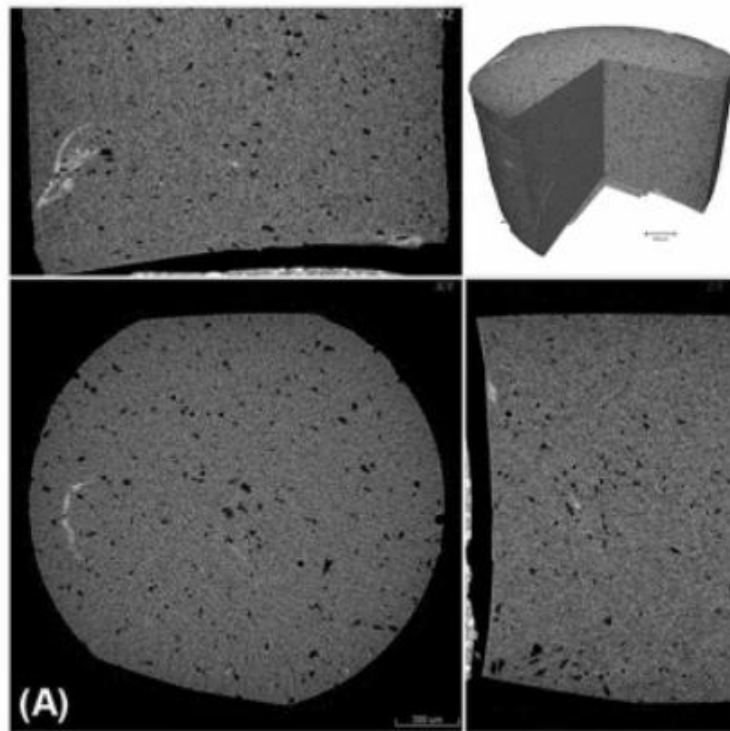
Figure 3-6 Micro XCRT imaging of dental resins providing an example of the internal structure detail that can be viewed (Haugen, et al., 2020).

The XRCT experimental method has the disadvantage of being open to operator opinion and therefore the same result may not be presented if two or more operators were to analyse the same collection of images. There is a potential source of difference in the selection of the middle portion of the granule which is required before fine-tuning the images before porosity analysis. As each granule is a different shape, what one operator assumes as the mid-point may not necessarily be that same as another operator. When fine-tuning the image within the CTAn software, multiple options can be changed. For example, when removing artefacts from the image, a sequence of images are presented and the operator chooses the one that they think is most representative. However, the most representative image may be different for another operator and therefore producing a different final image to be used in the next steps

of the analysis. In my opinion, XRCT is an excellent method for obtaining qualitative information about a sample, however any quantitative results should be used with caution.

3.4.5 Density

There are a number of methods available to measure the density of a material and is usually dictated by the type of density measurement required:

   I. Bulk

  II. Tapped

 III. Envelope

 IV. True

For the purpose of this investigation bulk, tapped and true densities were measured.
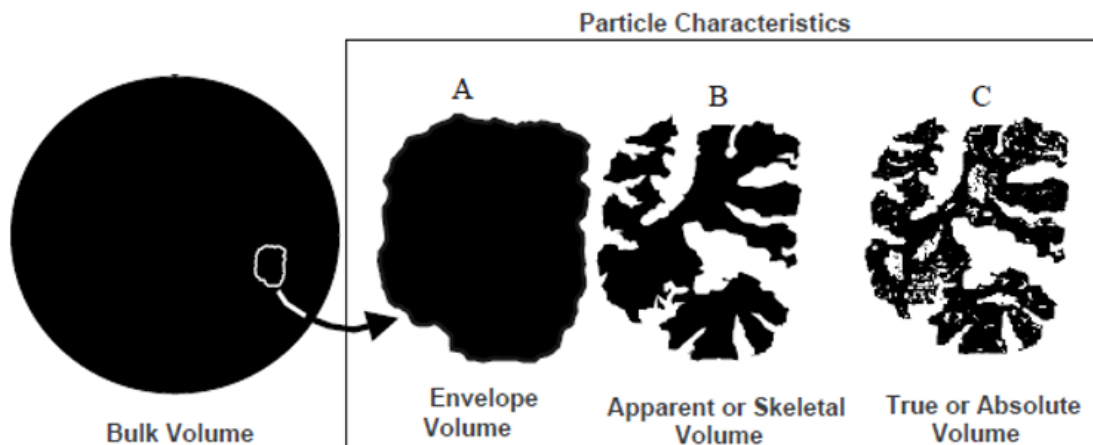
Figure 3-7 A pictorial representation of bulk, envelope, apparent and true density (Cement Science, 2013).

Bulk density is defined as the mass of powder occupying a given volume divided by that volume. Characterisation was carried out according to the European Pharmacopoeia (EDQM, Council of Europe, 2014). Granules were tested with no modification after the drying step of TSG. However, base (as received) powders were passed through a 1 mm sieve to break up any agglomerates that may have formed during storage. 100 g of powder or granules were weighed and then poured into a 250 ml graduated cylinder, gently levelled taking care not to compact the material. The bulk volume can then be used to determine the bulk density using Equation 3-3.

$$\rho_{bulk} = \frac{m}{V_0}$$
<div align="right">*Equation 3-3*</div>

where ρ_b is the bulk density, *m* is the mass of material and V_0 is the bulk volume.

Tapped density was determined using a tapped density tester (Coplay, JV2000, UK) and according to the method from the European Pharmacopoeia (EDQM, Council of Europe, 2014). Powders or granules were put into a 250 ml graduated cylinder according to the same method as that described for determining bulk density. The cylinder was secured on the cylinder support and 10, 500 and 1250 taps on the same sample were carried out and corresponding volumes V_{10}, V_{500} and V_{1250} were read. If the difference between V_{500} and V_{1250} exceeded 2 ml, the experiment was repeated in increments of 1250 taps until a difference of under 2 ml was observed. The tapped density, ρ_{tap}, was then calculated using Equation 3-4.

$$\rho_{tap} = \frac{m}{V_f}$$

<div align="right">*Equation 3-4*</div>

where m is the mass and V_f is the final tapped volume.

True density is defined as the absolute volume which is the volume occupied by the solid fraction of a particle and was determined using helium pycnometry (AccuPyc II 1340, Micromeritics, UK). A sample of known mass was placed in a chamber of known volume which is then evacuated before helium is injected and expanded into a reference chamber of known volume. The sample volume can then be calculated from the difference in pressure from measurements before and after. The gas displacement density can then be found by dividing the sample volume by its mass. An equilibration rate of 0.02 psig/min was used and 5 purges per sample. This method was based on that used by Hewitt (2015).

3.4.6   Flowability

Knowledge of the flowability of a powder aids in the prediction of the powder performance during processing. A powder that does not have good flowability characteristics may cause issues in formulation development which will need to be overcome before a process can be optimised.

The flowability of powders and granules was determined via two methods: firstly, Carr's Index and secondly, using a Schulze ring shear cell (RST-XS, Dietmar Schulze, Germany). Carr's Index (CI) and Hausner Ratio (H) are calculated using the bulk and tapped densities according to Equation 2-4 and Equation 2-5 respectively, detailed in Section 2.6.3. Due to both parameters

being based upon the same measurements, outcomes should be in close agreement, therefore only Carr's Index is used for the purpose of this thesis. It should be noted that measured bulk densities are affected by wall friction. In the situation of a powder with low density, if it is cohesive the level of compaction during tapping may be greatly influenced by the friction of the solid and the walls of the measurement container. The results can be used to compare powdered materials handled in a similar way for testing purposes, but it is not possible to extrapolate them to large-scale applications (Leturia, et al., 2014).

The Schulze ring shear cell described in Section 2.6.4 was used to measure the angle of internal friction, ∂, and flow factor coefficient, *ff*c. The internal angle of friction provides an indication of inter-particle friction and the *ff*c is a ratio of consolidation stress of the corresponding yield locus and the unconfined yield strength. The *ff*c is used as an index to rate the flowability of powders as detailed in Table 3-3 (Jenike, 1964).

Table 3-3 Classification of flow behaviour using ffc values (Schulze, 2010).

ffc value	Powder classification
ffc <1	Not flowing (cohesive)
1< ffc <2	Very cohesive
2< ffc <4	Cohesive
4< ffc <10	Easy flowing
10< ffc	Free flowing

Powder flow functions were constructed by performing yield locus test at pre-shear loads of 3, 6 and 9 kPa using a 31.37 cm^3 volume annular shear cell. Flow function coefficients (ffc $= \frac{\sigma_1}{\sigma_c}$) were determined from the 6 kPa pre-shear load results. The powder sample was

sheared to failure at six increasing, equally distributed normal stresses from 20% to 80% of the pre-shear load. This method was based on that previously used by Jager et al. (2015) and adapted for the current study during method development experimentation.

3.4.7   Surface area

The surface area of a solid material can identify information on void spaces and the surfaces of individual particles. The surface area of a powder influences further steps in a formulation development process such as processing properties, dissolution and bioavailability.

BET surface area analysis (TriStar II Plus, Micromeritics, Georgia, USA) was used to obtain surface area measurements for powders and tablets. The BET theory was an extension of the Langmuir adsorption isotherm which relates the monolayer adsorption of gas molecules onto a solid surface to the gas pressure of a medium above the solid surface at a fixed temperature. The BET theory extends the Langmuir theory to multilayer adsorption. BET surface area analysis usually uses nitrogen due to its availability, high purity and strong interaction with most solids. The surface is cooled using liquid nitrogen to obtain detectable amounts of adsorption because the interaction between gaseous and solid phases is usually weak. After adsorption layers are formed, data collected via highly accurate pressure sensors is displayed in the form of a BET isotherm, a plot of the amount of gas adsorbed as a function of relative pressure. There are five types of BET isotherm (Figure 3-8) (Mohammed, et al., 2020):

- Type I isotherms are observed when the adsorption is limited to a single layer,
- Type II isotherms occur when the amount adsorbed increases with increasing pressure and reaches a plateau when adsorption is completed,

- Type II isotherms are characterized by little initial adsorption,

- Type IV isotherms occur due to capillary condensation where gas condenses in capillary pores of the solid at pressures less than the saturation pressure of the gas, and

- Type V isotherms are similar to Type III isotherms as they show little adsorbate-adsorbent interaction but they occur on similar adsorbents as Type IV isotherms.
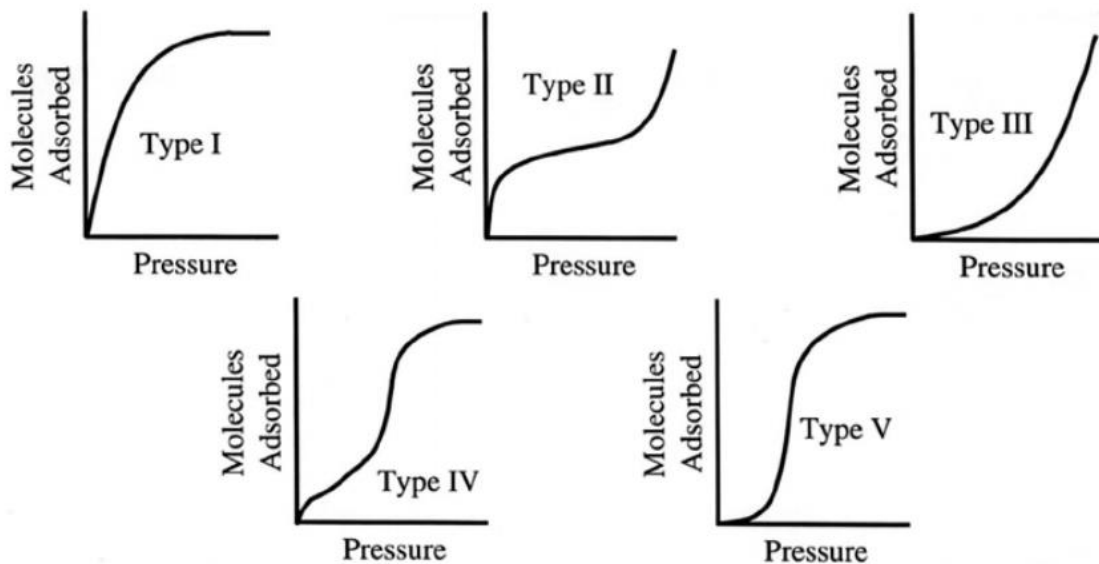
Figure 3-8 The five types of BET isotherm

Tablets were cut into four pieces using a tablet cutter before placing in the sample tube for testing. Powders were sieved through a 1 mm mesh to break up any agglomerates before placing in the tube for testing. Samples were placed into a sample tube ensuring minimum deposit of powder on the tube wall, then weighed and outgassed at 30 °C for 12 hours to remove any moisture. Due to small sample sizes (up to 1 g) within the sample tube, after consultation of dynamic vapour sorption (DVS) plots for each material and discussions with

equipment experts at AstraZeneca, 12 hours was determined to be a suitable length of time for outgassing. After this time, the sample was then weighed again to determine the dry mass of the sample before attaching to the instrument. Multipoint analysis (10 points) over the relative pressure range 0.05-0.22 at 77.3 K liquid nitrogen temperature was carried out. The MicroActive physisorption software (Version 2.03, Micromeritics, UK) was used to analyse data. The sorption isotherms obtained were interpreted using the BET model (Equation 3-5) (Brunauer, et al., 1938):

$$\frac{P}{V(P_0 - P)} = \frac{1}{V_m C_{BET}} + \frac{C_{BET} - 1}{V_m C_{BET}} \left(\frac{P}{P_0}\right)$$

Equation 3-5

where V is the volume of gas adsorbed at partial pressure, P, of adsorbate, V_m is the volume of gas adsorbed in the monolayer, P_0 is the saturation pressure of adsorbate at 77 K and C_{BET} is the BET constant that exponentially relates the heat of adsorption and condensation of the adsorbate. The linear form of the equation enables a plot of $P/V(P_0-P)$ versus P/P_0 from which C and V_m can be calculated. When outgassing has not been sufficient there is often difficulty in achieving a straight line from the BET plot or a negative value for C (Connelly, 2017), neither of which were observed in method development or final experimentation for the current study.

3.5 Tablet compression and characterisation

Compression of granules produced via TSG and, later in this thesis, compression of as-delivered excipient powders, took place utilising various methods. A universal testing machine (Zwick/Roell Z030, Leominster, UK) was used for uni-axial bulk confined compaction, more

specifically for applying models previously discussed, such as Kawakita and Heckel in Section 2.7.3. Later in the thesis, to provide a more accurate approach to high-speed tableting and closely relate the investigation to industry, compression simulators were used. Hydraulic compression simulators were used, firstly at Merlin Powder Characterisation Ltd. (Brierley Hill, UK) and secondly at AstraZeneca (Macclesfield, UK) (StylOne Evolution Single Station Tablet Press, Medelpharm, France). The use of the compression simulators ensured that the experiments were industrially relevant as they were set-up to mimic large-scale industrial tableting machines.

3.5.1   Uni-axial bulk confined compaction of granules

Uniaxial compactions were carried out within a close-fitting compression pellet die with an internal diameter of 10 mm or 13 mm (Specac, Kent, UK). Prior to each compression the die was lubricated by brushing with magnesium stearate in acetone and allowing to dry. Internal lubricants have not been used unless specifically stated, due to potential reduced tablet tensile strength in the presence of magnesium stearate within a powder (Paul & Sun, 2017). The die was tapped five times to remove large packing irregularities (Adams, et al., 1994). The granule bed was then compressed using a Universal Testing Machine (Zwick/Roell Z030, Leominster, UK) at a speed of 150 mm/min and upper force limit of 20 kN. The initial bed height was determined from the punch position at the start of loading. One or more of the compaction models proposed by Adams (1994), Heckel (Heckel, 1961), Kawakita and Ludde (1970) and Walker (1923) were then applied to the data using a Microsoft Excel spreadsheet.

3.5.2   Tableting using a compression simulator at Merlin Powder Characterisation

Compression experiments were carried out to investigate tablet tensile strength after changing TSG process parameters. Compression was undertaken using a lab scale hydraulic compression simulator (Figure 3-9) (Merlin Powder Characterisation, Brierley Hill, UK) to give high speed compaction data comparable to that found in industrial tablet production. Throughout the measurements, 10 mm flat faced tooling was used, and 350 mg of each sample was manually fed into the die. The die was lubricated using magnesium stearate 1% w/v in acetone before each compression. Tablets were compressed at a speed of 10 mm/s using 9 different target compression heights to give a range of data suitable for the production

of a tabletability profile. A single ended sine wave profile was used with a target 10 ms dwell time. During compression a measurement of maximum load was measured on upper and lower punches and the mean of the two peak forces was used to calculate punch pressure by dividing by the punch tip area. After compression, the height and diameter of each tablet was measured using digital callipers accurate to ±0.01 mm before diametrically compressing in a tablet hardness tester (Hollands C50, UK) to gain data required for tablet tensile strength calculations.

Figure 3-9 The hydraulic compression simulator used at Merlin Powder Characterisation.

The compaction simulator is able to simulate a wide range of industrial scale tableting presses. This allows for a reduction in formulation study times as the intended formulation can be tested for suitability at commercial scale early on in the development process. Due to a single punch and die within the simulator it can be a slow process to produce a large quantity of

tablets, especially as the die is being manually fed. A feed shoe can be used but the powder or granules would require internal lubrication with magnesium stearate and therefore alter the compression profile and tablet characteristics which was undesired in the current study.

3.5.3   Uni-axial bulk confined compression of powders

A 10 mm flat-faced die (Specac, Kent, UK) was used to produce tablets. The die was brushed with magnesium stearate 1% w/v in acetone to act as lubricant before each addition of powder and subsequent compaction. Powder samples were taken from the humidity chamber and placed in a 60 ml sample tube with screw-top lid immediately before compaction. Samples of 300 mg $\pm$ 20 mg powder were poured into the die from a weigh boat in a maximum of 2 minutes to minimise the amount of time the sample was open to lab conditions (21-24°C, 30-40% RH). Compression force was applied using a universal testing machine (Zwick Roell Z030, Leominster, UK) at a speed of 4 mm/min and at 6 compression pressures ranging between 30 and 390 MPa. Two tablets for each powder at each humidity and each compression pressure were produced. Feasibility studies were caried out prior to the main experiment and it was found that strong correlations were given with just one tablet tested, therefore the decision was made to test only two tablets for each condition at each pressure in the main study. Tablets were manually ejected from the die before measuring the mass using an analytical balance (ME Balance, Mettler Toledo, Leicester, UK) and diameter and height using digital callipers accurate to ±0.01 mm, within 1 hour of production. From these measurements the volume and density of the tablets were determined. Relative density, *D*, was calculated by

dividing tablet density by the true density of the powder. Tablet porosity, ε, was calculated using Equation 3-6.

$$\varepsilon = 1 - \frac{\rho_{tablet}}{\rho_{true}}$$ *Equation 3-6*

where ρ_{true} is the true density of the material (Sun, 2008). Heckel analysis as discussed in Section 2.7.3., was carried out on the compression data to find the yield pressure for each powder (Heckel, 1961).

3.5.4   Tableting using a compression simulator at AstraZeneca

A tableting simulator (StylOne Evolution Single Station Tablet Press, Medelpharm, France) (Figure 3-10) was used to produce tablets, using a 8 mm diameter, flat-faced tooling. The simulator process was controlled by computer software (Analis, Version 2.07, Medelpharm, France). Powders were equilibrated at various RH and were taken from desiccators immediately before compression, with the sample tube being minimally opened during experimentation. The instrument was calibrated before use in order to account for the deformation of the metal within each compression. Magnesium stearate 1% w/v in acetone was manually brushed on the punch and die and allowed to fully dry before compression. A Fette 2090 IC single rotary tablet press with 36 station B-turret was simulated with a punch speed of 250 mm/s to ensure the compression was industrially relevant. For compression of single materials, 160 mg ±10 mg of powder was weighed before compressing to a target tablet thickness which was changed in order to give compression pressures ranging between 30 MPa

and 300 MPa. A minimum of two tablets were produced for each compression pressure. All testing was performed in controlled environmental conditions of 25 °C and 45% RH.
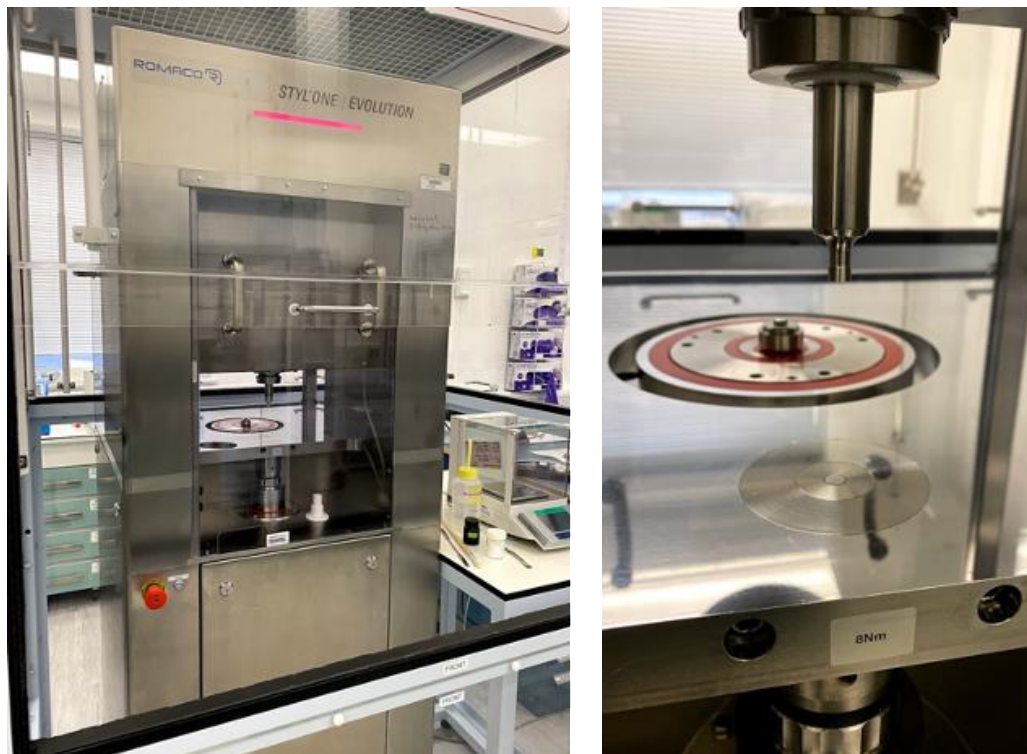
Figure 3-10 The Styl'One Evolution and 8 mm flat-faced die.

3.5.5 Diametric tablet compression

After compression, the mass of each tablet was measured using an analytical balance (Mettler Toledo, UK) along with diameter and height measurements by digital callipers accurate to ±0.001 mm before diametrically compressing to gain data required for tablet tensile strength calculations. Tablet strength is measured via diametric compression of vertically placed tablets (Figure 3-11) within the universal testing machine (Zwick/Roell, Leominster, UK) or texture analyser (TA.XTplus, Stable Micro Systems, UK). A tablet hardness tester can also be used (TBF 1000, Copley, Nottingham, UK) but provides less control over compression speed

and the inability to view a distance-force profile of the tablet breakage. The tablet tensile

strength is related to the load at the point of tablet fracture and calculated using Equation 3-7.

$$\sigma_t = \frac{2F}{\pi D_t t_h}$$ *Equation 3-7*

where F is the maximum diametrical compression force, D_t is the tablet diameter and t_h is the

tablet height. A tabletability profile can then be plotted as compaction pressure versus tablet

tensile strength. An example of a tabletability profile is given in Figure 2-12, Section 2.7.2.
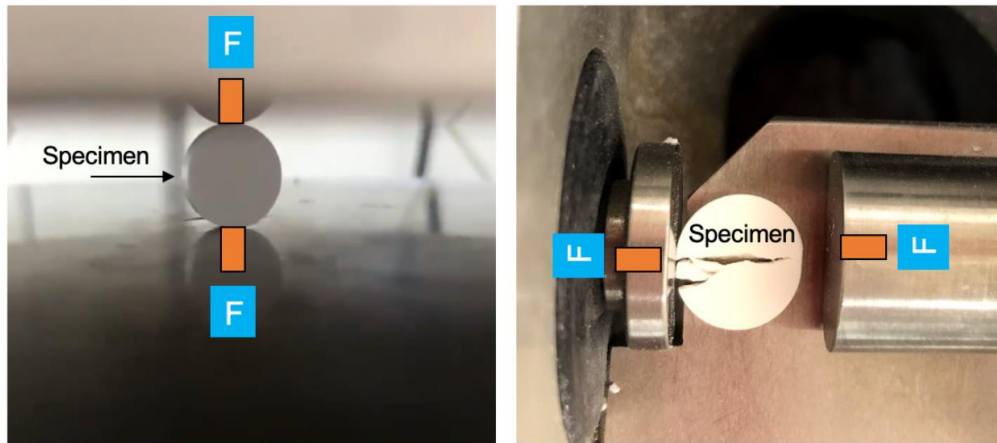
Figure 3-11 A demonstration of a diametrical compression. Force, F, is applied from platens above and below the specimen in (a) using a universal testing machine or each side of the horizontal specimen (b) in a tablet hardness tester.

3.5.6   Surface area analysis

BET surface area analysis (TriStar II Plus, Micromeritics, Georgia, USA) was carried out in order

to determine the surface area of tablets using the method described in Section 3.4.7. Tablets

were broken into quarters using a tablet cutting device before placing into the experimental

tube and degassing for 12 hours before measurement. It was noted that the surface area of

each tablet would change due to cutting into quarters. However, each tablet was treated the

same, therefore the relative differences between each one allows for comparison of results.

4   Investigating Twin Screw Granulation

4.1   Introduction

Granulation is commonly used prior to tableting to improve powder handling and ensure homogeneity of the product. Depending on the granulation process used, it may have a negative impact on tabletability. It is therefore important to understand how to optimise the granulation process to provide the required properties for tableting. The aim of this chapter is to examine the TSG process and the effect of the wet granulation process on tabletability of various pharmaceutical excipients. Granule and tablet properties were investigated using a range of techniques.

Sun & Kleinebudde (2016) reported that dry granulation causes a reduction in tabletability due to decreased compactibility of the granulated powder. A range of powders were considered, including those that are plastically deforming such as MCC and those that undergo brittle fracture, such as lactose. It was confirmed that there is not one single mechanism that can explain all observations. A previous study by Herting and Kleinebudde (2008) investigated the reasons for partial loss in compatibility after dry granulation and concluded that a work-hardening phenomenon was caused by a combination of particle size enlargement and hardening of material. Work-hardening is the region within a stress-strain relationship that occurs due to strength enhancement caused by plastic deformation[1] (Zhou & Qiu, 2010). The study showed that even if the size of granules is equal, the use of smaller particles as raw

---

[1] The stages of compression are discussed in more detail within Section 2.7.3.

material results in tablets with higher tensile strength due to higher specific surface area. Work-hardening and particle size enlargement cause partial loss in compactibility but this can be compensated by the production of smaller granules or base materials with small particle sizes (Herting & Kleinebudde, 2008).

The reduction in tabletability after wet granulation has been investigated utilizing a high shear mixer and applying the unified compaction curve (UCC) model that was originally developed to predict the loss in tabletability after roller compaction (a dry granulation process) (Farber, et al., 2008; Nguyen, et al., 2013). It was found that an increase in the liquid level and/or wet massing time caused a reduction in resulting tablet tensile strength. The TSG process differs greatly to high shear granulation, including shorter residence times, greater shear forces and being continuous in nature. Therefore, it may not be possible to use the UCC model for the TSG process without further investigation.

4.2   Materials and methods

4.2.1   Materials

Two commonly used pharmaceutical excipients were used for this study: Mannitol (Pearlitol 160C, Roquette, UK, median particle size ~160 μm) and α-Lactose monohydrate (Pharmatose 200M, DFE Pharma, Germany, d_{50} 35 μm and Fast Flo 316, Foremost Farms, USA, d_{50} 150 μm). Two types of lactose were used to provide an initial investigation of the impact of excipient production methods on the granulation process. Although particle size effects cannot be discounted, the spray-dried nature of Fast flo lactose results in material that is structurally different to that of Pharmatose. Fast Flo 316 is a spray-dried lactose and therefore has a

certain amount of 'built-in' porosity (Figure 4-1). Pharmatose 200M differs to Fast Flo 316 because it is a crystalline, milled lactose with a smaller particle size. The granulating fluid used was distilled water.
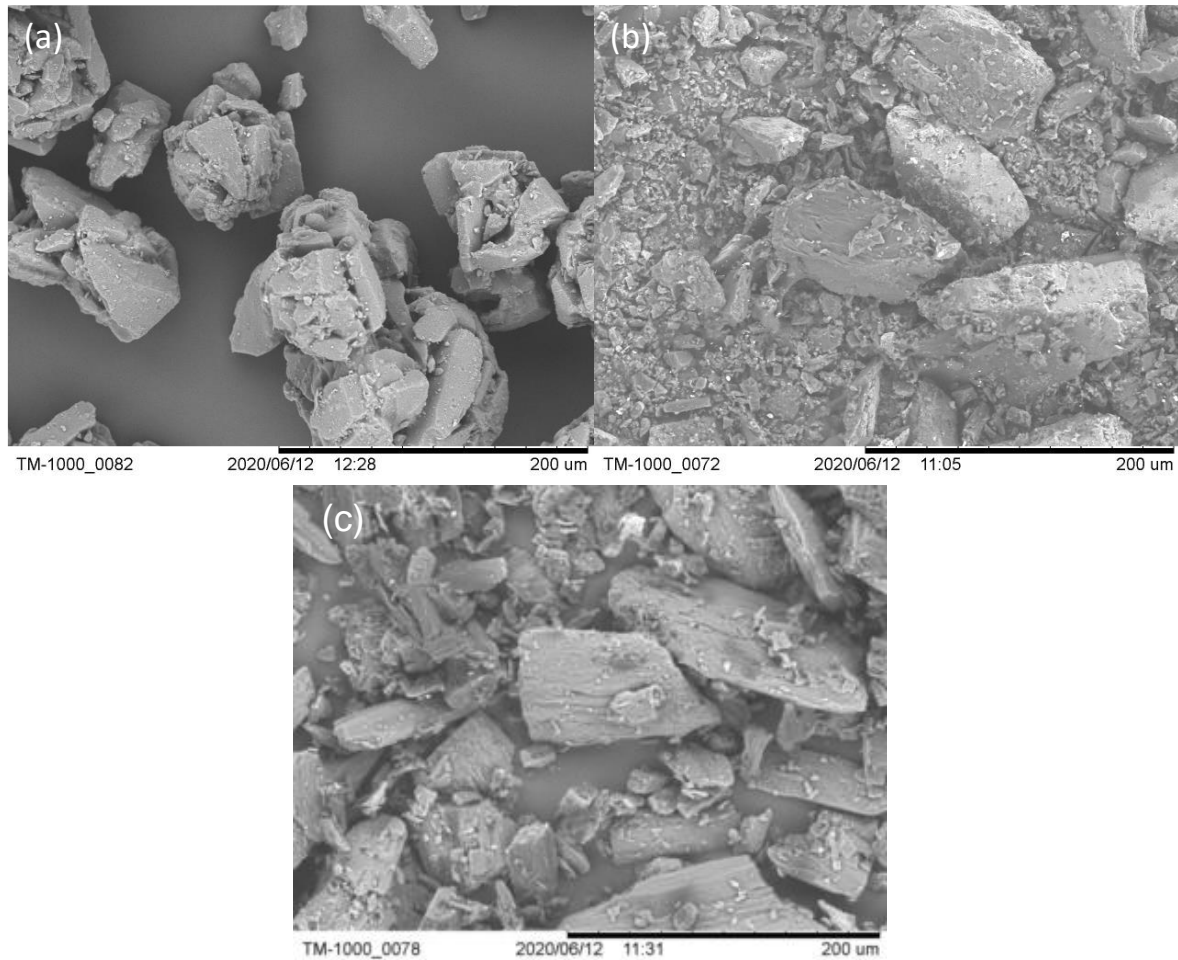
Figure 4-1 The structural differences between (a) Fast Flo 316 lactose, (b) Pharmatose 200M lactose and (c) Pearlitol 160C mannitol.

4.2.2   Methods

4.2.2.1   Granulation process

Granulation was performed using a lab scale co-rotating Twin Screw Extruder (Haake, Thermo Scientific, Germany) with a screw diameter (D) of 16 mm and length of 400 mm. Powder was fed into the barrel at the base of the screws via a volumetric twin screw feeder (T20, K-Tron Soder). Granulation fluid was added through a single injection port positioned approximately 9 diameters length from the base of the screws via an 8-roller peristaltic pump (REGLO Digital, Ismatec, Switzerland). The parameters used for the investigation were as follows:

I.   Barrel temperature 21 °C

II.   Powder feed rate 2 kg/h

III. Screw speed 400 rpm

IV.   0.11, 0.18 and 0.25 liquid to solid ratio (L/S)

Three different screw configurations were used (Figure 4-2). The configurations consisted of either conveying only elements (C) or kneading elements (K) making up 1 or 2 kneading zones and are described in terms of ratio of length to diameter. Each kneading zone consisted of four 60° forward kneading blocks which is the same as those used in previous studies by Seem (2015) on the same lab-scale extruder. Kneading blocks are available in offset angles of 30°, 60° or 90° which decide whether flow is forwarding or reversing. Kneading blocks offset at 30° or 60° will have some conveying capacity and push material along the screw. 90° blocks have no inherent conveying capacity and are dependent on pressure driven flow (Seem, et al., 2015). Thompson and Sun (2010) found that the angle of kneading elements affects granule

112

properties when the fill level is high and Van Melkebeke, et al. (2008) found that the porosity of granules produced with 30°, 60° and 90° offset angle kneading blocks were similar.

For the purpose of this study when 2 kneading zones are referred to, it is important to clarify that this is made up of 1 kneading zone immediately before the liquid injection port (pre-kneading section acting upon dry material) and 1 kneading zone later along the barrel (acting upon wet material). A pre-kneading zone was inserted to investigate the extent of the effect of a kneading zone without the presence of binder. The individual parameters used within the study are shown in Table 4-1. Once the TSG was operating at steady state (steady speed and torque output observed), approximately 200 g of granules were collected at the outlet and transferred to large trays in order to provide a shallow granule bed for drying. The granules were air-dried at ambient temperature and humidity for 72 hours before storage in airtight containers while awaiting characterisation.
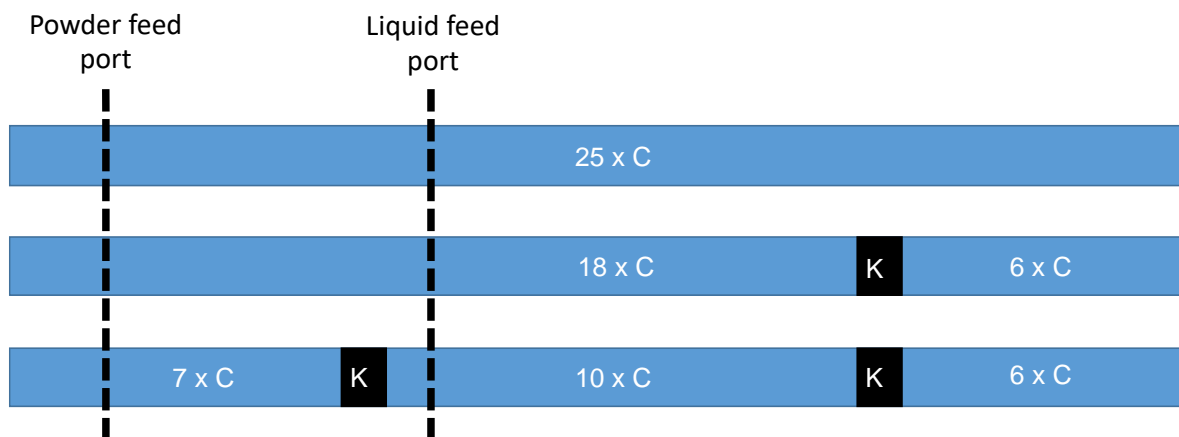
Figure 4-2 The three screw configurations used within the study. Each blue bar represents a screw barrel consisting of a total of 25 elements. C, conveying elements and K, kneading blocks. Each conveying element is 16 mm in length and a kneading block consists of 4x4 mm elements at 60º angles. The kneading blocks are aligned adjacent with conveying elements.

113

Table 4-1 Granulation parameters used within the study.

Experiment number	Material	Configuration	L/S ratio	Abbreviation
1			0.11	M C 0.11
2		Conveying only	0.18	M C 0.18
3			0.25	M C 0.25
4			0.11	M 1K 0.11
5	Mannitol	1 kneading zone	0.18	M 1K 0.18
6			0.25	M 1K 0.25
7			0.11	M 2K 0.11
8		2 kneading zones	0.18	M 2K 0.18
9			0.25	M 2K 0.25
10			0.11	FF C 0.11
11		Conveying only	0.18	FF C 0.18
12			0.25	FF C 0.25
13			0.11	FF 1K 0.11
14	Lactose (Fast Flo 316)	1 kneading zone	0.18	FF 1K 0.18
15			0.25	FF 1K 0.25
16			0.11	FF 2K 0.11
17		2 kneading zones	0.18	FF 2K 0.18
18			0.25	FF 2K 0.25
19			0.11	P C 0.11
20		Conveying only	0.18	P C 0.18
21	Lactose (Pharmatose 200M)		0.25	P C 0.25
22		1 kneading zone	0.11	P 1K 0.11
23			0.18	P 1K 0.18

Experiment number	Material	Configuration	L/S ratio	Abbreviation
24			0.25	P 1K 0.25
25			0.11	P 2K 0.11
26		2 kneading zones	0.18	P 2K 0.18
27			0.25	P 2K 0.25

4.2.2.2   Granule characterisation

Granule particle size distribution was carried out using the sieving method described in Section 3.4.2. Prior to sieving the granules were dried by distributing thinly on large trays and leaving them to dry at ambient temperature and humidity for a minimum of 72 hours.

Tabletability was assessed by producing tablets on a hydraulic compaction simulator at Merlin Powder Characterisation Ltd. as described in Section 3.5.2.

Granule structure was investigated using micro-CT as described in Section 3.4.4. The granules were selected from the 180 – 1400 μm size fraction as this represented the 'usable' granules most suitable for tableting.

Granule strength analysis was carried out using uniaxial compression tests via a Universal Testing Machine (Zwick/Roell Z030, Leominster, UK). A 13 mm round, flat-faced die (Specac, Kent, UK) was used with a moving top piston, lubricated by applying magnesium stearate 1% w/v in acetone with a brush and allowing to dry fully. For each compression, 500 mg of granules from the 180 – 1400 μm size fraction were manually fed into the die and tapped five times to remove any packing irregularities. The test was carried out twice for each sample at a speed of 150 mm/min and the upper force limit of 20 kN.

4.3   Results and discussion

4.3.1   Granule size distribution

Figure 4-3 shows images of wet granules of mannitol produced at increasing L/S and increasing kneading zones. The granules produced at 0.11 L/S using only conveying elements, consist of a large quantity of fines as there is insufficient and poorly distributed granulation liquid for the wetting process. The size of granules increases with an increasing L/S or kneading zones used in the TSG setup. At 0.25 L/S, with one kneading zone and one pre-kneading zone, the granules become over wetted, forming agglomerates too large for tableting purposes. Due to Figure 4-3 showing wet granules immediately after they exit the granulator, a particle size distribution of these granules cannot be given as there was no availability to carry out wet sieving of the material. The dry particle size data for the granules pictured in Figure 4-3 is given in Figures 4-4 and 4-5.
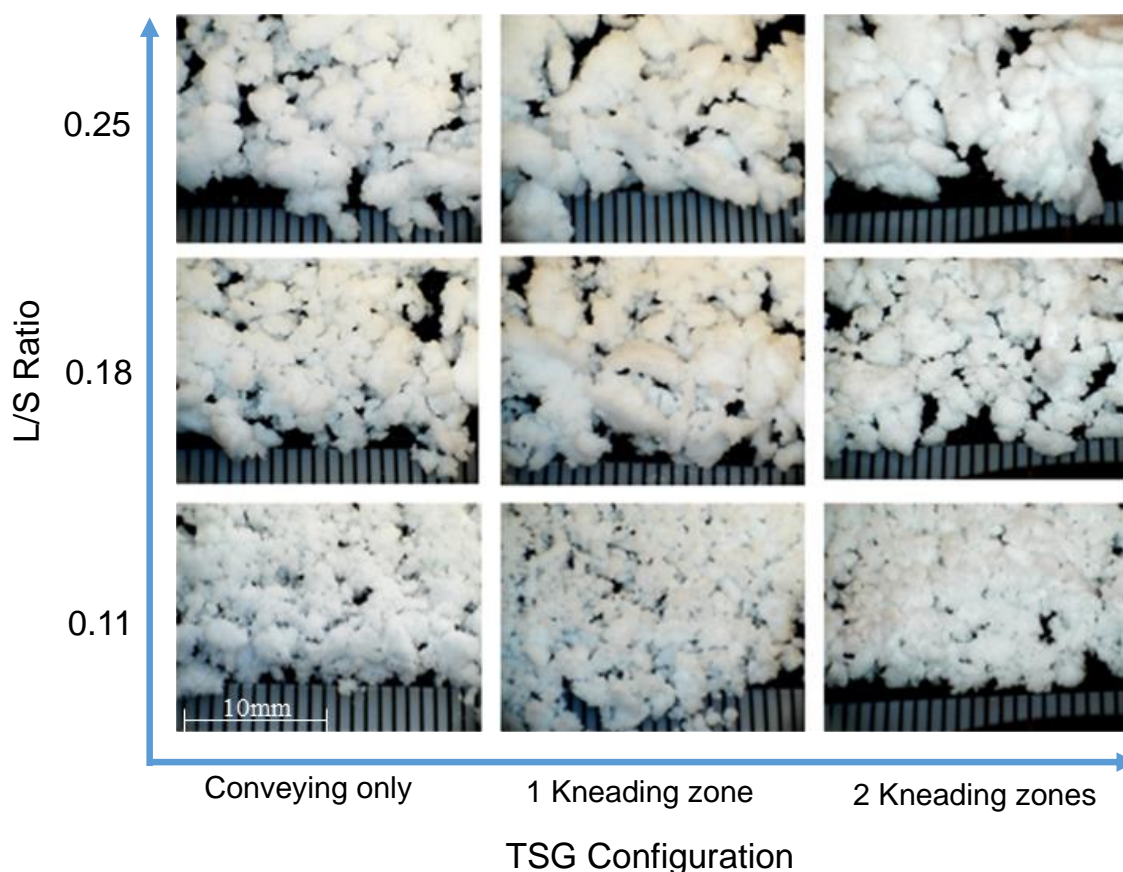
Figure 4-3 Wet granules produced using mannitol, showing the variation in outcomes after changing process parameters.

4.3.2 Sieving results

Sieving analysis was performed on all granules and cumulative distributions are shown in Figure 4-4. As the number of kneading zones and L/S are increased there is a shift to the right across the plots. This is most pronounced for Fast Flo, where a L/S of 0.25 and 2 kneading zones produce large granules that are unlikely to be useable without considerable drying and milling steps. For Pharmatose and mannitol, it is not until a L/S of 0.25 and the addition of 2 kneading zones that there is a considerable shift in the cumulative distribution to the right. However, the conclusions drawn from this data are limited as most of the observations are

based on weight differences in a single sieve. As work progressed throughout the EngD, it became apparent that sieving would not provide as detailed size distribution information as a dispersion method, such as QicPic or Malvern. However, at the time of TSG experimentation training on dispersion methods had not taken place resulting in the sieve method being the most appropriate available at the time.
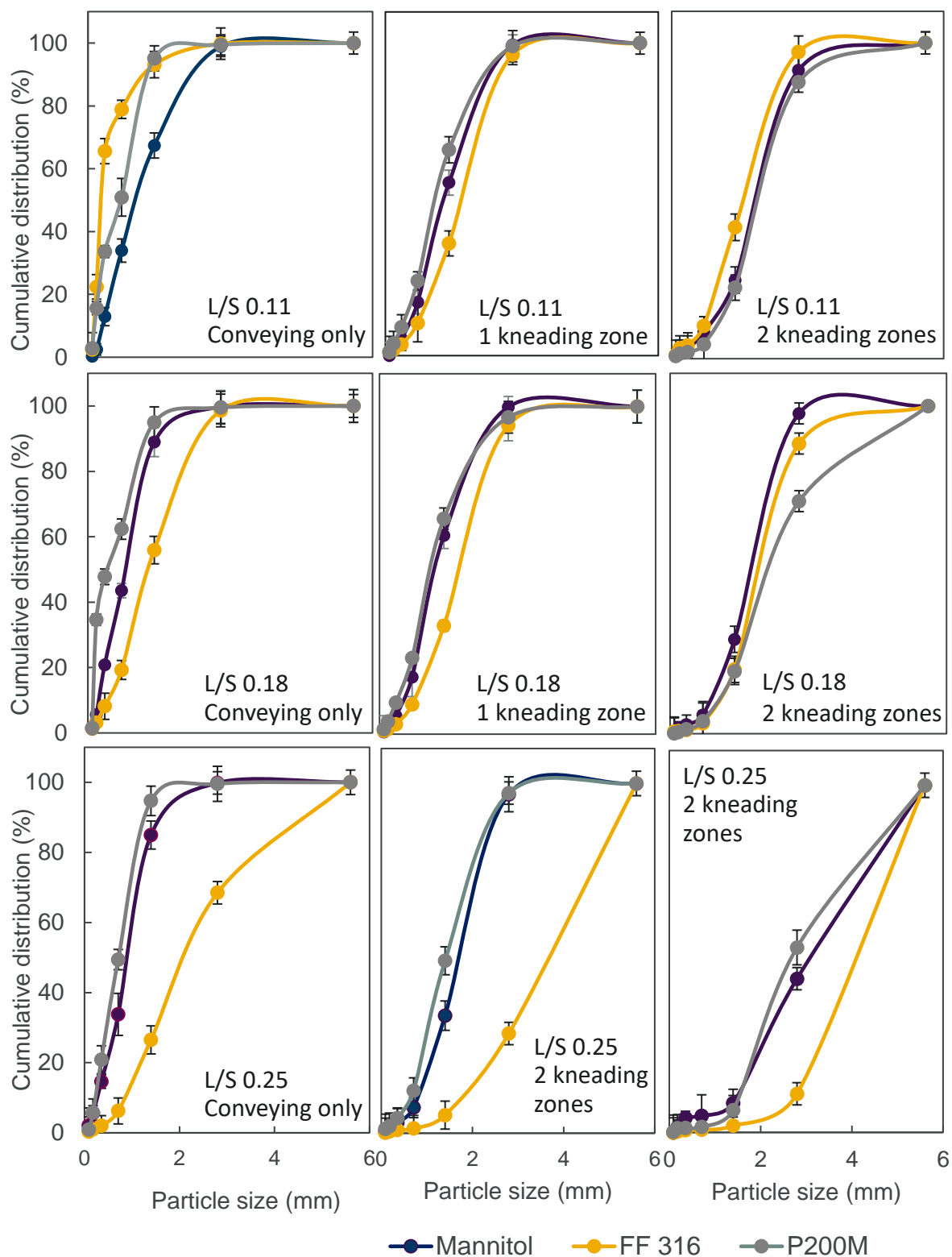
Figure 4-4 Cumulative mass percentage distribution for mannitol, FF316 and P200M at all L/S ratios and TSG set-ups. Error bars show minimum/maximum error, n=2.

Figure 4-5 shows the d_{50} and fractions separated into sizes under 180 μm, 180 – 1400 μm and over 1400 μm, which were then classified as 'fines', 'mid-sized' and 'over-sized' respectively for each material. The choice of 180-1400 μm being the 'usable' portion of the granule size distribution in based on an ideal choice being a d90 of 800 to 1200 μm with fines around 180 μm also being desirable (Hanningfield, 2020). Keeping fines to a minimum ensures good flow and uniform die filling which is important to ensure consistent uniformity of the active pharmaceutical ingredient (Hanningfield, 2020).

For mannitol, there are small quantities of fines with all screw configurations and L/S. Interestingly, even with conveying only elements and 0.11 L/S there are few fines. This would indicate good mixing and water dispersion within the system. However, this could also be attributed to the d_{50} of the base material being 160 μm and therefore the material that is added to the system is already larger that than in the case of Pharmatose with a d_{50} of 35 μm. A large number of fines within a pharmaceutical formulation could lead to segregation further downstream and therefore poor product homogeneity. For the purpose of a pharmaceutical product, if segregation occurs during the production process, this could lead to poor content uniformity (CU) within the product which is a source of risk to the patient due to the delivered dose being too high or low.

At a L/S of 0.25 there are large quantities of oversized granules for all materials, indicating over-wetting within the system. This is most apparent with a screw configuration containing two kneading zones due to the greater mixing and compressive forces acting upon the material within the barrel. This is mirrored in the high value for granule d_{50} (~3 mm) and these granules would not be suitable for further processing without considerable milling input.

Generally, across all materials, the granule d_{50} increases with increasing L/S and number of kneading elements. Screw configurations containing one or two kneading zones produce a higher number of fines with a L/S ratio of 0.11 than those produced with conveying only elements. This may be due to particle breakage occurring due to the shear stress applied by the kneading elements to the material, which in all cases, undergo brittle fracture. The addition of a second kneading zone acting upon dry material gives more opportunity for particle breakage and, at low L/S, less opportunity for later coalescence of material along the barrel length, thus resulting in more fines. Dhenge et al. (2012(a)) previously confirmed that kneading zones show simultaneous breakage and coalescence but this was dependent on the L/S used with a lower granule size corresponding to the reduction in L/S. The previous report was performed on a formulation of lactose, microcrystalline cellulose and disintegrant, croscarmellose sodium, therefore the mechanism of granule formation would be expected to be different but the overall principle of granule breakage with the addition of kneading zones comparable. Both kneading zones in the report by Dhenge et al. (2021(a)) were acting upon wet material and therefore the current study is of additional benefit to show the granule breakage that occurs when there is the presence of a kneading zone acting upon dry material.

Fast flo produces a large number of fines with conveying only elements and a L/S ratio of 0.11. However, with the addition of one or two kneading zones the quantity of fines is markedly reduced. The granule d_{50} increases in a linear manner with L/S and number of kneading zones. The presence of two kneading zones results in a large quantity of oversized granules, even at low L/S. This indicates that granule size is more dependent on screw configuration than liquid content for Fast Flo.

Much like for mannitol, the d_{50} of Pharmatose increases in a stepwise manner with increasing L/S and kneading zones. Large amounts of fines are observed with L/S of 0.11 and conveying only elements or one kneading zone. Interestingly, the d_{50} for this set-up is around that of the base material (Pharmatose d_{50} 35 μm versus TSG 0.11 L/S and 1 kneading zone 45 μm). This confirms the presence of ungranulated material being conveying along the length of the screw. The stepwise increase in d_{50} across L/S and number of kneading zones in a similar fashion to mannitol indicates that the granule size is more dependent on liquid content than screw configuration.
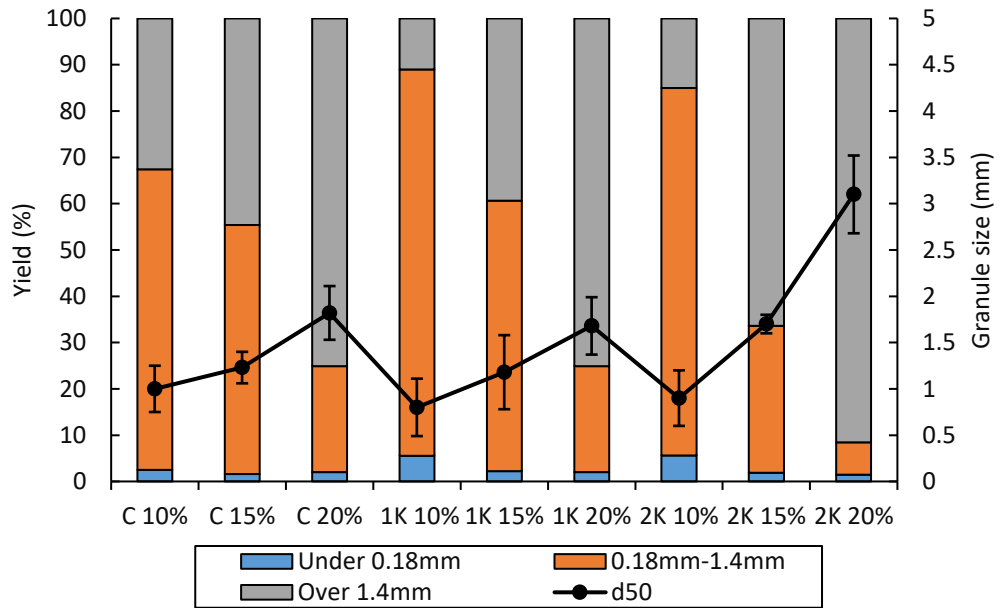
Figure 4-5 (a) Granule d$_{50}$ and yield information for mannitol.
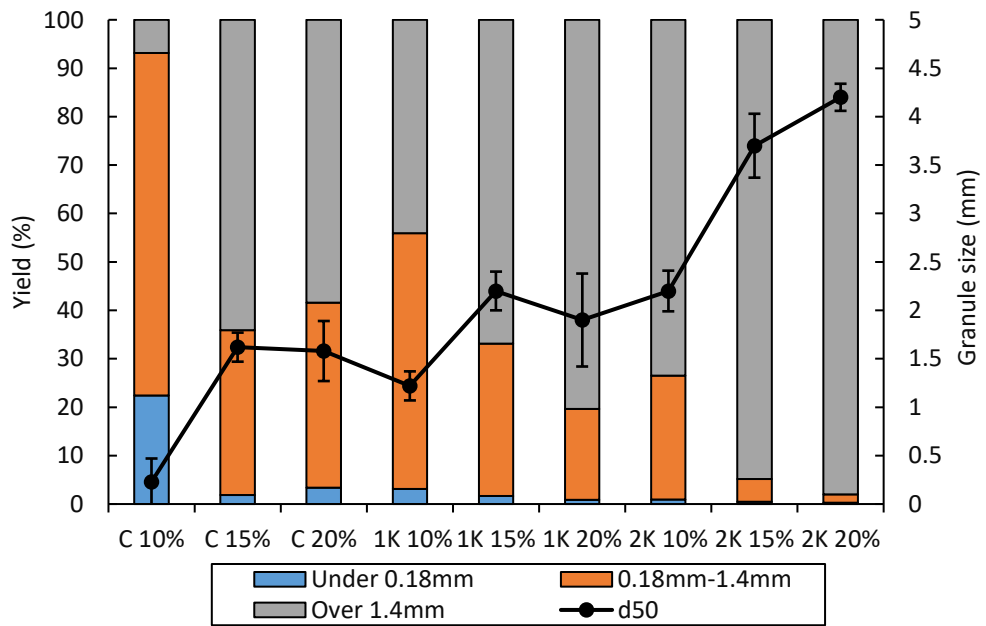
Figure 4-5 (b) Granule d$_{50}$ and yield information for Fast flo.
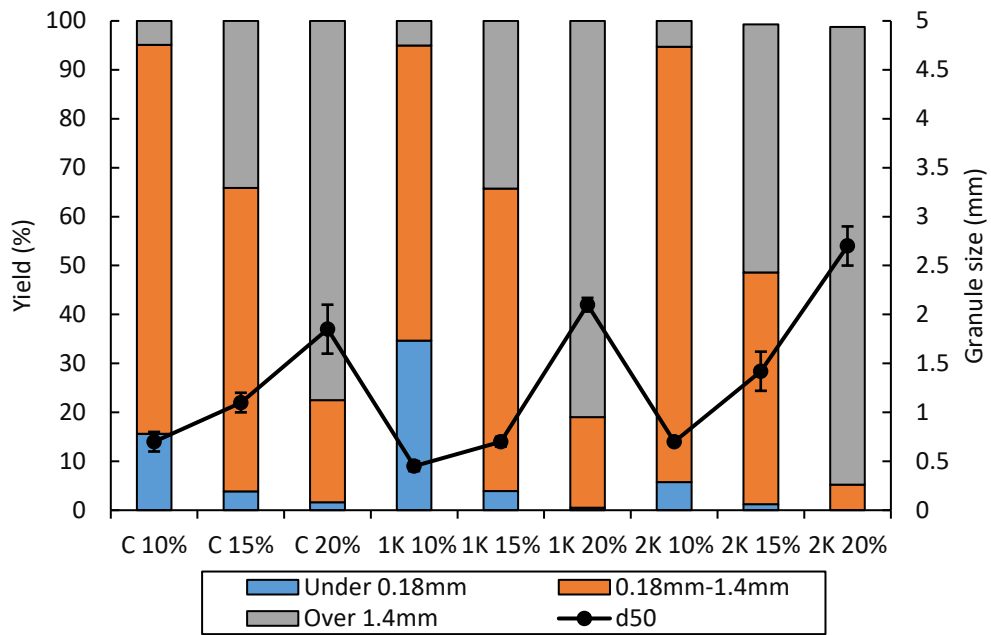
Figure 4-5 (c) Granule d$_{50}$ and yield information for Pharmatose.

4.3.3   Shape and morphology

Figure 4-6 and Figure 4-7 show the aspect ratio and sphericity for granules produced with conveying only elements and one kneading zone within the granule size range of 180 to 1400 µm. Batches of granules produced with 2 kneading zones did not have a high enough yield of useable granules to make characterisation possible. The granules produced have very similar values for both aspect ratio and sphericity for all materials, L/S and screw configurations. The aspect ratio ranges from 0.65 to 0.74, while the sphericity ranged from 0.76 to 0.79. There is no pattern to shape differences between varying L/S or screw configuration within the current study, however there are limitations to it being a small sample of the parameter space. Traditional batch methods of granulation, for example, high shear granulation produce granules with higher sphericity. Lee (2012) found the sphericity of granules produced by high shear granulation to be higher than that of those produced via TSG, quoting a value around

0.87. In corroboration with the current study, Lee (2012) also found little difference in sphericity or aspect ratio with changing process parameters, this may be due to only the granules from the usable size range, 180 to 1400 µm, being analysed. The sphericity values for TSG found by Lee (2012) agree with this study. Dhenge, et al. (2012(a)) found that granule shape varied considerably between TSG compartments, with the most spherical and largest agglomerates being produced in the first compartment. After the high compressive and shear forces on the material provided by kneading zones in later compartments, the agglomerates were broken and consolidated, producing a more elongated shape. The resultant granules at the end of the process had a similar sphericity and aspect ratio which seemed independent of the L/S used. The current study and findings within previous literature confirm that granule shape is more reliant on the TSG barrel set-up than L/S or material. However, this has only been shown in the current study for materials that undergo brittle fracture. It is likely that plastically deforming materials would respond differently to the TSG process.
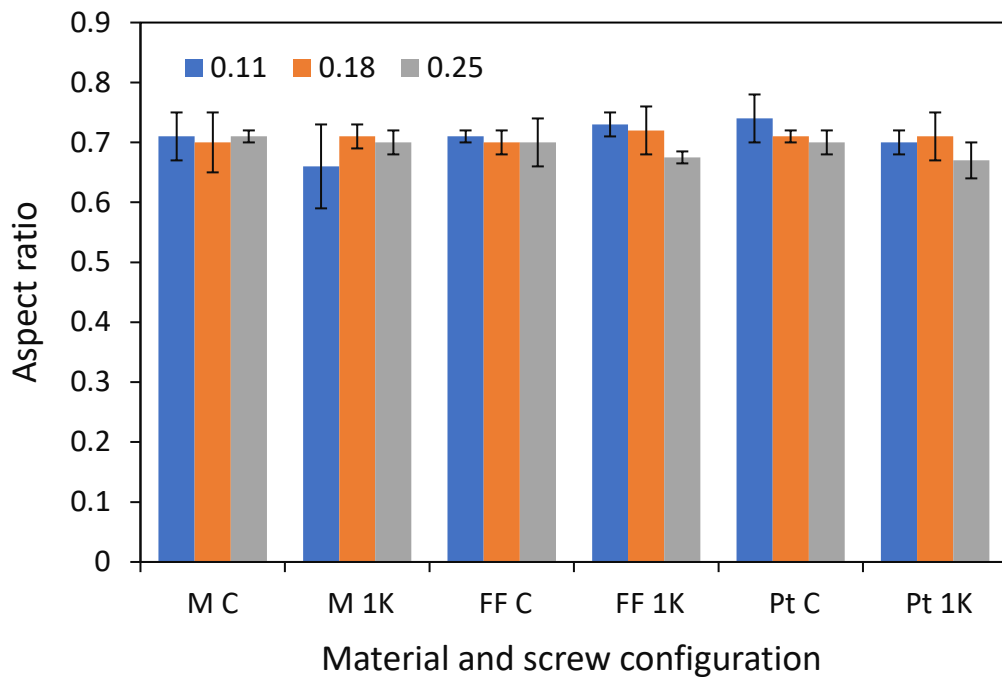
Figure 4-6 Aspect ratio values for materials (Mannitol, M, Fast Flo 316, FF, Pharmatose, Pt).
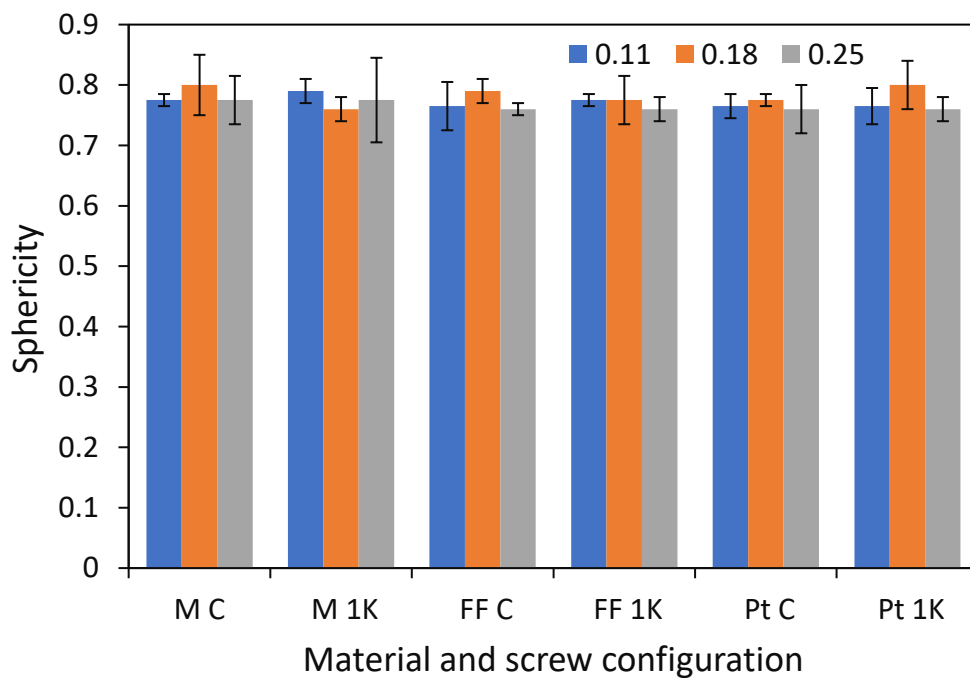
Figure 4-7 Sphericity values for materials (Mannitol, M, Fast Flo 316, FF, Pharmatose, Pt).

4.3.4 Internal structure and porosity of granules

Individual granules from each batch were chosen at random and imaged using XRCT. Figure 4-8(a) shows an XRCT image of the centre slice of two granules at the extremes of porosity observed. Further images can been seen in Figure 4-9, however Figure 4-8 has been provided to show the most extreme differences between granules produced with the same material but different process parameters. Figure 4-8(a) shows the most porous granule from all batches which was produced from mannitol, a L/S of 0.11 and conveying only elements. The porosity value is 57% and its internal structure resembles the shape of primary mannitol granules that are very loosely bound together. This is due to the limited amount of wetting at low L/S and the lack of kneading within the TSG barrel to increase shear force and growth between particles. Conversely, Figure 4-8(b) shows the least porous granule from all batches and was produced with mannitol, at a L/S ratio of 0.25 and 2 kneading zones within the barrel. The granule is clearly denser with a porosity value of 12% and has undergone more wetting, mixing and growth. Both granules have an irregular shape which is due to the slicing created by intermeshing screws within the barrel and, in the case of the granule shown in Figure 4-8 (b), the addition of 2 kneading blocks.
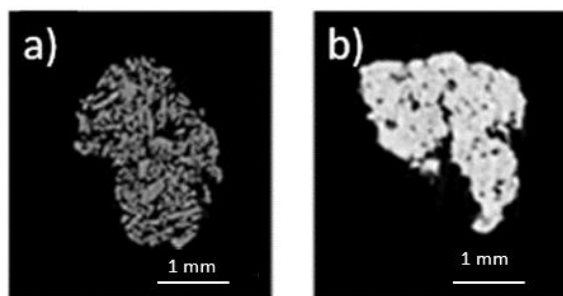
Figure 4-8 XRCT image of the centre slice of granules produced with (a) mannitol at L/S of 0.11 and conveying elements and (b) mannitol at L/S of 0.25 and 2 kneading zones.

The porosity of each batch of granules was measured and results are shown in Figure 4-9. Granules were chosen from each batch at random from within the 180 – 1400 µm size range. Due to the large amount of time required for each scan and only one granule being able to be imaged during each scan, only one granule for each material and process parameter was imaged. It should therefore be noted that this data is qualitative in nature and should be viewed with the limitations of XRCT (discussed in Section 3.4.4) in mind. For each material, the granule porosity reduces with increased L/S. This is a result of greater wetting and therefore agglomeration of granules as they are conveyed along the barrel. There is a large reduction in porosity when 2 kneading zones are used within the screw length.

There are limitations to XRCT for measuring granule porosity, for example, thresholding of the original image to a binary image is carried out by the operator and open to variability between each analysis. The resolution of the instrumentation is 2 µm, therefore pores below this size are not considered in the porosity calculation. It is also difficult to image multiple granules at once due to a reduction in resolution, making the sample size smaller than that which would be preferred to give preferable statistics. For the results presented in Figure 4-9, two granules

128

were imaged from each batch and the mean taken. This does not present statistically reliable data and solidifies the point that XRCT plays a larger role in qualitative rather than quantitative results.

Due to the spray-dried nature of Fast Flo and inherent porosity within the base material Figure 4-1(a) it may be assumed that the porosity of the resultant granules would differ to that of Pharmatose 200M. For the conveying only and 1 kneading zone set-up, Fast Flo produces granules of higher porosity which may indicate that the original structure is retained to a greater extent than that for Pharmatose 200M. However, for granules produced with 2 kneading zones and increasing L/S, a reduction in porosity for Fast Flo is seen when comparing to Pharmatose 200M. The increased shear force acting upon Fast Flo is likely to allow greater ingress of water into its original porous structure, allowing the material to be compacted together producing dense granules.
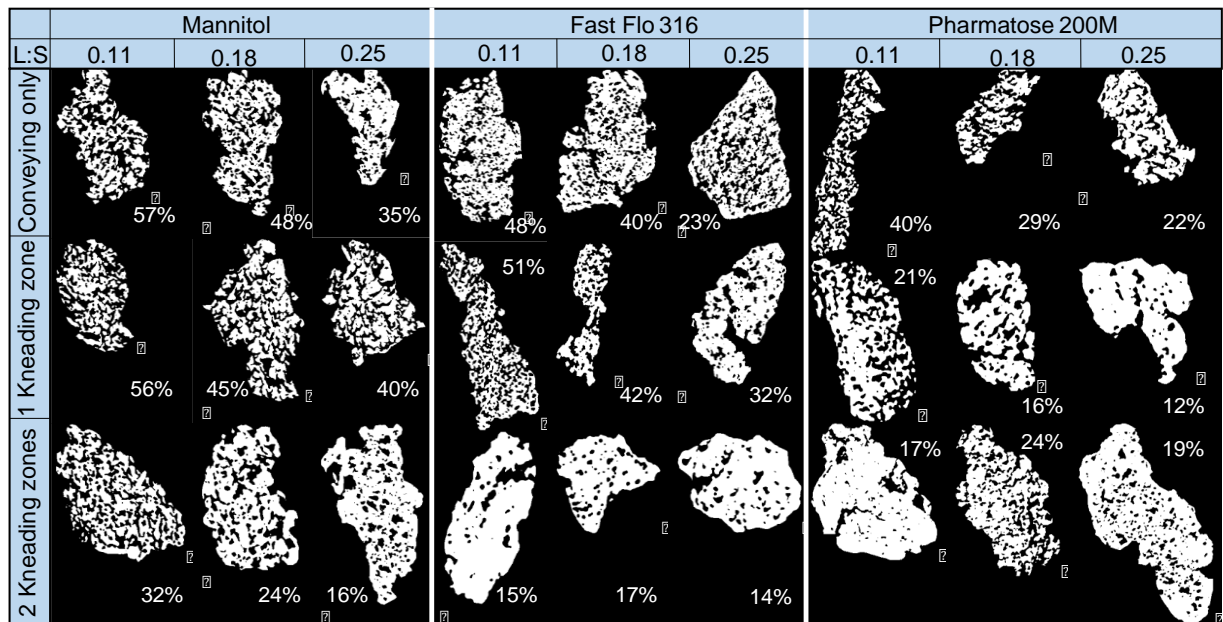
Figure 4-9 A matrix showing porosity values for granules produced from each material at varying L/S and TSG set-up.

Figure 4-10 shows material compaction occurring in a kneading area during TSG at steady state. The reduction in porosity is most likely due to the increased pressure on the material within each kneading zone and therefore compressive forces acting upon the granules to result in less porous structures (Thompson, 2015). However, because the addition of a second kneading section is situated before the granulation fluid inlet, kneading zones may produce enough compressive force to form agglomerates when dry.
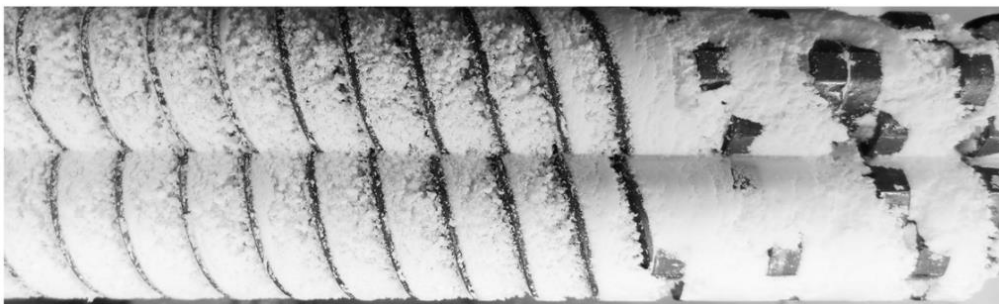
Figure 4-10 A photo showing the TSG barrel at steady state to demonstrate the high fill level within the kneading zone.

4.3.5   Investigating the role of the kneading zone prior to wetting

It should be noted that for screw configurations with one kneading zone, the kneading zone is located seven elements before the granule outlet (Figure 4-2). When a second kneading zone is added to the system it is located two element lengths before the liquid injection port. Even though any extra shear stress and compression acting upon the material from the addition of the second kneading zone is without binder, there is still a notable increase in granule size for all materials (Figure 4-5).

To investigate the effect of the kneading zone acting upon dry material, the TSG barrel was divided into 7 compartments. SEM micrographs of mannitol from each were taken after

stopping the equipment once steady state had been achieved. From Figure 4-11 it appears material taken from compartment 2 has already formed granule-like structures without the addition of any liquid binder. Granules from this compartment were fragile but well-formed and would be undergo the wetting process differently to the loose powder that would be present at the liquid injection port within a set-up containing conveying elements only.

Granule nucleus formation is described by capillary penetration of liquid through powder pores and the powder bed has been modelled as if it were a porous, non-deformable solid (Hapgood, et al., 2002). The wetting of a powder bed containing dry agglomerates would be different to that of a loose powder bed. Hapgood, et al. (2002) described the fluid drainage in a closley packed powder as being relitively uninhibited, much like the case of dry agglomerates in the current study. However, in irregular packed powder beds, macrovoids can form and as liquid penetrates into the powder bed the liquid front will be halted when the pore radius increases suddenly. The macrovid space does not contribute effectively to the capillary volume or surface area available for wetting. The increase in granule size and density in the case of two kneading zones being present is a result of the increased wetting at the start of the process.
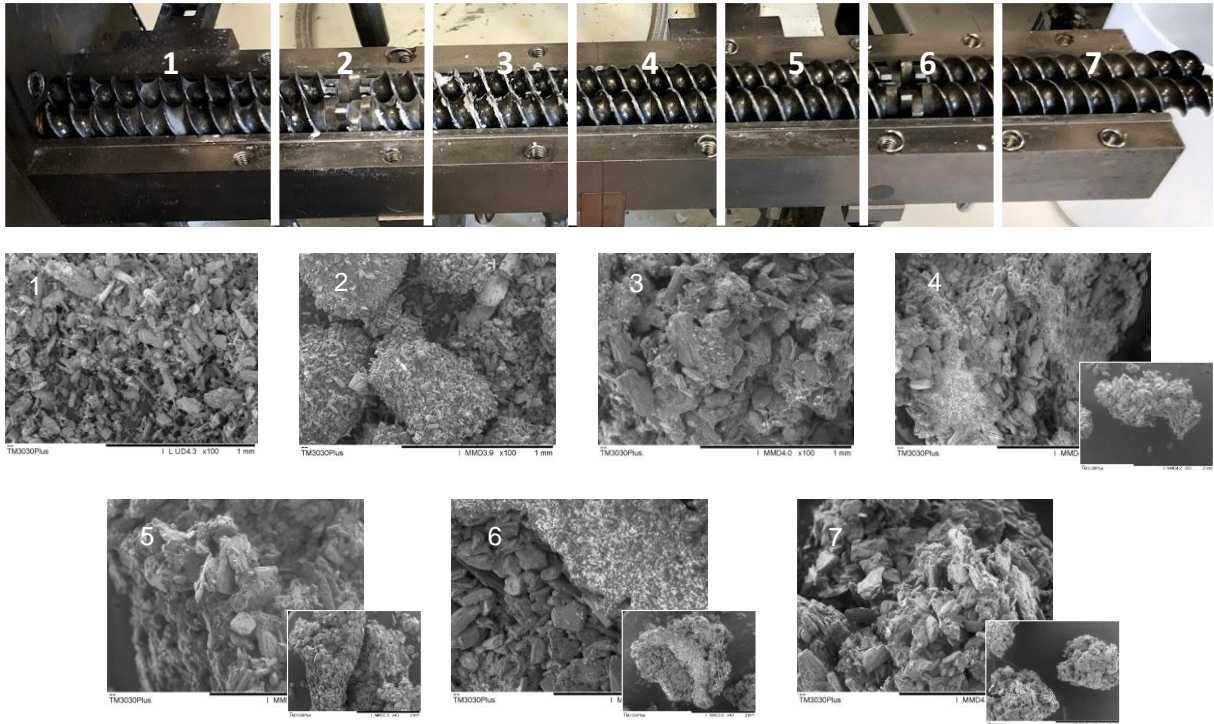
Figure 4-11 SEM micrographs of samples taken from compartments 1-7. Zones 2 and 6 are those with kneading blocks present and zone 3 is the liquid injection point. The process shown was run using mannitol, L/S 0.18 and 2 kneading zones.

4.3.6 Tabletability

A compaction study was performed using a compaction simulator (Merlin Powder Characterisation, Brierley Hill, UK) as described in Section 3.5.2. Results were used to plot the tabletability (tensile strength vs. compaction pressure) for batches of granules produced with conveying only elements and 1 kneading zone within the TSG barrel. Pitt et al. (2015) previously stated that, generally, a tablet tensile strength greater than 1.7 MPa will ensure the tablet is mechanically strong enough to withstand commercial manufacture and further manipulation before reaching the point of administration. However, tablets with a tensile strength of 2 MPa and greater should be the target to ensure a robust product. If the tablet

will not be subjected to large mechanical stresses, a tensile strength between 1 and 1.7 MPa may be allowable.

Figure 4-12 (a)-(c) shows the tabletability profiles for all three materials and process parameters.
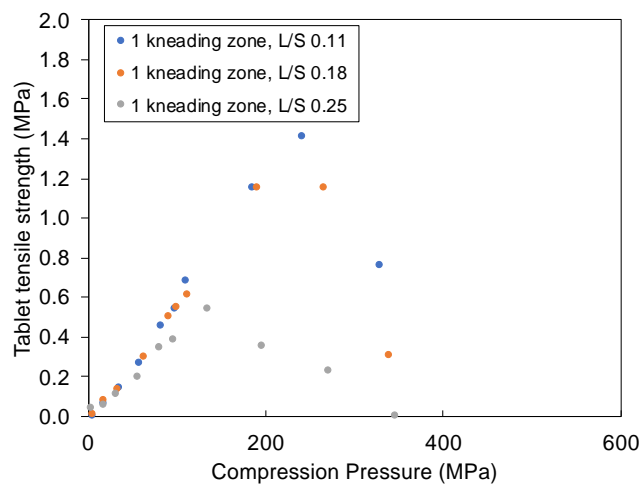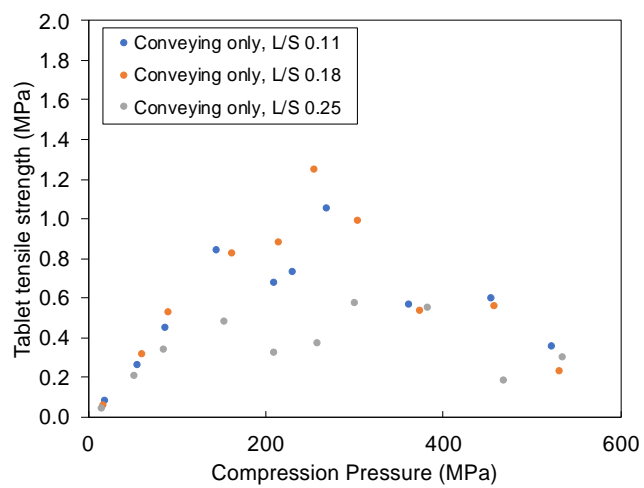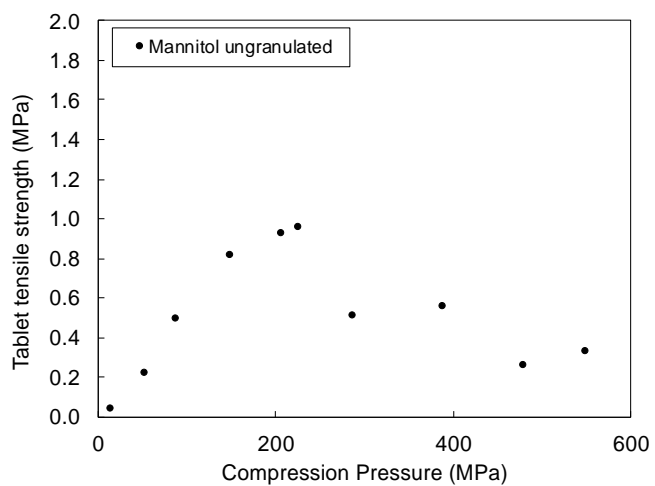
Figure 4-12 (a) Tabletability profiles for mannitol.
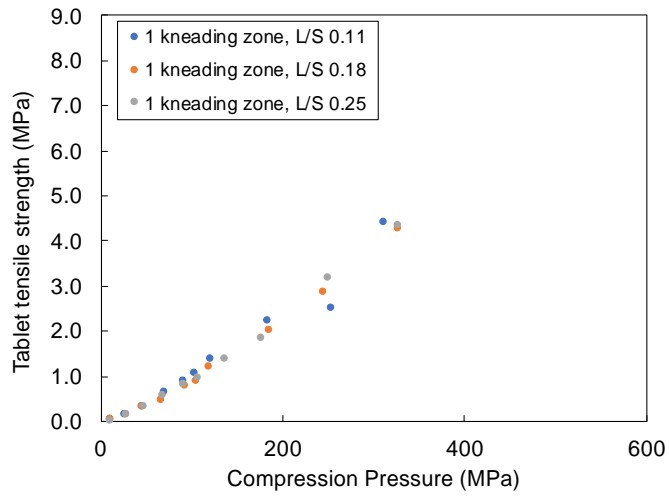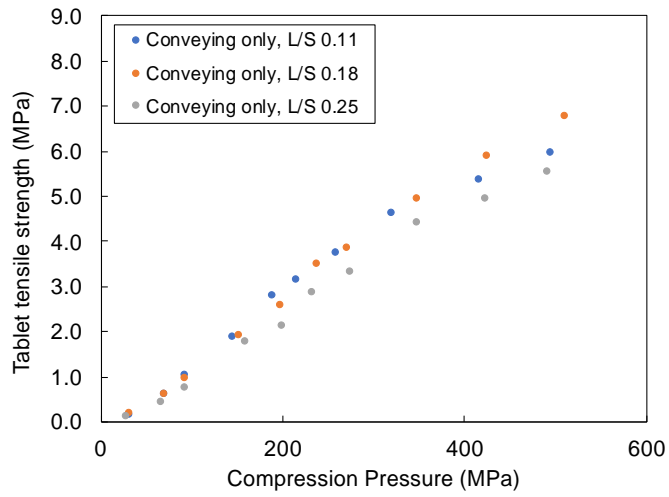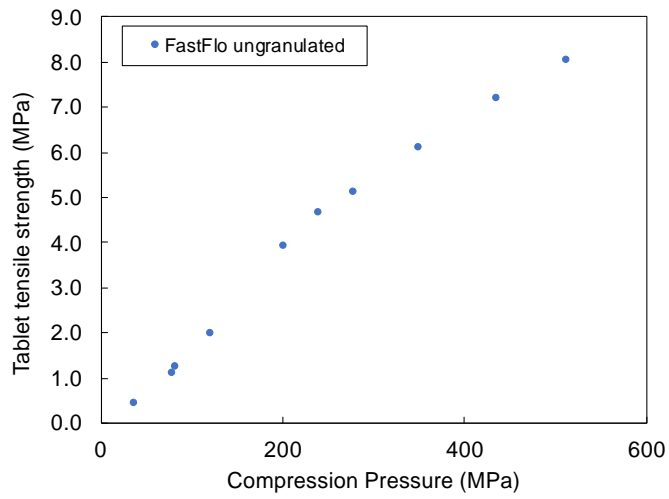
Figure 4-12 (b) Tabletability profiles for Fast flo.
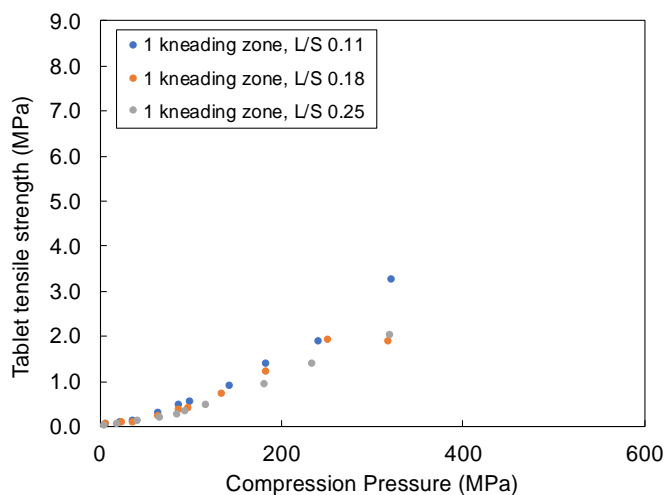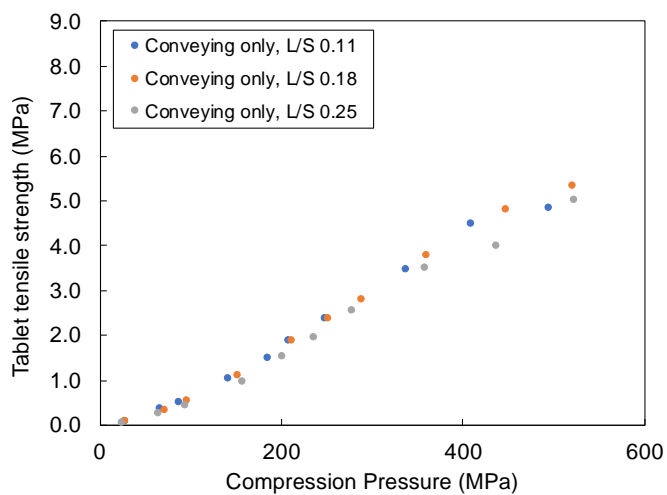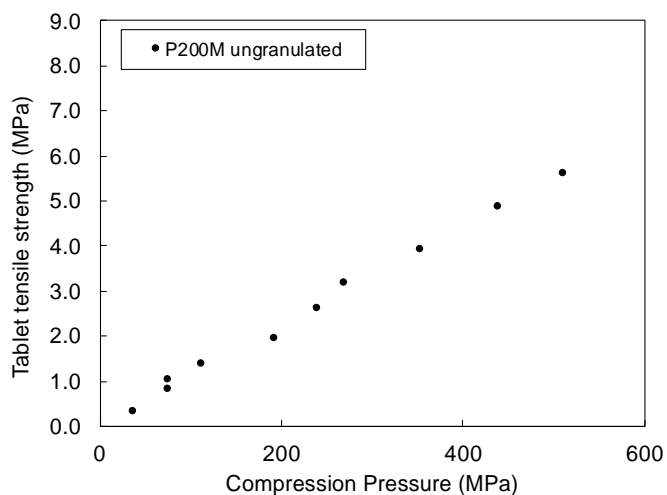
Figure 12 (c) Tabletability profiles for Pharmatose 200M.

Fast Flo produces tablets with a tensile strength above 1.7MPa starting with punch pressures of 120-190 MPa across all batches. Similarly, Pharmatose also starts to produce tablets with suitable tensile strength at around 200 MPa. Mannitol reacts very differently to compression and none of the batches produced tablets above 1.7 MPa. Mannitol gave the greatest yield of usable granules from earlier sieve analysis and produced granules with high porosity similar to Fast Flo. However, mannitol has a much lower tabletability than Fast Flo even though, as a material, it is easier to granulate (generally higher yields in the useable size range). Paul et al. (2019) investigated the tablet strength of different mannitol grades. A similar result to the current study was shown for the Pearlitol 160C grade, with an increase in tablet strength up to compression pressures of ~200 MPa and subsequent decrease in tablet strength. The finer, 25C grade did not show a similar drop in tabletability which agrees with the reduction in tabletability with increasing L/S, and therefore increasing granule size, in the current study. Paul et al. (2019) also found that there was a strong correlation between powder specific surface area (SSA) and tabletability, with higher SSA producing higher tablet strength. This also agrees with the current study, where a higher SSA would be expected for smaller granules and therefore exhibiting greater granule strength. This indicates that mannitol is likely to be highly dependent on available bonding surfaces for increased tablet strength.

Pharmatose shows a reduction in tabletability at L/S of 0.18 and 0.25 produced with 1 kneading zone. The Pharmatose granules produced with 1 kneading zone had considerably lower porosity than the granules produced with conveying only elements which may explain why they show a reduced tabletability. Tablets produced from Pharmatose are stronger than those produced with mannitol but not Fast Flo, suggesting that the decreased porosity of

Pharmatose granules over Fast Flo granules has a large effect on their tabletability. When ungranulated Fast Flo is compressed, it produces tablets above a tensile strength of 1.7 MPa at a pressure as low as 120 MPa, which is to be expected because the base material is porous and compactable, therefore producing stronger tablets without prior granulation. Ungranulated Pharmatose requires a compression pressure of approximately 200 MPa to produce tablets with a tensile strength above 1.7 MPa. Pharmatose, in contrast to Fast Flo, is a crystalline material with very little porosity, resulting in its compressibility being less than that of Fast Flo.

Neither Pharmatose nor Fast Flo gave an increase in tabletability after granulation. However, tabletability was increased for batches of mannitol produced with 1 kneading zone and L/S of 0.11 and 0.18. When the L/S was increased to 0.25 there was a very large reduction in tabletability with both conveying only elements and 1 kneading zone. The UCC model that has been applied to high shear wet granulation by Nguyen, et al. (2013) enables the prediction of tablet strength as a function of liquid added, wet massing time or binder flow rate. However, this model has been shown to accurately predict tablet strength for plastically deforming materials but less so for materials that undergo brittle fracture. Materials that undergo brittle fracture produce new bonding surfaces as compression takes place. Fragmentation is unlikely to take place to the same extent across different materials and is therefore difficult to model. The UCC model could not be applied to the current study, agreeing that it cannot be used for materials that undergo brittle fracture.

It was reported that an increase in tabletability was observed for mannitol, in agreement with the current study. Vanhoorne et al. (2016) previously reported that δ-mannitol undergoes

moisture-induced transformation to β-mannitol which improved its tabletability. The mannitol used in the current study is α-mannitol and further tests would be required to find if it has changed during wet granulation to confirm if this is the reason for its increased tabletability with specific process parameters.

4.3.7   Compaction modelling

Figure 4-13 shows stress strain curves for the three base materials in the study measured by uniaxial compaction. The difference in shape of the curves shows that there are some mechanical differences of the materials. Fast flo appears to show the highest level of deformation per unit stress. However, a stress strain curve alone does not provide enough information to give a definitive answer as to the mechanical properties of a powder.
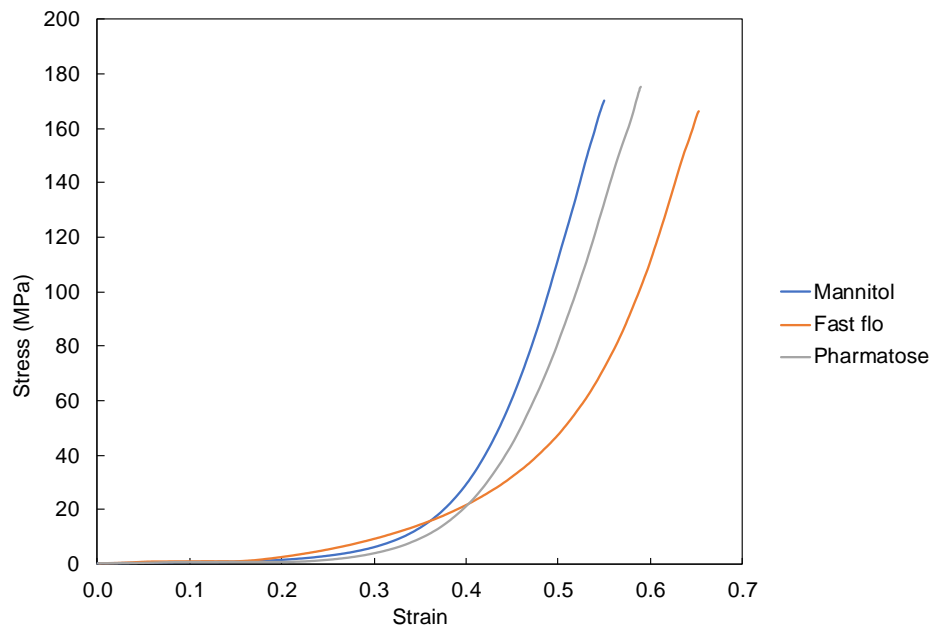
Figure 4-13 Stress strain curves for mannitol, Fast flo and Pharmatose base materials.

Upon compression of a granular bed, there is complex behaviour occurring due to the presence of both intergranular and intragranular pores. Kawakita and Adams models were applied to force displacement data to gain an understanding of the strength of individual granules during compaction (Kawakita & Ludde, 1970; Adams, et al., 1994).

The Kawakita model previously discussed in Section 2.7.3 was used. Linearisation of Equation 2-11 provides a plot from which the slope of stress divided by strain (σ/ε) as a function of compaction pressure will give the reciprocal of a and the intercept on the x axis will give the value for $1/ab$. The constant, a, relates to the initial powder porosity and the reciprocal of b gives an indication of the yield stress of particles. Figure 4-14 shows an example Kawakita plot, providing a good fit to experimental data within the range of 35 to 150 MPa, with R^2 value greater than 0.99. Kawakita plots were produced for each material and condition and used to identify the regions within which the Kawakita model gave a good fit to the experimental data. The regions were also chosen based on the areas where much of the plastic deformation would be expected to occur, where substantial changes in strain per unit stress occurs.

At very low compaction pressures (~1 MPa) there is a large deviation from the linearity of the rest of the plot. This was previously observed by Yap, et al. (2008) who provided a possible explanation as the transition from elastic to plastic deformation. This non-linear data was excluded from all plots to ensure a good fit to the experimental data.
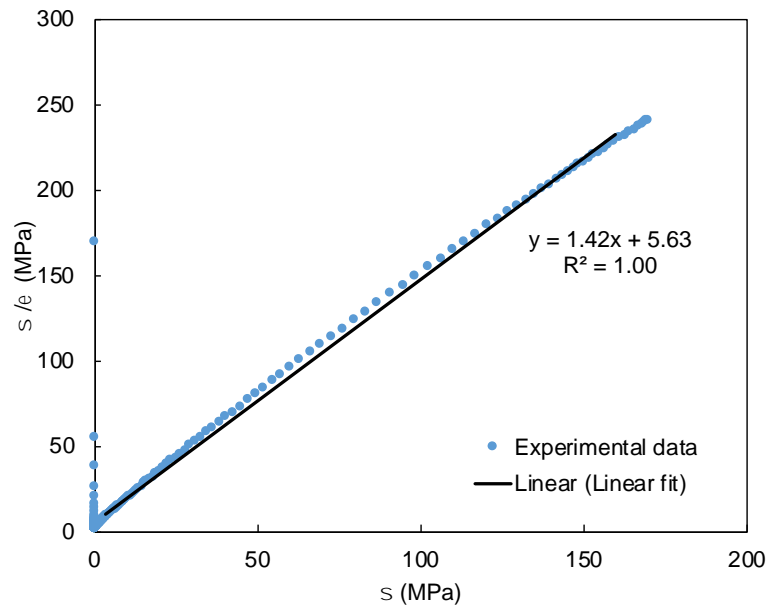
Figure 4-14 An example Kawakita plot for uniaxial compaction of mannitol, 0.11 L/S ratio and conveying only elements.

The Kawakita plot takes the initial packing of the powder bed into account (V_0) and determining this value is a sensitive process. Before compression the granule bed was filled into the die and tapped six times, therefore altering the degree of compaction by particle rearrangement and lowering the value for the constant, *a*, that is recorded.

The Kawakita parameters *a* and *b*$^{-1}$ derived from uniaxial compaction experimental results are shown in Table 4-2. For mannitol, values of *a* for granulated material is similar across the range of screw configurations and L/S, indicating little change in porosity obtained during the TSG process across the differing process parameters. For both lactose powders, there is a slight increase in the value of *a* which aligns with a decrease in porosity as more water or kneading sections are added into the system. The values for *a* are similar across lactose materials, showing that there is similar porosity of the granulated lactose materials with little dependence on the original manufacturing process of each particular brand.

The b^{-1} parameter values presented in Table 4-2 show that the original powders are stronger than the granulated material. This is to be expected as the granulated material is porous and therefore expected to pose a lower yield stress. For mannitol, there is an increase in granule strength with increasing L/S. Again, granules are less porous and therefore stronger as L/S is increased. The strongest granules are produced with two kneading zones and a L/S of 0.11 which corresponds to dense granules of low porosity as shown in Figure 4-9.

For Fast Flo, there is an increase in granule strength with increasing L/S for each configuration. However, the weakest granules are produced with two kneading zones and a L/S of 0.11. This may indicate that Fast Flo granules are more susceptible to breakage within the TSG barrel when two kneading zones are present and without extra water from increased L/S, there is not continued consolidation to produce strong granules. The results for Pharmatose seem somewhat anomalous and there is a decrease in granule strength with a conveying only set-up and increasing L/S. There is also a decrease in granule strength for two kneading zones and increasing L/S. This result does not appear to be explained by a real phenomenon that is occurring. It is most likely to be due to experimental error, however further investigation would be required to confirm this.

Table 4-2 Kawakita parameters for each material based on two repeats (standard error is indicated in parentheses).

Material	Configuration	L/S ratio	a	b^{-1} (MPa)	R^2
Mannitol (original powder)			0.66 (0.01)	7.13 (0.04)	0.991
Mannitol	C	0.11	0.53 (0.01)	4.55 (0.02)	0.990
	C	0.18	0.52 (0.01)	5.24 (0.01)	0.990

Material	Configuration	L/S ratio	a	b^{-1} (MPa)	R^2
	C	0.25	0.53 (0.01)	7.78 (0.02)	0.997
	1K	0.11	0.49 (0.01)	4.98 (0.04)	0.992
	1K	0.18	0.49 (0.01)	5.00 (0.01)	0.999
	1K	0.25	0.49 (0.01)	5.00 (0.02)	0.997
	2K	0.11	0.53 (0.01)	9.02 (0.02)	0.992
	2K	0.18	0.52 (0.01)	6.62 (0.02)	0.990
Fast flo (original powder)			0.51 (0.01)	15.01 (0.04)	0.991
	C	0.11	0.46 (0.00)	8.23 (0.01)	0.991
	C	0.18	0.45 (0.01)	8.89 (0.02)	0.990
	C	0.25	0.48 (0.02)	9.00 (0.02)	0.997
Fast flo	1K	0.11	0.46 (0.01)	7.18 (0.01)	0.991
	1K	0.18	0.46 (0.01)	7.79 (0.02)	0.991
	1 K	0.25	0.47 (0.01)	7.86 (0.02)	0.997
	2K	0.11	0.49 (0.02)	6.86 (0.01)	0.995
Pharmatose (original powder)			0.55 (0.01)	20.73 (0.03)	0.991
	C	0.11	0.47 (0.02)	8.33 (0.02)	0.991
	C	0.18	0.47 (0.01)	7.89 (0.02)	0.994
	C	0.25	0.48 (0.02)	7.53 (0.03)	0.994
	1K	0.11	0.47 (0.02)	6.83 (0.01)	0.998
Pharmatose	1K	0.18	0.48 (0.01)	8.29 (0.03)	0.991
	1K	0.25	0.50 (0.02)	7.75 (0.02)	0.993
	2K	0.11	0.49 (0.02)	7.16 (0.02)	0.991
	2K	0.18	0.48 (0.01)	6.55 (0.01)	0.990

Figure 4-15 shows data from the compaction of mannitol produced at a L/S of 0.11 and with conveying only elements for natural strain of 0 to 1.2. The plot shows both the experimental data and model first used by Adams, et al. (1994). The model was fitted to the experimental data using the solver function (Excel, Version 16.49, Microsoft) to extract values of α and τ_0. All data for each material and granulation setting was treated in the same way and a good fit was achieved above natural strains of 0.2. Values for α and τ_0 for each material and configuration are shown in Table 4-3. Differences at low strain levels may arise from differences in the preparation of the initial granule bed. Adams, et al. (1994) state within experimental methods that the die should be tapped to remove any irregularities. For the purpose of the current study, the die was tapped six times before each compression in an attempt to keep it the same throughout the experiment. However, due to operator variation, there is likely to be a difference in the initial rearrangement caused by tapping each time.
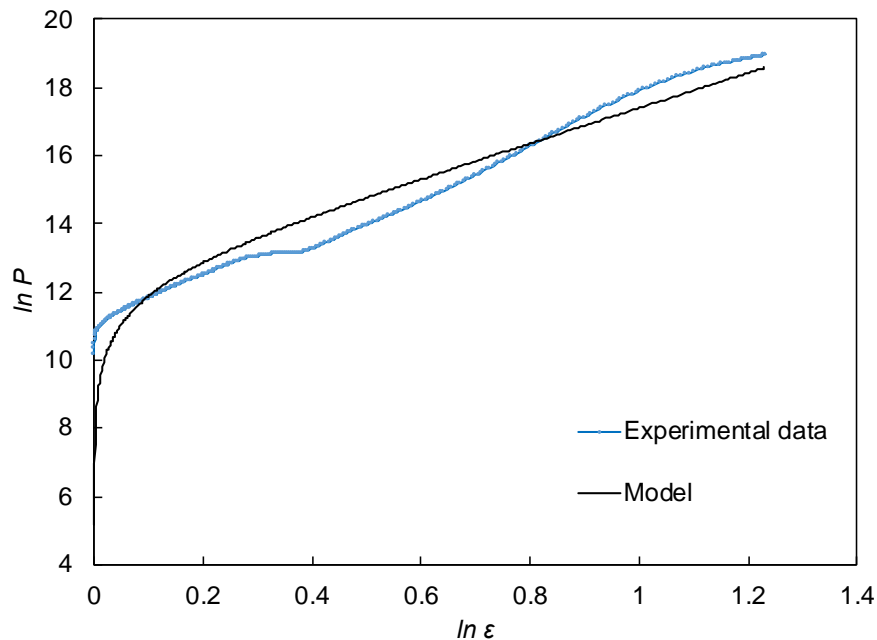
Figure 4-15 The Adams relationship for uniaxial compaction of mannitol, L/S 0.11 and conveying only elements.

144

Table 4-3 Adams model parameters for each material based on two repeats (standard error is indicated in parentheses).

Material	Configuration	L/S ratio	α	τ_0 (Mpa)
Mannitol (original powder)			10.27 (0.51)	1.55 (0.09)
Mannitol	C	0.11	5.12 (0.92)	1.10 (0.07)
	C	0.18	5.06 (0.22)	1.24 (0.09)
	C	0.25	8.50 (0.51)	0.40 (0.09)
	1K	0.11	5.60 (0.24)	1.41 (0.08)
	1K	0.18	4.64 (0.51)	1.14 (0.07)
	1K	0.25	4.59 (0.92)	1.16 (0.07)
	2K	0.11	5.82 (0.24)	1.49 (0.06)
	2K	0.18	5.54 (0.51)	1.17 (0.09)
Fast flo (original powder)			4.32 (0.81)	8.57 (0.05)
Fast flo	C	0.11	4.49 (0.57)	1.55 (0.01)
	C	0.18	4.19 (0.68)	1.92 (0.09)
	C	0.25	4.50 (0.58)	2.46 (0.02)
	1K	0.11	4.41 (0.71)	1.52 (0.05)
	1K	0.18	4.24 (0.91)	1.95 (0.09)
	1 K	0.25	4.12 (0.57)	2.38 (0.05)
	2K	0.11	4.70 (0.87)	2.18 (0.06)
Pharmatose (original powder)			6.83 (0.52)	3.20 (0.02)
Pharmatose	C	0.11	5.06 (0.67)	1.14 (0.02)
	C	0.18	4.95 (0.91)	1.06 (0.03)
	C	0.25	4.82 (0.78)	2.21(0.09)

Material	Configuration	L/S ratio	α	τ_0 (Mpa)
	1K	0.11	4.83 (0.72)	1.06 (0.03)
	1K	0.18	4.92 (0.81)	1.58 (0.09)
	1K	0.25	4.77 (0.73)	2.21(0.09)
	2K	0.11	5.10 (0.81)	1.29 (0.08)
	2K	0.18	4.93 (1.00)	1.00 (0.09)

Two uniaxial compactions of each material were carried out and the data was analysed based upon the first compaction. The α parameter suggests that, overall, more friction was present in the die for compressions of mannitol than either lactose grade. No other specific correlations can be made. The τ_0 parameter shows that the base material provides the strongest granule strength and, for both lactose grades, there appears to be an increase in granule strength with increasing L/S. For mannitol, granule strength decreases with increasing L/S.

When comparing Kawakita and Adams models, the following can be concluded:

I. The Kawakita model gives excellent fit to data above 1 MPa which is shown by consistently high R^2 values.

II. The Adams model can be applied over the full range of strain (0 – 1.2). However, there was not a good fit of the model to experimental data for any material or configuration.

A strong correlation between the Kawakita b^{-1} parameter and Adams τ_0 parameter has been shown by other authors (Adams, et al., 1994; Yap, et al., 2008). However, upon plotting the two parameters for the current study, no correlation was found (Figure 4-16). This is due to

the poor fit of the Adams model which may be due to inconsistent rearrangement during tapping of the die before the compression process. The Kawakita model is in a simpler form making it easier to apply to multiple powders, therefore this model is favored when comparing granules in the current study.
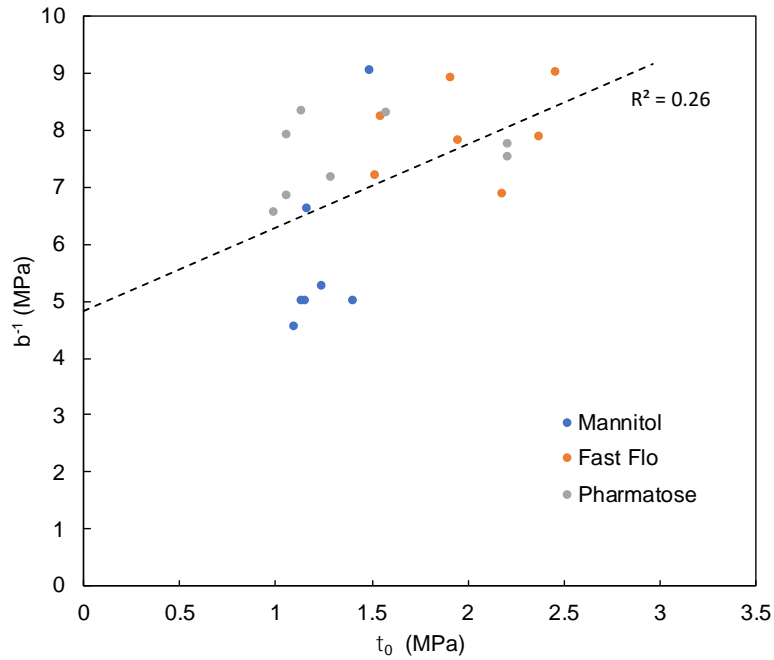
Figure 4-16 A plot of the Kawakita b^{-1} and Adams τ_0 parameters. The trendline is shown for all materials grouped together but materials are also shown separately for comparison.

4.3.8 Investigating hygroscopic powders

In the previous sections of this chapter, only non-hygroscopic powders were used. It was shown that water content plays a vital role in deciding the tensile strength of resultant tablets. Therefore, the decision was made to investigate hygroscopic powders, changing the water content of the powders by controlling the relative humidity (RH) they were stored at. Hydroxypropyl cellulose (HPC) and microcrystalline cellulose (MCC) were chosen as

hygroscopic powders. This section of experimental work was carried out as a feasibility for future work only. In the interest of experimental time, only one kneading zone and the lowest L/S ratio was used. As the materials being granulated were hygroscopic it was hypothesised that they would become 'over-wetted' quickly so the least intense process parameters were chosen.

4.3.9 Granulation and tableting of hygroscopic powders

Granulation was carried out using TSG set up, as before, with one kneading zone and 0.11 L/S using deionized water as the granulation fluid. Desiccator cabinets were set up at 65, 75 and 85% RH for storage of primary powders and granules. Before granulation, powders were taken from bulk containers stored at ambient temperature and humidity. Once granulation was carried out, granules were split into six smaller batches (~250 g each). The first three portions of the batch were left to dry at ambient room temperature and humidity for 72 hours, while the other three portions were placed in each of the desiccator cabinets. After 72 hours, the dried granules were put into each of the three desiccator cabinets. The drying and storage conditions are simplified in Table 4-4. After leaving the granules in desiccator cabinets for 28 days to reach equilibrium, they were tabletted using the Zwick Universal testing machine as in previous experiments. 500 mg of granules were compressed at 20 kN within a 10 mm die (Specac, Kent, UK) and at a speed of 4 mm/min.

Table 4-4 Drying and storage conditions for 6 granule batches. The symbol '-' indicates no drying step where granules were stored in the same conditions as eventual storage.

Batch	Drying step (72 hours)	Storage conditions for 28 days after initial 72 hours
1	20 °C/38% RH	20 °C/65% RH
2	20 °C/38% RH	20 °C/75% RH
3	20 °C/38% RH	20 °C/85% RH
4	-	20 °C/65% RH
5	-	20 °C/75% RH
6	-	20 °C/85% RH

Tensile strength testing for tablets produced from granules at each storage condition was carried out using the Zwick Universal testing machine at a speed of 1 mm/min and results are shown in Figure 4-17.
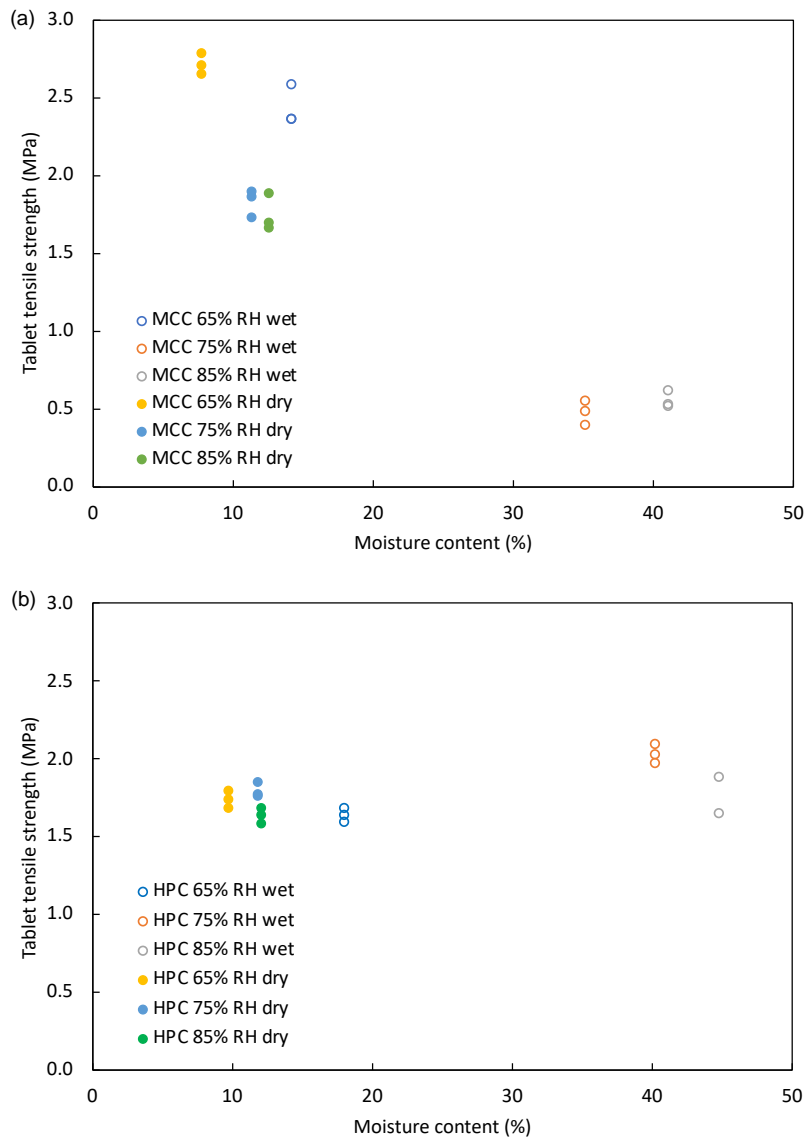
Figure 4-17 MCC (a) and HPMC (b) tablet tensile strength after granules have been stored in 65%, 75% and 85% RH immediately after granulation (wet, open symbols) and stored in 65%, 75% and 85% RH after drying for 72 hours (dry, closed symbols).

The plot shown in Figure 4-17 (a) confirms that for granules consisting of MCC that are dried at ambient temperature and humidity exhibit a reduction in tensile strength when stored at 75% or 85% RH. It is likely that the granules absorbed increasing amounts of moisture which disrupts the tablet bonding process due to the hygroscopic nature of MCC. This reinforces the

importance of controlled drying and storage conditions after granulation. The method of reduction in tabletability due to increased moisture is likely to be explained on the molecular level and dependent on where water lies within the tablet structure. As MCC is a plastic and hygroscopic material, water could potentially disrupt the cellulose chains causing expansion. Zarmpi, et al. (2017) indicated the importance of a Quality by Design (QbD) approach to excipient variability due to differences in, for example hygroscopicity, not only between materials but also between manufacturers of the same excipient. Therefore, it should be noted that an in depth understanding of material attributes is required to place the correct level of risk around each part of the manufacturing process.

HPC, although a hygroscopic material similar to MCC, showed a difference in tablet tensile strength behaviour. Tablets exhibited a similar level of strength independent of whether the granules were dried prior to placing in increasing levels of RH or having no drying step. This could be due to the material already being saturated at ambient RH and therefore there is no additional water uptake at increasing RH that could disrupt tablet integrity. Again, an understanding at the molecular level would be required to deconvolute the lack of change in tablet tensile strength with increased available moisture.

The effect of moisture on tablet tensile strength within hygroscopic materials is interesting and provides a potential impact on the prediction of tabletability. This is of particular interest within the pharmaceutical industry due to the reduction in pre-formulation studies if tabletability can be predicted based on base material attributes. The link between moisture and tablet tensile strength is a subject that will be studied further within this thesis.

4.4 Conclusions

The TSG investigation discussed within this chapter has led to the following conclusions:

I.   Granule size increases with increasing L/S and number of kneading zones. The addition of more granulating liquid has a higher impact on Fast Flo lactose than the other materials which is potentially a result of its porous nature due to its spray-dried production method.

II.   There is minimal impact on granule shape with changing process parameters. However, granule shape appears to be more reliant on TSG barrel set-up than L/S.

III. When a second kneading zone is added to the barrel length before the liquid addition port, there is evidence of agglomeration taking place without the presence of granulating fluid. This indicates that the kneading zone imparts considerable shear on the material leading to compaction and therefore small agglomerate formation.

IV.   For each material, the granule porosity reduces with increased L/S due to greater wetting and therefore agglomeration of granules. There is a large reduction in porosity when 2 kneading zones are used within the screw length which is expected due to the increased shear forces acting upon the material.

V.   Resultant tablet tensile strength is different for each material. Fast Flo produces the strongest tablets followed by Pharmatose and finally mannitol. A reduction in tablet tensile strength of granulated versus directly compressed base material is seen for Fast Flo and Pharmatose. However, in certain circumstances, an increase in tabletability after granulation is observed for mannitol.

VI. When comparing Kawakita and Adams models the Kawakita model is in a simpler form making it easier to apply to multiple powders. A more preferable fit to experimental data was also seen for the Kawakita model. Overall, there is an increase in granule strength with increasing L/S and number of kneading zones.

VII. For MCC, there is a high dependency on drying and/or storage RH for tablet tensile strength due to its hygroscopic nature. HPC, although hygroscopic, shows less dependency on storage RH. The relationship between MCC, water and tablet tensile strength will be investigated further in later chapters of this thesis.

The results presented in this section add to current literature in the form of a head to head comparison of single excipients processed with the same set of TSG process parameters. There have been several previous studies that have studied the effects of multiple process parameters on formulations (Sun & Thompson, 2009; Dhenge, 2013; Yu, et al., 2014; Vanhoorne, et al., 2016) which are unable to account for the properties of the resultant granules based on individual base material characteristics. Some prior research has granulated single excipients using TSG (Lute et al., 2018; Khorsheed, et al., 2019), however the effects of a kneading zone acting upon dry material was not studied and therefore the current study provides additional information.

5 Investigating the role of moisture in tablet compaction and tensile strength

5.1 Introduction

Identifying optimum tabletability process parameters for a formulation relies upon compaction testing and trial and error methods which is costly in both time and money. This step could be vastly reduced if there was an ability to predict the performance of a formulation within a given process. For this to be feasible there needs to be an understanding of the chemical, mechanical and physical properties of a powder and how these may impact the available bonding area during tableting. The dominating bond mechanism and the surface area over which these bonds are active are the main factors involved in determining the tabletability of a powder (Persson, et al., 2016).

The formation and use of bonding area within a tablet is related to the compaction conditions, mechanical properties and particulate properties (Sun, 2011). It has previously been found that plastic deformation is the most important mechanism for creating a large bonding area and this is affected by moisture for certain materials (Sun, 2008; Sun, 2011). However, plastic deformation does not create extra surface area, therefore it could be possible that the bonding area is increased by making the adjoining areas more intimate. Conversely, brittle fracture creates new surface area as compression is undertaken but effective bonds are not necessarily created between these areas.

Tablet tensile strength may vastly change in response to changes in moisture levels adsorbed or absorbed during storage (Sun, 2008), therefore the hygroscopicity of a material is an

154

important property to investigate before tableting. The addition of moisture may be of benefit to the final tablet strength. However, there is likely to be a need to quantify the 'ideal' moisture content in order to produce a tablet of preferential strength. This study aims to investigate the effect of moisture on tabletability for materials of various hygroscopicity in order to ascertain the extent of the role water plays in tablet bonding mechanisms.

5.2 Materials and methods

5.2.1 Materials

Four different, commonly used excipient powders were used in this study to provide a range of material properties (Figure 5-1). The powders used were:

- MCC (Avicel® PH101, FMC, Ireland), a semi-crystalline powder which is plastically deforming, hygroscopic and has a particle d_{50} of 70 μm.
- Starch 1500 (Starch 1500, Colorcon, USA), a partially pregelatinized maize starch. Starch is also hygroscopic and has a d_{50} value of 79 μm.
- α-lactose monohydrate (Pharmatose® 200M, DFE Pharma, Germany), a crystalline, non-hygroscopic material with a d_{50} of 35 μm.
- Dicalcium phosphate dihydrous (DCPD) (Di-Tab®, Innophos, USA) which is crystalline, non-hygroscopic and free-flowing. It has a d_{50} of 175 μm, making it the largest of the four materials.
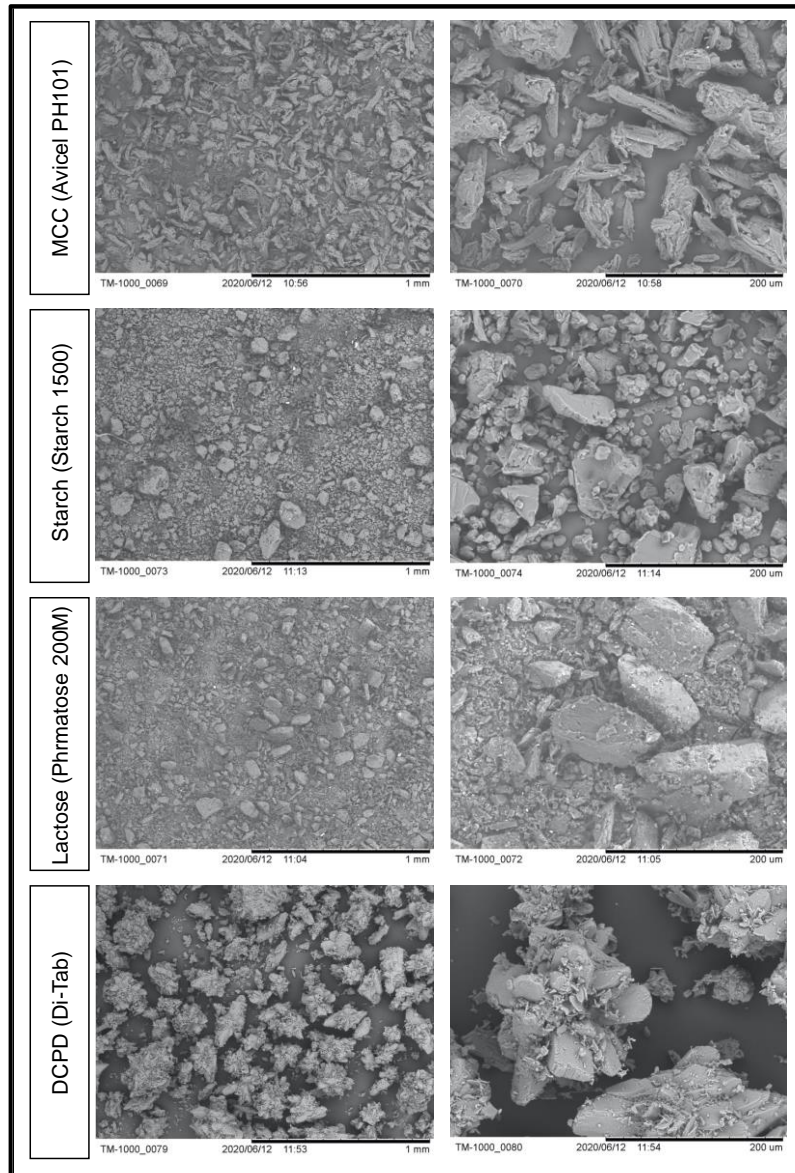
Figure 5-1 Scanning electron micrographs of the materials used within the study.

The powders were placed in humidity chambers from bulk containers as received and equilibrated for at least 28 days in Petri dishes to provide a shallow powder bed for moisture penetration. Saturated salt solutions were used to provide 11% (lithium chloride), 32% (magnesium chloride) and 55% (magnesium nitrate) RH. The mass of powders was recorded regularly to ensure the equilibrium of moisture content had been reached prior to running experiments.

5.2.2   Methods

Particle size distribution was carried out using laser diffraction as described in Section 3.4.2.

Particle morphology was assessed using scanning electron microscopy (SEM) as described in Section 3.4.3.

The *moisture content* of each powder was measured using a halogen moisture balance as described in Section 3.4.1. The moisture content of each powder was also verified by dynamic vapour sorption (DVS) for each powder to ascertain if moisture equilibrium had indeed been reached upon storage at 28 days. DVS was carried out according to the method described in Section 3.4.1.

True density was analysed using a helium pycnometer (AccuPyc II 1340, Micromeritics, UK) according to the method detailed in Section 3.4.5.

Bulk and tapped densities were investigated according to European Pharmacopoeia methods (EDQM, Council of Europe, 2014) detailed in Section 3.4.5.

Tablet compression was carried out using a 10 mm flat-faced die (Specac, Kent, UK) and universal testing machine (Zwick Roell Z030, Leominster, UK). Powders were removed from storage and tabletted in minimal time (maximum of 30 minutes) to ensure the effects of ambient room temperature and humidity were minimal. The moisture content of each powder was analysed immediately before tableting using a moisture analyser (HC103, Mettler Toledo, UK). The die was brushed with magnesium stearate 1% w/w in acetone using a paint brush and dried before each compaction. Powders were weighed (300 mg ± 20 mg) and

manually filled into the tablet die before tapping six times and placing onto the compression platform. Compactions were carried out at a speed of 10 mm/min and 6 compression pressures ranging between 30 and 390 MPa. Tablet tensile strength analysis was carried out by diametrical compression of each tablet using a universal testing machine (Zwick Roell Z030, Leominster, UK) as described in Section 3.5.4, no more than two hours after production. In previous literature, for example that of Egart, et al. (2014), diametrical compression is undertaken 24 hours after compression in order to assess the elastic recovery of the material. However, for the current study the short-term mechanics dependent on the water content of each material were of higher interest, therefore a shorter time frame for diametrical compression was used to ensure no drying effects would change the strength of the materials.

5.3   Results and discussion

5.3.1   Particle size distribution

Particle size analysis results are presented as cumulative distribution, Q3 (%) (Figure 5-2 (a)) and volume density distribution, q3 (Figure 5-2 (b)). Table 5-1 details the size parameters d_{10}, d_{50}, d_{90} and span. The average values across three measurements are presented with standard deviations. MCC is a mono dispersed system, lactose and starch appear to have three populations and DCPD is bimodal.

(a)

(b)
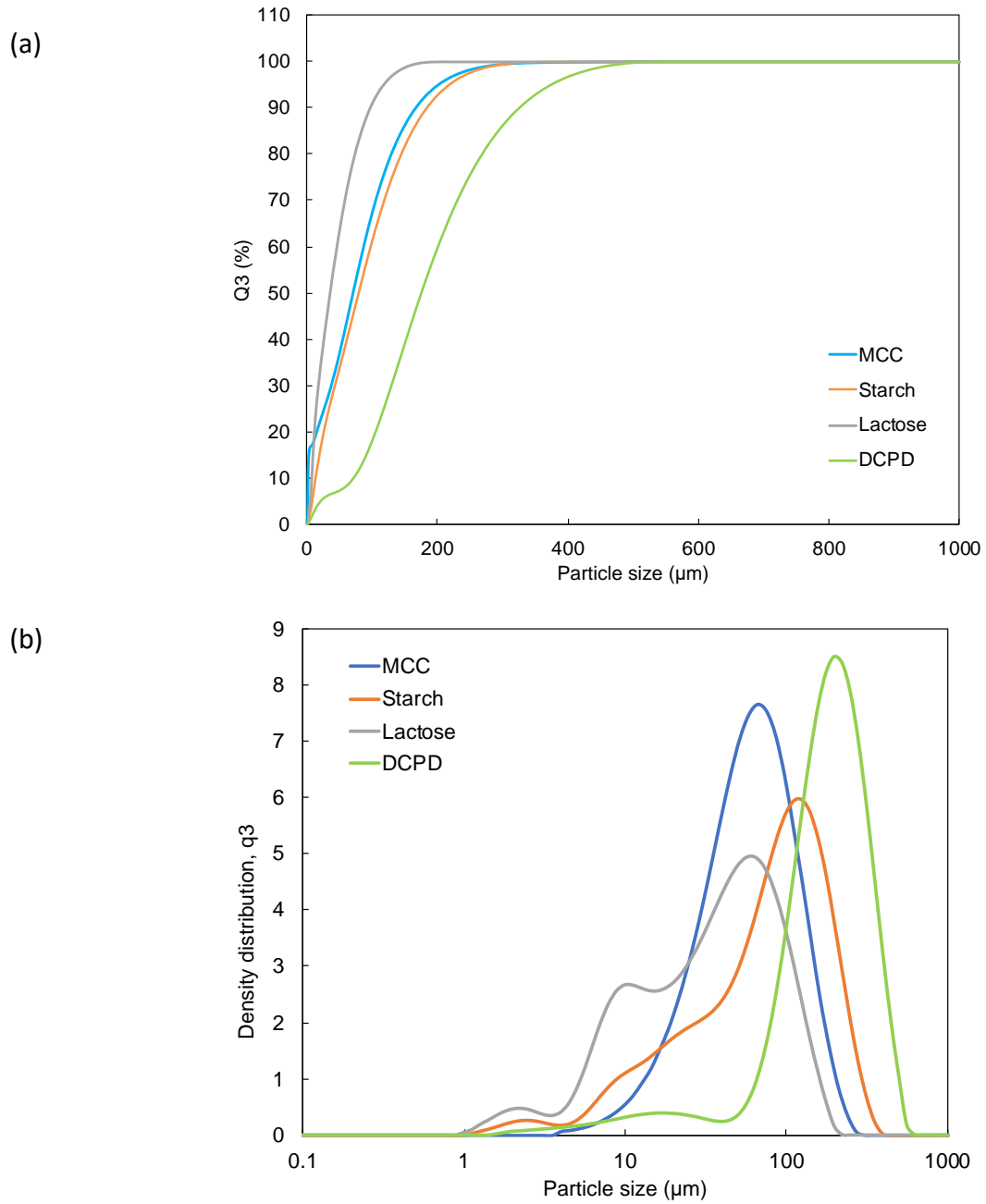
Figure 5-2 (a) The cumulative size distributions of each material and (b) Density distributions for each material. Results shown as the mean of three measurements.

Table 5-1 Particle size values for each material. Results are shown as the mean of three measurements ±SD (in parentheses).

Material	Size parameter	Value
MCC	d_{10} (µm)	23.5 (0.4)
	d_{50} (µm)	63.8 (2.1)
	d_{90} (µm)	139.0 (1.1)
	Span	1.8
Starch	d_{10} (µm)	12.8 (0.3)
	d_{50} (µm)	78.8 (1.9)
	d_{90} (µm)	182.9 (5.6)
	Span	2.2
Lactose	d_{10} (µm)	6.9 (0.1)
	d_{50} (µm)	35.0 (1.0)
	d_{90} (µm)	96.3 (1.4)
	Span	2.6
DCPD	d_{10} (µm)	71.4 (4.4)
	d_{50} (µm)	174.9 (0.5)
	d_{90} (µm)	324.6 (3.8)
	Span	1.5

DCPD has the largest particle size with a d_{50} of 175 µm. From Figure 5-3 it is possible to see more detailed structural information for DCPD and it appears that the material is made up of clusters of large crystals with smaller crystals deposited amongst them. This agrees with the description of Di-Tab provided by the manufacturer in that it is a granular form of dicalcium phosphate (Innophos, 2021). The smaller crystals that can be seen are likely to be tightly bound to the larger crystals as the d_{10} for DCPD is also large (71 µm) and, by eye, the small crystals would be considerably below this.

Lactose, similarly to DCPD, is a brittle material and has a smaller d_{50} which will provide some indication of size effects versus structural properties during compaction. Lactose is larger than both MCC and starch but has a smaller d_{10} which may be a result of its brittle nature and smaller fragments breaking off the larger crystals during manufacture or storage. According to the manufacturer of Pharmatose 200M (DFE Pharma, 2021) this grade of lactose is a highly consistent crystalline and mechanically milled product. The size parameters shown in Table 5-1 are in close agreement to those provided by the manufacturer, showing control over the milling process.

Starch, although similar, is larger in size than MCC. Both are smaller than lactose and DCPD but have larger d_{10} values than lactose.

5.3.2   Particle shape

The SEM images in Figure 5-3 show that MCC and lactose have a more elongated shape than the other materials, while lactose comprises a mixture of large and small particles. Larger particles within the distribution of MCC appear to have smaller particles that have agglomerated together, while larger particles of lactose appear to be whole crystals. Starch has a smooth appearance with smaller particles appearing more spherical than larger ones. Much like lactose, the larger particles within starch look to be made of single crystals rather than smaller agglomerated particles. DCPD is made up of elongated particles that have been formed into spherical agglomerates of the material and, as discussed in Section 5.3.1., smaller particles seem to be distributed around the centre of the primary agglomerates .
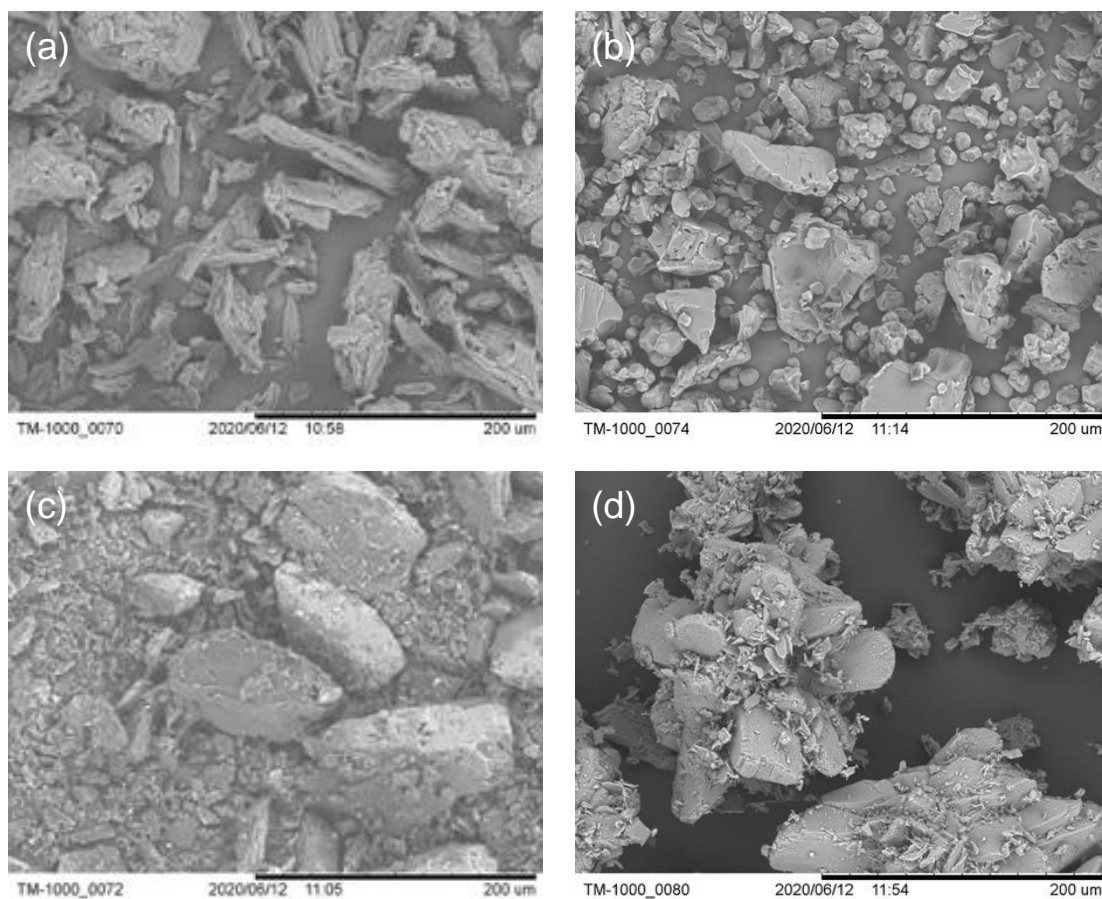
Figure 5-3 Scanning electron micrographs of the excipients used within the study (a) MCC, (b) Starch, (c) Lactose and (d) DCPD.

5.3.3 Moisture content

The moisture content of MCC increases with storage at increasing RH due to its hygroscopic nature, which can be attributed to the presence of hydroxyl groups on the cellulose chains and the relatively large surface area to volume ratio of microfibrils (Rowe, et al., 2009). Water can become tightly bound to its amorphous regions which are more hydrophilic than crystalline regions. Similarly, starch has both amorphous and crystalline regions leading to its hygroscopic nature. It has previously been reported that pregelatinized starch (as is the case for Starch 1500) exhibits a lower propensity for moisture than the original material

(Pharmaquest, Undated). However, it remains hygroscopic as shown by the increase in moisture content with increasing storage RH (Figure 5-4). No significant difference in moisture content is seen for lactose or DCPD with changing RH and overall, very little moisture is absorbed. This is due to their crystalline nature and lack of amorphous regions such as those within MCC and starch.
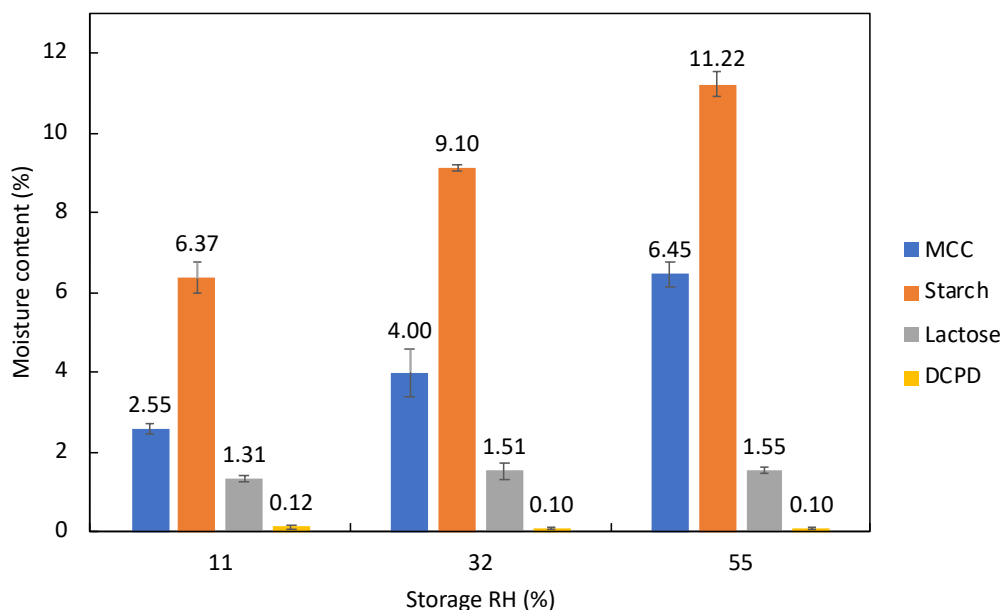
Figure 5-4 The moisture content of each material at given RH. Results represent the mean of three measurements ± SD (in parentheses).

The moisture content results were validated with DVS for each material and moisture sorption isotherms at 25°C are shown in Figure 5-5. There is little difference in the measured results for the stored samples and DVS plot for MCC and DCPD. The measured results for starch below ambient RH (40%) at which tableting took place, are above the DVS plot. This is most likely to be due to the material absorbing water from the air after removing the powder from the

desiccator cabinet. This shows the importance of tableting taking place as soon as possible after the powder is taken out of the individual storage conditions.

The results for lactose, although all measured quantities are similar to each other, lie above the DVS results. This could be a result of condensation upon the powder, or discrepancies in the moisture balance measurement. The measured moisture content values were carried out using an infra-red moisture balance which applies heat and may remove bound water, whereas DVS will not remove tightly bound water leading to discrepancies in results between the two techniques. The powders stored at all three humidity levels showed good agreement after testing each powder three times. The manufacturer specification for Pharmatose 200M (DFE Pharma, 2020) states a maximum loss on drying of 0.5%, therefore all results lie outside of specification.

Interestingly, there is a large hysteresis with starch, indicating that some moisture is retained within the material upon drying. The material tested was 'as received' and did not undergo any drying prior to the DVS process. This may be of some importance when considering the storage of the material as inherent changes may occur that are irreversible upon drying.
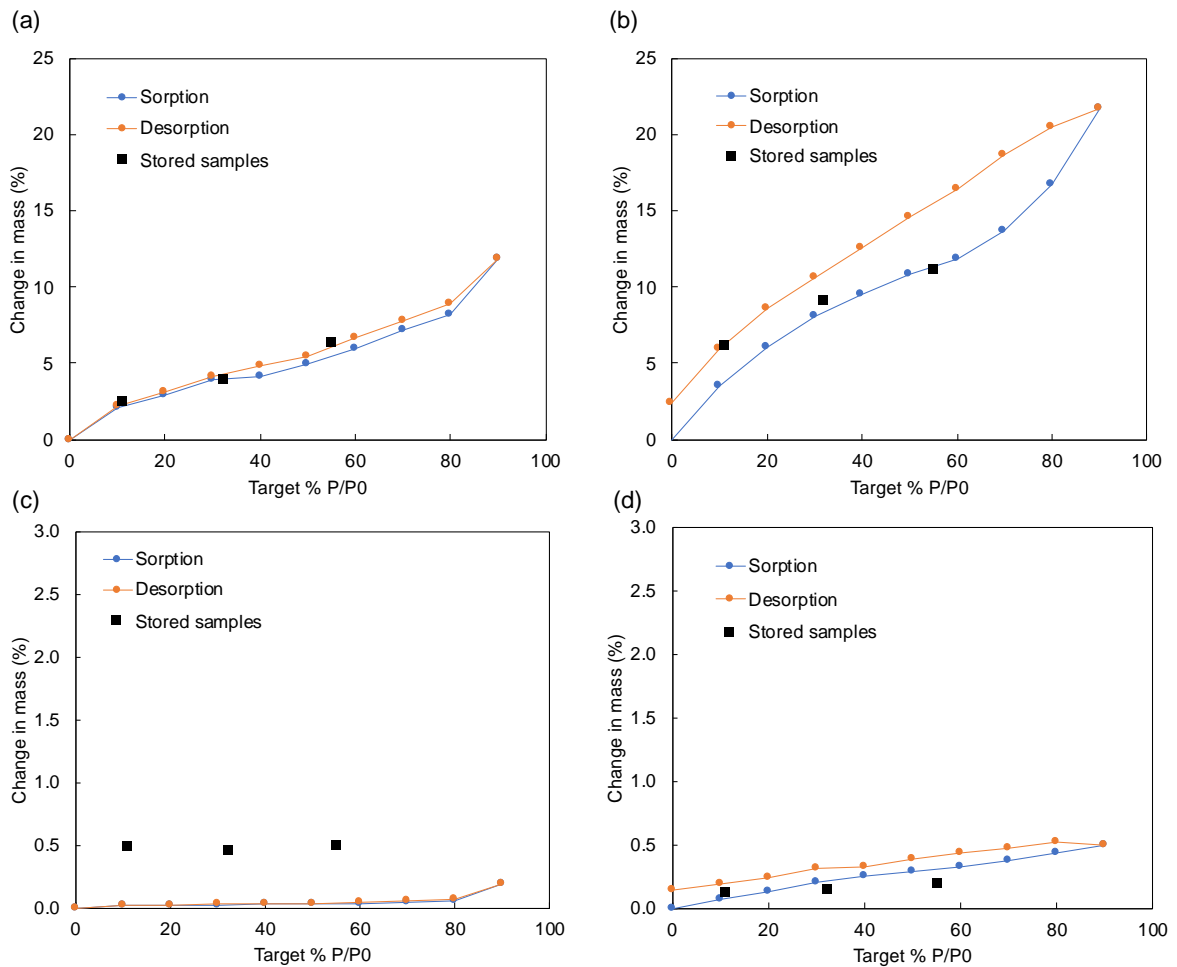
Figure 5-5 DVS results for (a) MCC, (b) starch, (c) lactose and (d) DCPD. Black squares represent the measured moisture content for powders stored at particular RH. Results shown as a mean of three measurements. Note the difference in the y axis scale between materials.

The moisture sorption data was fitted to the Guggenheim Anderson and De Boer (GAB) model (Equation 5-1) by non-linear regression in order to give values corresponding to the monolayer coverage of water (W_m) for each material (Sun, 2008).

$$W = \frac{W_m C' K' a_w}{(1 - K' a_w)(1 - K' a_w + C' K' a_w)}$$

Equation 5-1

where W is the weight ratio of water to dry solid, a_w is the water activity and C' and K' are parameters relating to the heat of sorption of the monolayer and intermediate layers respectively (Zografi, et al., 1984). Fitting the moisture sorption data to the GAB model by non-linear regression (Figure 5-6) results in the following values for MCC: W_m=3.07, C=21.45 and K=0.82. The monolayer coverage in the sample is achieved at 20% RH at 25 ºC. Data was treated in the same way for each material and the results are shown in Table 5-2.
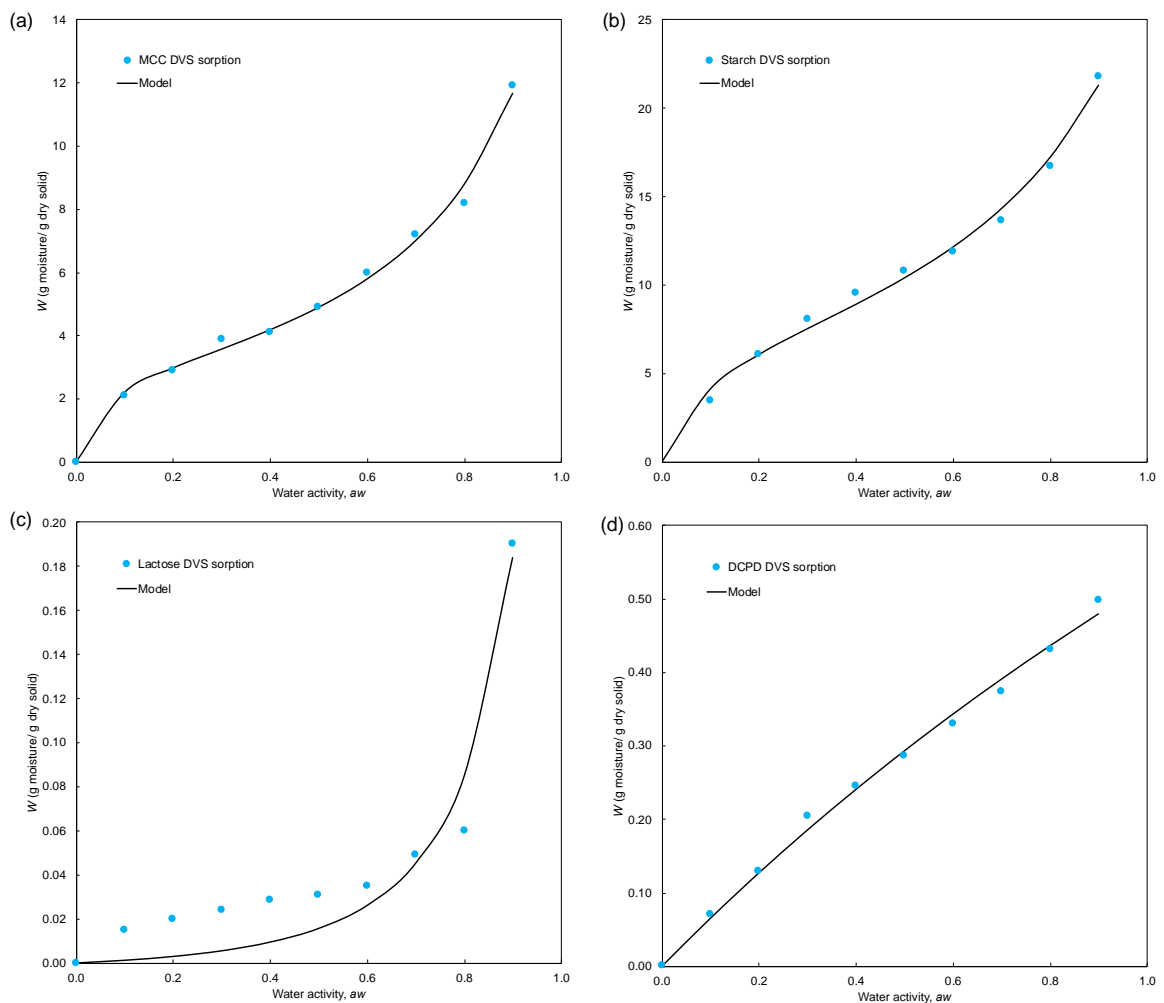
Figure 5-6 The GAB model fitted to DVS moisture sorption analysis data for (a) MCC, (b) starch, (c) lactose and (d) DCPD.

Table 5-2 GAB model parameters for each material. Note that for lactose and DCPD the calculated RH at which water monolayer is present is above 100% and is therefore not shown.

Material	W_m (%)	C	K	R^2	RH at which water monolayer is present (%)
MCC	3.07	21.45	0.82	0.97	20
Starch	7.40	13.41	0.74	0.98	25
Lactose	0.29	0.04	0.88	0.99	-
DCPD	2.05	20.72	0.02	0.99	-

Sun (2008) found that monolayer coverage for MCC is 3.43 wt% corresponding to an RH of 26%. The current study is also in agreement with previous findings Zografi, et al. (1984) where values of 3.0% and 3.3% are quoted for W_m of MCC and values between 8.6% and 9.8% for W_m of corn and potato starch. A different grade of MCC with a larger particle size is used within the study by Sun (2008) and it is unclear as to which grade of MCC is used for the Zografi, et al. (1984).

Any water that is present up to the water monolayer will be tightly bound to the cellulose particles (Zografi, et al., 1984). This water would not be available as liquid water and therefore could not act as a potential solvent for any other materials mixed with the excipient. Zografi, et al. (1984) proposed a model where water present within MCC and starch falls into three categories:

  I. Tightly bound water consisting of one water molecule per anhydroglucose unit;

  II. A second, less tightly bound water molecule per anhydroglucose unit; and

  III. Additional bulk water layers.

It was suggested that for MCC, water present up to 70% RH falls in the 'non-free' water categories. This model will be further discussed in Section 5.3.5.

A suspension of 4 g/10 ml MCC in water was prepared and left overnight. The suspension became a paste, indicating a physical change in the properties of MCC. However, powder x-ray diffraction (PXRD) results showed no difference between the wet and dry MCC, therefore the crystalline structure remained unchanged. The authors concluded that the physical changes were a result of interactions between water and amorphous cellulose. It is unclear as to the method used for carrying out XRD on the paste. Further work could suggest whether the extent to which the material is hygroscopic changes upon wetting and subsequent drying by comparing DVS results of intial and wet/dry cycled material.

5.3.4   Density

The true, bulk and tapped densities of all materials are reported in Table 5-3. Equation 2-4 was used to calculate the corresponding Carr's Index. Density measurements for each differing moisture content of MCC and starch were carried out. Due to only small variation, the mean of all powders is quoted in Table 5-3.

Table 5-3 Showing physical properties and calculated flowability indicators for each material. Results shown as the mean of three measurements ±SD (in parentheses).

Physical property	Material			
	MCC	Starch	Lactose	DCPD
True density (g/cm^3)	1.58 (0.00)	1.49 (0.01)	1.55 (0.02)	2.28 (0.05)
Bulk density (g/cm^3)	0.28 (0.02)	0.62 (0.03)	0.57 (0.02)	0.89 (0.03)
Tapped density (g/cm^3)	0.43 (0.02)	0.78 (0.06)	0.85 (0.01)	1.05 (0.05)
Carr's Index (%)	35 (Very poor)	21 (Passable)	33 (Very poor)	15 (Good)
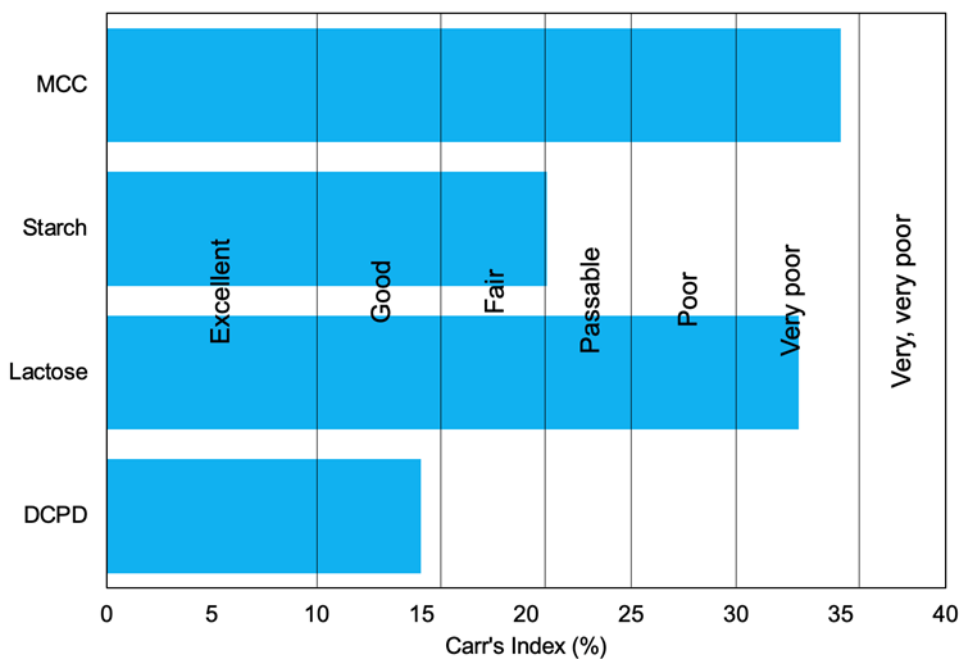
Figure 5-7 A comparison of the Carr's Index for all powders.

Bulk density results are in close agreement with the literature data from Rowe, et al. (2009) where the bulk density for MCC, starch, lactose and DCPD were reported as 0.32, 0.59, 0.57 and 0.92 g/cm^3 respectively. Similarly, the tapped density results are in agreement with Rowe,

et al., (2009) with values of 0.45, 0.88, 0.84 and 1.17 g/cm^3 for MCC, starch, lactose and DCPD respectively. The tapped density for each material is higher than bulk density due to the movement in the powder bed cause by tapping which reduces the volume of the powder, therefore increasing density.

The true density for MCC (Avicel PH101) is within the range of 1.46-1.58 g/cm^3 stated in previous literature (Gustafsson, et al., 2003; Rowe, et al., 2009; Schiano, 2017). Sun (2004) used a novel method to derive the true density of MCC from compaction data stating that helium pycnometry is not a suitable method for samples that have water associated due to the release of water when exposed to the dry helium atmosphere. This was previously discussed in Section 2.6.3. In a later paper (Sun, 2008) calculated the true density of MCC (Avicel PH102) with a water content between 3.3% and 5.1% at ~1.46 g/cm^3 which is 0.12 g/cm^3 lower than the true density found in the current study. The true density of MCC with water contents above 5.1% decreases with increasing water content due to the swelling propensity of MCC at high humidity. The value for MCC true denstiy in the current study is higher than that found by Sun (2008). However, the grade of microcrystalline cellulose was different, therefore a like-for-like comparison cannot be made.

The true density of Starch (Starch 1500) is also in agreement with literature, which is in the range of 1.49-1.52 g/cm^3 (Wu, et al., 2005; Rowe, et al., 2009). Rowe, et al. (2009) states the true density of lactose (Pharmatose 200M) to be 1.545 g/cm^3 and is therefore in agreement with the current study. Finally, the true density of DCPD is within the range of 2.32-2.43 g/cm^3 in previous literature (Zhang, et al., 2003; Rowe, et al., 2009; Choi, et al., 2010), and is in close agreement with the result of 2.28 g/cm^3 within this investigation.The Carr's index can be

calculated as described in Section 3.4.6 to investigate the flowability of each material and the results are shown in Table 5-3 and Figure 5-7. The results show that MCC and lactose have very poor flowability, while starch is passable and DCPD has good flowability (Figure 5-7). These results were expected after observations made during the handling of the powders and density results. Particle interactions (cohesivity or interlocking) prevent poured particles from settling completely during bulk density measurements. Tapping the powder bed dislodges particles to permit denser packing. A larger difference between bulk and tapped densities indicates more interactions that hinder flow of the powder. Starch and DCPD have more similar bulk and tapped densities than MCC and lactose and this is shown in the Carr's Index values. MCC and lactose are both irregularly shaped (Figure 5-3), leading to lower bulk densities, and therefore poorer flow, than those for the more spherical shaped starch and DCPD. DCPD has the highest flowability due to its granular nature. From this work it should be noted that flowability of individual excipients should be taken into account when thinking about the design of a formulation. If a high quantity of a poorly flowing material is used, it may decrease the flowability of the entire formulation and have implications on the manufacturing process.

5.3.5 Tabletability and the effect of water content

The strength a tablet attains under a given pressure is known as its tabletability (Sun & Kleinebudde, 2016). *Figure* 5-8 (a-d) shows the tabletability profiles for each material at all RH values.

a) MCC
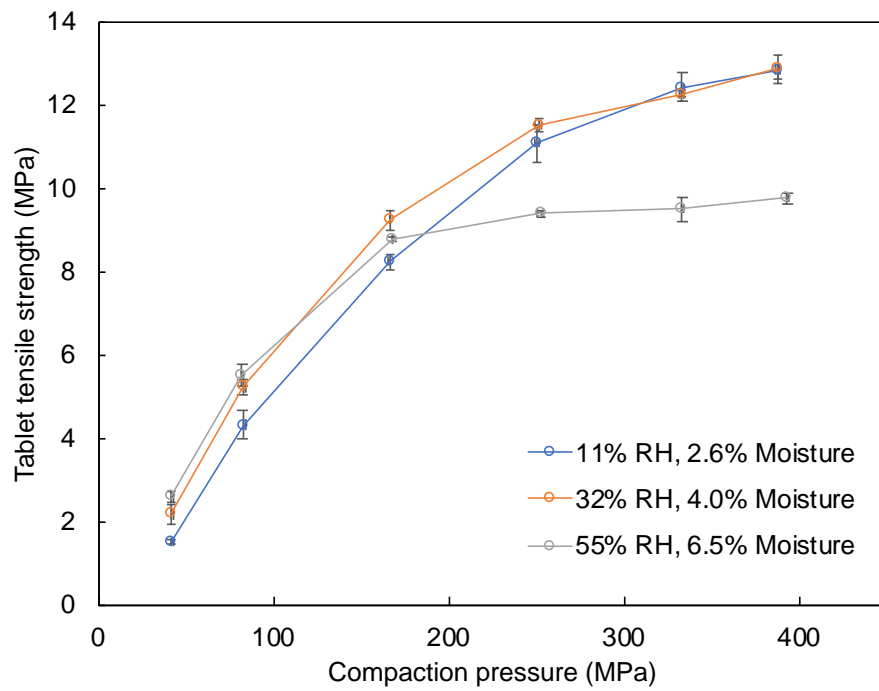
b) Starch
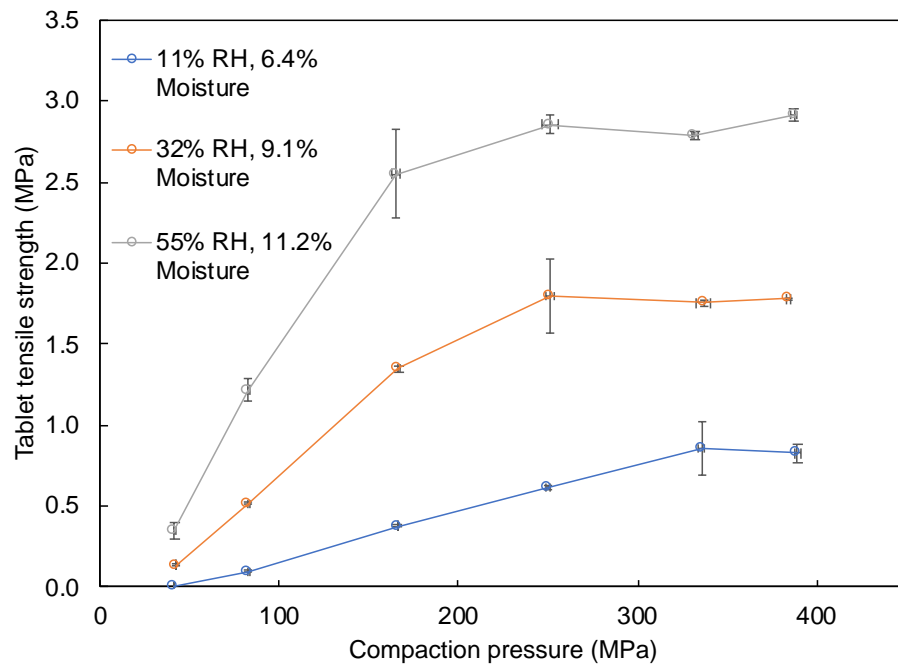
c) Lactose
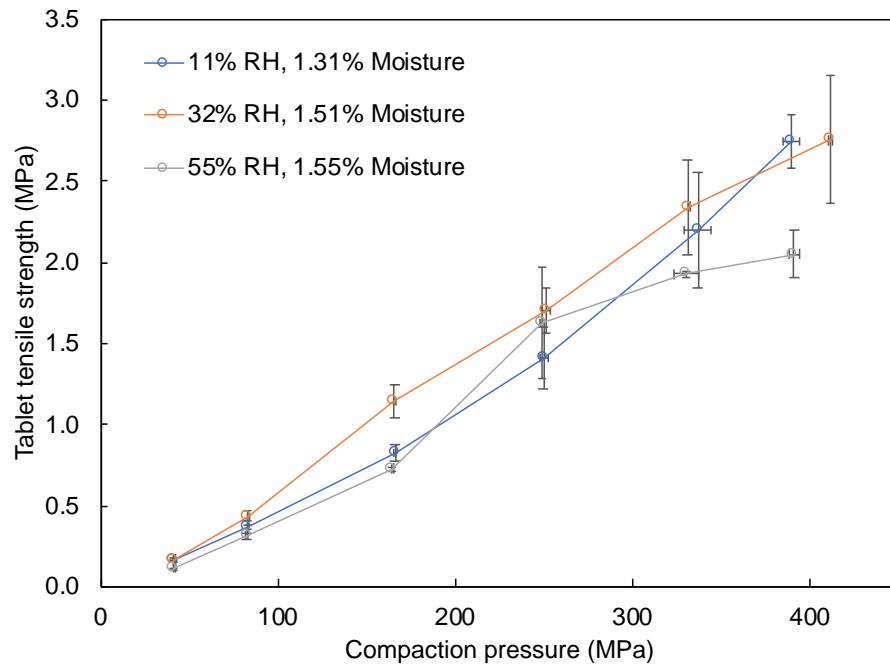
d) DCPD
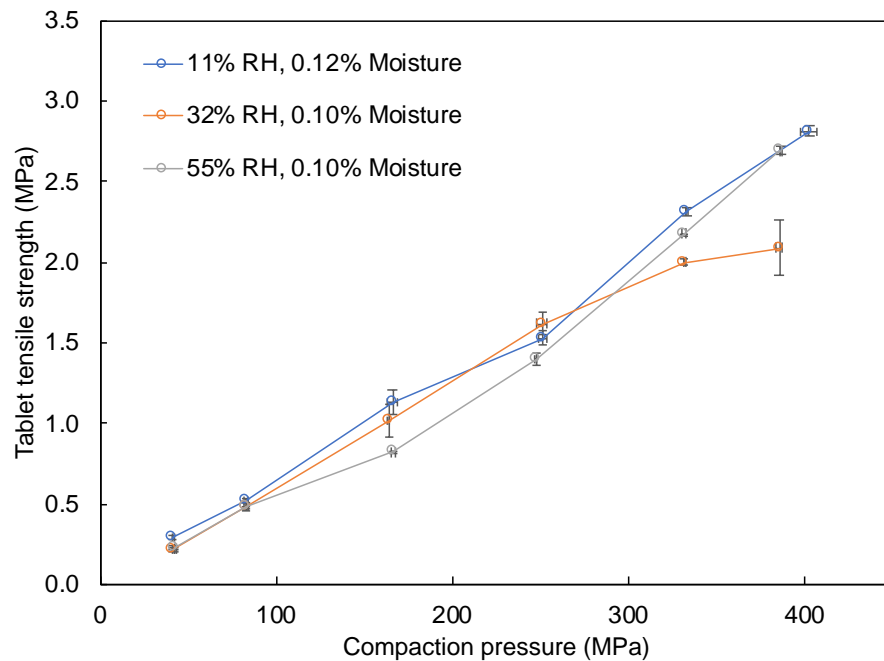
Figure 5-8 Tabletability profiles for (a) MCC, (b) Starch, (c) Lactose and (d) DCPD.

It has been suggested to withstand manufacturing steps and distribution, tablets should have, at a minimum, tensile strengths of 1.7 MPa with porosities of 10-20% (Pitt, et al., 2015; Etzler, et al., 2012). MCC demonstrates the minimum tablet strength at minimal compaction pressures across all moisture content levels. DCPD and lactose reach the minimum tensile strength requirements at maximum compaction pressure. The minimum required tensile strength is only reached at the highest moisture content (11.2%) and ~120 MPa compaction pressure for starch. For starch (*Figure* 5-8(b)), there is a point at which the tablet tensile strength plateaus and the compaction pressure at which this occurs changes depending on the moisture content of the material. The last data point before the plateau is also noisiest at this point for all three data sets suggesting that there is a key point at which the material

changes depending on the moisture content and pressure applied. Starch 1500 is a partially pre-gelatinised starch and therefore contains both soluble (gelatinised) and insoluble fractions. Cunningham (Undated) confirmed that the insoluble and smaller particle size fraction comprises of intact starch grains, whereas the larger particle size fraction is made up of granular and soluble pregelatinised starch. Starch has a propensity to swell with increasing moisture content resulting in a change in particle size. It could be possible for the larger, granular fraction to swell more than the smaller fraction, therefore considerably changing the bulk of the material depending on moisture content. The point at which each data set plateaus can be explained by the rupture of the larger size fraction when enough compaction pressure is applied and this is likely to be a lower compaction pressure for increasing moisture content due to the higher moisture content contained within the startch particles due to osmotic pressure. Once the material has ruptured there will be more 'free' water within the structure resulting in no further increase in tablet strength with increasing compaction pressure.

From Figure 5-5 (b) it should be noted that the DVS plot shows a hysteresis for starch. It could be hypothesised from this with the data shown in Figure 5-5 that pre-wetted material that was then stored at 11% RH could provide stronger tablets given that they would likely contain more moisture than the original material.

For MCC, the results are in agreement with previous studies (Sun, 2008) where the authors recommend that the optimum tabletability of MCC occurs after storage between 21.6% and 38.2% RH corresponding to moisture contents of 3.1% and 4% respectively. For the current study if RH during storage and tableting process is kept between 11% and 32% corresponding to moisture contents between 2.6% and 4.3%, the greatest tablet tensile strength is observed.

The study by Sun (2008) stored MCC at 0% RH which gave a moisture content of 1.5% so it is important to note that the tabletability of completely dry material has not been tested. Amidon and Houghton (1995) stated that the tensile strength of MCC compacts was independent of moisture content below 5% and then decreased as the moisture content increased further. The current study disagrees with this as there is a difference in tabletability between MCC containing 2.6% and 4.0% moisture. At compaction pressures above ~300 MPa a difference in tablet strength is not observed. However, before this point the material containing 4.0% moisture produces stronger tablets than that containing 2.6% moisture. This difference is most pronounced at compaction pressures between 80 and 170 MPa (Figure 5-9).

Figure 5-9 shows tabletability of MCC at compaction pressures under 200 MPa in more detail. Here it is clear that at low compaction pressures (below ~115 MPa), powder containing 4.0% and 6.5% moisture produce the strongest tablets. In agreement with previous studies by Sun (2008), the water that is present further plasticizes the MCC and therefore produces a more deformable material under pressure. Above compaction pressures of ~115 MPa, the extra water that is present hinders the tableting process, acting as a lubricant, allowing MCC chains to slide easily across each other rather than producing stronger interactions.

Above 20% RH, there is the potential for more water than that which will present as a monolayer on the material, and, as discussed earlier, will fall into category 3 of the model suggested by Zografi, et al. (1984). Additional water will be present as bulk water layers. However, Zografi, et al. (1984) suggested that water present up to 70% RH would be 'non-free' and would not cause issues in routine handling of the materials. The current study disagrees with this assumption due to the loss in tabletability observed at compaction

pressures over 200 MPa and 55% RH. At 11% RH (2.6% moisture), there is less water present than that corresponding to the water monolayer, therefore no extra plasticization will occur, resulting in tablets of lower tensile strength. A moisture content of 4% provides enough water to increase the plasticization of MCC to produce a strong tablet. However, when considering an industrial setting, it may be possible for conditions to be in excess of 32% RH and therefore produce tablets of lower strength. This confirms the need for tight control over atmospheric conditions when using hygroscopic materials such as MCC.
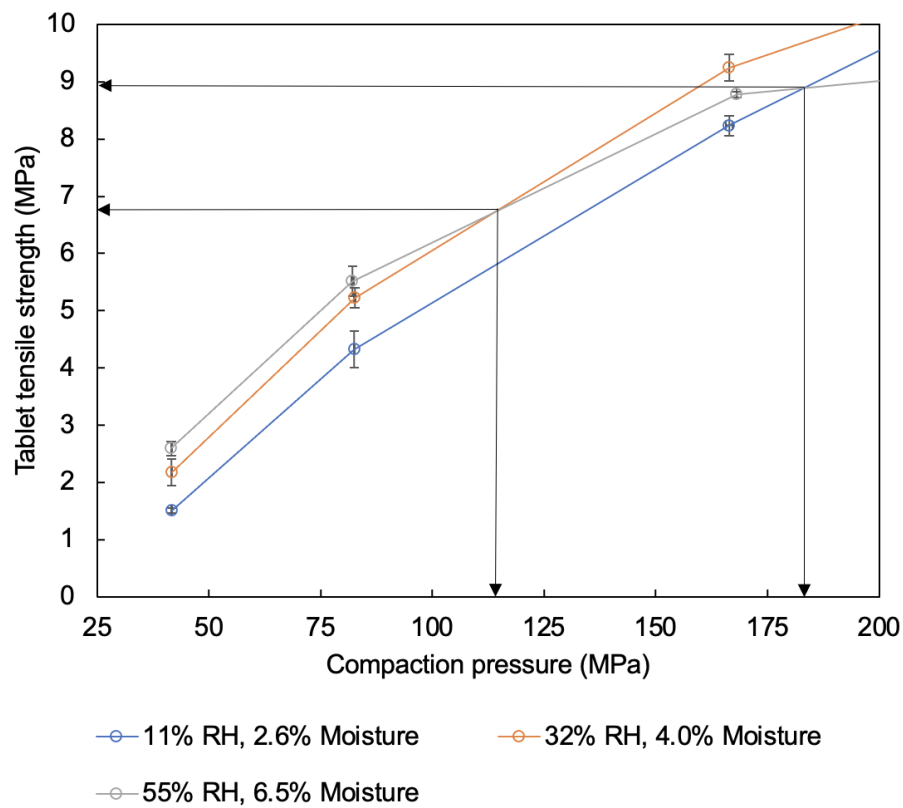
Figure 5-9 MCC tabletability profiles under 200 MPa compaction pressure. Arrows highlight the point at which the powder containing 6.5% moisture begins to lose strength in comparison to powders with lower moisture content.

Similarly to MCC at low compaction pressures, there is an increase in tablet tensile strength with increasing moisture for starch and this trend continues even at higher compaction pressures. Across all RH storage levels starch produces tablets with lower tensile strength than those with MCC stored at the coressponding RH. There is a large difference in the resultant tablet tensile strength with increasing moisture content across the compaction pressure range. For example, there is a more than ten-fold increase in tablet strength at a compaction pressure of 80 MPa for tablets produced from starch containing 6.2% moisture (tensile strength = 0.1 MPa) and starch containing 11.24% moisture (tensile strength = 1.2 MPa). At the highest compaction pressure, ~390 MPa, there is an even greater difference of 2.1 MPa. For all moisture contents tested, the tablet tensile strength seems to plateau over a compression pressure of 300 MPa and there is no increase in strength even with an increase in compaction pressure. The plateau occurs at progressively lower compaction pressure as moisture increases. According to Table 5-2 a water monlayer is present for starch at an RH of 29% or 7.4% moisture. Conversely to MCC, the tablet tensile strength increases past the moisture content corresponding to the water monolayer. This may indicate that, at moisture contents above 7.4%, water is able to penetrate the starch structure allowing intermolecular attraction to continue at the surface and avoid lubrication of the particles. Another explanation may be provided by the structure of starch. Due to the pre-gelatinization process which is used in the manufacture of Starch, the material is composed of two polymers, amylose and amylopectin (Colorcon Inc., 2016). Colorcon Inc. (2016) states that amylose exhibits strong intermolecular bonding and swells significantly when wetted. The additional tablet strength observed with increasing moisture in the current study may be a result, at least in part, of the strongly bonded amylose. As it swells with aditional water, the strong

intermolecular bonds may be broken and then reformed as it is compressed. The newly produced bonding surfaces are likely to be different to the original, possibly increasing available surface area, and producing strongly bonded tablets.

The moisture content of lactose and DCPD does not change significantly, and this is illustrated by little change in the tabletability profiles for all three storage RH levels (*Figure* 5-8 (c) and (d)). The relationship between compaction pressure and tablet tensile strength for lactose and DCPD is linear and they both reach a similar maximum tensile strength between 2.5 and 3 MPa at 400 MPa compaction pressure. Due to the linear nature of the tabletability profiles for both lactose and DCPD it is likely that the maximum potential tablet tensile strength has not been obtained, even at 400 MPa. This is a result of the brittle nature of each material. New bonding surfaces are being produced throughout the entire tabletability profile and therefore a reduction in porosity and higher resultant tablet tensile strength.

5.3.6   Differences in tablet breakage

Each material undergoes breakage during diametrical compression in a different way due to their differing material attributes. Figure 5-10 highlights the plastic nature of MCC in comparison to other materials. Each picture is taken from a high-speed video taken during the diametrical crushing of a tablet and shows the point at which the tablets break. Starch, lactose and DCPD undergo a rapid break in the centre of the tablet, whereas the breakage of MCC is slower and does not result in two fully-separated sides as with the other materials. The MCC tablet appears to break from a central point that radiates towards the upper and lower edges of the tablet before other breakage occurs from the edges inward. Interestingly, the breakage

of a starch tablet appears to be more similar to that of lactose and DCPD, resulting in a fast breakage producing two large pieces. These observations were noticed across all of the tablet breakage that was carried out for the production of the tabletability profiles presented in this chapter. The result was highly repeatable with tablets following the breakage pattern shown in Figure 5-10 for all materials highly regularly.
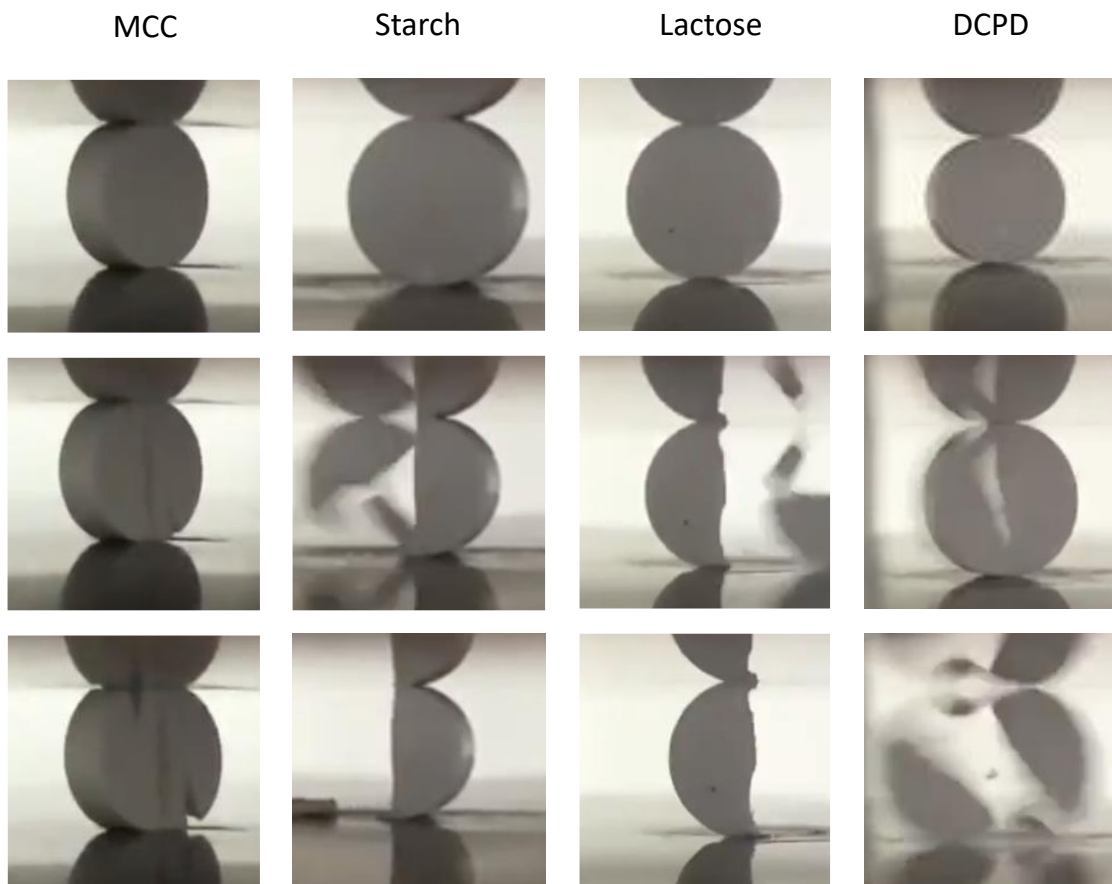
Figure 5-10 Still photos taken from high-speed videos of individual tablet crushing for each material.

During tablet tensile strength testing it is possible to extract data to produce force-displacement curves for the crushing of each tablet to further investigate and visualise tablet breakage (Figure 5-11). For MCC at each storage RH, there is an initial peak indicating the first

break along the tablet followed by a prolonged wide peak before finally approaching 0 N of force. For lactose and DCPD, the initial breakage peak is followed by a rapid return to 0 N of force due to complete failure of the tablet, almost instantly. Starch appears to have a mixture of the force-distance profiles of MCC and DCPD or lactose. At a low compaction pressure of 43 MPa, the breakage profile for starch is more reminiscant of that for MCC with a lower and broader peak after the initial break suggesting some material plasticity. However at 170 and 395 MPa of compaction pressure, starch tablets appear to break and rapidly return to 0 N of force indicating complete failure.
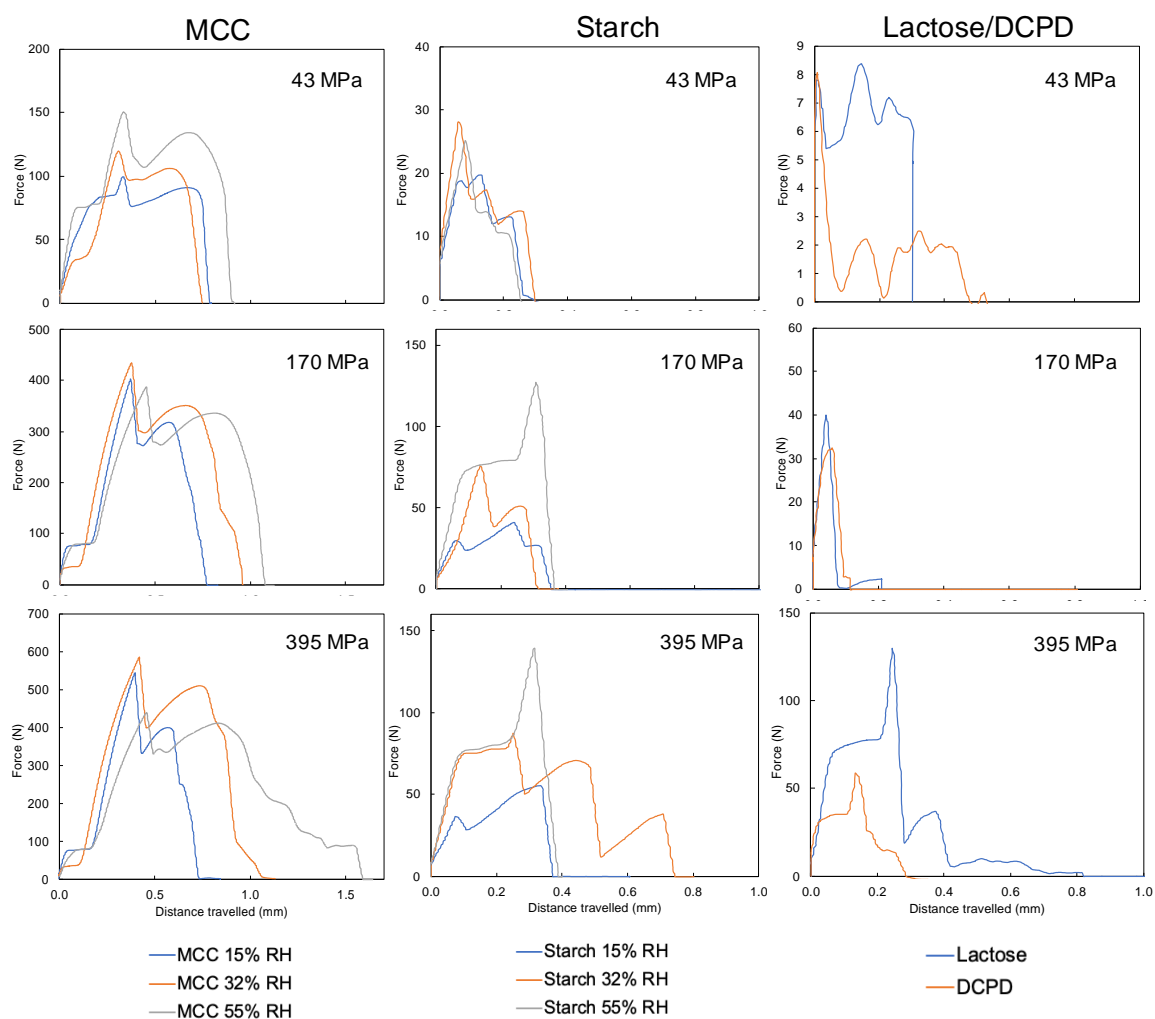
Figure 5-11 Tablet crushing force-displacement profiles for tablets produced with 43, 170 and 395 MPa compaction pressure. Tablets produced from materials stored at all RH values are shown for hygroscopic materials MCC and starch. Only tablets produced from material stored at 32% RH shown for non-hygroscopic materials lactose and DCPD. Note difference in scale for each plot.

To further deconvolute the difference in break between MCC and starch, SEM micrographs were taken of the fracture surface (Figure 5-12). The fracture surface of MCC looks very different to the structure of the primary particles shown in Figure 5-3. The particles seem to have deformed and are in close contact with each other; by eye, the material appears plastic

in structure. When comparing the primary starch particles from Figure 5-3 to the fracture surface in Figure 5-12 the original particle shape can still be identified after tablet compression. Rearrangement is required to fill gaps between the particles as the porosity is reduced. There are two possibilities depending on the particle size distribution of the material:

I.   Firstly, there is a large volume of small particles, so these form a continuous phase with larger particles dispersed within it. In this case, the accommodation of volume change will be through particles moving closer together.

II. Secondly, there is a small volume of small particles, so the larger particles form the continuous phase. In this case the accommodation of volume reduction will be through larger particles rearranging, undergoing rotation, fracturing or deforming to allow particles to come closer together.

There is no evidence of particle breakage upon fracture of the starch tablet, it appears that the original particles are still intact as in Figure 5-3. From the second of the starch images in Figure 5-12(b) it appears that there are large particles in contact with each other. In the third image of Figure 5-12(b) there is evidence of cleavage of particles in the bottom-left corner. As mentioned earlier in Section 4.3.6, the tabletability of starch increases with increasing moisture content. There is no obvious evidence of increasing plasticity upon studying Figure 5-12(b) and comparing it to the base material in Figure 5-3 as the particles show a similar structure even at the high compression pressure of 300 MPa. This suggests that rather than increasing the plasticity of the material, additional water increases water bonding within the structure or produces other mechanical changes leading to stronger tablets.
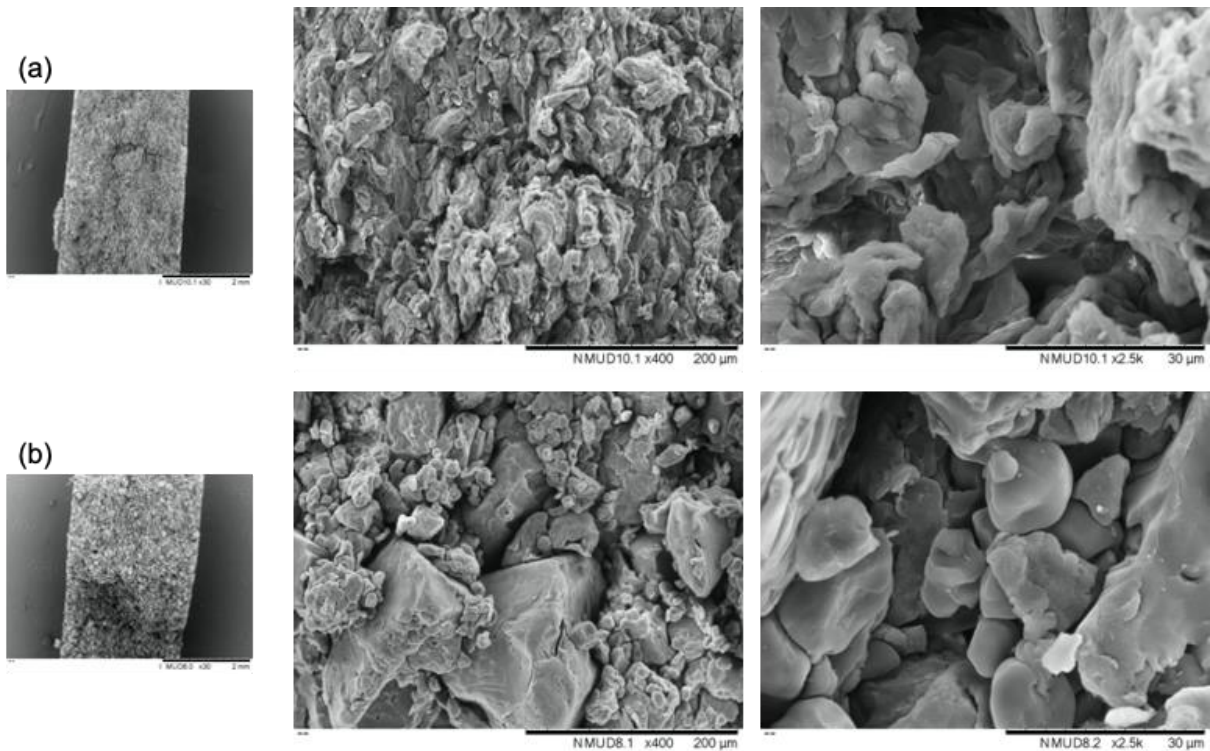
Figure 5-12 SEM micrographs of the tablet fracture surface of (a) MCC and (b) Starch. Tablets were produced with 300 MPa compression pressure after material had been stored at 32% RH.

5.3.7 Compressibility and the effect of water

Tabletability and the process of tablet breakage shows distinct differences between materials that are hygroscopic (MCC and starch) and non-hygroscopic (lactose and DCPD). For this reason, the following areas of compressibility and compactibility will be discussed for each of the two sets of materials separately. Tablet porosity was calculated by taking out of die measurements for tablets. Tablet dimensions were measured within two hours of production to ensure water content remained close to those values measured before tableting.

5.3.7.1 Non-hygroscopic materials

As expected, due to the lack of water uptake, there is no difference in compactibility between powders stored at different RH for lactose or DCPD. For lactose, there is a rapid decrease in porosity at low compression pressures, indicating a rapid progression of particle rearrangement and breakage. DCPD shows a slower rate of particle rearrangement, partly due to its lower porosity as an uncompressed powder bed, and also due to less rearrangement and fracture at lower compaction pressures. As shown in Figure 5-7, DCPD has a lower calculated Carr's Index value which indicates improved flow over that of lactose. The increase in flowability will lead to preferable packing in the initial powder bed for DCPD, and therefore lower porosity, than that of the initial lactose powder bed. However, beyond 50 MPa of compaction pressure, both lactose and DCPD show a similar reduction in porosity and this is unaffected by the RH the powders have been stored at. Even at the highest compaction pressures, around 400 MPa, there appears to be a continuing reduction in porosity for both materials. This indicates that there is still the potential for the material to fragment and compress further which is mirrored by the linear relationship noted between compaction pressure and tablet tensile strength in Figure 5-8. If the materials are continuing to fragment at this point, there is an increase in bonding surface area, and it continues to be effective due to not only the decrease in porosity, but also the increase in tablet tensile strength.

The minimum porosity reached is ~0.1 which is to be expected because it is unlikely that a tablet could ever be compressed to the extent that it would equal the materials true density.

As part of the experimental procedure, the calibration of the equipment was checked and no errors were found.
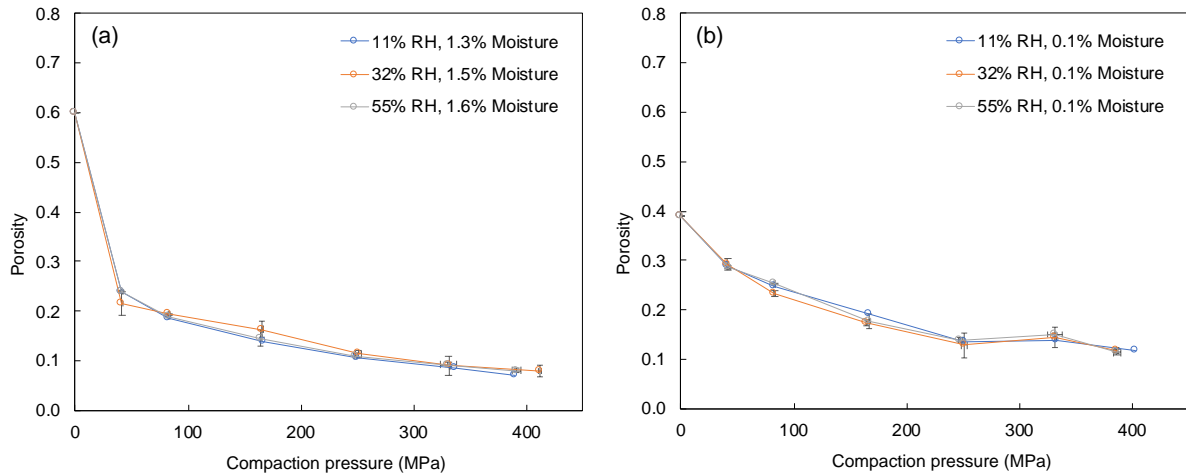
Figure 5-13 Compactibility profiles for (a) lactose and (b) DCPD.

5.3.7.2 Hygroscopic materials

Unlike the non-hygroscopic materials, both MCC and starch reach a minimum porosity within the compaction pressures studied (Figure 5-14). For MCC, the minimum porosity is attained at 180 MPa for the powder containing the highest amount of moisture (6.5%). This confirms that the contact area between particles has been maximised at this point due to the additional plasticization by water present within the material. At equal compression pressures, MCC containing less moisture corresponds to higher porosity values and therefore a lower bonding area. This confirms the lower deformability of drier material due to the lack of enough water to plasticize the material sufficiently.

MCC with 4% moisture content, exhibits an increase in contact area due to increasing compression pressures past 180 MPa and up to 250 MPa where the porosity value begins to

level out. Interestingly, the driest MCC (2.6% moisture) shows a continuous reduction in porosity past the wetter material, up to ~350 MPa and has a lower porosity than the wetter materials at the maximum compaction pressure. Due to less water present within the powder bed, there is more available volume for MCC particle-particle interactions, but this does not lead to stronger tablets. As shown in Section 5.3.5, MCC containing 2.6% moisture only reaches the same tablet tensile strength as MCC containing 4% moisture at the highest compaction pressures. The faster porosity reduction and higher tablet tensile strength below ~250 MPa for MCC at 4% moisture shows that water leads to more intimate bonding of MCC. However, even with drier material at 2.6% moisture, with enough compaction pressure, this same intimate bonding can be reached, indicating that the presence of water is more important if tableting at lower compaction pressures is required. Much like the point at which no extra tablet strength can be gained past ~180 MPa for the wettest material (6.4% moisture) due to no further space availability for porosity reduction, at 400 MPa and 4% moisture there is no availability for further compaction.

The difference in compactibility based on moisture content is even more pronounced for starch. Similarly to MCC, the powder with the highest moisture content reaches a lower porosity at a faster rate than the powders with lower moisture content. However, starch containing the lowest moisture content (6.4%) appears to still be reducing in porosity even at the highest compaction pressures, indicating there may still be potential to create stronger tablets at this point. Tablets produced from powder stored at 32% RH show a plateau in porosity at 250 MPa and for 55% RH the plateau begins at 200 MPa. This is in agreement with

the tabletability profiles for starch (*Figure* 5-8(b)) where maximum tablet strengths are generated at the same compaction pressures as those for minimum porosity.
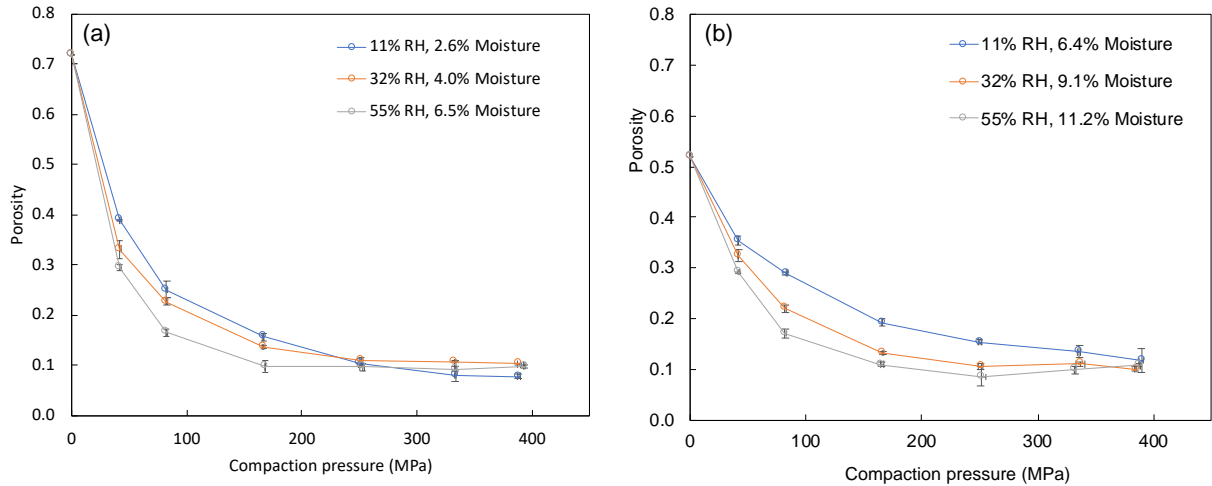
Figure 5-14 Compactibility profiles for (a) MCC and (b) Starch.

It is interesting that all materials, both non-hygroscopic and hygroscopic, have a minimal attainable porosity at around 0.1. It would be unlikely to generate a tablet with zero porosity, even at the highest compaction pressures used within this study and there may be error within the equipment used. Although height calibration was carried out regularly while using the universal testing machine, there may be some error when taking height measurements due to the presence of the die in-between the two compression platens. However, a minimum porosity that is similar across all materials indicates maximum densification has been reached within the die and compaction pressures used.

5.3.8   Heckel and Walker analysis

The effect of moisture on compactibility can also be studied by using the empirically based Heckel and Walker models as discussed in Section 2.7.3. The compressibility of materials was

investigated by using a range of compression pressures between 40 and 400 MPa and evaluating tablets within 2 hours after production. An out-die method was selected due to previous investigations by Egart, et al. (2014) where it was found that the in-die method results in overestimating the compressibility of powders. In-die coefficients depend on the elasticity of the material, whereas out-die coefficients evaluate plastic deformation only. Again, the hygroscopic and non-hygroscopic materials will be discussed independently of each other.

The Heckel equation (Heckel, 1961) was derived assuming that particles will undergo plastic deformation with the application of pressure. The volume reduction of a powder bed obeys first-order kinetics where the 'reactants' are the pores (Equation 5-2)

$$\ln\left(\frac{1}{1-D}\right) = kP + \text{A}$$

Equation 5-2

where D is the relative density (or solid fraction) and 1-D is the void fraction (or tablet porosity) at pressure, P. The dimensionless constant, A, is related to the bulk density of the powder upon initial filling and particle rearrangement and fracture upon increasing pressure. The constant, k, describes the influence of pressure in increasing the density of the tablet (Sun & Grant, 2001) and the reciprocal of k represents yield pressure, P_y (Hersey & Rees, 1971).

The Walker model (Walker, 1923) is based on the change of a tablet's volume with respect to compression pressure (Equation 5-3).

$$V' = -w' \times logP + V'_{sp}$$

<div align="right">*Equation 5-3*</div>

where *V'* is the specific volume of the tablet, *w'* is the Walker coefficient represented by the slope of a plot of *logP* against specific volume. The Walker coefficient expresses the volume reduction corresponding to one-decade change in pressure, *P*. V'_{sp} is the specific volume at 1 MPa of pressure (Sonnergard, 1999).

5.3.8.1   Heckel and Walker analysis of non-hygroscopic materials

The data was analysed according to the Heckel and Walker models (Figure 5-15 and Figure 5-16) and an excellent fit was seen for both which is reflected in the R^2 values quoted in Table 5-4. A higher value for P_y indicates lower compressibility due to the material demonstrating greater resistance of the particles to deformation. If a mean value for yield pressure, P_y, is taken across all three storage conditions for lactose and DCPD, it is found that the materials have similar levels of compressibility (291 and 270 MPa respectively). The values for Walker coefficient are also similar across all storage conditions and between materials.
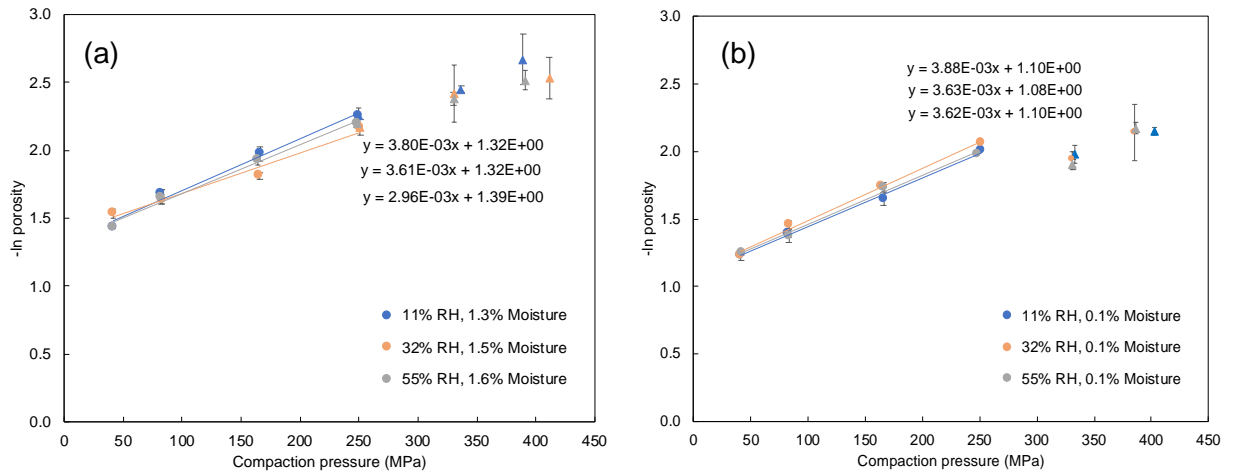
Figure 5-15 Out-of-die Heckel plots for (a) lactose and (b) DCPD. Circular data points indicate those used in the Heckel calculation and triangular data points indicate those above the compression range used for the calculation.
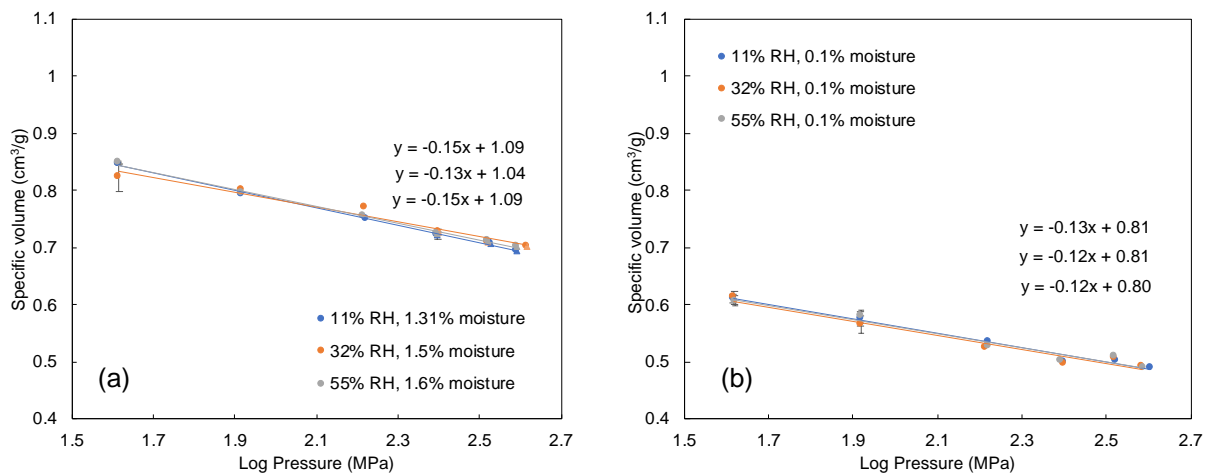
Figure 5-16 Walker plots for (a) lactose and (b) DCPD.

Table 5-4 The yield pressure (P_y or the reciprocal of K), A, Walker parameter (-w'x100) and V'$_{sp}$ with corresponding R values for lactose and DCPD.

Material and storage humidity	Moisture (%)	P_y (MPa)	A	R^2	-w' x 100 (%)	V'$_{sp}$	R^2
Lactose 11%	1.3	263	1.32	0.99	15	1.09	0.98
Lactose 32%	1.5	333	1.32	0.94	13	1.04	0.96
Lactose 55%	1.6	278	1.39	0.99	15	1.09	1.00
DCPD 11%	0.1	278	1.10	0.98	13	0.81	1.00
DCPD 32%	0.1	256	1.08	0.99	12	0.81	0.97
DCPD 55%	0.1	278	1.10	0.99	12	0.80	0.96

5.3.8.2   Heckel and Walker analysis of hygroscopic materials

Unlike the results seen for lactose and DCPD, unsurprisingly the Heckel and Walker coefficient values differ depending on the moisture content of the material for both MCC and starch (Table 5-5). For MCC, the yield pressure shows a step-change at the highest moisture content (6.5%) when comparing with the lower moisture content of 2.6 or 4%. This implies that at the higher moisture content the material is more compressible due to increased plasticity. It is important to note that focusing on the compressibility coefficients in isolation is not indicative of the material properties at higher compressive forces. As shown in the tabletability profile (*Figure* 5-8(a)) and compactibility profile (Figure 5-14(a)), even though MCC at the highest moisture content provides a faster rate of porosity reduction and greater tabletability up to 180 MPa, at higher compaction pressures the material does not gain any further tablet strength. Therefore, in this situation, if there is any further increase in plasticity due to water content it does not result in the strongest tablets.

Starch also shows a decrease in yield pressure and therefore increase in plasticity with increasing moisture content. However, unlike for MCC, this difference is across the entire range of moisture content. At the highest storage RH, the moisture content of starch was 11.2% versus a moisture content of 6.5% for MCC. Even though more moisture is present within starch, the yield pressure is higher than that for MCC stored at the highest RH, being 133 and 119 MPa respectively. As mentioned before, the higher plasticity within MCC with the highest moisture content does not equate to stronger tablets at higher compaction pressures.
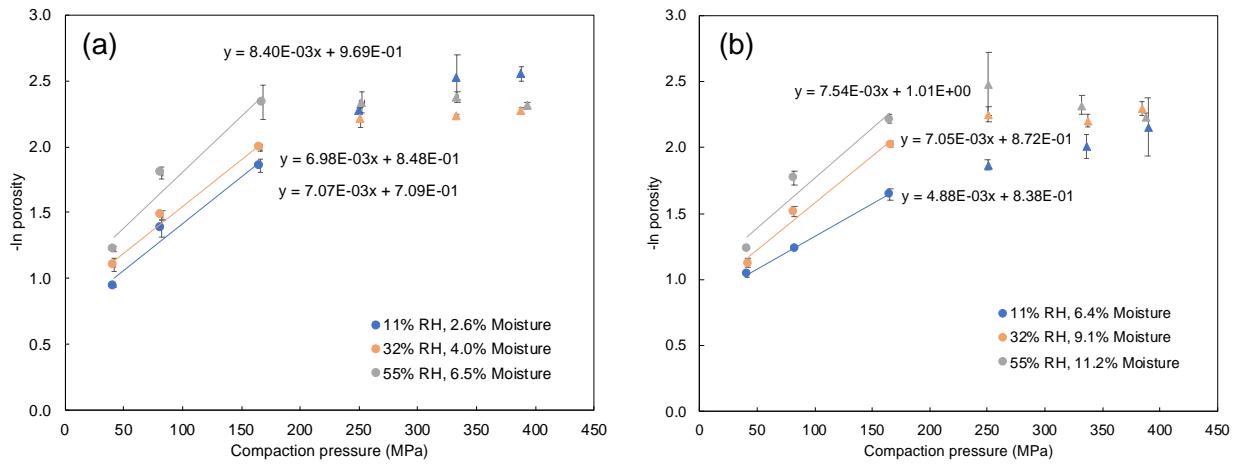
Figure 5-17 Out-of-die Heckel plots for (a) MCC and (b) starch. Circular data points indicate those used in the Heckel calculation and triangular data points indicate those above the compression range used for the calculation.
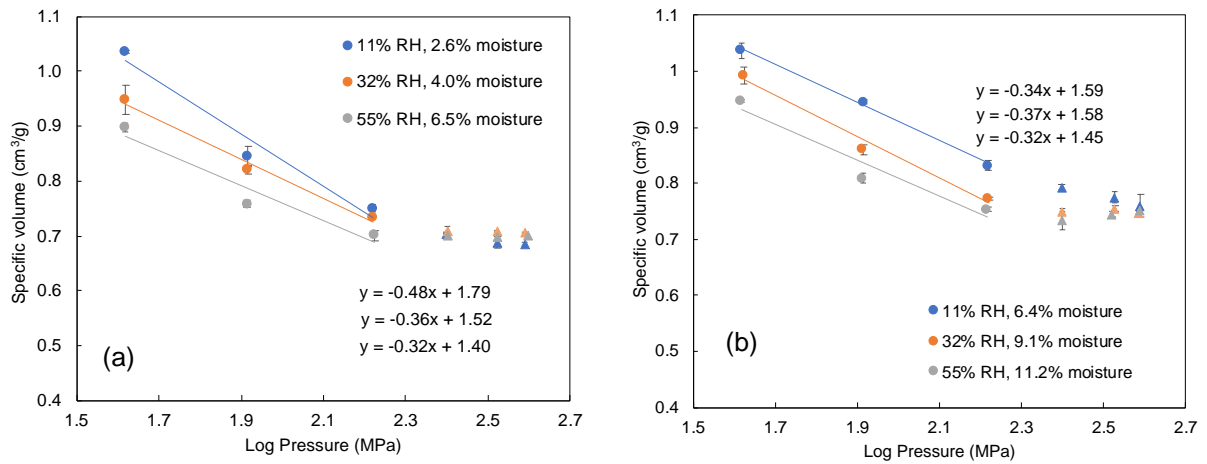
Figure 5-18 Walker plots for (a) MCC and (b) starch.

Table 5-5 The yield pressure (P_y or the reciprocal of K), A, Walker parameter (-w'x100) and V'_{sp} with corresponding R values for MCC and starch.

Material and storage humidity	Moisture (%)	P_Y (MPa)	A	R^2	-w' x 100 (%)	V'_{sp}	R^2
MCC 11%	2.6	141	0.71	0.95	48	1.79	0.96
MCC 32%	4.0	143	0.85	0.99	36	1.52	0.99
MCC 55%	6.5	119	0.97	0.97	32	1.40	0.94
Starch 11%	6.4	204	0.84	1.00	34	1.59	1.00
Starch 32%	9.1	141	0.87	0.99	37	1.58	0.98
Starch 55%	11.2	133	1.01	0.94	32	1.45	0.94

The R^2 values for the Walker results were slightly lower than those for Heckel. The compressibility of MCC and starch stored at the lowest RH showed that MCC is more compressible. However, the compressibility of MCC reduces with increasing moisture according to the Walker model. A moisture content of 2.6% results in a compressibility value of 48%, and the highest moisture content of 6.5% results in considerably lower compressibility

of 32%. This result contradicts the hypothesis that additional moisture results in increased plasticity of MCC and supports that there is more than just increased plasticity at play when finding the 'ideal' water content of the materials for tabletability. The Heckel and Walker models appear contradictory when considering the resistance to deformation. The Heckel model shows yield stress reducing but the Walker model shows compressibility reducing with increasing moisture. It suggests that moisture content plays an important role when considering these models. Any changes in MCC structure due to moisture content would result in mechanical differences in the material and therefore lead to changes in tabletability. As discussed earlier in Section 5.3.5, any additional water available over that of the water monolayer may also be crucial in determining the tabletability of the material, suggesting that water not only plasticises the material but also aids or hinders bonding at particle interfaces depending on the quantity present.

5.3.9 Compactibility and the effect of water

5.3.9.1 Compactibility of non-hygroscopic materials

Tablet porosity has previously been quoted as a measure of the tableting process due to the relationship with tablet tensile strength (Etzler, et al., 2012). Ryshkewitch (1953) showed that the logarithm of the tensile strength is inversely proportional to the tablet's porosity (Equation 5-4).

$$\sigma_t = \sigma_0 e^{-b'\varepsilon} \hspace{4cm} \textit{Equation 5-4}$$

where σ_t is the tablet tensile strength, σ_0 is the maximum tensile strength at zero tablet porosity and *b'* is an empirical constant.

Figure 5-19 shows a Ryshkewitch-Duckworth plot for lactose and DCPD. For both materials, as porosity decreases, tensile strength increases. The fit to the model confirms that, for non-hygroscopic materials, tablet tensile strength is not dependent on storage RH due to high correlation coefficients (Figure 5-19). The fit of the model gives the parameter, *b'*, which relates the rate at which tablet tensile strength increases as a function of porosity, therefore how the reduction of free volume within the tablet is achieved or bonding capacity. The model also gives the tensile strength at zero porosity, σ_0. Values for both *b'* and σ_0 are given in *Table 5-6*.

In the case of a material such as lactose that undergoes brittle fracture, small particles fill gaps between the larger particles and as compaction pressure increases the material breaks, resulting in a larger surface area for particle-particle contacts to be made. As the value for *b'* increases, porosity reduces, and more contacts are made. However, the larger area available for bonding does not necessarily mean that it is effective contact. Contact between asperities formed due to brittle fracture are less efficient than the contact made via plastic deformation due to the applied stress per contact point being relatively smaller leading to a lower bonding strength. DCPD has a lower bonding capacity than lactose but the surfaces created during brittle fracture are more effective resulting in stronger tablets and therefore higher values for σ_0.
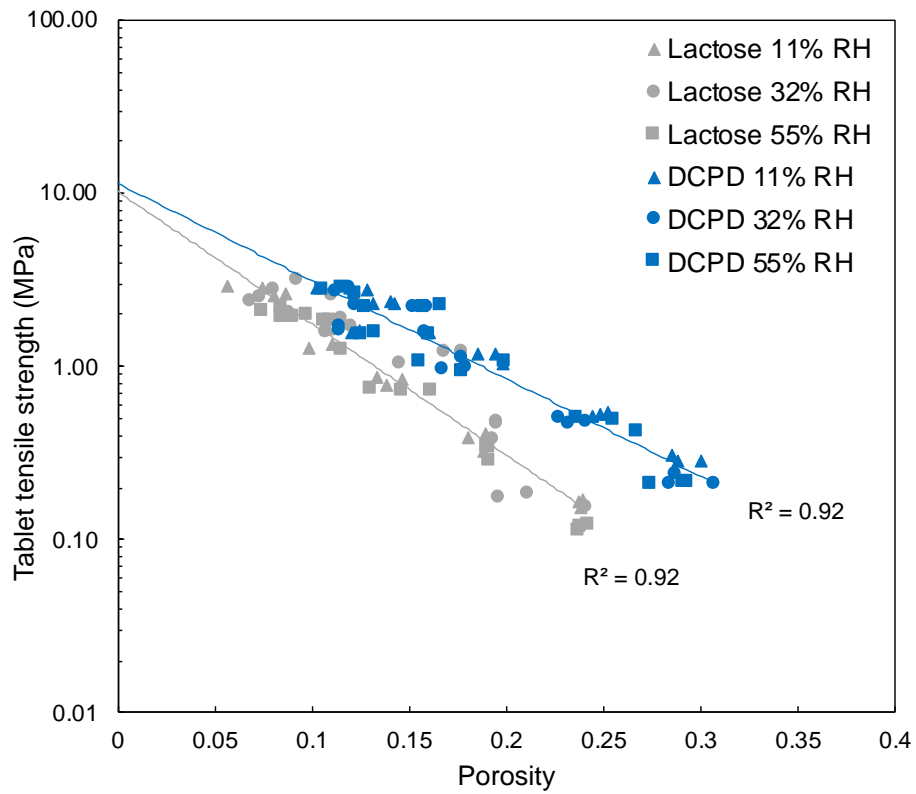
Figure 5-19 Tablet tensile strength as a function of porosity for lactose and DCPD. Straight lines are fitted to the Ryshkewitch-Duckworth equation.

Table 5-6 The tablet strength at zero porosity, $\sigma 0$, and b parameter from the Ryshkewitch-Duckworth equation.

Material and storage humidity	Moisture content	σ_0 (MPa)	b'	R^2
Lactose 11%	1.3	8.1	16.8	0.98
Lactose 32%	1.5	7.2	13.5	0.85
Lactose 55%	1.6	10.8	18.5	0.98
DCPD 11%	0.1	13.6	13.0	0.95
DCPD 32%	0.1	14.6	13.5	0.92
DCPD 55%	0.1	14.6	13.5	0.94

The tableting results from the granulation investigation detailed in Chapter 4 were used to compare directly compressed lactose from the current study (Pharmatose 200M) with granulated lactose. Both Pharmatose 200M and Fast Flo 316 lactose grades had previously been granulated and tableted using a lab scale hydraulic compression simulator (Merlin Powder Characterisation, Brierley Hill, UK). The same die dimensions of 10 mm flat faced tooling were used. However, the tableting speed was considerably faster than the current study at 10 mm/s versus 0.2 mm/s respectively. The data from both investigations is plotted in Figure 5-20 and fitted to the Ryshkewitch-Duckworth model. Table 5-7 shows that both granulated lactose grades have higher values for σ_0, with Fast Flo resulting in the strongest tablets. However, Fast Flo has the lowest bonding capacity.

It has been suggested in earlier publications that there is no dwell time (or compression speed) dependence for the Ryshkewitch-Duckworth equation (Etzler, et al., 2012; Tye, et al., 2005) which would seem to disagree with the current study. Figure 5-20 shows a distinct difference between materials and compression speed when applying the equation. On closer examination of the data presented by Etzler, et al. (2012), there appears to be a considerable difference in model fit between the shortest dwell time of 9 ms and longest dwell time of 90 s which points towards a compression speed dependence for the equation. At faster compression speeds there would likely be a difference in particle rearrangement and breakage. For example, for a brittle material, a faster compression speed may lead to more breakage in the first stages of the compression due to particle asperities coming into contact with each other faster and unavailable time for them to potentially slide past one another as they may with slower compression speeds.

The current study shows a difference between directly compressed and wet granulated material, but it is difficult to deconvolute whether the difference is due to the change in mechanical properties due to wet granulation. Within the granules there is likely to be solid bridges that have formed by partial dissolution and recrystallisation of adjacent particles. This may explain the higher tablet tensile strength for the granulated material as there will be a higher proportion of strong bonds within the structure than that of the non-granulated material at the same porosity.
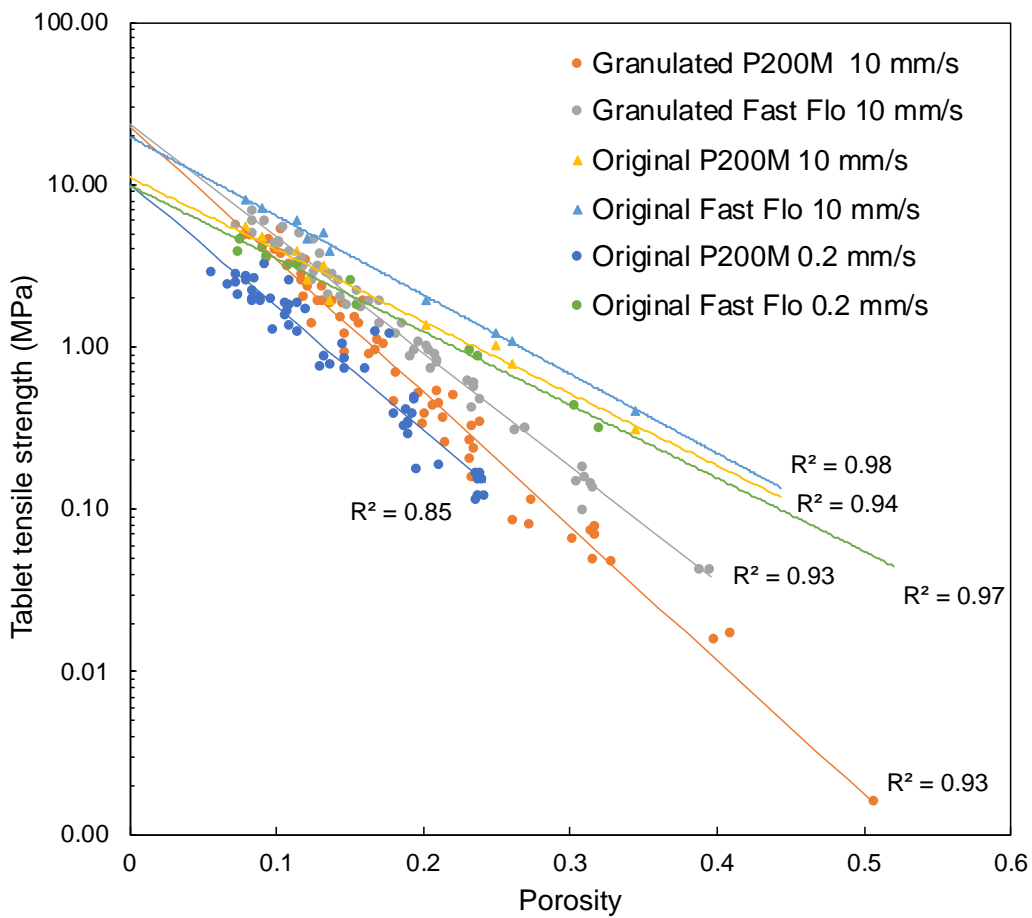
Figure 5-20 Tablet tensile strength as a function of porosity for original and granulated lactose products, note original Pharmatose and Fast Flo are shown at compression speeds of both 10 mm/s and 0.2 mm/s. Straight lines are fitted to the Ryshkewitch-Duckworth equation.

Table 5-7 The tablet strength at zero porosity, σ_0, and k parameter from the Ryshkewitch-Duckworth equation for original and granulated lactose products.

Material	σ_0 (MPa)	b'	R^2
Lactose: Moisture study	10.2	17.5	0.92
Lactose: Granulated P200M	23.2	19.0	0.98
Lactose: Granulated Fast Flo	24.1	16.3	0.99

5.3.9.2   Compactibility of hygroscopic materials

MCC forms stronger tablets at all equivalent porosities compared with all other directly compressed materials and this is shown by the high values for σ_0 (Table 5-8) across all moisture contents. For a material such as MCC that undergoes ductile deformation of particles, there is rapidly increasing intimate contact with increasing compaction pressure allowing for the formation of hydrogen bonds between adjacent cellulose particles. The data points corresponding to MCC stored at 55% RH, (6.5% moisture) all lie below the line fitted to data for MCC stored at 11% and 32% RH (2.6% and 4.0% moisture respectively). The added moisture results in a lower tablet tensile strength at the same porosity in contrast to tablets with a lower moisture content. As stated earlier, the presence of moisture within the tablet may act as a plasticiser allowing the material to undergo more efficient plastic deformation. However, over a certain moisture level, the water acts as a hindrance to hydrogen bond formation due to larger gaps between the material and therefore lower effective contact area. The value for bonding capacity, b', is considerably lower for MCC at any moisture content than all other materials. Again, this may be due to its plastically deforming nature. As compression of the material increases there is no formation of new bonding surface area but rather the surfaces already present are forced closer together; there is no increase in bonding capacity as the compression takes place. Conversely, materials that undergo brittle fracture continually increase their bonding capacity throughout the tablet compression process by fracturing and creating new surface area.

Table 5-8 The tablet strength at zero porosity, σ_0, and k parameter from the Ryshkewitch-Duckworth equation.

Material and storage humidity	Moisture content	σ_0 (MPa)	b'	R^2
MCC 11%	2.6	22.2	6.8	0.99
MCC 32%	4.0	26.9	7.5	0.99
MCC 55%	6.5	17.3	6.5	0.99
Starch 11%	6.4	4.3	12.9	0.97
Starch 32%	9.1	6.1	11.6	0.99
Starch 55%	11.2	8.0	10.7	0.97
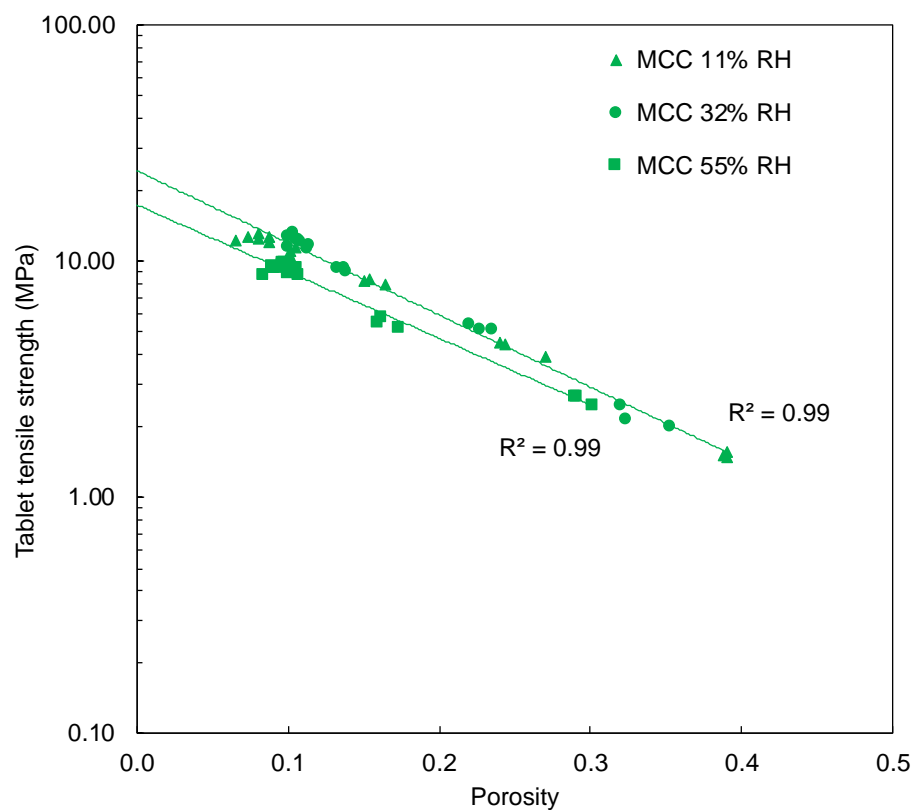
Figure 5-21 Tablet tensile strength as a function of porosity for MCC. Straight lines are fitted to the Ryshkewitch-Duckworth equation, MCC stored at 11% and 32% RH appear on the same line and MCC stored at 55% RH is fitted to a separate line.

Starch does not show a similar fit to the model, with data from each RH showing separate lines of fit. Bonding capacity reduces with increasing moisture content even though the tablet tensile strength at zero porosity increases with increasing moisture content. At the same pore fraction but with increasing moisture content, it is possible to gain a stronger tablet. This points towards water playing a key role in the formation of a strong tablet. Starch swells upon contact with water, therefore morphological changes are likely to be the overarching reason for tablet tensile strength gain. This would also explain the reduction in bonding capacity due to a reduction in surface area as the material swells. However, the increase in tablet tensile strength may also be, even if only in part, due to water bonding within the material.
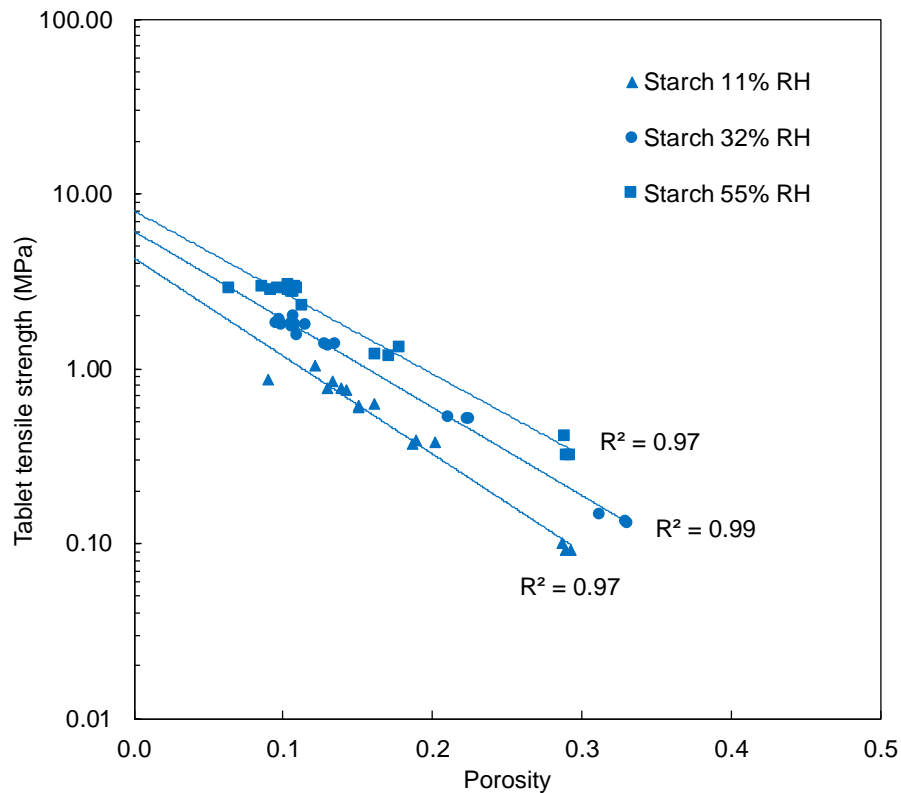
Figure 5-22 Tablet tensile strength as a function of porosity for starch. The straight line is fitted to the Ryshkewitch-Duckworth equation.

5.3.10 The effect of compression and moisture on tablet surface area

The surface area changes as a tablet undergoes compression and can be analysed using BET surface area analysis (TriStar II Plus, Micromeritics, Georgia, USA) as described in Section 3.5.5. The measurement of surface area via BET nitrogen adsorption is a time-consuming process, therefore a decision was made to test one plastically deforming material, MCC, and one material that undergoes brittle fracture, lactose. Differences in surface area as compression took place was assessed by measuring the surface area of tablets compressed at four compressive forces.

The surface area values for MCC and lactose primary powders are shown in Table 5-9. MCC has a higher surface area than lactose due to its layered structure. For the purpose of this investigation, it has been assumed that the uncompacted powder has the same surface area regardless of moisture content. Part of the process for measuring surface area involves outgassing and drying of the material and therefore would not allow for measurement of surface area at various moisture content. It is likely that the surface area for uncompacted material would be different depending on moisture content, however, the experimental procedure was the same for each sample to allow for direct comparison.

Table 5-9 BET surface area values for MCC and lactose primary powders.

Material	BET surface area (m^2g)
MCC	1.203 ± 0.001
Lactose	0.521 ± 0.001

Figure 5-23 shows the change in surface area as a function of compaction pressure. In agreement with previous findings in this study, a linear reduction in surface area with increasing compaction pressure can be seen in all MCC samples, indicating plastic deformation and minimal breakage of primary particles. The surface area also reduces with increasing moisture within the sample indicating that BET appears to be measuring available surface area. The effect of moisture on reducing MCC surface area is likely due to increased bonding i.e., the additional plasticisation has allowed for more surfaces to come together. It also implies that with additional moisture content there is less effective bond strength due to the presence of water between surfaces preventing hydrogen bonding between adjacent surfaces.

For lactose, a crystalline material that undergoes brittle fracture, there is an initial increase in surface area with compaction pressure due to particle breakage. At a compaction pressure of 191 MPa, the surface area reaches its maximum value of 1.09 m^2/g before reducing to 0.84 m^2/g at a compaction pressure of 255 MPa. The tensile strength from tabletability profiles for lactose presented earlier (*Figure* 5-8(c)), continues to rise past 255 MPa, therefore suggesting a further reduction in surface area past this point would occur.
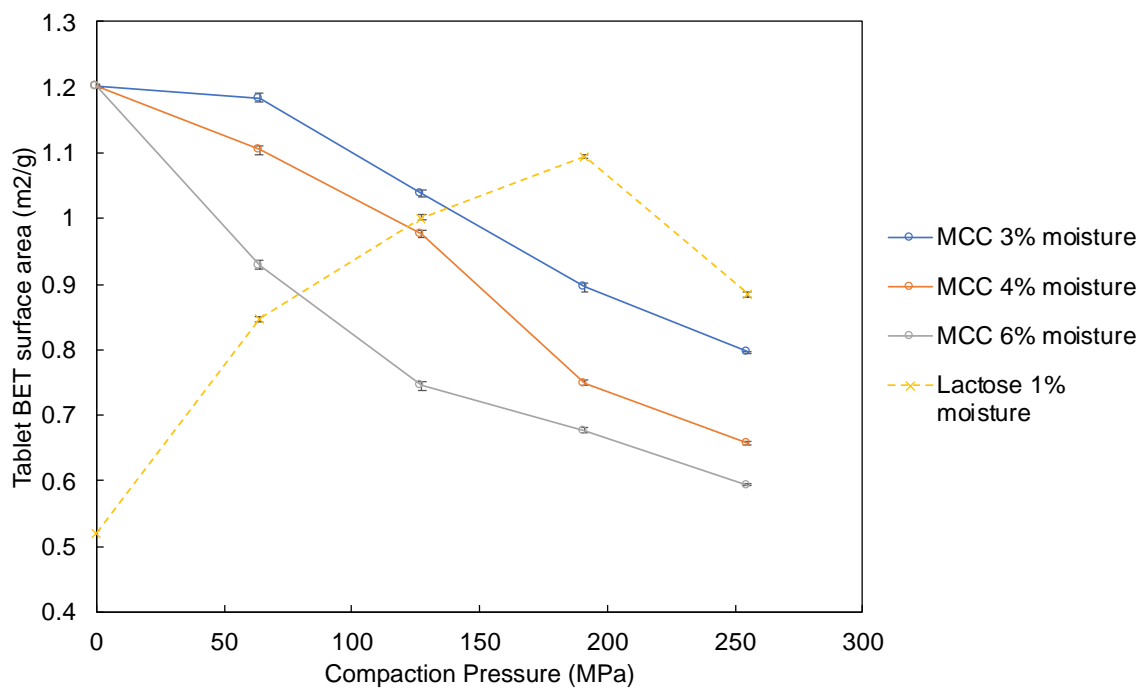
Figure 5-23 Surface area as a function of compaction pressure for MCC at each RH and lactose at 32% RH

5.3.11 The effect of surface area on tablet tensile strength

Figure 5-24 shows plots of tablet surface area against tablet tensile strength for MCC and lactose. Tablet tensile strength increases with decreasing surface area for MCC at all moisture levels and is a linear function of the available surface area. The highest moisture content results in tablets with the lowest surface area. This agrees with the earlier suggestion that an increase in water content leads to more intimate particles within the tablet structure. However, at higher compressive forces the water becomes a hinderance to tablet strength due to over-lubrication of the tablet, therefore equivalent surface area values for the high and low moisture content to do not result in equivalent tablet tensile strength.

Lactose shows a linear increase in surface area and tensile strength during the compression phase corresponding to breakage and rearrangement of the material (Figure 5-24). Once a maximum surface area of 1.1 m^2/g is reached a rapid reduction in surface area with increase in tensile strength is observed.
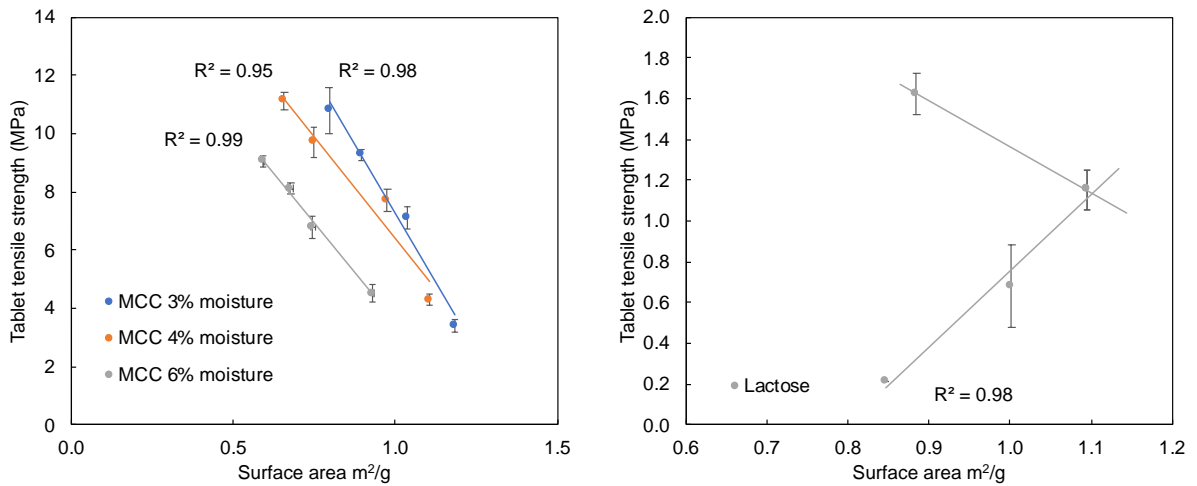
Figure 5-24 Tablet surface area versus tablet tensile strength of tablets produced from (a)
MCC and (b) lactose. Note the difference in scale for each graph.

Table 5-10 Surface area (m^2/g) and tensile strength (MPa) of MCC at 3%, 4% and 6%
moisture content and lactose at 0.5% moisture content. Tablets were compressed to ± 5 MPa
of the figures stated.

Material	Moisture content (%)	Compression pressure (MPa)	Surface area (m^2/g)	Tablet tensile strength (MPa)
MCC	3	0	1.203 ± 0.001	0 ± 0.0
		64	1.184 ± 0.007	3.4 ± 0.2
		127	1.038 ± 0.005	7.1 ± 0.4
		191	0.896 ± 0.007	9.3 ± 0.2
		255	0.796 ± 0.001	10.8 ± 0.8
	4	0	1.203 ± 0.001	0 ± 0.0
		64	1.105 ± 0.007	4.3 ± 0.2
		127	0.976 ± 0.005	7.7 ± 0.4
		191	0.749 ± 0.004	9.7 ± 0.5
		255	0.657 ± 0.002	11.1 ± 0.3
	6	0	1.203 ± 0.001	0 ± 0.0

Material	Moisture content (%)	Compression pressure (MPa)	Surface area (m²/g)	Tablet tensile strength (MPa)
		64	0.929 ± 0.007	4.5 ± 0.3
		127	0.745 ± 0.004	6.8 ± 0.4
		191	0.677 ± 0.007	8.1 ± 0.2
		255	0.594 ± 0.001	9.1 ± 0.2
Lactose	1.5	0	0.521 ± 0.001	0 ± 0.0
		64	0.847 ± 0.004	0.2 ± 0.0
		127	1.002 ± 0.004	0.7 ± 0.2
		191	1.095 ± 0.003	1.2 ± 0.1
		255	0.884 ± 0.003	1.6 ± 0.1

The surface area measurements for MCC tablets can also be used to further probe morphological changes to the material due to moisture. By plotting tablet porosity against tablet surface area (Figure 5-25), it becomes apparent that the surface area changes with moisture content at the same porosity, indicating that morphological changes have taken place with the addition of water. The change is greatest between 3% and 4% moisture and little difference is observed between 4% and 6% moisture. At 6% moisture, for the same value of porosity, there is a reduction in tablet tensile strength compared to those containing 3% and 4% moisture even though there is no considerable difference in surface area. This confirms that any absorption of moisture, and therefore morphological change, has already occurred at a moisture content between 3% and 4%. There is only a small difference in tablet surface area depending on porosity between MCC of each moisture content.
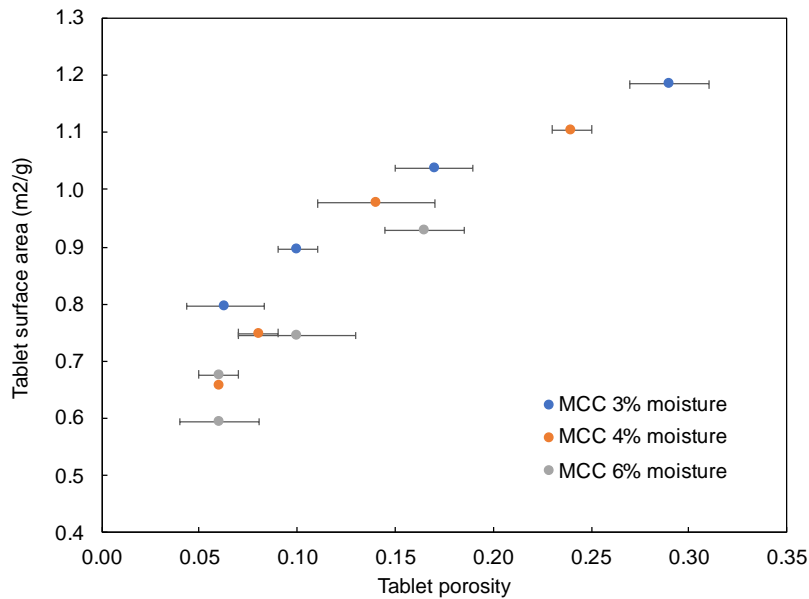
Figure 5-25 The relationship between tablet porosity and tablet surface area for MCC at various moisture content. Error bars indicate the standard deviation of an n=3 experiment.

SEM micrographs of the tablet fracture surface were taken for both lactose and MCC at a range of tablet compaction pressures (Figure 5-26). As compaction pressure increases for lactose, a reduction in the number of visible small particles can be observed. At 127 MPa, the small particles are still distinguishable from the larger ones. At 191 MPa, it is more difficult to distinguish between the larger and smaller particles due to the considerable reduction in porosity. At this point, the highest surface area has been achieved and it can be assumed considerable consolidation of the material is taking place, therefore making it more difficult to distinguish individual particles.

It is more difficult to observe changes with increasing compaction pressure for MCC and definite conclusions cannot be drawn. MCC appears to have a more uniform particle shape and size than lactose. The plastic nature of MCC is apparent as the particles appear to change

shape and become more intimate in a striated manner. Potential differences may be

obtainable with a larger data set and sophisticated image analysis in future work.
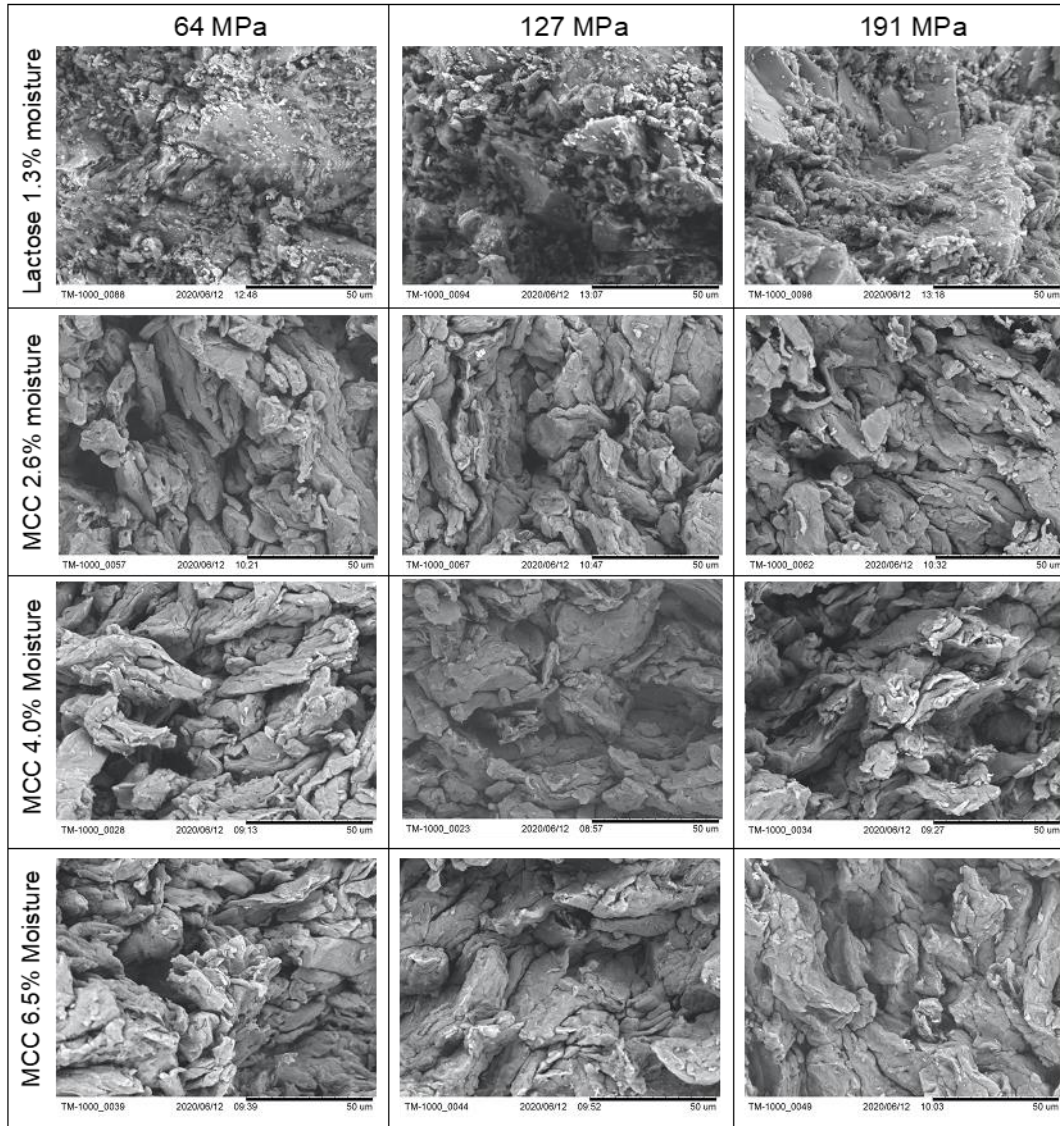
Figure 5-26 SEM micrographs of tablet fracture surfaces for lactose (32% RH) and MCC (15%, 32% and 55% RH) at the range of compaction pressures corresponding to those shown in Figure 5-23.

5.4 Conclusions

The investigation into the role of moisture in tablet compaction and tensile strength in this chapter has led to the following conclusions:

I. The presence of water within the materials and its effect on final tablet strength was shown to influence materials of hygroscopic nature. The tabletability of MCC increases with increasing moisture at low compression pressures (under ~115 MPa), however, at higher pressures, a moisture content above 4% produces weaker tablets. A reduction in tabletability, even for the highest moisture content of 11.2%, is not seen for starch. Starch tablet tensile strength increases with both increasing compaction pressure and moisture.

II. The tabletability of MCC reaches a maximum before a moisture content of 6.5%. At compaction pressures below 115 MPa, MCC containing 6.5% moisture produces the strongest tablets. However, above this value, the tablet tensile strength begins to plateau and even with addition application of pressure, no further tensile strength can be attained. Immobile water layers at the MCC particle surfaces could, to a point, enhance particle-particle interactions but after the formation of multiple water layers, the additional water that is present reduces tablet strength by disruption of or reduced number of intermolecular forces.

III. A maximum moisture content that hinders tablet tensile strength for starch was not found. Even at 11% moisture, there was an increase in tablet tensile strength over the lower moisture content. However, the compaction pressure relating to maximum tensile strength within each moisture level shifted to a lower value with increasing

moisture. The point at which a critical mechanical characteristic change takes place in the swollen starch particles changes with moisture content, indicating that individual starch particles swell upon storage in increasing RH and they have the potential to burst once enough pressure has been applied during the tableting process.

IV. Materials such as lactose and DCPD, that are non-hygroscopic and undergo brittle fracture, show a linear trend for tablet strength under compression. The mechanical properties of these materials are unaffected by changes in RH.

The results presented in this section add to the current body of work by comparing hygroscopic and non-hygroscopic materials in one study. A previous study by Sun (2008) provided an in-depth look into the effects of moisture on the tabletting of MCC, the current study not only confirms some of the findings but also expands the range of moisture content tested and provides a comparison to starch, another hygroscopic commonly used excipient.

6 Investigating microcrystalline cellulose tabletability and storage

6.1 Introduction

Previous researchers have concluded that the moisture content of MCC impacts the resulting tablet tensile strength after compaction due to differing extents of plasticisation of the material (Khan et al. (1988), Nicholas et al. (1999) and Sun (2008)). With increased plasticisation there is a greater contact area for solid bridges to occur and therefore increased tablet tensile strength. This chapter investigates the importance of liquid bridge bonding within MCC tablets based on previous investigations (Chapter 5) showing increased tabletability with increasing moisture. Siming & Wan (2013) showed that liquid bridges can have comparable bond strength to van der Waals forces and therefore any increase in tablet tensile strength is unlikely to be due to plasticisation effects alone.

6.2 Materials and methods

6.2.1 Materials

MCC (Avicel® PH101, FMC, Ireland) was used within the study. Powder was placed in 60 ml sample pots (no more than 45 ml fill) in desiccators previously equilibrated to 3%, 22%, 43% and 75% RH using saturated salt solutions of caesium fluoride, potassium acetate, potassium carbonate and sodium chloride respectively. Powders were left to equilibrate for 28 days before tableting. The mass of powders was recorded regularly to ensure the equilibrium of moisture content had been reached prior to running experiments. Moisture content was assessed using an infra-red moisture balance immediately before tableting (HG63, Mettler

Toledo, UK). The same infra-red moisture balance was used to dry material fully (30 minutes at 120°C) to give the data point at 0 within Figure 6-1. Moisture content was validated using DVS (Figure 6-1). The measured moisture content of MCC is in close agreement with those found from DVS of the material.
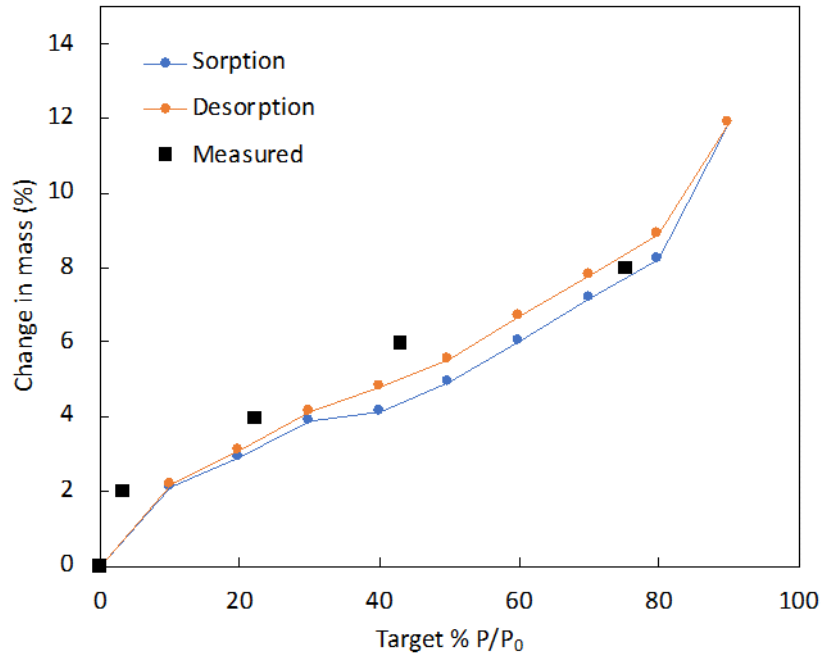
Figure 6-1 DVS results for MCC powder. Black squares represent the measured moisture content of powders via moisture balance.

6.2.2 Powder densities

Bulk, tapped and true densities were measured according to Section 3.4.5 for each powder.

6.2.3 Flowability

The Schulze ring shear cell (Dietmar Schulze, Wolfenbuttel, Germany) described in Section 3.4.6 was used to investigate flow function (ffc) and effective angle of internal friction for MCC

stored at all four RH. Each powder sample was passed through a #18 sieve (1000 µm openings) to break up any loose agglomerates formed during storage. To control the effects of moisture uptake, each sample was taken from the desiccator, prepared and placed in the testing cell within a 15-minute period. All tests were performed in a controlled environment at room temperature and 43% RH.

The relationship between unconfined yield strength (σ_c) and effective angle of internal friction (δ) as a function of major principal stress (σ_1) was determined. Powder flow functions were constructed by performing yield locus test at pre-shear loads of 3, 6 and 9 kPa using a 31.37 cm^3 volume annular shear cell. These three normal stresses were applied, with the fourth being a repeat of the first stress applied (3 kPa). Flow function coefficient (ffc $= \frac{\sigma_1}{\sigma_c}$) were determined from the 6 kPa pre-shear load results. The powder sample was sheared to failure at six increasing, equally distributed normal stresses from 20% to 80% of the pre-shear load and results are presented as the mean of three repeats. This method was based on recommendations from Schulze (2010 and 2013).

6.2.4   Tableting

Tableting was carried out using the Styl'One Compression Simulator as described in Section 3.5.3. Compaction pressures ranged from 50 MPa to 290 MPa, and all tablets were compressed with settings based on the Fette 2090 IC single rotary tablet press with 36 station B-turret, simulated with a punch speed of 250 mm/s to ensure the compression was industrially relevant. For each tablet, the 8 mm die was manually filled with 160 ± 10 mg

powder after lubricating by brushing the die with 1% w/w magnesium stearate in acetone and allowing to dry. Tablet properties were measured according to Section 3.5.4.

6.3 Results and discussion

6.3.1 Powder densities

As stated in Section 5.3.3, the water required for monolayer coverage of MCC was lower than that of materials that undergo brittle fracture such as lactose and DCPD. It is thought water can penetrate the MCC material causing swelling within the striated structure. This concept can be further corroborated by the increasing bulk density of MCC with increasing moisture content (Table 6-1). The increase in bulk density suggests that water is causing the material to swell. Interestingly, the true density of MCC increases with increasing moisture content. This is in agreement with the findings of Sun (2008) and explained by MCC not being 100% crystalline. The increase in true density may be due to the antiplasticization effects of water on amorphous polymers where adsorbed moisture is tightly bound with disordered polymer chains. There is no significant expansion of the solid and a net reduction of the free volume in the amorphous polymer (Sun, 2008).

Table 6-1 Moisture content, bulk density, tapped density and true density values for MCC stored at four different RH values. Results are shown as the mean of three measurements ± SD (in parentheses).

Storage humidity (%)	Moisture content (%)	Bulk density (ρ_b) (g/cm³)	Tapped density (ρ_{tap}) (g/cm³)	True density (ρ_{true}) (g/cm³)
Dried material	0.2	0.32 (0.01)	0.43 (0.02)	1.540 (0.002)
3	1.9	0.32 (0.01)	0.44 (0.01)	1.546 (0.003)
22	4.4	0.34 (0.02)	0.47 (0.00)	1.555 (0.002)
43	5.6	0.34 (0.01)	0.48 (0.01)	1.567 (0.004)
75	8.1	0.38 (0.01)	0.54 (0.00)	1.577 (0.005)

6.3.2   Flowability

6.3.2.1   Effect of moisture content

From the bulk and tapped densities quoted in Table 6-1, the Carr's Index can be calculated (Figure 6-2). Powders stored at all RH show results consistent with very, very poor flow. Flowability decreases slightly with increasing moisture content.
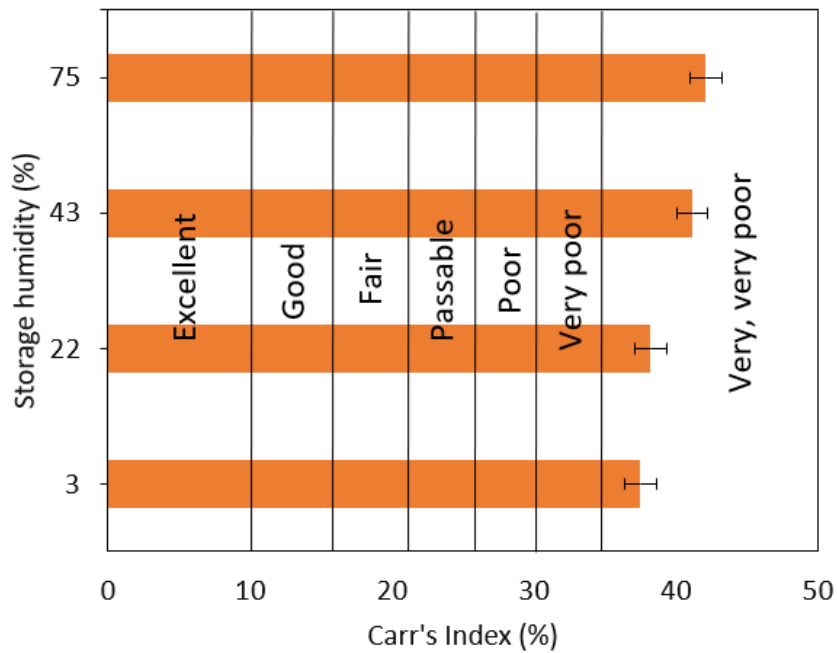
Figure 6-2 The Carr's Index for MCC stored at increasing RH. Error bars indicate standard error.

A Schulze Ring Shear Tester was also used to characterise flowability of powders with differing moisture content. The Jenike flow function coefficient (ff_c) was plotted against powder moisture content (Figure 6-3). Values for ff_c reduced with increasing moisture content, indicating reducing flowability with increasing moisture in agreement for the indication given from bulk and tapped densities. The relationship between ffc and moisture content is not linear, therefore it is unlikely that moisture content is the only parameter that influences the flowability of the material.
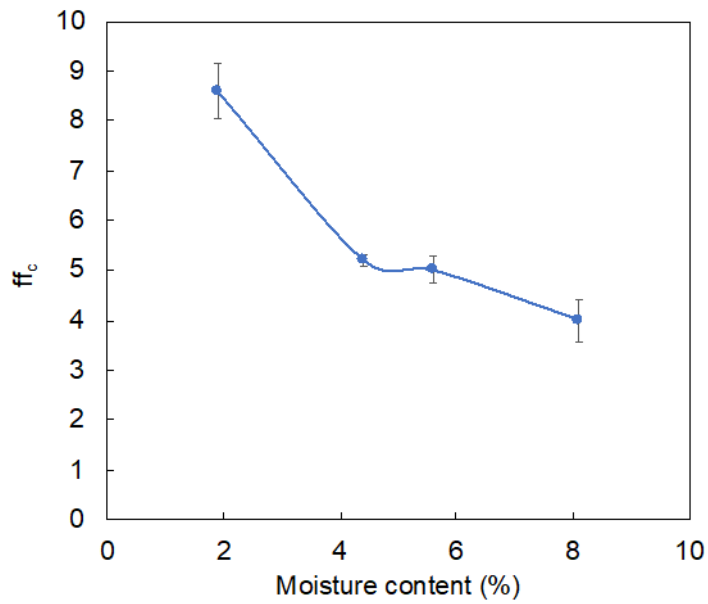
Figure 6-3 Jenike flow function coefficient (ffc) versus powder moisture content. Error bars represent the standard deviation of three repeats.

6.3.2.2   Effect of moisture on powder flow function

Figure 6-4 shows an example plot obtained from a yield locus test and indicates the unconfined yield strength (σ_c) and major principal stress (σ_1).
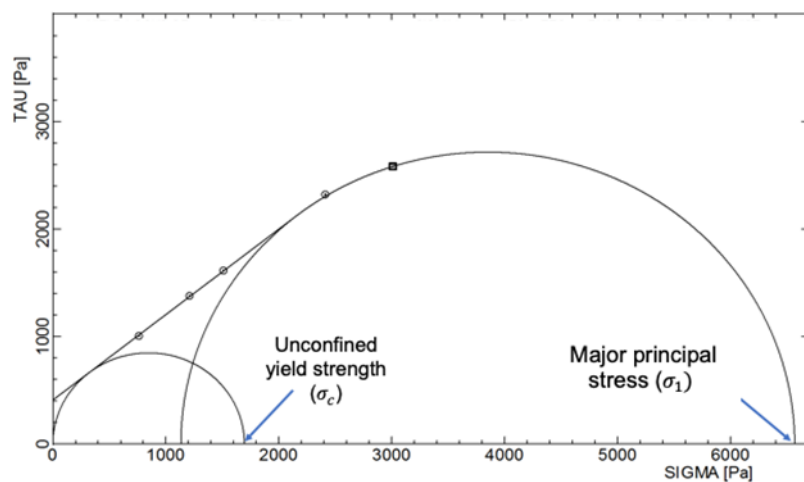
Figure 6-4 An example of the yield locus test indicating unconfined yield stress and major principal stress. Example test shown is for MCC stored at 43% RH and pre-shear of 3000 Pa.

Unconfined yield strength, σ_c, is the shear stress required to initiate flow within the bulk solid after consolidation by a known amount and can be defined by Equation 6-1. The degree of consolidation, or major principal stress (σ_1), is the pressure required to critically consolidate the powder bed prior to deformation (Jager, et al., 2015).

$$\sigma_c = 2c\frac{1+sin\delta}{cos\delta}$$
<div align="right">*Equation 6-1*</div>

where c is cohesion and δ is the angle of internal friction. Cohesion is a measure of the bonding strength of a material. The angle of internal friction is the force required for particles to slide across one another (Jager, et al., 2015).

Figure 6-5 shows a powder flow function plot for MCC at each moisture content. Unconfined yield strength increases with increasing moisture content. However, little difference can be seen between moisture contents of 4.4% and 5.6%. As consolidation stress increases, MCC particles are forced closer together, increasing inter-particulate forces and therefore cohesion/adhesion also increases. For MCC containing 8.1% moisture, due to the greater amount of water, there is likely to be a greater number of liquid bridges between particles as well as other interparticulate forces such as electrostatic interactions, hydrogen bonding and van der Waals forces. The sum of these results in a greater shear force being required for flow. This result is interesting because even though there is greater cohesion within the powder containing the highest moisture content (8.1%) during the shear cell test, it does not lead to extra tensile strength in tablets produced from the same powder (further discussion in Section 6.3.3). The major principal stress does not change considerably with moisture content. The

major principal stress is the greatest stress acting on any plane in the powder. For the same normal stress, a major principal stress indicates a greater shear stress and higher internal angle of friction (Schulze, 2010). This experiment we performed a total of two times and caution should be taken when viewing the results as the variability shown is most likely expected variability within the experimental procedure.
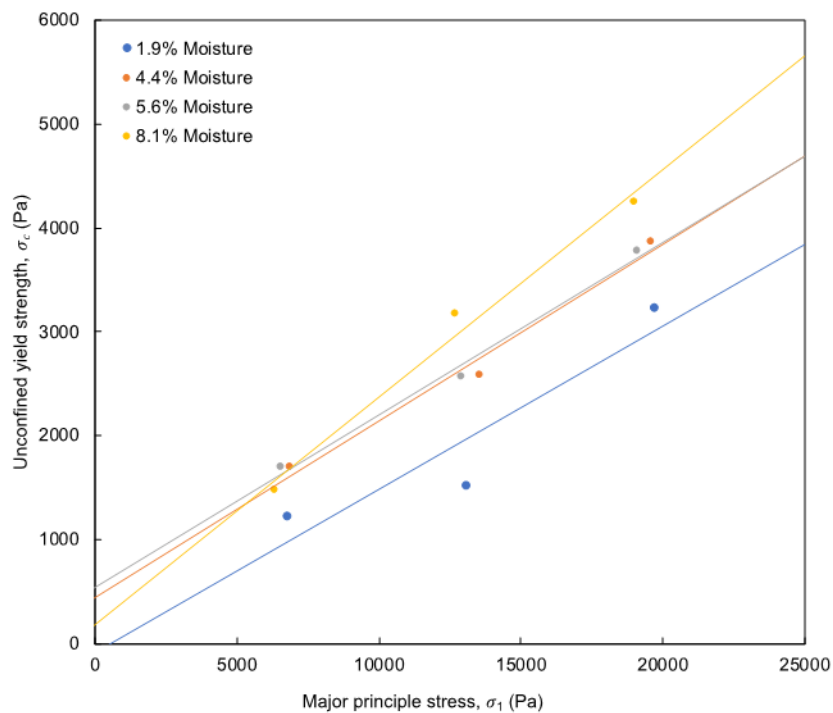
Figure 6-5 Powder flow functions for MCC stored at 3%, 22%, 43% and 75% RH (n=2).

6.3.3   Tabletability

Figure 6-6 shows the tabletability profiles of powders that have been stored at each RH and powder dried prior to tableting. In agreement with previous findings in Section 5.3.5, the tensile strength of tablets produced with MCC containing 0% - 6% moisture increases throughout the profile and even at the highest compression pressure they continue to gain

strength. However, MCC containing 8% moisture (stored at 75% RH) reaches a maximum strength of 11 MPa before plateauing and no further increase in tablet strength can be gained with increasing compression pressure. Interestingly, the material that has been dried prior to tableting demonstrates a considerable reduction in tabletability in comparison to the other powders. This suggests that the presence of water leads to greater bonding within the material in the form of water bonding between MCC particles and also contributes to increasing plasticity of the material. MCC containing 4% and 6% moisture demonstrate similar tabletability, reaching a maximum tensile strength of ~13.5 MPa. From Table 5-2 it can been seen that, according to the GAB model, the quantity of water in the MCC sample required to produce a monolayer is 3.07%. However, the tabletability profile for MCC containing 6% moisture shows an increase in tablet strength with moisture above that required to form a monolayer. Water present over a quantity of 3.07% and up to ~6% may result in stronger tablets due to increased water bonding and not yet be present in large enough quantities to provide a lubricating effect on the material.

Figure 6-6(b) shows the tablet tensile strength of each powder below 100 MPa compression pressure. At compression pressures below 60 MPa, the order of tabletability runs in order of increasing moisture content, with MCC containing 8% moisture gaining the highest tablet tensile strength. This is in agreement with previous flowability tests, which are run at low compression pressures, where the highest moisture content gives the greatest amount of cohesion. This additional cohesion at lower pressures does not lead to stronger compacts being formed at higher pressures. As increasing water adsorbs onto the particle surface and penetrates the MCC structure, taking up space both internally and externally, it is potentially

acting as a lubricant at higher pressures. As the water is present in a greater volume than that required to fill the monolayer, it is acting as a hinderance rather than increasing the amount of water bonding between particles.
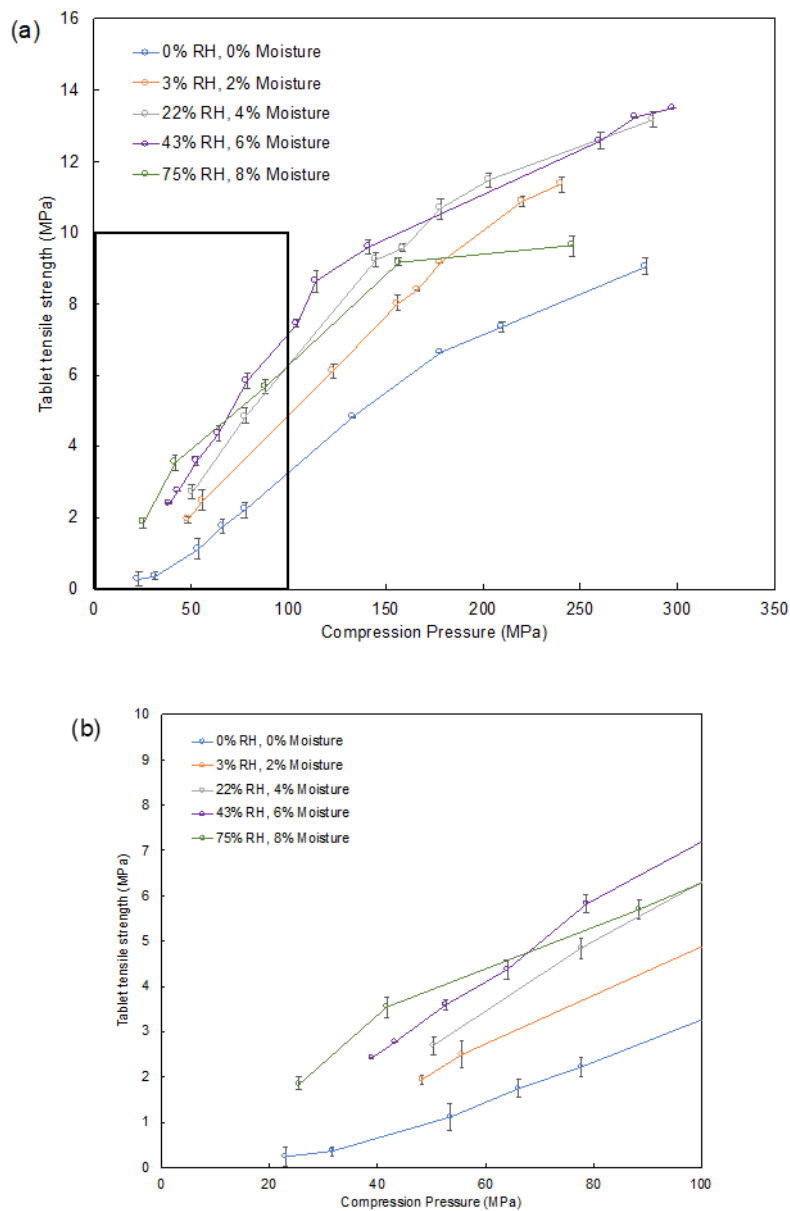
Figure 6-6 (a) Tabletability profiles for MCC stored at a range of RH and dried before tableting. (b) A closer view of the tabletability of powders at compression pressures below 100 MPa (shown by the outlined area in (a)).

6.3.4 Compressibility

Figure 6-7 shows the compressibility profiles for powder stored at each RH. The relationship follows a power law. The reduction in porosity for the dried material is far slower than any other which is in agreement with other results that point towards the drier material being less plastically deformable. The other powders then follow in order of increasing compressibility with increasing moisture. It is important to note that even at the highest compression pressures, zero porosity is not reached but similar minimum porosity values are observed for MCC that has been stored at 3%, 22%, 43% and 75% RH. The rate of reduction in porosity at low compression pressures is faster for 43% RH and 75% RH powders. This may be due to the presence of increased amounts of water leading to a more plastically deforming material and therefore more efficient reduction in powder bed porosity at low compression pressures. More efficient bonding may also take place due to the increasing presence of water bonding.
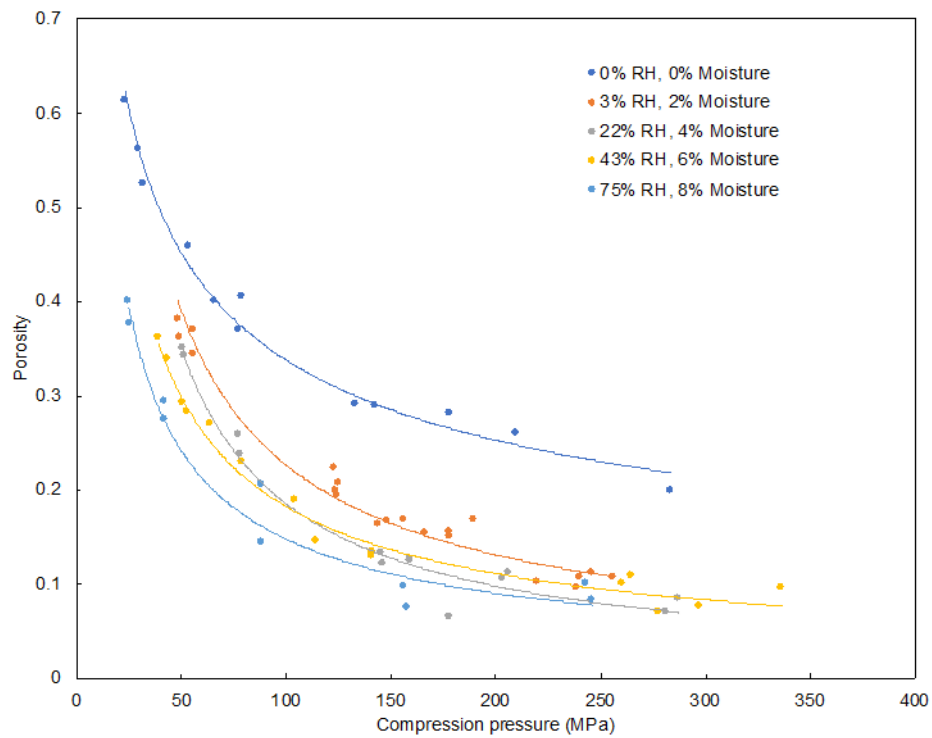
Figure 6-7 Compressibility profiles for powder stored at each RH with corresponding moisture content.

6.3.5   Investigating tablet storage conditions

Further investigation was carried out to study the effect of water on tablet tensile strength upon storage. Additional tablets were produced from powders that had been stored at 3%, 22%, 43% and 75% RH and then placed back into either the same RH that the original powder had been stored at or into a different RH to investigate the effects of 'drying' or 'wetting' of the tablets after production. Tablets were stored for 28 days in order to ensure equilibrium.

Figure 6-8 shows a matrix used to visualise the effects of storage of tablets at various RH. The matrix has been separated into green and red shaded areas to indicate where an increase (green) and decrease (red) in tablet tensile strength has been observed. For tablets produced

from MCC powder stored at 3% RH and then stored at increasingly higher humidity (corresponding to the first row within the matrix), a reduction in tablet strength can be seen with each increasing step of RH when compared to the tablets originally produced and strength tested immediately after production. Tablets originally produced and then placed back into 3% RH remain at a similar tensile strength after storage, suggesting no structural changes to the tablet have taken place. Interestingly, tablets that are placed into 75% RH result in weak tablets that have lower tensile strength than those produced originally from MCC stored at 75% RH (8% moisture). In this instance, water has penetrated the tablet and MCC structure, disrupting hydrogen bonding and forcing apart the bonds originally formed during tablet compression.

The second row within the matrix shows MCC that has been stored at 22% RH and placed back into increasing RH from left to right. When placed into 3% RH, there is no change in tensile strength suggesting no significant mechanical changes have taken place that could result in a stronger or weaker tablet. Even though the 3% RH is a drier environment than the 22% RH, it cannot be concluded that drying of the tablets has taken place. Further work would be required to assess the drying propensity of a tablet at different RH and controlled temperatures as a DVS plot of the base material would not provide an accurate picture as the material has not undergone densification. It would be expected that the drying time of a tablet would be different to that of a loose powder. When placed back into 22% RH there is a decrease in tablet strength for tablets produced at 225 MPa. At first it may be thought the small decrease in tablet tensile strength is due to elastic recovery of the tablet upon storage. However, Zhang, et al. (2017) found that MCC tablets produced at higher compaction

pressures showed less elastic recovery than those produced at lower pressures. The author concluded that this was due to higher compaction pressures (210-300 MPa) enabling stronger particulate interactions, creating a denser tablet structure. The particle-particle attraction force obstructed material expansion. The water that is available within 22% RH is likely to penetrate the densely packed tablet and enable elastic recovery to take place, therefore weakening the tablet. There is a considerable reduction in tablet strength when tablets are stored at 43% and 75% RH. It could be suggested that water has penetrated the tablet and caused expansion and increased porosity resulting in a weaker tablet. However, from Figure 6-9 it can be seen that there is little to no change in tablet porosity within the stored tablets when compared to the original tablets. This means, either the change in porosity due to water is on a scale too small to be seen within the resolution of the tablet measurements taken, or the water can make a mechanical change to the material without creating a change in porosity.

The third row of the matrix shows MCC that has been stored at 43% RH before tableting and placed back into increasing RH from left to right. A slight increase in tablet tensile strength can be seen at a storage of 3% RH suggesting some drying and reduction in porosity as confirmed by Figure 6-9. When placed back into the same RH of 43%, there is a decrease in tablet tensile strength which is more pronounced for tablets produced at higher compaction pressures. Similar to the effects observed for tablets stored at 22% RH, it is unlikely that this trend is due to elastic recovery of the material. Tablets become even weaker when stored at 75% RH where a tablet produced with 250 MPa compaction pressure loses half its tensile strength, dropping from 12 to 6 MPa.

The fourth and final row of the matrix shows the most notable difference in tablet strength upon storage. For tablets produced from powder taken from 75% RH and then stored at 3%, 22% and 43% RH there is a considerable increase in tablet strength after 28 days. Interestingly, the produced with powder from 75% RH and then stored at 3% RH are stronger than tablets produced and stored at 3% RH. This indicates that the presence of water has had a marked effect on tablet strength both at the time of compression and over time. Even at a compaction pressure of 125 MPa, the stored tablets are stronger than those produced or stored at any other condition. This could be key information for future industrial applications where lower compaction pressures are required for either material or process purposes. Again, there is no considerable change in porosity for tablets stored at 3%, 22% and 43% RH, indicating that tablet shrinkage due to water evaporation has not occurred.
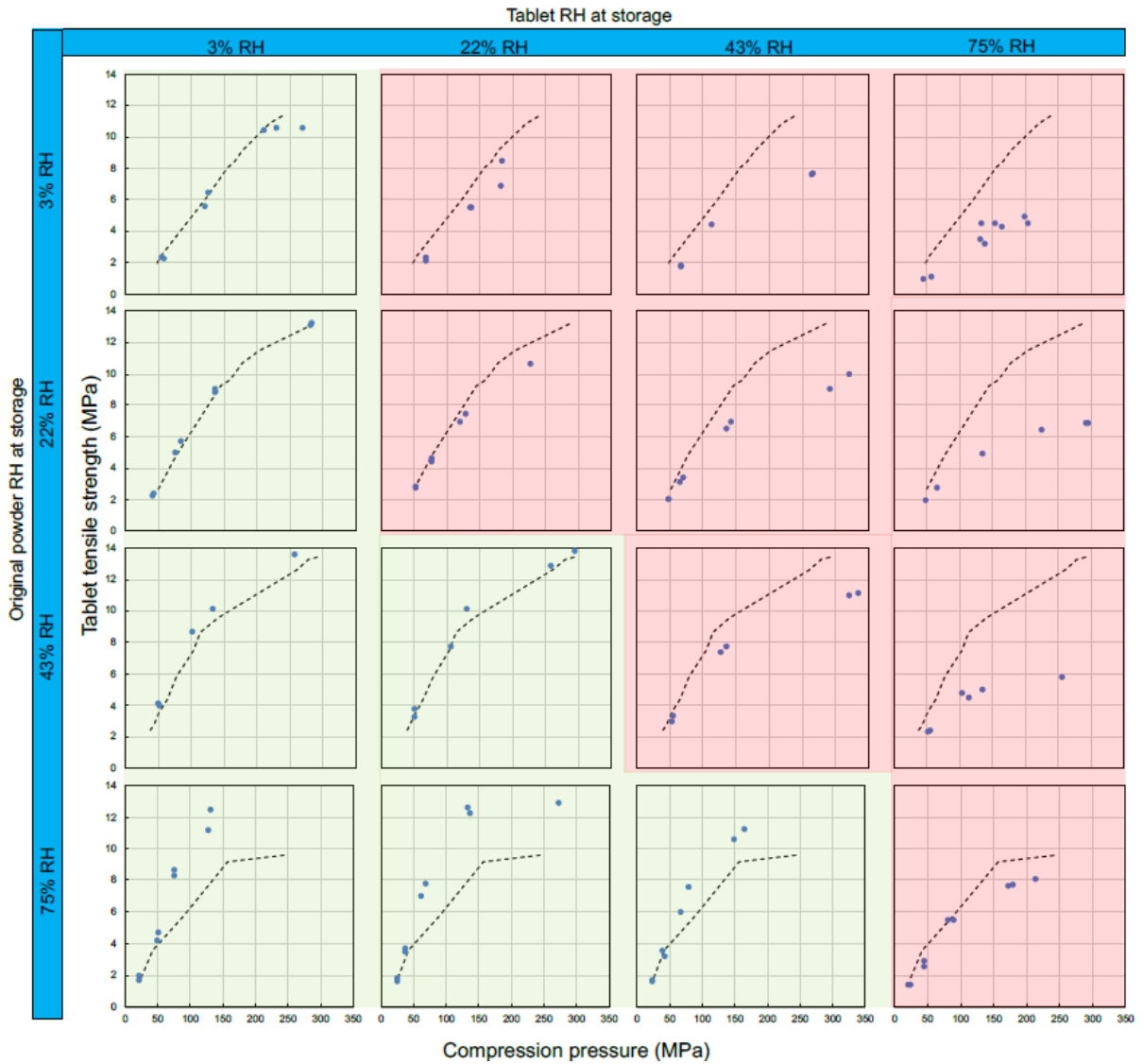
Figure 6-8 A matrix showing the difference in tablet tensile strength upon storage at each RH. Black dotted lines represent the tabletability profile of the original powder stored at RH indicated from the vertical axis of the matrix. Blue dots represent the tensile strength of tablets after storage in the RH indicated on the horizontal axis of the matrix for 28 days. Red and green shaded areas indicate a reduction or increase in tablet tensile strength respectively.
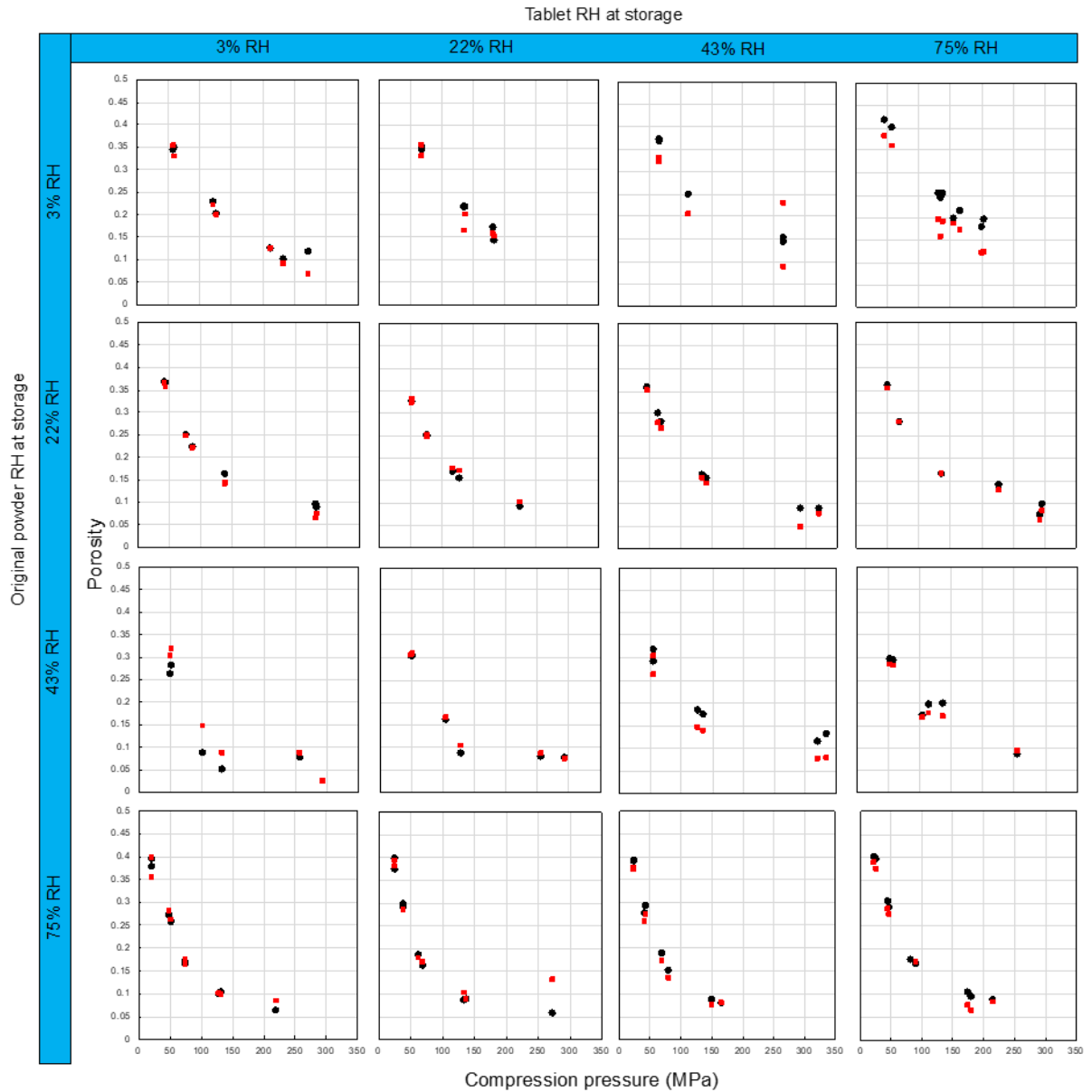
Figure 6-9 A matrix showing tablet compressibility profiles upon storage at each RH. Red circles represent the compressibility profile of the original powder stored at RH indicated from the vertical axis of the matrix. Black circles represent the porosity change of the same set of tablets after storage in the RH indicated on the horizontal axis of the matrix for 28 days.

Previous work by Zhang, et al. (2017) showed that MCC tablets exhibited continuous volume expansion upon storage and concluded that this was due to water absorption from the surroundings and elastic recovery. It was also shown that mannitol, which undergoes brittle fracture exhibited expansion immediately after production due to elastic recovery and then shrinkage on storage due to solidification. To further asses the behaviour of the material, the height and diameter of each tablet immediately after compression was compared to its dimensions after 28 days of storage at varying RH. The elastic recovery after storage (V_{ERS}) was calculated using to determine the time and storage RH-dependent dimension change in both radial and axial directions using Equation 6-2. Tablet dimensions were taken using digital callipers accurate to ±0.001 mm within 60 minutes after production and after 28 days of storage at varying RH.

$$V_{ERS}\ (\%) = \frac{V - V_{ej}}{V_{ej}} \times 100$$

<div align="right">*Equation 6-2*</div>

where *V* is the tablet volume after 28 days storage and V_{ej} is the tablet volume immediately after ejection from the production process.

Figure 6-10 (a) shows an increase in tablet volume on storage at increasing RH. As expected, the largest increase in volume is for tablets stored at 75% RH, indicating that the tablet has absorbed water and undergone elastic recovery. The difference in volume expansion due to water absorption and elastic recovery is unknown as a moisture content after storage was not recorded. However, when tablets are placed back into 3% RH (the RH from which original MCC powder was taken for tablet production), there is very little volume increase and, due to water

absorption being unlikely at this point, the tablet expansion is expected to be entirely due to elastic recovery. At storage of 3% RH, tablets undergo less volume increase with increasing production compaction pressure. This is in agreement with previous findings by Zhang, et al. (2017). As storage RH increases the volume expansion seems less dependent on production compaction pressure and more dependent on exposure to moisture. This suggests that the orignial bonding within the tablet is disrupted by water to the same extent no matter how close the contact of the original material under the original compression.

Figure 6-10 (b) shows the change in tablet volume after tablets are produced from original material stored at 22% RH and then stored at varying RH. There is a decrease in tablet volume when placed back into 22% RH or 3% RH. At 3% RH there is a larger volume decrease for tablets compressed at 130 and 200 MPa which indicates material that was already closer together as a result of higher compaction pressure can become a denser compact after water loss and solidification. Figure 6-8 confirms that at 3% RH storage, this solidification results in stronger tablets. When tablets are stored at 43% or 75% RH there is volume expansion due to water absoprtion which results in less intimacy between particles and weaker tablets.

The greatest amount of volume reduction was seen within tablets produced from powder originally stored at 43% RH and then placed in 3% RH for 28 days (Figure 6-10 (c)). This resulted in stronger tablets as shown in Figure 6-8. Interestingly, for tablets compressed at 60 and 130 MPa and stored at 43% or 75% RH, there is considerable volume expansion but no change in volume for tablets compressed at 200 MPa. Tablets compressed at 200 MPa may have undergone enough consolidation to stop water from the atmosphere entering the tablet and being able to force material apart. In this case, the particle-particle attraction force inhibits

233

expansion during relaxation, this may include water bridges that have formed due to the water that is present within the tablet. The greater expansion seen, even at higher compression, for tablets stored at 3% RH shows that water bonding within the tablet is important to inhibit the expansion process. In the previous study by Zhang, et al. (2017) it was found that MCC tablets produced at 210 MPa and kept at ambient RH (45%) demonstrated a volume change of 1.8% at 500 minutes compared to a 3% increase in volume for tablets produced at 68 MPa. This is in agreement with the current study. However, it is unclear as to why tablets compressed at 130 MPa demonstrate a larger volume increase than tablets produced at 60 MPa. The same is true for tablets stored at 75 % RH in Figure 6-10 (d). The trend for tablets produced from powder taken from 75% RH and stored at varying RH is similar to that seen for those produced from powder at 45% RH. At 3%, 22% and 43% storage RH there is a range of volume change from -4.2 – 0.5%. When tablets are placed into 75% RH there is expansion, confirming that further expansion of the material is possible even thought the tablets were produced from material that had previously been stored at 75% RH. However, part of the expansion may be due to material losing some of the origial moisture contained within it during the production process and then absorbing the moisture again once put back into 75% RH.
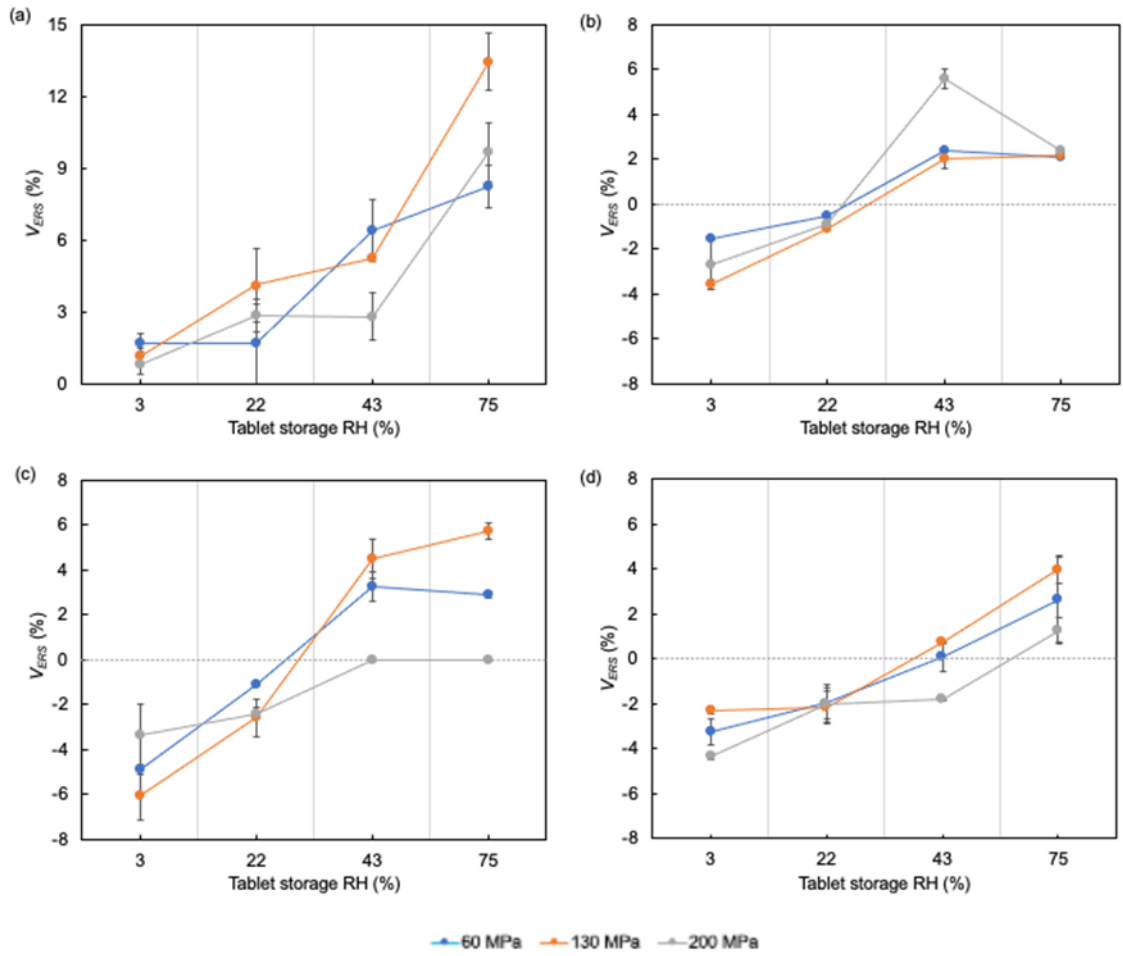
Figure 6-10 Tablet volume change with increasing storage RH for tablets produced at 3 compaction pressures and with MCC originally stored at (a) 3% RH, (b) 22% RH, (c) 43% RH and (d) 75% RH.

6.4 Conclusions

This section provides an in-depth study of the effects of moisture on MCC and further expands the work carried out by Sun (2008). As a result of further investigations into the relationship between water and the tabletability of MCC presented in this chapter the following conclusions can be made:

I.   At low compression pressures below 60 MPa, tabletability of MCC increases with increasing water content. Material containing 8% moisture demonstrates that adsorbed water can occupy free space and increase tablet strength through additional plasticisation of MCC until higher compressive forces are applied. At compressive forces over 60 MPa, the additional water present within the material fills space between particles, allowing them to slide over one another and any plasticisation effects from water are cancelled out by its lubricating effects. This further confirms the conclusions made in Chapter 5 of this thesis.

II. The strength of tablets changes according to the RH they are stored in post-production. When tablets produced from low moisture-containing material are placed in a higher RH for storage, they undergo volume expansion which results in a weakening of the tablet. The tablet can take up water from the atmosphere which penetrates the tablet structure, pulling apart the strong bonds that had formed between MCC particles as a result of the initial tablet compression process.

III. The flowability of MCC reduces with increasing moisture content highlighting the increased particle-particle interactions due to the presence of water. This could have

implications for the processibility of a formulation in industry and should be taken into account when choosing process conditions and equipment.

IV. The results of this chapter confirm the importance of maintaining a controlled level of environmental moisture during the processing of formulations containing MCC to ensure target tablet tensile strength is both attained and maintained.

7 The role of magnesium stearate in the reduction of tablet tensile strength

7.1 Introduction

The negative effect of magnesium stearate is widely known and MCC is often referred to as a material with high lubrication sensitivity (Roberts & Rowe (1986), Hiestand (1997), Paul & Sun (2017)). MCC undergoes plastic deformation and therefore any MgSt that is distributed on the particle surface will remain in place to inhibit effective bonding between MCC surfaces throughout compression. Materials that undergo brittle fracture, such as lactose, are less sensitive to the addition of MgSt due to the production of new effective bonding surfaces throughout fragmentation during compression. There has been little investigation as to whether MCC lubrication sensitivity is exaggerated with the presence of moisture within the tablet. Past literature reports that the reduction in tablet strength is due to a reduction in interparticulate bonding which, in turn, increases the relaxation of tablets (Zuurman, et al., 1999). Koskela, et al. (2018) reported that MCC is a particularly lubricant-sensitive material and over-lubrication occurred with all MCC grades. Upon longer blending times in a Turbula mixer the tensile strength of tablets was reduced. It is important to understand the negative effects the presence of magnesium stearate in various concentrations may have on a tablet to ensure quality. The addition of magnesium stearate results in increased tablet brittleness, therefore changing the fracture behavior under stress (Paul & Sun, 2017). Problems such as chipping, lamination and high friability may occur in tablets with increased brittleness and therefore produce a sub-standard tablet.

7.2   Materials and methods

7.2.1   Materials

MCC (Avicel® PH101, FMC, Ireland) was used within the study, both as a single material and mixed with 0.5%, 1% and 2% w/w magnesium stearate (MgSt) (Mallinckrodt, Ireland). A mixer shaker (Turbula T2F, GM, USA) was used to disperse the three concentrations of MgSt within MCC for 15 minutes and at 50 rpm. The mixing conditions were chosen based on the previous study by Paul & Sun (2017) where the longest mixing time was 15 minutes at only 25 rpm. To ensure sufficient mixing had taken place, a speed of 50 rpm was chosen for the current study. Both MCC and MgSt were taken from ambient conditions and the moisture content of the mixed powders was measured using an infra-red moisture balance (HG63, Mettler Toledo, UK) and found to be 3.88% (±0.12) based on three measurements of each formulation immediately after mixing. The powders were then placed in open 60 ml sample pots (no more than 45 ml fill) in desiccators previously equilibrated to 3%, 22%, 43% and 75% RH using saturated salt solutions of caesium fluoride, potassium acetate, potassium carbonate and sodium chloride respectively. Powders were left to equilibrate for 28 days before tableting. The mass of powders was recorded regularly to ensure the equilibrium of moisture content had been reached prior to running experiments. Powder moisture content was assessed using the infra-red moisture balance immediately before tableting.

7.2.2   Powder densities

Bulk, tapped and true densities were measured, in triplicate, according to Section 3.4.5 for each powder from ambient temperature and humidity.

7.2.3   Powder Flowability

The Schulze ring shear cell described in Section 2.6.4 was used to measure the flow function coefficient, ffc. A pre-shear load of 5000 Pa and normal load at shear of 1500, 2200, 3150 and 4800 Pa were used to obtain yield loci within a standard cell of 30 ml. The cohesion of a sample was calculated by extrapolating the yield loci to zero normal stress.

7.2.4   Tableting

Tableting was carried out using the Styl'One Compression Simulator as described in Section 3.5.3. Settings were based on the Fette 2090 IC single rotary tablet press with 36 station B-turret, simulated with a punch speed of 250 mm/s. These settings were chosen to mimic those used within an industrial setting. For each tablet, the die was manually filled with 150 ± 10 mg powder and not lubricated prior to fill. Compaction pressure ranged from 60 MPa to 250 MPa. Tablet properties were measured according to Section 3.5.4.

7.2.5   Experimental design

The effects of the amount of MgSt, the storage RH and compression pressure were evaluated by a multilevel full-factorial design (Table 7-1). The design and analysis was completed using MODDE software (Version 12.0, Umetrics MKS AB, Umeå, Sweden).

Table 7-1 Factor names and levels.

Factor	Factor levels
MgSt concentration (%w/w)	0, 0.5, 1
Powder storage RH (%)	3, 22, 43, 75
Compression Pressure (MPa)	60, 150, 250

Tablets produced with MgSt concentration of 2% w/w were excluded due to initial experiments showing excessive lamination in tablets, even at the lowest compression pressure. The design contained 117 experiments including three centre point replicates. The centre point experiments contained powders stored at 22% RH, containing 0.5% w/w MgSt and a compression pressure of 150 MPa.

7.3   Results and discussion

7.3.1   Powder moisture content

Table 7-2 shows the moisture content of each powder immediately before tableting. There is no significant difference between different concentrations of magnesium stearate or the primary MCC powder.

Table 7-2 The moisture content of each powder immediately before tableting. Results are shown as the mean of three measurements ±SD (in parentheses).

Material	Storage RH (%)	Moisture content (%)
MCC	3	2.2 (0.05)
	22	4.4 (0.02)
	43	5.6 (0.03)
	75	8.9 (0.01)
MCC + 0.5% w/w MgSt	3	2.4 (0.06)
	22	4.1 (0.04)
	43	5.8 (0.02)
	75	8.7 (0.03)
MCC + 1% w/w MgSt	3	2.5 (0.02)
	22	4.1 (0.03)
	43	5.7 (0.01)
	75	8.5 (0.03)
MCC + 2% w/w MgSt	3	2.3 (0.01)
	22	4.1 (0.03)
	43	5.9 (0.02)
	75	8.2 (0.03)

7.3.2   Powder densities

Table 7-3 shows the measured density values for MCC, MgSt and subsequent mixtures of each. As MgSt concentration is increased bulk and tapped density decrease due to the lower bulk and tapped densities of MgSt primary powder. The resultant value for Carr's Index indicates poor or very poor flow for all of the powders. Although still poor, a concentration of 2% MgSt

provides improved flowability compared with lower concentrations due to MgSt providing lubrication within the formulation.

Table 7-3 Bulk, tapped and true density of powders taken from ambient temperature and humidity with corresponding Carr's index value. Results are shown as the mean of three measurements ± SD (in parentheses).

Material	Bulk density (g/cm3)	Tapped density (g/cm3)	True density (g/cm3)	Carr's Index (%)
MCC	0.28 (0.02)	0.43 (0.02)	1.58 (0.00)	35 (very poor)
MgSt	0.14 (0.01)	0.21 (0.01)	1.02 (0.00)	33 (poor)
MCC + 0.5% w/w MgSt	0.26 (0.02)	0.40 (0.03)	1.54 (0.00)	35 (very poor)
MCC + 1% w/w MgSt	0.25 (0.01)	0.39 (0.03)	1.54 (0.00)	36 (very poor)
MCC + 2% w/w MgSt	0.25 (0.02)	0.37 (0.01)	1.53 (0.00)	32 (poor)

7.3.3   *Flowability measured using Schulze Ring Shear Tester.*

Flowability was measured for each powder using the Schulze ring shear tester and the results are presented in Table 7-4 in terms of flow function (ffc). A higher value for ffc denotes materials with higher flowability (Jenike, 1964). Results are given as the mean of three measurements. As the concentration of MgSt increases, there is an increase in ffc at low moisture content (2.2%) but similar ffc values are observed across MgSt concentrations at higher moisture content levels.. MCC with no MgSt at the lowest moisture content, is classified as easy-flowing according to an ffc value of 8.6. With the addition of 2% w/w MgSt, the material becomes free-flowing (Schulze, 2010). This confirms that the MgSt is acting as a lubricant and would improve manufacturability by reducing friction between the formulation and manufacturing equipment. Even though MgSt increases the flowability of the driest

material, this is not the case when additional moisture is added to the system. Using Figure 7-1 to visualise ffc results, it is clear that any advantage gained by using MgSt within the formulation at 2.2% moisture content, is rapidly lost with the addition of moisture.

Table 7-4 The ffc values for each powder sample. Results are shown as the mean of three measurements $\pm$ SD (in parentheses).

Material	Moisture content (%)	ffc
MCC	2.2 (0.05)	8.6 (0.4)
	4.4 (0.02)	5.2 (0.2)
	5.6 (0.03)	5.0 (0.1)
	8.9 (0.01)	4.0 (0.5)
MCC + 0.5% w/w MgSt	2.4 (0.06)	9.0 (0.6)
	4.1 (0.04)	4.9 (0.4)
	5.8 (0.02)	4.7 (0.2)
	8.7 (0.03)	4.1 (0.3)
MCC + 1% w/w MgSt	2.5 (0.02)	10.0 (0.4)
	4.1 (0.03)	4.9 (0.1)
	5.7 (0.01)	4.7 (0.2)
	8.5 (0.03)	3.9 (0.2)
MCC + 2% w/w MgSt	2.3 (0.01)	11.0 (0.6)
	4.1 (0.03)	5.6 (0.2)
	5.9 (0.02)	4.0 (0.2)
	8.2 (0.03)	3.7 (0.3)
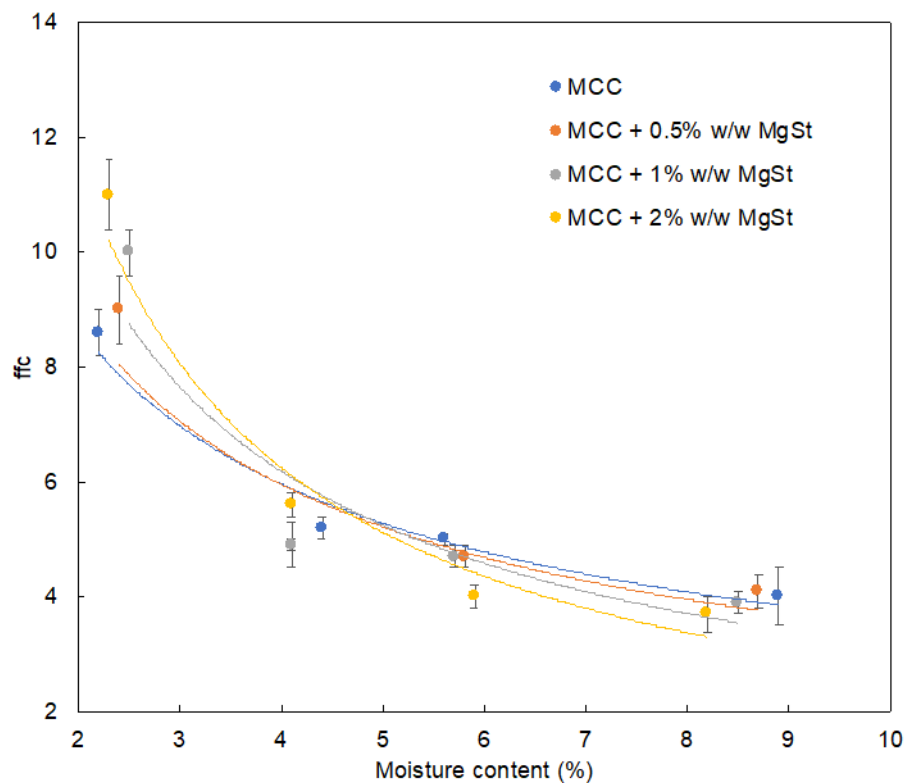
Figure 7-1 The relationship between MgSt concentration, moisture content and ffc.

7.3.4 The effects of moisture content, compression pressure and magnesium stearate concentration on tabletability

Figure 7-2 shows the tabletability profiles for each concentration of MgSt based on the RH the powder had been stored at prior to tableting. Tablets containing no lubricant show minimal loss in tabletability with increasing moisture content up to 6% moisture. At 8% moisture there is a reduction in tabletability. After storage at 75% RH, and therefore a moisture content of 8%, the tablet tensile strength of tablets begins to plateau at 200 MPa for the 0% w/w MgSt powder. The highest tablet tensile strength values were obtained with powder stored at 22% RH with no MgSt present and a compaction pressure of 250 MPa.

The reduction of tablet tensile strength with increasing MgSt is clear in Figure 7-2, however it does not appear to be further exacerbated by any increase in moisture until a moisture content of 8% in introduced.. At compaction pressures over 100 MPa, tablets were unable to be produced from 1% MgSt powder stored at 75% RH and even at the lowest compaction pressures tablets could not be produced with 2% MgSt powder from the same RH. During tableting of MCC containing 2% w/w MgSt, it was noted that lamination occurred when applying compression pressure (Figure 7-3). Capping or lamination occurs when the interparticulate bonding produced during the compaction process is weak and therefore cannot withstand the elastic recovery that takes places during decompression (Sun, et al., 2018). The reduction of interparticle attraction, and therefore, reduced resistance against relaxation was also confirmed by (Zuurman, et al., 1999) where a decrease of ~8.5 MPa tablet tensile strength was observed in non-lubricated versus lubricated tablets. The presence of MgSt hinders the tablet compression process leading to a lack of effective bonding within the tablet.
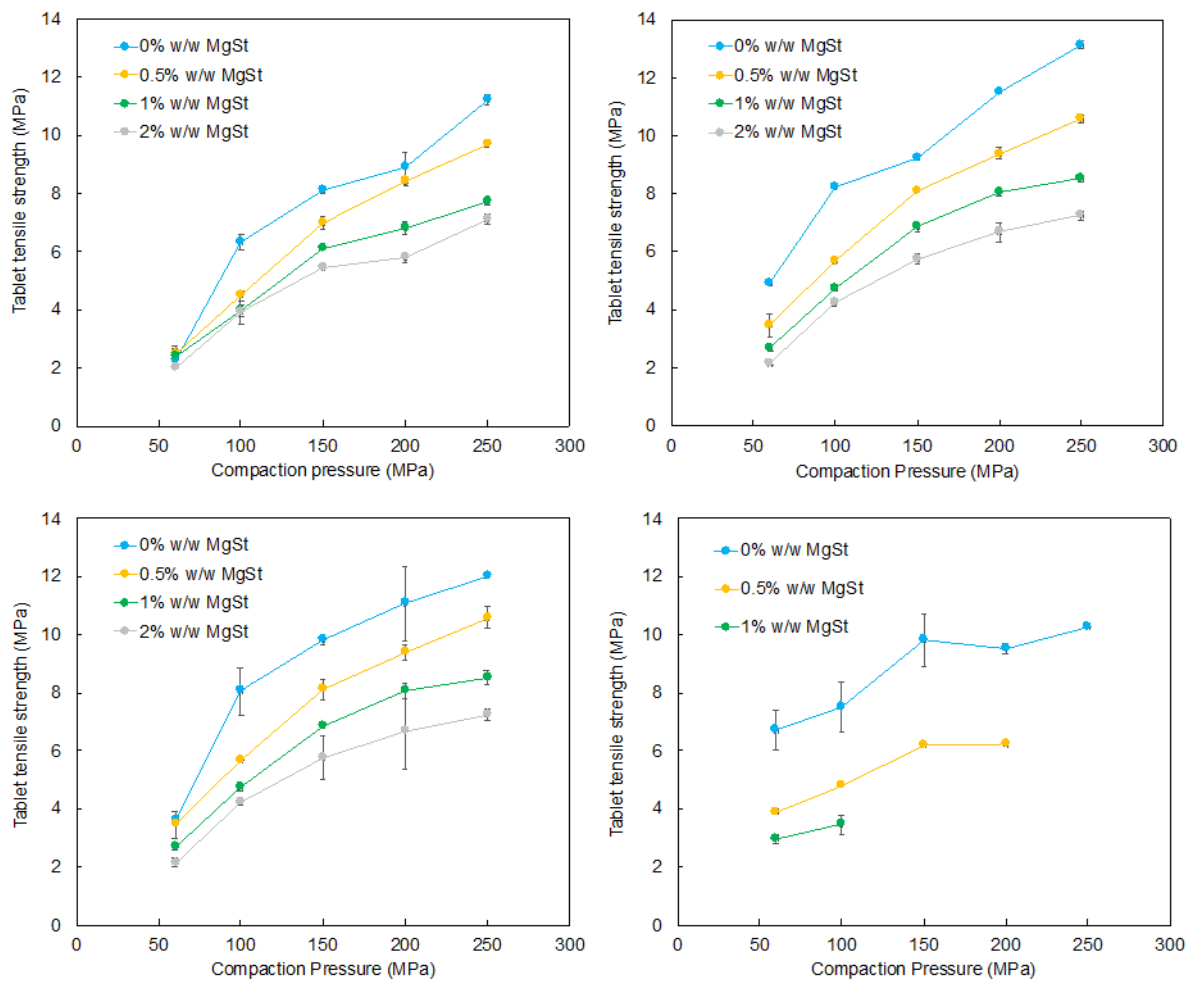
Figure 7-2 Tabletability profiles for each concentration of magnesium stearate stored at (a) 3%, (b) 22%, (c) 43% and (d) 75% RH corresponding to 2%, 4%, 6% and 8% ±1% moisture respectively. Tablets could not be produced from MCC containing 2% MgSt at any compaction pressure when stored at 75% RH.

Figure 7-3 Demonstrating the failure of MCC tablets produced from material containing 2% w/w MgSt and stored at 75% RH.

7.3.5   Modeling

A stepwise regression technique was employed using MODDE software (Version 12.0, Umetrics MKS AB, Umeå, Sweden) to model the effects of variables (MgSt concentration, storage RH and compression pressure) as shown by Equation 7-1. The least significant terms were excluded from the model as long as the predictive power value (Q^2) increased.

$$y = a_1 \cdot MgSt + a_2 \cdot RH + a_3 \cdot CP + a_4 \cdot RH^2 + a_5 \cdot CP^2 + a_6 \cdot MgSt \cdot RH + a_7 \cdot MgSt \cdot CP + a_8 \cdot RH \cdot CP + c$$

Equation 7-1

Where y is tablet tensile strength (MPa), MgSt is magnesium stearate concentration (%w/w), RH is storage humidity of the original powder (%), CP is compaction pressure (MPa), a_1 to a_8 are coefficients and c is a constant. The equation for the tablet tensile strength response is presented in Table 7-5. The R^2 and Q^2 values for the model were 0.89 and 0.87 respectively, indicating a high goodness of fit and high predictive relevance. This is also shown by a plot of

observed versus predicted results in Figure 7-4. This model has limitations, it will likely only

hold for the process parameters and tablet geometries used within the current study. A

broader experimentational study would be required to fine-tune the model to allow for

differing conditions.

Table 7-6 shows a *p* value <0.0001 for tablet tensile strength which indicates a significant

effect of interactions between control factors and their mutual interactions. A normal

probability plot for residual errors of the response variable is shown in Figure 7-4. The plots

show normal distribution and data is distributed along a straight line.

Table 7-5 Showing the coefficient values a_1 to a_9 and constant for the tensile strength response. Statistical significance is shown by p.

	Coefficient	p
a_1	-2.196	<0.0001
a_2	-0.964	<0.0001
a_3	2.419	<0.0001
a_4	-2.109	<0.0001
a_5	-1.246	<0.0001
a_6	-1.375	<0.0001
a_7	-0.901	<0.0001
a8	-1.976	<0.0001
c	8.182	<0.0001
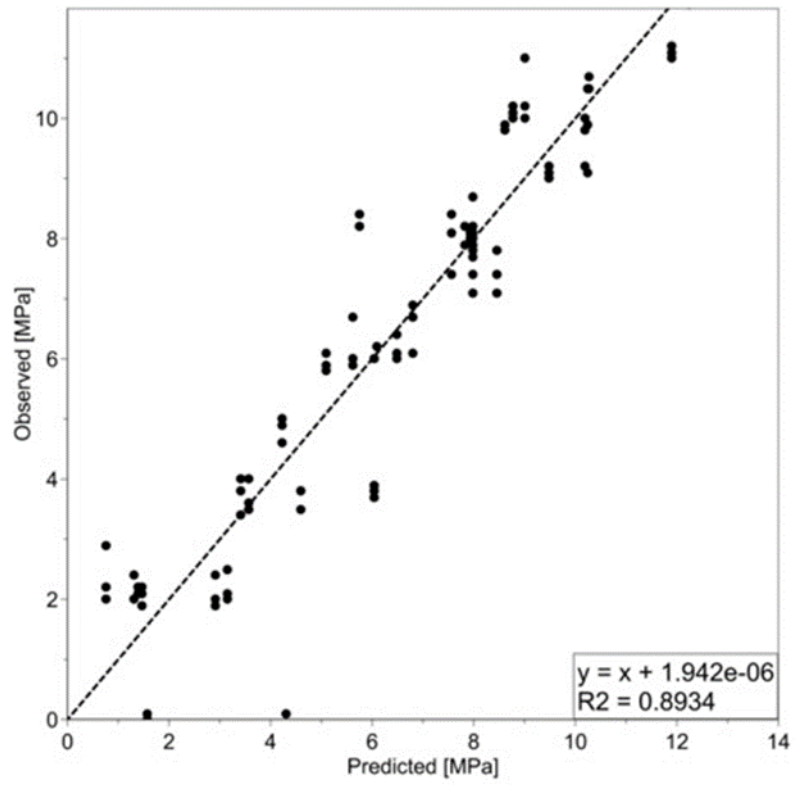
Figure 7-4 Observed versus predicted results for the presented model

Table 7-6 Analysis of variance (ANOVA) of the dependent variable.

Responses	F value	*p* value	R squared	Adjusted R squared	Q2 value
y, Tensile strength	113	<0.0001	0.89	0.89	0.87
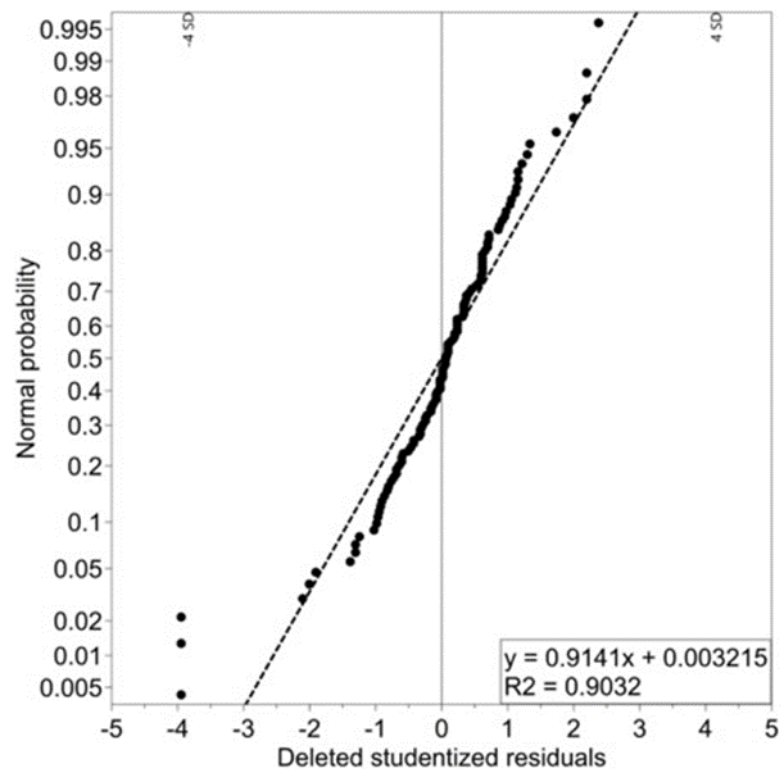
Figure 7-4 A normal probability plot for residual errors of the response variable (tablet tensile strength).

Figure 7-5 shows a response 4D contour plot for tablet tensile strength based on MgSt concentration. The 4D contour plot can be used to predict tablet tensile strength according to moisture and MgSt quantities. This is useful for pre-formulation work because a number of scoping experiments can be avoided. Formulations can contain multiple components, however, the contour plots presented in Figure 7-5 provide a good starting point for formulations that are predominantly produced with MCC. MCC is a hygroscopic excipient and therefore more likely to exhibit different behavior in the presence of moisture compared to its non-hygroscopic counterparts. In laboratory scale pre-formulation studies, the environmental conditions may not be as strictly controlled as those in a good manufacturing practice (GMP) industrial unit (Nally, 2016). Therefore, it is important to understand the

impact environmental RH may have on tablet tensile strength and how this may differ in a GMP environment.

Tablet tensile strength decreases with increasing storage RH and MgSt concentration. Interestingly, the effect of MgSt concentration is much less pronounced at low compression pressures, where tablet strength appears similar for concentrations of 0.5 and 1% w/w. For the higher MgSt concentration, tablet strength is slightly reduced at higher storage RH. Above compression of 100 MPa, the presence of MgSt hinders tablet formation and a considerable reduction in resultant tablet strength is observed. From Figure 7-5 it can be seen that the presence of some moisture due to storage in RH of between 22% and 43% is beneficial to tablet bonding, therefore resulting in increased tablet strength. This may be due by either increased plasticity of the MCC with additional moisture, increased water bonding in the tablet, or both. However, the effect of the 'ideal' amount of moisture is reduced with increasing MgSt concentration. There is a marked reduction in tablet tensile strength when increasing concentration from 0.5% to 1% w/w. This is exacerbated by additional moisture which indicates that it is not just saturation of the MCC particle surfaces by MgSt alone, but the MgSt and water work together to impede bonding within the tablet. The mechanism of this is discussed later in Section 7.3.6.1.
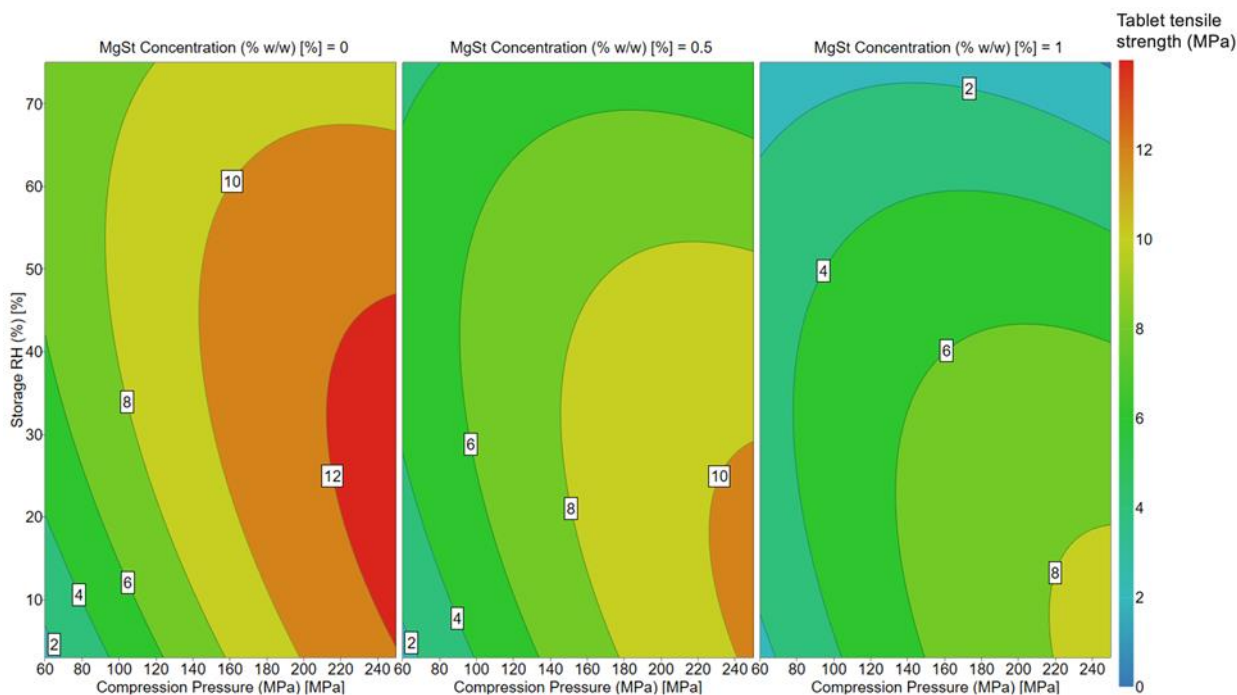
Figure 7-5 A response 4D contour plot based on MgSt concentration for tablet tensile strength.

7.3.6 Raman Spectroscopy

Raman spectroscopy is a technique that can be used to find information about chemical structure, phase, crystallinity and molecular interactions. Scattered light is used to measure the vibrational energy modes of a sample. The technique relies upon inelastic scattering of photons which is known as Raman scattering. Raman spectroscopy measures the energy gap between vibrational levels within a molecule, however not all vibrational modes can be detected using Raman spectroscopy. For a vibrational mode to be detected it must be 'Raman active' (Kafle, 2020). As it can use these properties to identify molecules it is a useful technique for locating areas of magnesium stearate within a tablet. For this section, a feasibility study was carried out as part of a package of work at AstraZeneca and thanks go to Stephanie Brooks for providing the Raman Spectroscopy data for this section.

253

7.3.6.1   Raman spectroscopy and increasing magnesium sulphate concentration

Firstly, tablets produced from 0.5, 1 and 2% w/w MgSt in MCC stored at 3% RH and compressed at a pressure of 170 MPa (±10 MPa) using a Styl'One Compression Simulator (as described in Section 3.5.3). The tablet surface was then imaged using a Raman imaging microscope (Thermo DXRxi) with experimental details as follows:

I.   Laser Frequency: 780 nm

II.   Laser Power: 24.0 mW

III.   Objective: 20x long working distance

IV.   Exposure Time: 0.50000 sec

V.   Number of Scans: 2

VI.   Image Pixel Size: 4 µm

VII.   Aperture: Confocal pinhole 50 micron

VIII.   Spectral range: $3,300cm^{-1}$ to $50cm^{-1}$

Tablets were secured to a microscope slide with double-sided Sellotape and a total area of approximately 0.9 x 1.3 mm was analysed per sample. Reference spectra showed good discrimination between MCC and MgSt and a simple peak ratio was successful for profiling MgSt distribution. It should be noted that the analysis was carried out on a clean tablet surface due to Raman spectroscopy requiring a flat surface to act upon. Using the tablet surface may not give a reliable representation of the internal composition, however, no external lubrication was used during the tablet compression process. Therefore, the concentration of magnesium sulphate on the tablet surface should be representative of that throughout the

internal profile of the tablet. If the tablet had been broken in two, the surface would have been uneven and therefore providing unreliable results. If the tablet was cut, it could have led to smearing of magnesium sulphate, again providing unreliability in the results.

Figure 7-6 shows the Raman spectra for the three tablets with increasing concentrations of MgSt. Blue shows areas with no detectable MgSt and green shows areas of mixed MCC and MgSt but with significant MgSt concentration. There is an obvious increase in the areas containing MgSt with increasing concentration. Interestingly, at 2% MgSt, instead of there being an even distribution of small particles, there are multiple areas of what seems to be larger clusters of MgSt.

Lakio, et al. (2013) used Raman spectroscopy to find the distribution of MgSt in MCC depending on blending time. One concentration of MgSt was used (1% w/w) with blending times ranging from 1 to 90 mins. With a blending time of 2 minutes, there were clear areas of high concentration MgSt and these areas dispersed to an increasing extent at 30 and 60 minutes. However, even at 60 minutes blending time, there are still large areas of highly concentrated MgSt. The increased dispersion of MgSt with mixing time was coupled with a decrease in tablet tensile strength. Other authors have made reference to a 'magnesium stearate film' across the surfaces of host particles which decrease interparticulate bonding (Wurster, et al., 2008). However, the current study and that by Lakio, et al. (2013) disagrees with the presence of a film and the evidence points more towards the presence of MgSt clusters on the host particle surface.
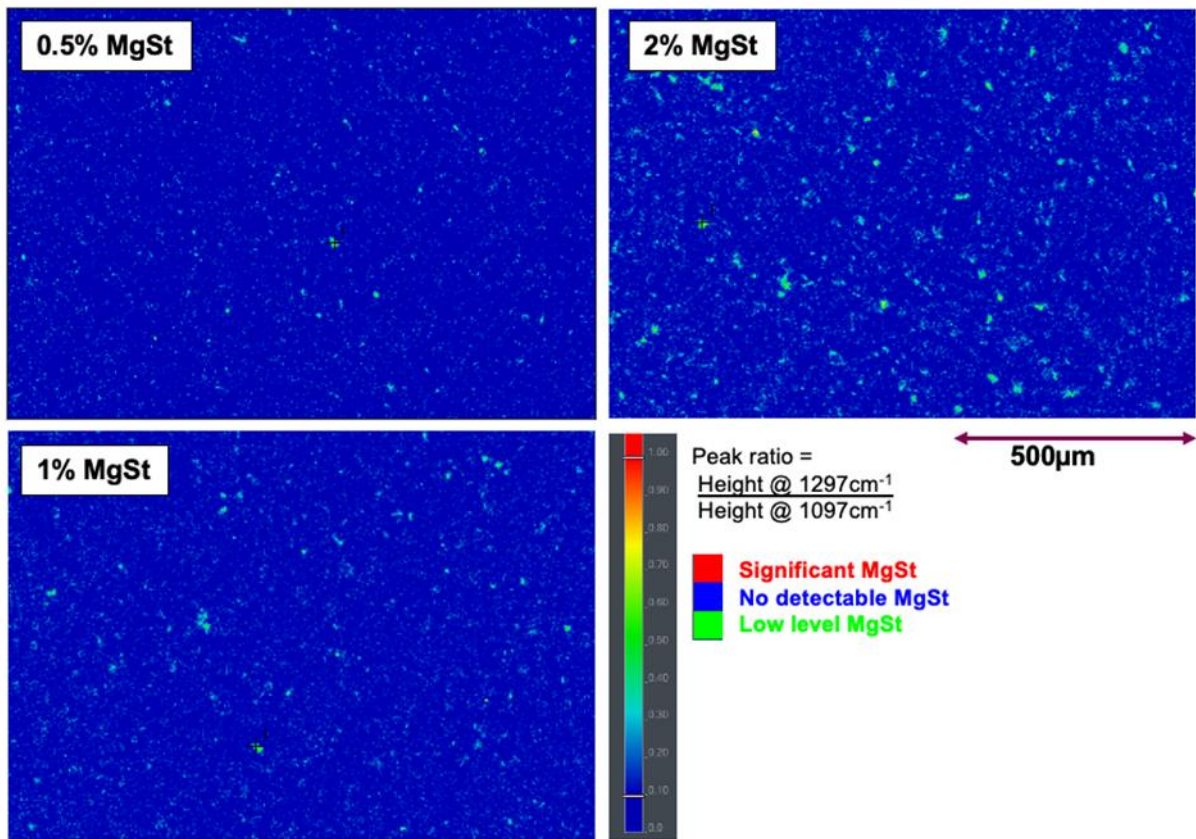
Figure 7-6 Raman spectra of tablets containing 0.5, 1 and 2% MgSt stored at 2% RH.

The second part of the study focused on the distribution of MgSt within a tablet depending on moisture content. MCC powders containing 1% w/w MgSt were stored at 0%, 15%, 30% and 55% before tableting as before at 170 MPa (±10 MPa) using a Styl'One Compression Simulator as described in Section 3.5.3. The tablet surface was then imaged using Raman spectroscopy as before which produced the images shown in Figure 7-7. In contrast to the images shown in Figure 7-6, the MgSt appears to be less evenly distributed and larger areas of highly concentrated MgSt increase in number with increasing storage RH and therefore moisture content. Figure 7-8 shows this in more detail.
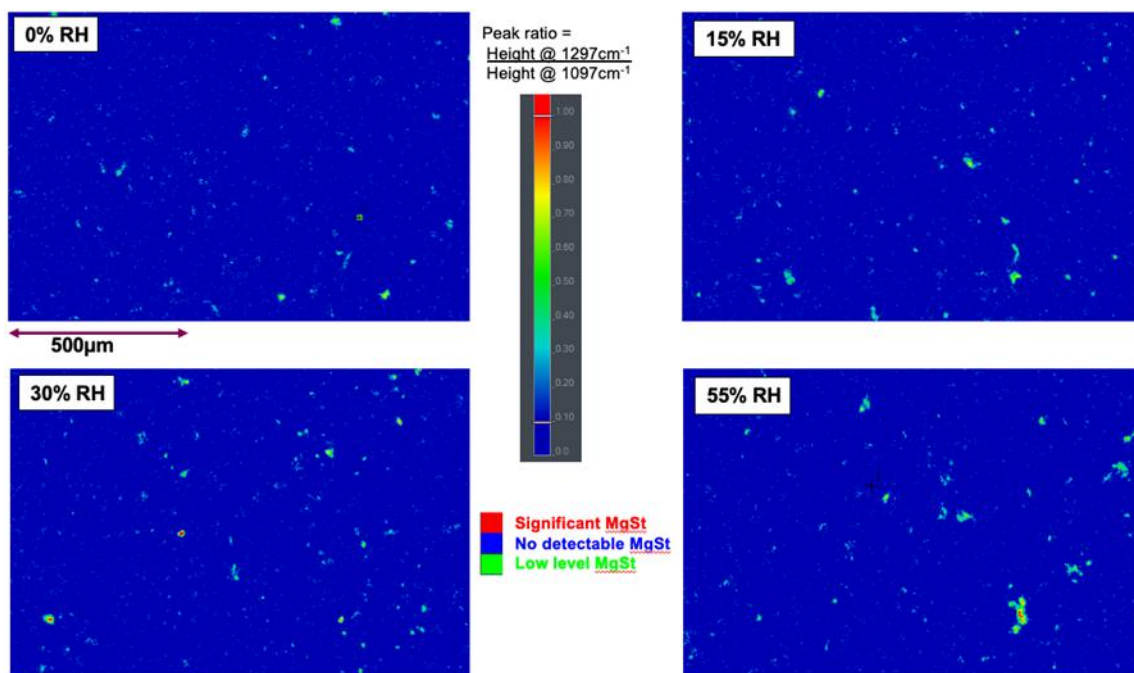
Figure 7-7 Raman spectra of tablets containing 1% MgSt that have been produced from powders stored at 0, 15, 30 and 55% RH.
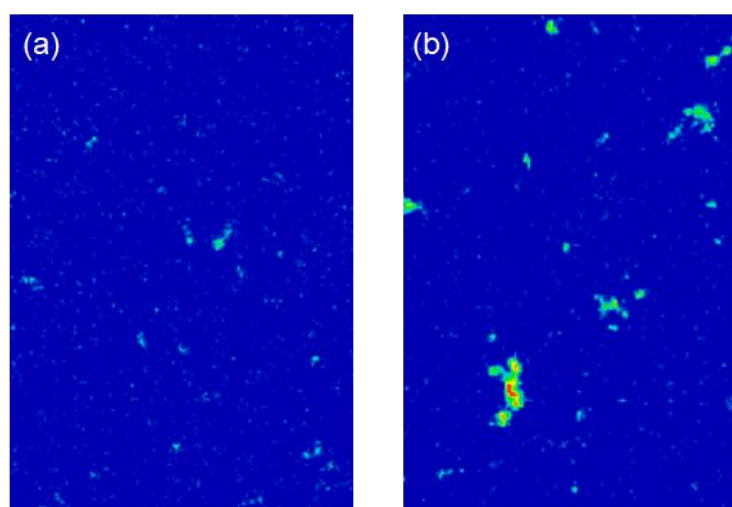
Figure 7-8 Raman spectra showing (a) tablets produced with 1% w/w MgSt in MCC powder stored in 0% RH and (b) tablets produced with 1% w/w MgSt in MCC powder stored in 55% RH.

The larger areas of highly concentrated MgSt in Figure 7-8 (b) show that the previously suggested 'film' of MgSt over the surface of the MCC particles is less likely at higher moisture content. MgSt is highly hydrophobic and therefore in the presence of increased water it will have a tendency to clump as it will be attracted to other MgSt particles. As discussed in Section 7.3.4., the tabletability of MCC is vastly decreased in the presence of increasing concentration of MgSt and water content. At low concentrations of MgSt there is still the potential for MCC surfaces to be exposed to one another resulting in effective bonding. When a higher concentration of MgSt is introduced, there is greater coverage of the MCC surface resulting in less availability of effective bonding. With both 1% or 2% MgSt and 8% moisture, there are areas of high water concentration and MgSt concentration which will both hinder the potential effective bonding between MCC surfaces. This effect is further explained by Figure 7-9. Unfortunately this work could not be extended and explored further due to the Covid-19 pandemic and the UK national lockdown. The experiment was carried out as a feasibility and should be treated as such. However, the promising results show that this method should be explored further in future work.

Water
MCC surface
Magnesium stearate

1. With low levels of moisture and lack of MgSt, MCC particle surfaces can come into close contact for bonding during compression.

2. The addition of low concentration MgSt inhibits some MCC particle surfaces coming into contact, therefore creating a weaker tablet.

3. At higher water content, the hydrophobic MgSt is attracted to like particles forming areas high in MgSt concentration and inhibiting bonding to a greater extent. At this point there would be a high incidence of lamination within the tablet.

Figure 7-9 Demonstrating the increase in MgSt and water content leading to the inhibition of tablet bonding.

7.4 Conclusions

There are multiple studies reporting the high lubrication sensitivity of MCC (Roberts & Rowe (1986), Hiestand (1997), Paul & Sun (2017)), however, after an extensive literature search, there was no evidence of studies that investigated the interaction of MCC and water and the effects of lubrication. Chapter 7 has investigated the role magnesium stearate has in reducing the tabletability of MCC tablets in the presence of differing levels of moisture. The following conclusions can be drawn:

I. The presented results have demonstrated a reduction in tabletability of MCC with both increasing MgSt concentration and increasing moisture content. The lubrication sensitivity of MCC is exacerbated by additional moisture within the tablet.

II. At the highest concentration of MgSt and moisture, tablet production was unsuccessful at all compaction pressures. The resultant laminated tablet structure is a product of highly concentrated areas of hydrophobic MgSt inhibiting the close contact of MCC particles to form a solid tablet.

III. The addition of MgSt to MCC promotes flowability, shown by higher ffc values for MgSt-containing powders. However, the increased flowability is reduced by the presence of water. At the highest moisture content, even with the highest content of MgSt (2% w/w), there are lower ffc values than MCC alone.

IV. Raman spectroscopy can be used to effectively detect MgSt distribution within tablets, showing clear differences between both increasing MgSt concentration and MgSt distribution with or without the presence of moisture.

V. At low MgSt concentration, the lubricant appears to form a film over the surface of the MCC. However, upon additional MgSt concentration, it forms increasing larger areas of clustered MgSt particles rather than a covering over the entire MCC surface.

8 Functionalized mannitol case study: An introduction to future work

8.1 A note on the Covid-19 pandemic

This is the final Chapter of the thesis which contains experimental results. It should be noted that soon after the experimental work for this chapter began, the Covid-19 pandemic was underway resulting in much of the laboratory work being cut short due to the UK national lockdown. The findings presented within the chapter and any conclusions drawn are very much based around the feasibility of the study and should be treated as a starting point for future work that could take place.

8.2 Introduction

The tableting behavior of a material is dependent upon its chemical structure, solid-state structure and particle properties (Sun, 2017). Tablet tensile strength is a result of bonding area and bonding strength. Factors such as plasticity, brittleness and particle size can change bonding area and therefore if these can be controlled across the powders being tested, the influence of surface free energy alone on tabletability can be assessed.

The surface characteristics of a material are a key part of understanding the interactions it may have with other materials and phases. The surface nature of powders can vary; for example, crystal habits may expose different functional groups at the surface, impurities may be present or there could be a change in polymeric form. As demonstrated in Chapter 7 of this thesis, the addition of magnesium stearate, has a marked difference on the compactibility of a tablet due to the lubricant changing the particle surfaces, altering the ability of the

microcrystalline cellulose to undergo particle-particle adsorption. Thus, the energy of the different particle surfaces involved in inter-particulate bonding is a key factor for determining the tensile strength of a tablet.

Differences in cohesion between molecules and the resultant surface energy can be explained by different types of interactions. Temporary fluctuations of the charge distribution in molecules are called dispersive interactions, or more commonly known as van der Waals forces. Polar interactions occur between permanent dipoles and, for example, hydrogen bonds. The surface energy of a material is the sum of dispersive and polar parts. Surface energy measurements are used to investigate wettability and adhesion characteristics and within pharmaceutical science they can be used to describe interactions such as drug adsorption, cohesion, adhesion, coating performance and lubricant sensitivity (Steele, et al., 2008). As shown in Figure 8-1 a material that produces a low contact angle upon investigation with angle goniometry, results in higher wettability and a higher surface energy value. A high contact angle results in a more hydrophobic surface and lower surface energy. Angle goniometry requires the solid to be a flat, non-porous surface, however the use of this technique for compacts is questionable due to the complication of angle measurement due to surface roughness and surface accessible pores (Steele, et al., 2008).
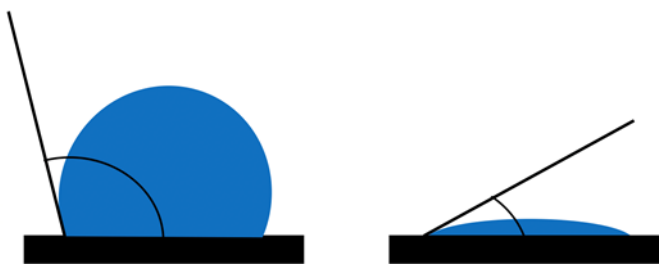
Figure 8-1 An illustration to demonstrate the wetability of a material. On the left, a large contact angle, therefore a badly wetting material. On the right, a small contact angle, therefore a material with good wetability.

Inverse gas chromatography (IGC) is a commonly used alternative to angle goniometry and uses the measurement of the retention volumes of non-polar and polar probes after passing through a packed column of the material under investigation.

Fichtner et. al. (2008) state that the fracture energy of a compact together with the microstructure control the tablet strength, therefore the fracture energy will show some proportionality with the surface energy of solids sharing similar microstructures. It is important to note that in order to compare tablets produced with powders of differing surface energy, the microstructure must be similar, therefore similar porosities must be obtained (Fichtner, et al., 2008). As a tablet is being compressed the surface area may considerably change and therefore the surface energy may constantly change with increasing pressure.

In the investigation by Fichtner, et. al. (2008), lactose was spray-dried with different proportions of surfactant to alter the surface energy of each powder and, although the resultant powders had similar bulk density, true density and surface area, there is not a detailed result quoted for particle size. Lactose deforms by brittle fracture, therefore creating

new bonding area as compression takes place. However, this mechanism may be altered by the spray-drying process. This is acknowledged by the authors, stating that the spray-drying process produces porous particles and potential differences in particle density and pore structure. The dispersive surface energy values for lactose alone was 49.11 mJ/m^2, with 0.001% w/w surfactant 47.91 mJ/m^2 and with 0.01% w/w surfactant 46.30 mJ/m^2. The difference in dispersive surface energy between powders with surfactant compared to lactose without surfactant was shown to be statistically significant. However, it was not statistically significant for difference between the two surfactant concentrations. The work concluded that a reduction in particle dispersive energy increased the pressure needed to form a compact of a predetermined tensile strength.

An opportunity presented to investigate the tabletability of functionalized mannitol powders with variations in particle surface energies. Four functionalized mannitol powders were provided by Ioana Dumitru, PhD student, Imperial College London.

Figure 8-2 shows the chemical structure of standard mannitol. The powders provided by Imperial College London were modified to contain one of three other functional groups: -Ph, -CH$_3$ and -CF$_3$, each resulting in a different surface energy value while keeping other particle properties the same.
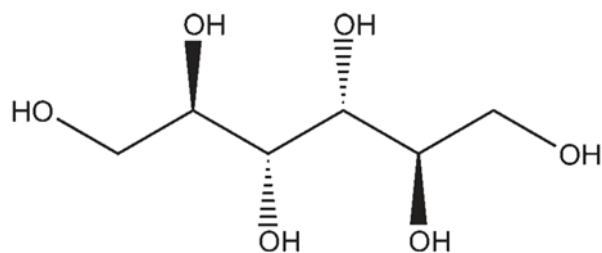
Figure 8-2 The chemical structure of 'as received' mannitol (Rowe, et al., 2009).

8.3 Materials and methods

8.3.1 Materials

Four functionalized mannitol powders were provided by Imperial College, London. The surface chemistry of mannitol (Pearlitol 160C, Roquette, UK) was independently controlled by grafting different silanes via a hydrolytic deposition process to produce surfaces with different wetting behavior. The surfaces produced were -Ph, -CF_3 and -CH_3. The 'as received' mannitol has a -OH functional group.

Surface energy data was provided by Ioana Dumitru (Imperial College, London) using Inverse gas chromatography (IGC Surface Energy Analyser, Surface Measurement Systems, UK) and results are provided in Table 8-1. Minimal method details are available as the work was carried out at another institution. 'As received' mannitol has the highest dispersive surface energy value followed by Ph, CF_3 and finally CH_3 derivatives. The value of 70.1 mJ/m^2 for 'as received' (Pearlitol 160C) mannitol is in close agreement with the figure of 70.7 mJ/m^2 reported by Cares Pacheco, et al. (2014).

Table 8-1 Single point dispersive surface energy values for each mannitol derivative.

Material	Dispersive surface energy, γ_s^d (mJ/m²)
Ph	46.7
OH	71.8
CF$_3$	34.2
CH$_3$	30.2

From the single point dispersive data it can be noted that increased hydrophobic character, or decreased wettability of the materials occurs as follows: -OH < -Ph < CF$_3$ < CH$_3$. It is expected that a decrease in surface energy will result in a decrease in tablet tensile strength. This hypothesis is supported by Fichtner, et al. (2008) by confirming that the strength of bonding forces between particles is controlled by surface energy.

8.3.2 Methods

8.3.2.1 Particle and powder properties

Imaging was carried out using SEM microscopy (TM-1000, Hitachi, Japan) as described in Section 3.4.3. for each excipient powder.

Particle size distribution was carried out for each material via laser diffraction, using a dry dispersion module (Mastersizer 3000, Malvern Instruments Ltd., Malvern, UK). A dispersion pressure of 0.5 bar was set for all powders. Powders were passed through a 1000 μm sieve prior to dispersion and determinations were carried out in triplicate.

Powder bulk density was determined by pouring a measured mass of powder into a 10 ml measuring cylinder using a funnel. Bulk density was then calculated by dividing the volume of powder by the measured powder mass. Measurements were carried out in triplicate.

Powder true density was determined using helium pycnometry (AccuPyc II 1340, Micromeritics, UK) as described in Section 3.4.4.

8.3.2.2 Tableting

The Styl'One Compression Simulator was used for tableting as described in section 3.6.3. Compaction pressure ranged from 60 MPa to 500 MPa, and all tablets were compressed with settings based on a simulated machine (Korsch XL100-Euro B) at a speed of 5 rpm. A slower tableting speed was used to minimise the onset of capping which has been observed when tableting mannitol in previous experiments. For each tablet, the die was manually filled and lubricated prior to fill by brushing with 1% w/w magnesium stearate in acetone and allowing to dry. Tablet properties were measured according to Section 3.5.5. Tablet hardness testing was carried out using a texture analyser (TA.XT PlusC, Stable Micro Systems, Surrey, UK).

8.4 Results and discussion

8.4.1 Particle and powder properties

8.4.1.1 Imaging

Figure 8-3 shows the SEM images for each powder. There is not a significant difference in the appearance between the bulk of each material. However, the OH sample had fine, 'hair-like', crystals distributed on the surface (Figure 8-4) which were not present in any other powder.

These crystals may produce an increase in surface area available for bonding and therefore an increase in tablet tensile strength which has been observed for the OH derivative (Figure 8-7). Detailed surface area data was not provided with the surface energy data upon delivery of the material. Information was given which suggested that the surface area was similar for all derivatives, however upon the observations made via SEM it does not appear that this is the case. Unfortunately, surface area measurements could not be taken due to experimental work being cut short by the Covid-19 pandemic. If future work could take place with these materials, it would be recommended to test the surface area by nitrogen adsorption BET.
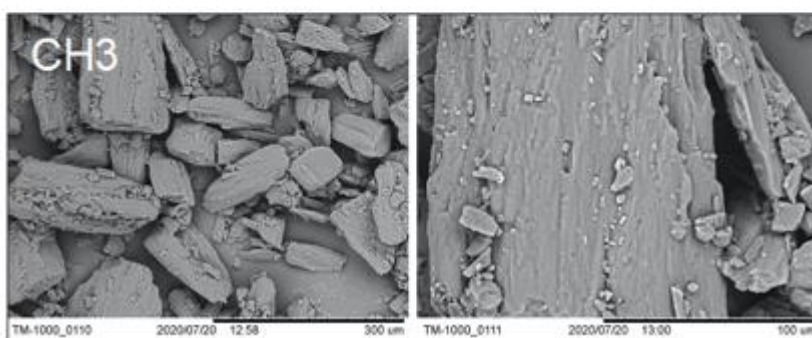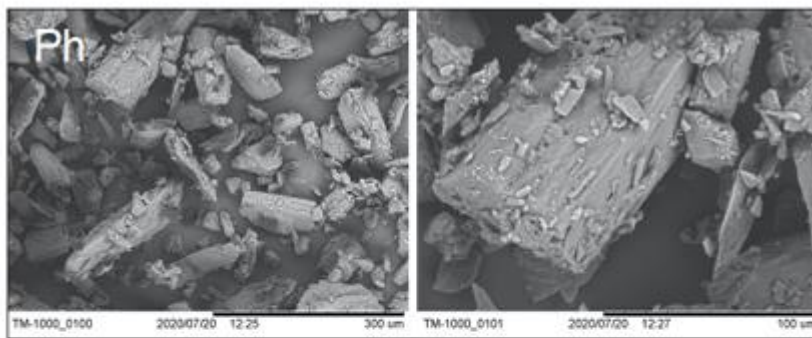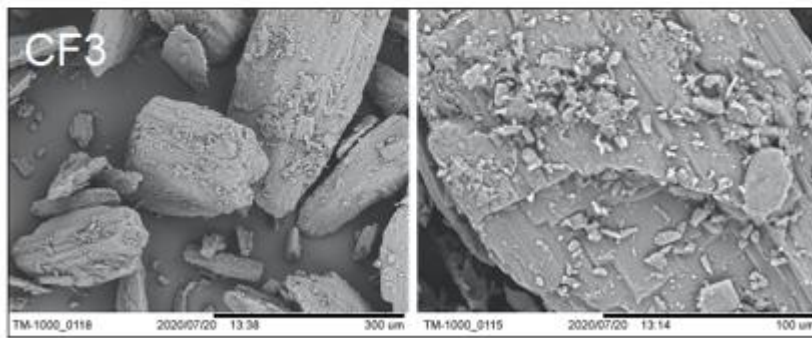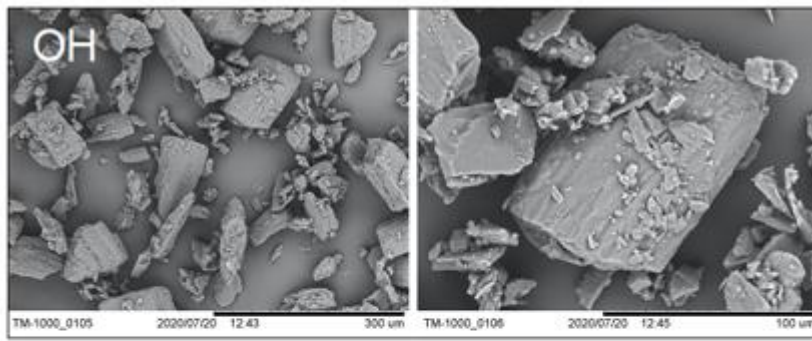
Figure 8-3 SEM images of each mannitol derivative powder.
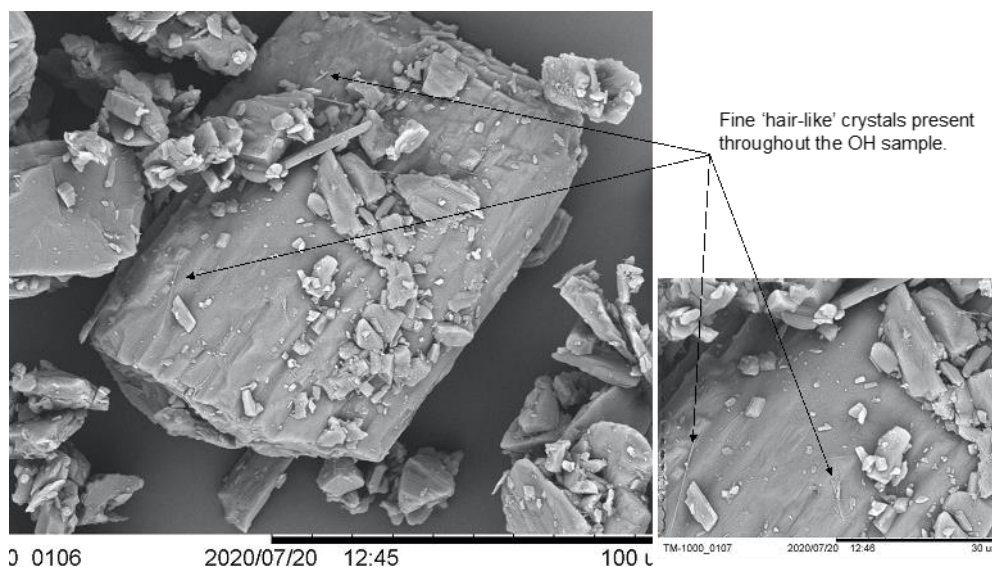
Figure 8-4 An SEM image highlighting the 'hair-like' crystals present on the OH sample.

8.4.1.2 Particle size distribution

The particle size distribution for each mannitol derivative is shown in Figure 8-5. All powders show monomodal distribution. Both CF_3 and CH_3 show a slight peak around 1000 μm which indicates some agglomeration of the material. When handling CF_3 and CH_3 powders it was noted that agglomerates easily formed, even after passing through a sieve (Figure 8-6). Agglomeration is a process which occurs when particles are assembled to form larger agglomerates, where the original particles can still be distinguished (Cuq, et al., 2013). The reason for agglomeration in the CF_3 and CH_3 derivatives is unknown and requires further investigation. The materials are non-hygroscopic and have low moisture levels, therefore agglomeration is not expected to occur due to water ingress to the material on storage.

271
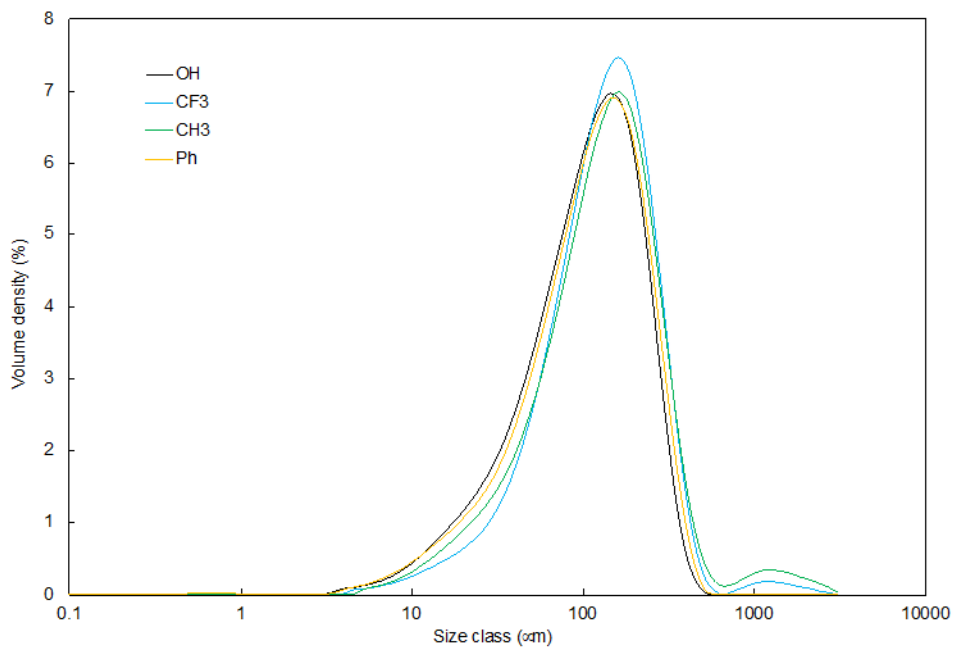
Figure 8-5 The particle size distribution for each mannitol derivative.

Figure 8-6 An example of the observed agglomerates within the mannitol-CF3 sample.

8.4.1.3   Powder true density

Table 8-2 shows the true density values for each powder. Although the difference is small, there is an increase in true density as follows: Ph<OH<CF$_3$<CH$_3$. The small difference in material true density is unlikely to lead to any differences in tablet tensile strength.

Table 8-2 The true density values for each mannitol derivative. Results are shown as the mean of three measurements ±SD (in parentheses).

Material	True density (g/cm^3)
Ph	1.481 (0.003)
OH	1.488 (0.004)
CF$_3$	1.493 (0.001)
CH$_3$	1.498 (0.008)

8.4.2   Tabletability

Figure 8-7 shows the tabletability profiles for each powder. The OH modified mannitol demonstrates the highest tabletability, gaining a maximum tensile strength of 1.6 MPa at 280 MPa compression pressure (Table 8-3). The other powders do not produce tablets with similar tensile strengths at the same compression pressure with decreasing tabletability as follows: CF$_3$, Ph and CH$_3$ (Table 8-3). For all powders, after maximum tablet tensile strength has been reached there is a decrease in strength with increasing compression pressure. The profiles can be divided into two parts: firstly, brittle fracture leads to the formation of increased bonding surface area and the formation of a tablet compact at a maximum compression pressure before, secondly, a failure of the compact with increasing compression pressure. In the first

region, corresponding to the compression pressures up to those shown in Table 8-3, the increase in tablet tensile strength with increasing compression pressure or 'rate of compactibility' is dependent on the powder used. Within this region, OH and CF_3 increase in tensile strength at a similar rate. However, at ~150 MPa, CF_3 appears to plateau and no additional strength can be gained with increasing compression pressure. Both Ph and CH_3 have slower rates of compactibility, however the tensile strength gained begins to plateau at around 150 MPa in a similar fashion to CF_3. It is important to note that surface energy of a particle that undergoes brittle fracture is likely to change as the material creates newly exposed faces as compression takes place. Further characterisation would be required to quantify these differences. In the second region, the tablet strength reduces even though there is an increase in compression pressure and observations made in this region found that tablets had undergone lamination which can be described as horizontal layering. Lamination can occur for a number of reasons, most regularly shear stresses developing as the tablet is ejected from the die or tensile stress developing at the centre of the tablet (Mazel & Tchoreloff, 2021).

As mentioned earlier in Section 4.3.6., Paul et al. (2019) found that the tablet strength of mannitol was dependent on surface area. Although all of the mannitol derivatives supplied were done so with the understanding that they had similar specific surface areas, this should be confirmed with nitrogen adsorption BET to ensure that this is not the reason for the differences in tabletability.
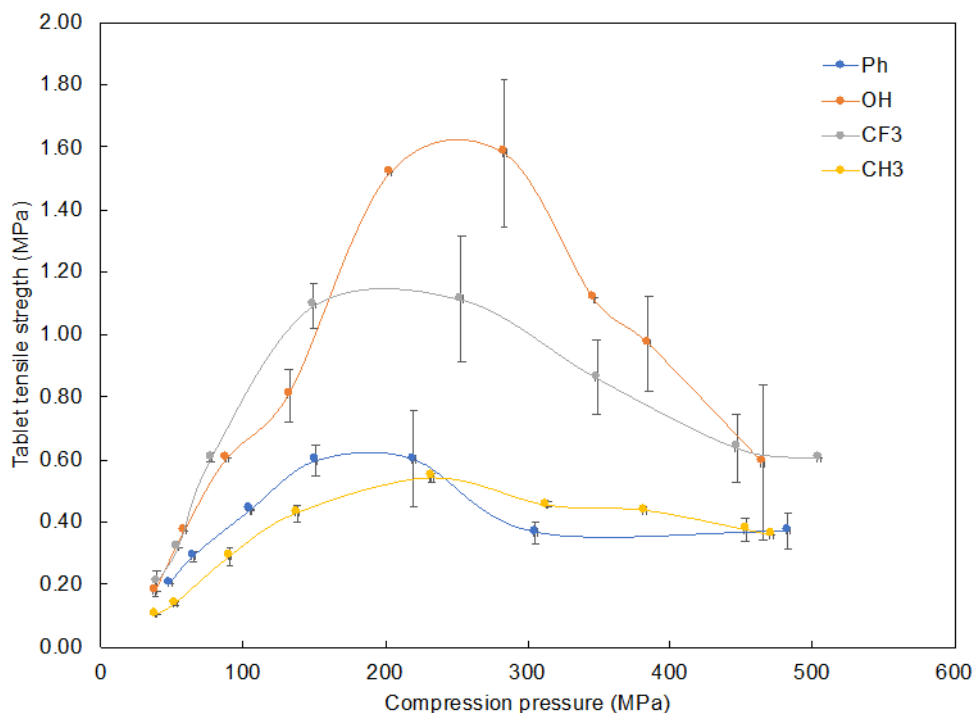
Figure 8-7 Tabletability profiles for all four mannitol derivatives. Error bars indicate standard deviation.

Table 8-3 The maximum tablet tensile strength acquired and corresponding compression pressure.

Material	Maximum tablet tensile strength (MPa)	Compression pressure required for maximum tensile strength (MPa)
CH_3	0.5	230
Ph	0.6	150
CF_3	1.1	150
OH	1.6	240

It was noted during tablet strength testing that there was a distinct difference in the appearance of the tablet fracture for each mannitol derivative. The OH and Ph derivatives underwent a 'clean break' along the centre of the tablet, resulting in two halves. This appeared

to be the same for all OH and Ph tablets produced at any compaction pressure. The CH3 and CF3 tablets broke in a different pattern which became more obvious for tablets produced at higher compressive forces. The top and bottom faces of the tablet sheared away from the body leaving a smaller tablet structure behind. An example of these two mechanisms is shown in Figure 8-8.
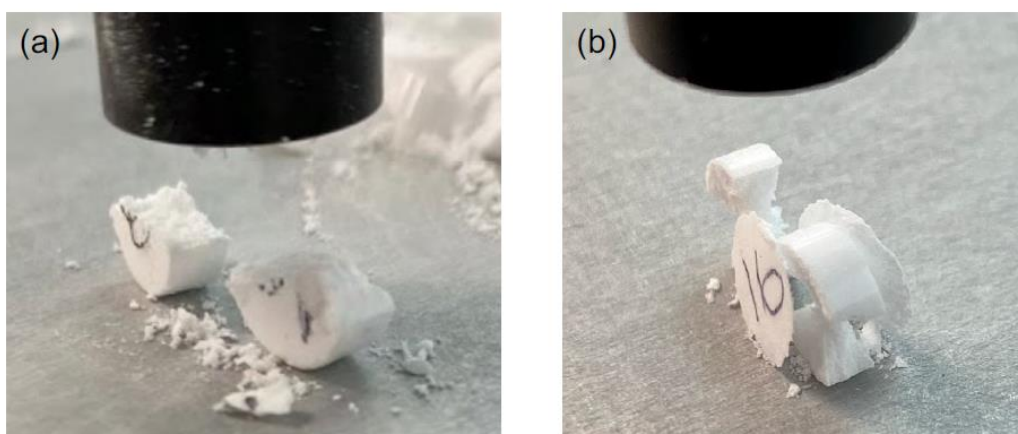
Figure 8-8 An example of the tablet fracture upon tensile strength testing of tablets produced from (a) OH and (b) CH3 mannitol derivatives.

8.4.2.1   Tablet compression properties

Tablet porosity decreased with increasing compression pressure for all powders in a non-linear fashion (Figure 8-9). The compressibility of OH, CF_3 and CH_3 mannitol powders are similar indicating that the mechanism of tablet compression was the same for each powder. However, the Ph derivative falls below the others, which may suggest a difference in micro-structure as the tablet is being compressed. For OH, CF_3 and CH_3 powders it can therefore be assumed that the inter-particulate contact area per fracture area was controlled by the particle mechanics rather than the surface energy.
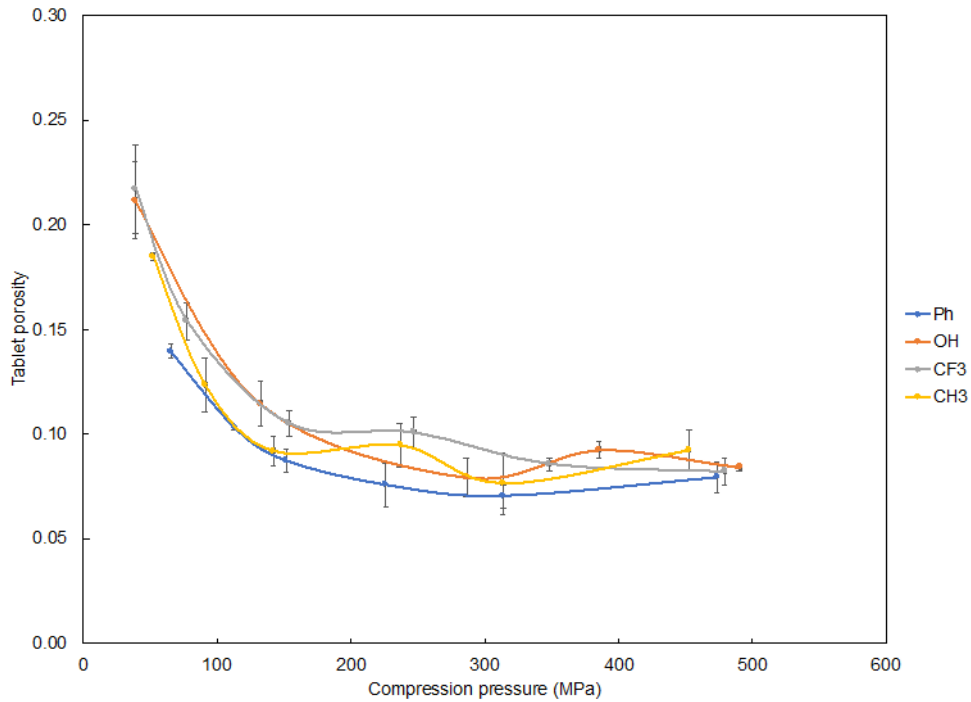
Figure 8-9 Compressibility profiles for all four mannitol derivative powders. Error bars indicate the standard deviations.

Heckel plots were produced for each powder both in-die and out-of-die. The slope of the linear regression line (solid, black lines in Figure 8-10 and Figure 8-11) relates to the Heckel coefficient and the reciprocal value, yield pressure (P_y), is a measure of the compressibility of the powder. A lower value for P_y indicates greater compressibility. Table 8-4 details both the in-die and out-die values for P_y and shows that for in-die evaluation the most compressible materials are the Ph and CH_3 derivatives. For in-die evaluation, Mannitol OH and CF_3 have the largest tablet porosity but are the least compressible materials (P_y values of 132 MPa and 125 MPa respectively). A high particle porosity is required for a well-compressible material; however, the compressibility of a material is also dependent upon its deformation properties. Different outcomes are noted with out-die evaluation, where the P_y values show much less distribution across the materials and OH and CH_3 derivatives are most compressible (P_y values

277

of 152 MPa and 137 MPa). There is not a correlation in rank order of yield pressure with dispersive surface energy for either in-die or out-die measurements. The fit of the data for both in-die and out-die evaluation was acceptable for all materials (Table 8-4), shown by R^2 of 1.00 for all in-die data and over 0.90 for all out-die data.
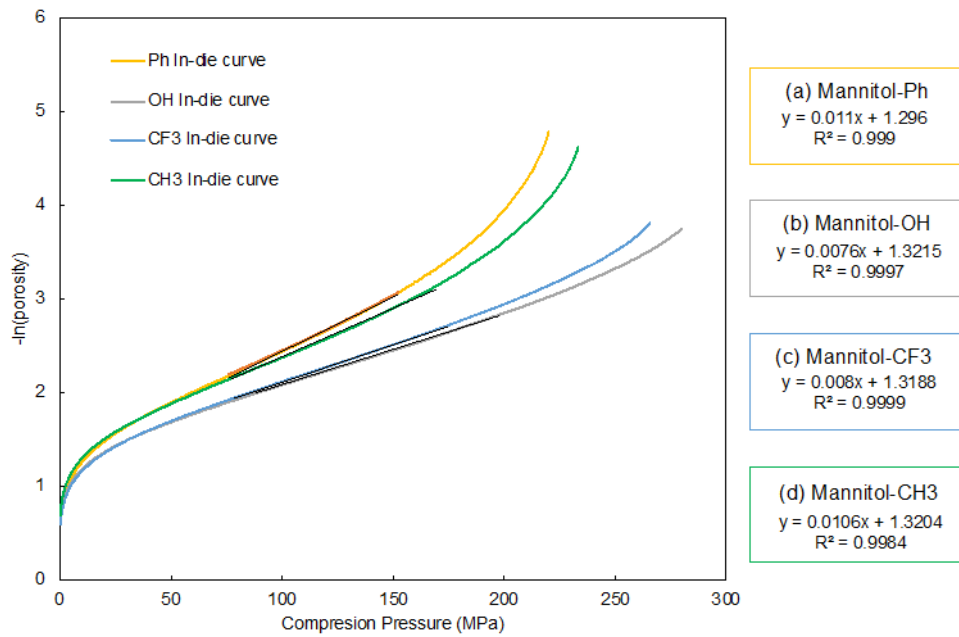
Figure 8-10 In-die Heckel profiles for (a) mannitol-Ph, (b) mannitol-OH, (c) mannitol-CF₃ and (d) mannitol-CH₃.
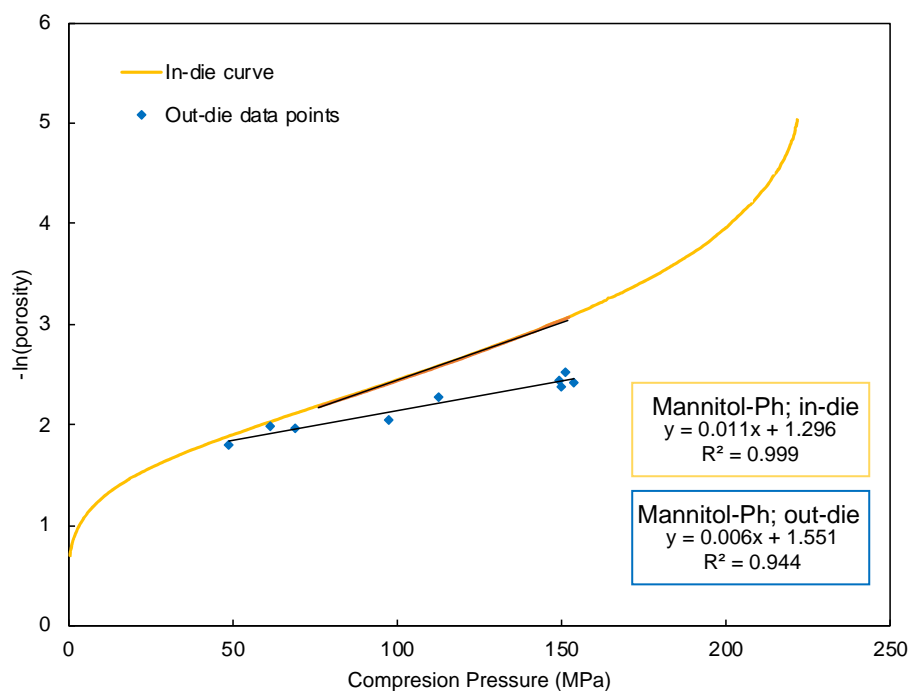
Figure 8-11 An example of an in-die Heckel curve and out-die data points for Mannitol-Ph.

Table 8-4 In die and out of die yield pressure values for each powder.

Material	Dispersive surface energy (mJ/m^2)	P_y			
		In die (MPa)	R^2	Out of die (MPa)	R^2
Mannitol-Ph	46.7	88	1.00	169	0.94
Mannitol-OH	71.8	132	1.00	152	0.95
Mannitol-CF$_3$	34.2	125	1.00	164	0.93
Mannitol-CH$_3$	30.2	94	1.00	137	0.90

Figure 8-12 shows the relationship between the material dispersive surface energy and the maximum tensile strength attained for each mannitol derivative. The 'as received' material, the OH derivative, has the highest surface energy and the highest tablet tensile strength. Interestingly, the Ph derivative demonstrates low tabletability even though it has the second

highest surface energy value. This indicates that it is not surface energy alone that decides the maximum tensile strength a tablet can gain under compression. The CH_3 derivative has the lowest surface energy and tablet tensile strength. The low R^2 value for the plot suggests there is an unlikely trend between surface energy and tensile strength. However, further work is required to ensure that all materials have the same material attributes with the exception of surface energy.
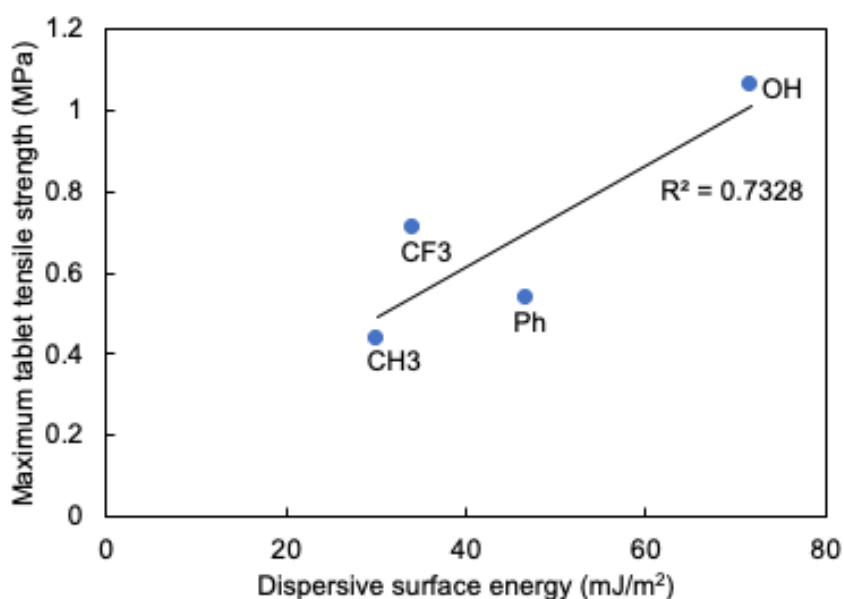
Figure 8-12 A plot showing the relationship between dispersive surface energy and the tablet tensile strength at 9% porosity for each material.

8.4.2.2   Compression properties of mixed materials

Each mannitol derivative powder was mixed as a 50 %w/w blend with each of the other derivative powders. Powders were provided pre-mixed and sieved through a 1 mm mesh. The same tableting parameters as those in Section 8.2.2.3 were used to produce tablets and therefore tabletability profiles for each mix of powder (Figure 8-13)
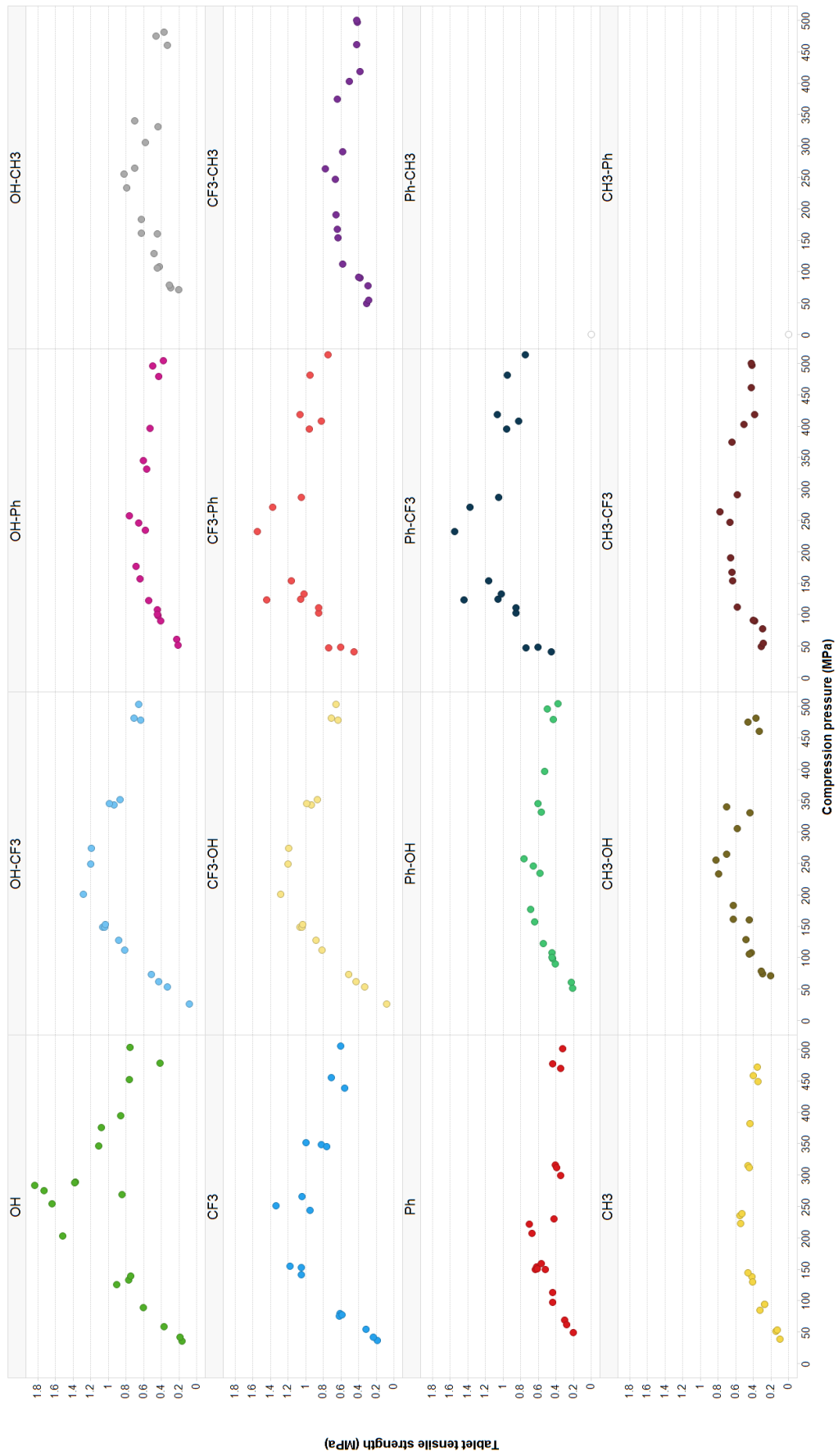
Figure 8-13 A matrix showing the tabletability profiles for base mannitol derivatives and 50/50 blends of each.

The far-left column of the matrix shown in Figure 8-13 demonstrates the reducing tabletability of the mannitol derivative base materials as discussed previously. Tabletability runs in the order from strongest to weakest: OH>CF$_3$>Ph>CH$_3$. For 50% w/w blends of OH and other materials it was demonstrated that all other materials reduce the tabletability of the original material, and as expected, this effect was most extreme with the addition of Ph and CH$_3$ powders. The OH-Ph blend gives a tabletability profile similar to that of the Ph base material, with similar maximum tensile strengths obtained. However, the Ph-CF$_3$ blend shows increased tabletability over the original Ph material and a higher maximum tensile strength than the individual CF$_3$ material. The presence of CF$_3$ masks the poor tabletability of Ph entirely. The same is not true for the CH$_3$-CF$_3$ blend, where the tabletability profile is similar to the original CH$_3$ material which shows poor tableting performance. Further investigation is required to find the underlying mechanism for the masking ability of CF$_3$ to Ph.

8.5 Conclusions

The differences in dispersive energy between modified mannitol samples led to a change in tablet tensile strength when compared to the 'as received' material. The resultant tabletability does not always correlate to an increase in maximum tablet tensile strength in order of increasing dispersive surface energy. This suggests that there is a difference in the material which is yet to be characterised or considerable changes to the material upon the action of compressive force. When the Ph and CH$_3$ mannitol derivatives, which give the lowest tablet tensile strength as base materials, are added to a 50% w/w mixture with the CF$_3$ derivative, tablet tensile strength is increased. The CF$_3$ derivative masks the Ph and CH$_3$ properties which may point towards preferable mechanical properties of the fluorinated mannitol upon

compression. In the absence of other material characteristics which determine tabletability, dispersive surface energy has shown to be an important property in determining final tablet properties. However, mannitol undergoes brittle fracture upon compression and therefore may expose faces of material with differing surface energy to that of the starting material. It would be recommended to repeat this work upon a plastically deforming material to ensure surface energy remains the same throughout tablet compression.

8.6 Further work

8.6.1 Surface energy and tableting

The investigations detailed within Chapter 8 were part of a case study that presented as a result of a collaboration with Imperial College London and it is work that is ongoing. A literature search was carried out to find dispersive surface energy values for materials that have been investigated within this thesis in order to increase the background of the relationship between surface energy and tablet tensile strength. Table 8-5 provides a summary of the findings.

Table 8-5 Results of a literature search for material dispersive surface energy values and BET surface area values quoted from Section 5.3.11.

Material	Dispersive surface energy (mJ/m²)	Reference	BET surface area (m²/kg)
Lactose (P200M)	49.11	(Fichtner, et al., 2008)	521
	45.4	(Das, et al., 2011)	
MCC (Avicel PH101)	36.4	(Steele, et al., 2008)	1203

The dispersive surface energy data can be used with BET surface area data shown in Table 8-5 to determine the surface energy per gram of material (Steele, et al., 2008). The BET surface area value for mannitol derivatives was assumed to be the same for all materials due to knowledge passed on by the manufacturer and taken as 410 m^2/kg from literature (Cares-Pacheco, et al., 2014). The product of surface energy (mJ/m^2) and the BET specific surface area (m^2/kg) provides a value for specific surface energy (mJ/kg). Steele, et al. (2008) quoted that the specific surface energy is related to the potential bonding energy within a tablet with a higher value for specific surface energy resulting in greater tabletability. Figure 8-14 shows the exponential relationship between specific surface energy and tablet tensile strength. However, this relationship should be viewed with caution due to MCC being an outlier to all other materials shown on the plot. The tablet tensile strength relates to that for tablets produced at 9% porosity as the important of the relationship between tablet strength and porosity has been shown previously in this thesis. The complex relationship between material characteristics and tensile strength is dependent on many factors and therefore a linear relationship between specific surface energy and tablet tensile strength is not expected. It is also important to note that previous work by Steele, et al. (2008) found that the dispersive surface energy of MCC changed depending on the RH during surface energy experimentation. However, different MCC grades were used to those in the current study. Any future work should take into account the surface energy differences within MCC due to water content.
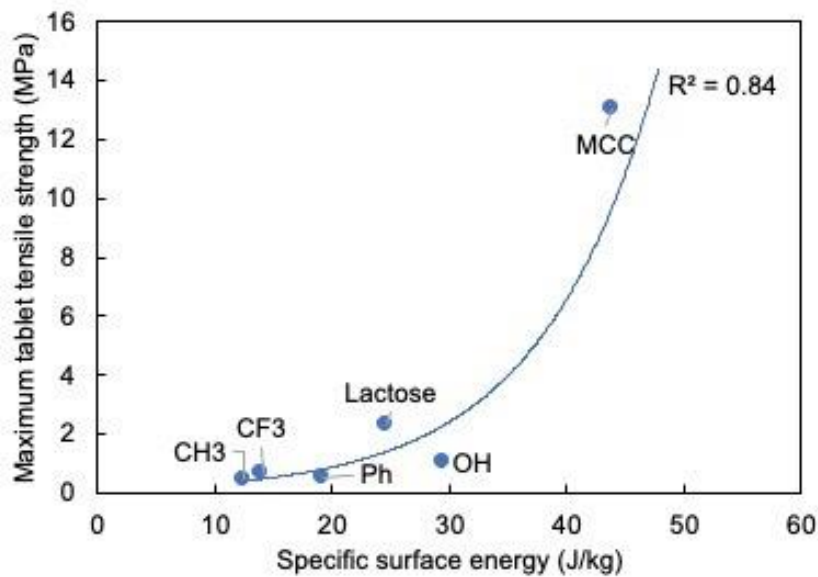
Figure 8-14 A plot showing an exponential relationship between specific surface energy and tablet tensile strength for a range of materials at 9% porosity. MCC value is that for material stored at 43% RH.

Surface energy appears to be one of many material attribute in the tabletability of a given powder and the work carried out has provided a positive introduction to further work that could be carried out in this area. Further work is required to determine the extent to which dispersive and polar interactions are deciding the cohesion between powder molecules during compression. So far, this study has only investigated the effect of dispersive surface energy. However, polar interactions that occur between permanent dipoles and permanent and induced dipoles act with dispersive surface energy to produce the total surface energy (or surface tension) of a material. This partnered with the influence of other powder characteristics will hopefully lead to the future of tablet tensile strength prediction and ever decreasing pre-formulation study time.

9 Conclusions

9.1 Initial objectives revisited

The initial objectives stated at the start of this thesis were:

I. Investigate the TSG process and how it modifies pharmaceutical excipients to give required granule attributes for tableting by changing process parameters.

II. Improve the understanding of tabletability surrounding bonding mechanisms by an in-depth study of pharmaceutical excipients.

III. Explore the mechanical properties of pharmaceutical excipients and whether these properties can be used in the future of tablet strength prediction studies.

9.2 Objective I

Objective I was addressed in Chapter 4 of this thesis where TSG process parameters were explored and the result on the tabletability of pharmaceutical excipients. Compaction studies using a compaction simulator confirmed the difference in tabletability based on TSG process parameters used. A comparison of compaction modelling was performed which assessed the granule strength based on process parameters used and identified potential models to be carried forward within the thesis.

9.3 Objectives II and III

Objectives II and III are addressed within Chapters 5 to 8 where the properties of a number of pharmaceutical excipient properties were explored. The difference in tabletability of hygroscopic and non-hygroscopic materials was assessed and the impact of water within each

material as a result of storage RH made clear. For hygroscopic materials such as MCC and starch, there is an increase in tabletability with increasing moisture content. The difference between materials undergoing plastic deformation and brittle fracture was also investigated and the resultant impact on the tablet compaction process. Brittle materials such as lactose provide additional bonding surfaces during initial compaction before reaching a critical point at which material consolidation takes place to form the final compact. The importance of surface energy was also identified as a key source of information for future studies.

MgSt was confirmed to cause substantial loss in tabletability with increasing concentration in MCC tablets. This effect was exacerbated by moisture and an explanation for tablet lamination at high MgSt and moisture content was proposed.

Although a definitive answer cannot be given as to the exact bonding mechanisms present per material, it is clear that multiple factors responsible for tablet strength are at play. Tablet porosity, the surface area of the base material, moisture content and the surface energy of the base material have all been identified as key parameters in the prediction of tabletability. The importance of control of RH during tablet storage has been highlighted for hygroscopic materials due to changes in tablet strength taking place over time. For MCC, absorbed water can increase the number of solid bridges by increasing the plasticisation of the material and excess water present at particle surfaces leads to greater particle-particle interactions. Once water content is present in excess and can form bulk water between particle surfaces, tablet bonding is hindered and a reduction in tablet tensile strength is observed.

A comprehensive and thorough study of tablet properties based on the moisture content of materials has been carried out. This information can be used to inform future pre-formulation studies and reduce the amount of experimental time required through better prediction of tablet compaction based on material properties.

10 References

Adams, M. J., Mullier, M. A. & Seville, J. P. K., 1994. Agglomerate strength measurement using a uniaxial confined compression test. *Powder Technology,* Issue 78, pp. 5-13.

Aliofkhazraei, M., 2015. Surface Energy. 1st ed. London: IntechOpen.

Amidon, G. E., Meyer, P. J. & Mudie, D. M., 2017. Chapter 10 - Particle, Powder, and Compact Characterization. In: *Developing Solid Oral Dosage Forms: Pharmaceutical Theory and Practice.* s.l.:Elsevier, pp. 271-293.

Amixon Mixing Technology, Undated. Agglomeration. [Online]
Available at: https://www.amixon.com/en/glossary/agglomeration-granulation
[Accessed February 2022].

Ashland, 2019. *Klucel EXF.* [Online] Available at:
https://www.ashland.com/file_source/Ashland/Documents/PHA19-
028_Klucel_EXF_SellSheet_A4_spotWG9_ms.pdf [Accessed January 2020].

Aulton, M. E. & Taylor, K. M. G., 2013. Aulton's Pharmaceutics: The Design and Manufacture of Medicines. 4 ed. s.l.:Elsevier.

Beretta, M. et al., 2020. Investigation into powder tribo-charging of pharmaceuticals. Part I: Process-induced charge via twin screw feeding. International Journal of Pharmaceutics, Volume 591.

Bocquet, L., Charlaix, E., Ciliberto, S. & Crassous, J., 1998. Moisture-induced ageing in granular media and the kinetics of capillary condensation. *Nature,* Volume 396, pp. 735-737.

Boundy, M., Leith, D. & Polton, T., 2006. Method to Evaluate the Dustiness of Pharmaceutical Powders. *The Annals of Occupational Hygiene,* 50(5), pp. 453-456.

Brunauer, S. S., Emmett, P. H. & Teller, E., 1938. Adsorption of gases in multimolecular layers. *Journal of the American Chemical Society,* Volume 60, pp. 309-319.

Cardona, J. et al., 2018. Image analysis framework with focus evaluation for in situ characterisation of particle size and shape attributes. Chemical Engineering Science, Issue 191, pp. 208-231.

Cares-Pacheco, M. G. et al., 2014. Physicochemical characterization of D-mannitol polymorphs: The challenging surface energy determination by inverse gas chromatography in the infinite dilution region. *International Journal of Pharmaceutics,* 475(1-2), pp. 69-81.

Cement Science, 2013. What is density? How to distinguish different density definitions?. [Online]
Available at: https://www.cementscience.com/2013/03/what-is-density-how-to-distinguish-different-density-definitions.html
[Accessed January 2022].

Charoo, N. A., 2020. Critical excipient attributes relevant to solid dosage formulation manufacturing. Journal of Pharmaceutical Innovation, Volume 15, pp. 163-181.

Choi, D. H. et al., 2010. Material properties and compressibility using Heckel and Kawakita equation with commonly used pharmaceutical excipients. *Journal of Pharmaceutical Investigation,* 40(4), pp. 237-244.

Colorcon Inc., 2016. *Starch 1500 Application Data,* s.l.: Colorcon.

Conceição, J. et al., 2014. Technological excipients of tablets: Study of flow properties and compaction behaviour. *American Journal of Medical Sciences and Medicine,* 2(4), pp. 71-76.

Connelly, A., 2017. *Andy Connelly.* [Online]
Available at: https://andyjconnelly.wordpress.com/2017/03/13/bet-surface-area/
[Accessed 2022].

Cunningham, C. R., Undated. *Starch Contrasts.* [Online] Available at:
https://www.colorcon.com/products-formulation/all-products/excipients/tablets/starch-1500/item/139-starch-contrasts [Accessed January 2021].

Cuq, B. et al., 2013. Agglomeration/granulation in food powder production. In: *Handbook of food powders.* s.l.:Woodhead Publishing, pp. 150-177.

Das, S. C. et al., 2011. Use of surface energy distributions by inverse gas chromatography to understand mechanofusion processing and functionality of lactose coated with magnesium stearate. *European Journal of Pharmaceutical Sciences,* 43(4), pp. 325-333.

DFE Pharma, 2020. *DFE Pharma Pharmatose 200M.* [Online]
Available at: https://www.dfepharma.com/ [Accessed July 2020].

DFE Pharma, 2021. *Pharmatose 200M.* [Online]
Available at: https://dfepharma.com/en/Excipients/Expertise/Oral-Solid-
Dose/Lactose/Milled/Pharmatose-200M [Accessed January 2021].

DFE Pharma, Undated. *Wet granulation of milled lactose,* s.l.: DFE Pharma.

Dhenge, R. M. et al., 2011. Twin screw wet granulation: Effect of powder feed rate. *Advanced Powder Technology,* Issue 22, pp. 162-166.

Dhenge, R. M., Cartwright, J. J., Hounslow, M. J. & Salman, A. D., 2012(a). Twin screw granulation: Steps in granule growth. *International Journal of Pharmaceutics,* Volume 438, pp. 20-32.

Dhenge, R. M., Cartwright, J. J., Hounslow, M. J. & Salman, A. D., 2012(b). Twin screw wet granulation: Effects of properties of granulation liquid. *Powder Technology,* Volume 229, pp. 126-136.

Dhenge, R. M. et al., 2010. Twin screw wet granulation: Granule properties. *Chemical Engineering Journal,* Volume 164, pp. 322-329.

Dhenge, R. M. et al., 2013. Twin screw granulation using conveying screws: Effects of viscosity of granulation liquids and flow of powders. *Powder Technology,* Volume 238, pp. 77-90.

Djuric, D. et al., 2009. Comparison of two twin-screw extruders for continuous granulation. *European Journal of Pharmaceutics and Biopharmaceutics,* Volume 71, pp. 155-160.

Doldán, C. et al., 1995. Dicalcium phosphate dihydrate and anhydrous dicalcium phosphate for direct compression: a comparitive study. *International Journal of Pharmaceutics,* Issue 124, pp. 69-74.

Dr. Dietmar Schulze, 2018. *Ring Shear Tester RST-XS.s,* s.l.: Schulze.

EDQM, Council of Europe, 2014. *European Pharmacopoeia.* 8th ed. Strasbourg: s.n.

Egart, M. et al., 2014. Compaction properties of crystalline pharmaceutical ingredients according to the Walker model and nanomechanical attributes. *International Journal of Pharmaceutics,* Volume 472, pp. 347-355.

El Hagrasy, A. S. et al., 2013. Twin screw wet granulation: Influence of formulation parameters on granule properties and growth behaviour. *Powder Technology,* Volume 238, pp. 108-115.

Emady, H. N., Kayrak-Talay, D., Schwerin, W. C. & Lister, J. D., 2011. Granule formation mechanisms and morphology from single drop impact on powder beds. *Powder Technology,* Volume 212, pp. 69-79.

Ennis, B. J., 2005. Theory of granulation: an engineering perspective. In: D. M. Parikh, ed. *Handbook of Pharmaceutical Granulation Technology.* NY: Taylor & Francis, p. Chapter 2.

Etzler, F. M. et al., 2012. Tablet tensile strength: An adhesion science perspective. *Journal of Adhesion Science and Technology,* 25(4-5), pp. 501-519.

Eyjolfsson, R., 2015. Design and Manufacture of Pharmaceutical Tablets. s.l.:Elsevier.

Farber, L. et al., 2008. unified compaction curve model for tensile strength of tablets made by roller compaction and direct compression. *International Journal of Pharmaceutics,* Volume 346, pp. 17-24.

FDA, 2006. Guidance for Industry Q8 Pharmaceutical Development, s.l.: Food and Drug Administration CDER.

Fichtner, F. et al., 2008. Effect of surface energy on powder compactibility. *Pharmaceutical Research,* 25(12), pp. 2750-2759.

Fonteyne, M. et al., 2013. Real-time assessment of critical quality attributes of a continuous granulation process. *Pharmaceutical Development Technology,* 18(1), pp. 85-97.

Freeman Technology, Undated. About the FT4 powder rheometer. [Online]
Available at: https://www.freemantech.co.uk/powder-testing/ft4-powder-rheometer-powder-flow-tester
[Accessed January 2022].

Garekani, H. A. et al., 2001. Crystal habit modifications of ibuprofen and their physicomechanical characteristics. *Drug Development and Industrial Pharmacy,* 27(8), pp. 803-809.

Granutools, Undated. Granudrum. [Online]
Available at: https://www.granutools.com/en/granudrum
[Accessed January 2022].

Greenspan, L., 1976. Humidity fixed points of binary saturated aqueous solutions. *Journal of research of the National Bureau of Standards - A. Physics and Chemistry,* 81A(1), pp. 90-96.

Gustafsson, C., Lennholm, H., Iversen, T. & Nyström, C., 2003. Evaluation of surface and bulk characteristics of cellulose I powders in relation to compaction behaviour and tablet properties. *Drug Development and Industrial Pharmacy,* 29(10), pp. 1095-1107.

Hanningfield, 2020. Perfecting particle size sistribution (PSD) for tableting. [Online]
Available at: https://www.hanningfield.com/perfecting-particle-size-distribution-tableting/
[Accessed February 2021].

Hapgood, K. P., Litster, J. D., Biggs, S. R. & Howes, T., 2002. Drop penetration into porous powder beds. *Journal of Colloid and Interface Science,* Volume 253, pp. 353-366.

Haugen, H. J. et al., 2020. Nano-CT as tool for characterization of dental resin composites. Scientific Reports, Volume 10.

Heckel, R. W., 1961. Density-pressure relationship in powder compaction. *Transaction of the metallurgical society,* Issue 221, p. 671.

Hersey, J. A. & Rees, J. E., 1971. Deformation of particles during briquetting. *Nature,* p. 230.

Herting, M. G. & Kleinebudde, P., 2008. Studies on the reduction of tensile strength of tablets after roll compaction/dry granulation. *European Journal of Biopharmaceutics,* 70(1), pp. 372-379.

Hiestand, E. N., 1997. Mechanical properties of compacts and particles that control tableting success. Journal of Pharmaceutical Science, Volume 86, pp. 985-990.

Hiremath, P., Nuguru, K. & Agrahari, V., 2019. Chapter 8: Material attributes and their impact on wet granulation process performance. In: *Handbook of Pharmaceutical Wet Granulation.* s.l.:Elsevier, pp. 263-315.

Houwink, R. & De Decker, H. K., 1971. *Elasticity, Plasticity and Structure of Matter.* 3rd ed. Cambridge: Cambridge University Press.

Ilić, I. et al., 2013. Deformation properties of pharmaceutical excipients determined using in-die and out-die method. *International Journal of Pharmaceutics,* Volume 446, pp. 6-15.

Innophos, 2021. *Innophos Excipients.* [Online] Available at: https://www.innophos.com/ingredients/ingredient-categories/excipients [Accessed January 2021].

Iveson, S. M. & Lister, J. D., 1998. Growth regime map for liquid-bound granules. *AIChE Journal,* Volume 44, pp. 1510-1518.

Iyer, R. M. et al., 2014. The impact of roller compaction and tablet compression on physicochemical properties of pharmaceutical excipients. *Pharmaceutical Development and Technology,* 5(19), pp. 583-592.

Jager, P. D., Bramante, T. & Luner, P. E., 2015. Assessment of pharmaceutical powder flowability using shear cell-based methods and application of Jenike's methodology. *Journal of Pharmaceutical Sciences,* Volume 104, pp. 3804-3813.

Jenike, A. W., 1964. *Storage and flow of solids.* Salt Lake City: University of Utah.

Joiris, E. et al., 1998. Compression behaviour of orthorhombic paracetamol. *Pharmaceutical Research,* 15(7), pp. 1122-1130.

Kaerger, J. S., Edge, S. & Price, R., 2004. Influence of particle size and shape on flowability and compactibility of binary mixtures of paracetamol and microcrystalline cellulose. *European Journal of Pharmaceutical Science,* Issue 22, pp. 173-179.

Kafle, B., 2020. Chapter 8 - Raman Spectroscopy. *Chemical Analysis and Material Characterization by Spectrophotometry*, pp. 245-268.

Kawakita, K. & Ludde, K.-H., 1970. Some considerations on powder compression equations. *Powder Technology,* Issue 4, p. 61.

Kayrak-Talay, D., Dale, S., Wassgren, C. & Lister, J., 2013. Quality by design for wet granulation in pharmaceutical processing: Assessing models for a priori design and scaling. *Powder Technology,* Issue 240, pp. 7-18.

Keleb, E. I., Vermeire, A., Vervaet, C. & Remon, J. P., 2002. Continuous twin screw extrusion for the wet granulation of lactose. *International Journal of Pharmaceutics,* Volume 239, pp. 69-80.

Khan, P., Pilpel, N. & Ingham, S., 1988. The effect of moisture on the density, compaction and tensile strength of microcrystalline cellulose. Powder Technology, Volume 54, pp. 161-164.

Khorsheed, B., Gabbott, I. & Reynolds, G. K., 2019. Twin-screw granulation: Understanding the mechanical properties from powder to tablets. Powder Technology, Volume 341, pp. 104-115.

Koskela, J. et al., 2018. The effect of mechanical dry coating with magnesium stearate on flowability and compactibility of plastically deforming microcrystalline cellulose. *International Journal of Pharmaceutics,* Volume 537, pp. 64-72.

Kuentz, M. & Leuenberger, H., 1999. Pressure susceptibility of polymer tablets as a critical property: a modified Heckel equation. *Journal of Pharmaceutical Science,* Volume 88, pp. 174-179.

Kumar, A. et al., 2016. Development of a process map: A step towards a regime map for steady-state high shear wet twin screw granulation. *Powder Technology,* Volume 300, pp. 73-82.

Lakio, S. et al., 2013. Challenges in detecting magnesium stearate distribution in tablets. *AAPS PharmSciTech,* 14(1), pp. 435-444.

Lee, K. T., Ingram, A. & Rowson, N. A., 2012. Twin screw wet granulation: The study of a continuous twin screw granulator using Positron Emission Particle Tracking (PEPT) technique. *European Journal of Pharmaceuticas and Biopharmaceutics,* Volume 81, pp. 666-673.

Leturia, M. et al., 2014. Characterization of flow properties of cohesive powders: A comparitive study of traditional and new testing methods. *Powder Technology,* Volume 253, pp. 406-423.

Li, L. & Iskander, M., 2019. Evaluation of dynamic image analysis for characterizing granular solids. Geotechnical Testing Journal.

Lister, J., 2016. *Design and Processing of Particulate Products.* Cambridge: Cambridge University Press.

Litster, J. & Ennis, B., 2004. *The Science and engineering of granulation processes.* s.l.:Kluwer Academic Publishers.

Liu, H. et al., 2017. Optimization of critical quality attributes in continuous twin-screw wet granulation via design space validated with pilot scale experimental data. *International Journal of Pharmaceutics,* Volume 525, pp. 249-263.

Liu, L. X. et al., 2008. Effect of particle properties on the flowability of ibuprofen powders. *International Journal of Pharmaceutics,* Volume 362, pp. 109-117.

Lute, S., Dhenge, R. & Salman, A., 2018. Twin screw granulation: Effects of properties of primary powders. *Pharmaceutics,* 10(2).

Mallinckrodt, 2019. *Measurably Superior Stearates.* [Online]
Available at: https://www.mallinckrodt.com/globalassets/documents/10004827-3_stearates-brochure_with-rspo_final_no-opdp-sub_122319.pdf
[Accessed January 2021].

Malvern Instruments Worldwide, 2013. *Application Note: Wet or liquid dispersion method development for laser diffraction particle size measurements,* s.l.: Malvern Instruments Limited.

Malvern Panalytical, 2022. Laser Diffraction. [Online]
Available at: https://www.malvernpanalytical.com/en/products/technology/light-scattering/laser-diffraction
[Accessed January 2022].

Mate, C. M., 2007. Physical origins of surface forces. In: Tribology on the small scale: A bottom up approach to friction, lubrication and wear. s.l.:Oxford Scholarship.

Mazel, V. & Tchoreloff, P., 2021. Lamination of pharmaceutical tablets: Classification and influence of process parameters. Journal of Pharmaceutical Sciences.

Meier, R. et al., 2016. Granule size distributions after twin-screw granulation - Do not forget the feeding systems. *European Journal of Pharmaceutics and Biopharmaceutics,* Volume 106, pp. 59-69.

Mohammed, I. et al., 2020. A review on polymer, gas, surfactant and nonoparticle adsorption modeling in porous media. Oil & Gas Science and Technology, 75(77).

Nally, J. D., 2016. *Good manufacturing practices for pharmaceuticals.* 6th ed. s.l.:CRC Press.

Nathier-Dufour, N. et al., 1993. Comparison of sieving and laser diffraction for the particle size measurements of raw materials used in foodstuff. *Powder Technology,* 76(2), pp. 191-200.

Nguyen, T. H., Morton, D. A. V. & Hapgood, K. P., 2013. Application of the unified compaction curve to link wet granulation and tablet compaction behaviour. *Powder Technology,* Volume 240, pp. 103-115.

Nicolas, V. et al., 1999. Preformulation: Effect of moisture content on microcrystalline cellulose (Avicel PH-302) and its consequences on packing performances. *Drug Development and Industrial Pharmacy,* 25(10), pp. 1137-1142.

Odeku, O. & Itiola, O., 2003. Effects of interacting variables on the tensile strength and the release properties of paracetamol tablets. Tropical Journal of Pharmaceutical Research, 2(1), pp. 147-153.

Paul, S. et al., 2018. Comparative analyses of flow and compaction properties of diverse mannitol and lactose grades. *International Journal of Pharmaceutics,* Issue 546, pp. 39-49.

Paul, S. & Sun, C. C., 2017. Lubrication with magnesium stearate increases tablet brittleness. *Powder Technology,* Volume 309, pp. 126-132.

Paul, S., Tajarobi, P., Boissier, C. & Sun, C. C., 2019. Tableting performance of various mannitol and lactose grades assessed by compaction simulation and chemometrical analysis. International Journal of Pharmaceutics, Volume 566, pp. 24-31.

Persson, A., Nordström, J., Frenning, G. & Alderborn, G., 2016. Compression analysis for assessment of pellet plasticity: Identification of reactant pores and comparison between Heckel, Kawakita, and Adams equations. *Chemical Engineering Research and Design,* Volume 110, pp. 183-191.

Peter Greven, 2018. Ligamed. [Online]
Available at: https://www.peter-greven.de/fileadmin/user_upload/dweber/PG/PDFs/Broschueren/PG_Pharma_2018_GB.pdf
[Accessed January 2022].

Pharmaquest, Undated. *Hygroscopicity, powder rheology and compaction properties.* [Online]
Available at:
http://pharmaquest.weebly.com/uploads/9/9/4/2/9942916/powder_rheologyhygrocompaction.pdf
[Accessed August 2020].

Pitt, K. G. et al., 2015. Compression prediction accuracy from small scale compaction studies to production presses. *Powder Technology,* Volume 270, pp. 490-493.

Pitt, K. & Sinka, C., 2001. Tabletting. In: *Handbook of Powder Technology.* s.l.:Elsevier, pp. 736-776.

Retsch, 2015. Retsch Sieve Analysis. [Online]
Available at: https://www.retsch.com/dltmp/www/53e4b562-5294-4711-9111-636500000000-b8e580d34c65/expert_guide_sieving_en.pdf
[Accessed January 2022].

Roberts, R. & Rowe, R., 1986. The effect of the relationship between punch velocity and particle size on the compaction behaviour of materials with varying deformation mechanisms. *Journal of Pharmacy and Pharmacology,* 8(38), pp. 567-571.

Roberts, R. J. & Rowe, R. C., 1986. Brittle fracture propensity measurements on 'tablet-sized' cylindrical compacts. Journal of Pharmaceutics and Pharmacology, Volume 38, pp. 526-528.

Roquette, 2022. Pearlitol 160C. [Online]
Available at: https://www.roquette.com/innovation-hub/pharma/product-profile-pages/pearlitol-160c-mannitol
[Accessed January 2022].

Rosato, A. & Windows-Yule, C., 2020. Sgregation in Vibrated Granular Systems. 1st ed. s.l.:Academic Press.

Rowe, R. C., Mckillop, A. G. & Bray, D., 1994. The effect of batch and source variation on the crystallinity of microcrystalline cellulose. *International Journal of Pharmaceutics,* Issue 101, pp. 169-172.

Rowe, R. C., Sheskey, P. & Quinn, M. E., 2009. *Handbook of pharmaceutical excipients.* 6th Edition ed. London: Pharmaceutical Press.

Ryshkewitch, E., 1953. Compression strength of porous sintered alumina and zirconia. *Journal of the American Ceramic Society,* Volume 36, pp. 65-68.

Sørensen, A. H., Sonnergaard, J. M. & Hovgaard, L., 2005. Bulk Characterization of Pharmaeutical Powders by Low-Pressure Compression. *Pharmaceutical Development and Technology,* Volume 10, pp. 197-209.

Sahputra, I. H., Alexiadis, A. & Adams, M. J., 2019. Effects of moisture on the mechanical properties of microcrystalline cellulose and the mobility of the water molecules as studied by the hybrid molecular mechanics-molecular dynamic simulation method. *Journal of Polymer Science,* Volume 57, pp. 454-464.

Saito, Y., Fan, X., Ingram, A. & Seville, J. P. K., 2011. A new approach to high-shear mixer granulation using positron emission particle tracking. *Chemical Engineering Science,* Issue 66, pp. 563-569.

Schiano, S., 2017. Dry granulation using roll compaction process: Powder characterization and process understanding, s.l.: University of Surrey.

Schulze, D., 2010. *Flow properties of powders and bulk solids.* [Online]
Available at: https://www.dietmar-schulze.de/grdle1.pdf [Accessed April 2020].

Schulze, D., 2013. Shear Testing of Powders for Process Optimization. *Annual Transactions of the Nordic Rheology Society*, Volume 21, Issue 21, pp. 99-106.

Seem, T. C. et al., 2016. Asymmetric distribution in twin screw granulation. *European Journal of Pharmaceutics and Biopharmaceutics,* Issue 106, pp. 50-58.

Seem, T. C. et al., 2015. Twin screw granulation - A literature review. *Powder Technology,* Issue 276, pp. 89-102.

Seville, J. P. K. & Wu, C., 2015. *Particle technology and engineering.* Oxford: Butterworth-Heinemann.

Shotton, E. & Ganderton, D., 1961. The strength of compressed tablets. *Journal of Pharmacy and Pharmacology,* Volume 13, pp. 144-152.

Siming, Y. & Wan, M. P., 2013. Mathematical Models for the van der Waals force and capillary force between a rough particle and surface. *Langmuir,* Volume 29, pp. 9104-9117.

Sonnergard, J. M., 1999. A critical evaluation of the Heckel equation. *International Journal of Pharmaceutics,* Volume 193, pp. 63-71.

Steele, D. F. et al., 2008. Surface energy of microcrystalline cellulose determined by capillary intrusion and inverse gas chromatography. *The AAPS Journal,* 10(3), pp. 494-502.

Sun, C., 2017. Role of surface free energy in powder behaviour and tablet strength. In: K. L. Mittal & F. M. Etzler, eds. *Adhesion in pharmaceutical, biomedical and dental fields.* s.l.:Scrivener Publishing LLC, pp. 75-88.

Sun, C. C., 2004. A novel method for deiving true density of pharmaceutical solids including hydrates and water-containing powders. *Journal of pharmaceutical sciences,* 93(3), pp. 646-653.

Sun, C. C., 2008. Mechanism of moisture induced variations in true density and compaction properties of microcrystalline cellulose. *International Journal of Pharmaceutics,* Issue 346, pp. 93-101.

Sun, C. C., 2011. Decoding powder tabletability: Roles of particle adhesion and plastcitiy. *Journal of Adhesion Science and Technology,* Volume 25, pp. 483-499.

Sun, C. C. & Kleinebudde, P., 2016. Mini review: Mechanisms to the loss of tabletability by dry granulation. *European Journal of Pharmaceutics and Biopharmaceutics,* Volume 106, pp. 9-14.

Sun, C. & Grant, D. J. W., 2001. Influence of elastic deformation of particles on Heckel analysis. *Pharmaceutical Development and Technology,* 6(2), pp. 193-200.

Sun, W., Kothari, S. & Sun, C. C., 2018. The relationship among tensile strength, Youngs's modulus, and indentation hardness of pharmaceutical compacts. *Powder Technology,* Volume 331, pp. 1-6.

Sympatec, 2021. *Particle Shape Analysis.* [Online] Available at: https://www.sympatec.com/en/particle-measurement/glossary/particle-shape/ [Accessed January 2021].

Tarlier, N. et al., 2018. Deformation behaviour of crystallized mannitol during compression using rotary tablet press simulator. *International Journal of Pharmaceutics,* 547(1-2), pp. 142-149.

Thapa, P., Lee, A. R., Choi, D. H. & Jeong, S. H., 2017. Effects of moisture content and compression pressure of various deforming granules on the physical properties of tablets. *Powder Technology,* Issue 310, pp. 92-102.

The United States Pharmacopeial Convention, 2012. <786> Particle size distribution estimation by analytical sieving. In: The United States Pharmacopeia. s.l.:s.n., pp. 336-339.

Thompson, M. R., 2015. Twin screw granulation - a review of current progress. *Drug Development and Industrial Pharmacy,* 8(41), pp. 1223-1231.

Thompson, M. R. & Sun, J., 2010. Wet granulation in a twin-screw extruder: Implications of screw design. *Journal of Pharmaceutical Sciences,* 99(4), pp. 2090-2103.

Thoorens, G. et al., 2014. Microcrystalline cellulose, a direct compression binder in a quality by design environment. International Journal of Pharmaceutics, Volume 473, pp. 64-72.

Tu, W.-D., Ingram, A. & Seville, J., 2013. Regime map development for continuous twin screw granulation. *Chemical Engineering Science,* Volume 87, pp. 315-326.

Tye, C. K., Sun, C. C. & Amidon, G. E., 2005. Evaluation of the effects of tableting speed on the relationships between compaction pressure, tablet tensile strength and tablet solid fraction. *Journal of Pharamceutical Science,* 94(3), pp. 465-472.

Van Melkebeke, B., Vermeulen, B., Vervaet, C. & Remon, P., 2008. Validation of a continuous granulation process using a twin-screw extruder. International Journal of Pharmaceutics, Volume 356, pp. 224-230.

Vanhoorne, V. et al., 2016. Improved tabletability after polymorphic transition of delta-mannitol during twin screw granulation. *Internation Journal of Pharmaceutics,* Volume 506, pp. 13-24.

Vanhoorne, V. et al., 2016. Continuous twin screw granulation of controlled release formulations with various HPMC grades. International Journal of Pharmaceutics, Volume 511, pp. 1048-1057.

Vercruysse, J. et al., 2015. Impact of screw configuration on the particle size distribution of granules produced by twin screw granulation. *International Journal of Pharmaceutics,* Volume 479, pp. 171-180.

Vercruysse, J. et al., 2012. Continuous tein screw granulation: influence of process variables on granule and tablet quality. *European Journal of Pharmaceutics and Biopharmaceutics,* 82(1), pp. 205-211.

Viana, M., Jouannin, P., Pontier, C. & Chulia, D., 2002. About pycnometirc density measurements. *Talanta,* Volume 57, pp. 583-593.

Vonk, P. et al., 1997. Growth mechanisms of high-shear pelletisation. *International Journal of Pharmaceutics,* 157(1), pp. 93-102.

Walker, E. E., 1923. The properties of powders VI: the compressibility of powders. *Transactions of the Faraday Society,* Volume 19, pp. 73-82.

Willecke, N. et al., 2018. A novel approach to support formulation design on twin screw wet granulation technology: Understanding the impact of overarching excipient properties on drug quality attributes. *International Journal of Pharmaceutics,* Issue 545, pp. 128-143.

Wu, C. et al., 2005. A simple predictive model for the tensile strength of binary tablets. *European Journal of Pharmaceutical Sciences,* Volume 25, pp. 331-336.

Wurster, D. E., Likitlersuang, S. & Chen, Y., 2008. The influence of magnesium stearate on the Hiestand tableting indices and other related mechanical properties of maltodextrins. *Pharmaceutical Development and Technology,* 10(4), pp. 461-466.

Yap, S. F., Adams, M. J., Seville, J. P. K. & Zhang, Z., 2008. Single and bulk compression of pharmaceutical excipients: Evaluation of mechanical properties. *Powder Technology,* Volume 185, pp. 1-10.

You, S. & Pun Wan, M., 2013. Mathematical models for the Van der Waals Force and capilliary force between a rough particle and surface. *Langmuir,* Volume 29, pp. 9104-9117.

Yu, W. & Hancock, B. C., 2008. Evaluation of dynamic image analysis for characterizing pharmaceutical excipient particles. *International Journal of Pharmaceutics,* Issue 361, pp. 150-157.

Yu, S. et al., 2014. Granulation of increasingly hydrophobic formulations using a twin screw granulator. International Journal of Pharmaceutics, Volume 475, pp. 82-96.

Zarmpi, P. et al., 2017. Biopharmaceutical aspects and implications of excipient variability in drug product performance. *Biopharmaceutics,* Volume 111, pp. 1-15.

Zhang, J., Wu, C., Pan, X. & Wu, C., 2017. On identification of critical material attributes for compression behaviour of pharmaceutical diluent powders. *Materials,* Volume 10, p. 845.

Zhang, Y., Law, Y. & Chakrabati, S., 2003. Physical properties and compact analysis of commonly used direct compression binders. *AAPS PharmSciTech,* 4(4), p. Article 62.

Zhou, D. & Qiu, Y., 2010. Understanding material properties in pharmaceutical product development and manufacturing: powder flow and mechanical properties. *Journal of validation technology,* Issue Spring 2010, pp. 65-77.

Zografi, G., Kontny, M. J., Yang, A. Y. S. & Brenner, G. S., 1984. Surface area and water vapor sorption of microcystalline cellulose. *International Journal of Pharmaceutics,* Volume 18, pp. 99-116.

Zuurman, K., Van der Voort Maarschalk, K. & Bolhuis, G. K., 1999. Effect of magnesium stearate on bonding and porosity expansion of tablets produced from materials with different consolidation properties. *International Journal of Pharmaceutics,* Volume 179, pp. 107-115.